Climatic Behavior and Associated Variations Using CMIP Models over KKSD Basins in West Bengal

Thesis Submitted by

GAURAV PATEL

Index No.: D-7/E/143/21

Doctor of Philosophy (Engineering)

School of Water Resources Engineering

Faculty of Interdisciplinary Studies, Law and Management

Jadavpur University

Kolkata, India

2025

This dissertation is dedicated to Lord Hanuman, family and guides whose boundless love, guidance, and unwavering support have been my greatest strength. Their belief in me, even in moments of doubt, has been the driving force.

अतुलितबलधामं हेमशैलाभदेहं,

दनुजवनकृशानुं ज्ञानिनामग्रगण्यम् |

सकलगुणनिधानं वानराणामधीशं,

रघुपतिप्रियभक्तं वातजातं नमामि || ..... (Shri Hanumat Stawan stotram)

Whose power is incomparable, whose body is as massive as a mountain of gold. Who defeated the demons and is foremost among the knowledgeable. Who possesses all qualities and is the chief of the monkeys. Who is the beloved devotee of Lord Rama and is known as the son of the wind. I pay my respects to him.

JADAVPUR UNIVERSITY
KOLKATA – 700 032, INDIA

INDEX NO.: **D-7/E/143/21**

Title of Thesis:

Climatic Behavior and Associated Variations Using CMIP Models over KKSD Basins in West Bengal

Name, Designation and Institution of the Supervisors

Dr. Subhasish Das
Associate Professor and Joint Director
School of Water Resources Engineering
Jadavpur University
Kolkata 700 032, West Bengal, India

Dr. Rajib Das
Assistant Professor
School of Water Resources Engineering
Jadavpur University
Kolkata 700 032, West Bengal, India

List of Journal Publications

1. Patel, G., Das, R. and Das, S. (2023). Is the extreme temperature trend changed in last two decades compared to last seven decades? Case study from Eastern India. Journal of Earth System Science, 132(3), 140. https://doi.org/10.1007/s12040-023-02158-2 (**Q3, SCIE, SCOPUS**)
2. Patel, G., Das, S. and Das, R. (2023). Identification of Best CMIP6 Global Climate Model for Rainfall by Ensemble Implementation of MCDM Methods and Statistical Inference. Water Resources Management, 37(13), 5147–5170. https://doi.org/10.1007/s11269-023-03599-6 (**Q1, SCIE, SCOPUS**)
3. Patel, G., Das, S. and Das, R. (2024). Determine the best method for analysing long-term (120 years) annual and seasonal rainfall trends in four east India river basins. Journal of Earth System Science, 133(2), 70. https://doi.org/10.1007/s12040-024-02282-7 (**Q3, SCIE, SCOPUS**)
4. Patel, G., Das, S. and Das, R. (2024). Accuracy of historical precipitation from CMIP6 global climate models under diversified climatic features over India. Environmental Development, 50, 100998. https://doi.org/10.1016/j.envdev.2024.100998 (**Q2, SCIE, SCOPUS**)
5. Patel, G., Das, R., Das, S. and Mukherjee, I. (2025). Innovative trend analysis of long-term rainfall variation over West Bengal, India. Mausam (Accepted) (**Q4, SCIE, SCOPUS**)
6. Patel, G. and Das, S. (2025). Multi-Temporal Evaluation of CMIP6 Models for Maximum Temperature in East India: Improving Climate Dynamics Understanding. Stochastic Environmental Research and Risk Assessment. (2^{nd} Revision) (**Q1, SCIE, SCOPUS**)

List of Presentations in National/International Conferences

1. Patel, G., Das, S. and Das, R. (2022). MCDM approach to select best CMIP6 Global Climate Models (GCMs) for Dwarkeswer and Kangsabati basins in India. vol. 2022, Art. no. GC51B-01, 2022. [based on the article presented in the **American Geophysical Union (AGU)** Fall Meeting 2022, Chicago, Illinois, 12-16 December, 2022. *https://agu2022fallmeeting-agu.ipostersessions.com/default.aspx?s=E6-5E-C6-6C-C9-A9-54-5B-24-58-59-5D-20-A9-D8-23*].

2. Patel, G., Das, S. and Das, R. (2024). Influence of normalization techniques in CMIP model selection using an MCDM method MOORA. In Swain, B.P. and Dixit, U.S. (eds.), Recent Advances in Civil Engineering. ICSTE 2022. Lecture Notes in Civil Engineering, vol 431. Springer, Singapore. https://doi.org/10.1007/978-981-99-4665-5_6 (**SCOPUS**) [*based on the article presented in the International Conference on Science, Technology and Engineering (ICSTE 2023), NIT Manipur, 17-18 February, 2023*]

3. Patel, G., Das, S. and Das, R. (2025). Unraveling Extreme Temperature Dynamics over West Bengal: A Decadal Investigation Utilizing Very High-Resolution Gridded Dataset. In S. Vadhera et al. (eds.), Advances in Green Energy Technologies, Lecture Notes in Electrical Engineering 1314, https://doi.org/10.1007/978-981-96-0861-4_3 (**SCOPUS**) [*based on the article presented in the International Conference on Green Energy and Sustainable Technology, (ICGEST 2023), NIT Kurukshetra, 07-09 April, 2023*]

4. Patel, G., Das, S. and Das, R. (2025). A Comprehensive Seasonal Temperature Assessment of Historical Climate Model Accuracy. In One-Day National Symposium titled "Seventy-Five Years of Accomplishments of Mausam: Quarterly Journal of Meteorology, Hydrology, and Geophysics". (*Mausam Symposium*)

PROFORMA – 1

"Statement of Originality"

I, **Gaurav Patel (D-7/E/143/21)** registered on **2nd August 2021** do hereby declare that this thesis entitled **"Climatic Behavior and Associated Variations Using CMIP Models Over KKSD Basins in West Bengal"** contains literature survey and original research work done by the undersigned candidate as part of Doctoral studies.

All information in this thesis have been obtained and presented in accordance with existing academic rules and ethical conduct. I declare that, as required by these rules and conduct, I havefully cited and referred all materials and results that are not original to this work.

I also declare that I have checked this thesis as per the "Policy on Anti Plagiarism, Jadavpur University, 2019", and the level of similarity as checked by iThenticate software is **08%**.

Gaurav Patel
Signature of Candidate:

Date: 27.01.2025

Certified by Supervisor(s):(Signature with date, seal)

1. Subhasish Das 27/01/25

Dr. Subhasish Das
Associate Professor & Joint Director
School of Water Resources Engineering
Jadavpur University
Kolkata - 700032

2. Rajib Das 27/01/2025

Dr. RAJIB DAS
Assistant Professor
School of Water Resources Engineering
Jadavpur University
Kolkata-700 032

CERTIFICATE FROM THE SUPERVISORS

This is to certify that the thesis entitled "**Climatic Behavior and Associated Variations Using CMIP Models Over KKSD Basins in West Bengal**" submitted by **Mr. Gaurav Patel**, who got his name registered on **2nd August 2021** for the award of the Ph.D. degree of Jadavpur University is absolutely based upon his own work under the supervisions of **Dr. Subhasish Das**, Associate Professor and Joint Director and **Dr. Rajib Das**, Assistant Professor of School of Water Resources Engineering, Jadavpur University and that neither his thesis nor any part of the thesis has been submitted for any degree or any other academic award anywhere before.

1. Subhasish Das 27/01/25

THESIS ADVISOR

Dr. Subhasish Das
Associate Professor and Joint Director
School of Water Resources Engineering
Jadavpur University

Dr. Subhasish Das
Associate Professor & Joint Director
School of Water Resources Engineering
Jadavpur University
Kolkata - 700032

2. Rajib Das 27/01/2025

THESIS ADVISOR

Dr. Rajib Das
Assistant Professor
School of Water Resources Engineering
Jadavpur University

Dr. RAJIB DAS
Assistant Professor
School of Water Resources Engineering
Jadavpur University
Kolkata-700 032

ACKNOWLEDGEMENTS

The author wishes to express his heartfelt gratitude towards his thesis supervisors Dr. Subhasish Das, Associate Professor and Joint Director, and Dr. Rajib Das, Assistant Professor of the School of Water Resources Engineering (SWRE), Jadavpur University (JU), for their valuable guidance and continuous encouragement in planning, wholehearted involvement, advice, support execution and presentation of this thesis. It was their initiation, constant encouragement, and help rendered in developing the experimental facilities in the Computational Lab of the School of Water Resources Engineering, Jadavpur University that enabled the author to carry out a major part of the present thesis work.

He is also indebted to his supervisors for helping and providing moral support during the tenure of his Ph.D. work.

Heartfelt gratitude to Prof. (Dr.) Asis Mazumdar, Professor and Director, School of Water Resources Engineering, Jadavpur University for his encouragement during the research.

Thanks, are also due to all the staff members of the SWRE, JU, for their co-operation during the investigation.

Special thanks are also due to Mr. Buddhadev Nandi, Mrs. Koushani Sarkar, and other Research Scholars of SWRE, JU, for their help during this journey.

Last but not least, the author would like to dedicate this thesis to his family, and friends (Mr. Kaushal Kumar, Ph.D. student of MNIT Bhopal) without whose motivation and constant backup, the completion of this thesis might be a distant dream to the author.

Date: 27.01.2025

Place: SWRE, Jadavpur University

Gaurav Patel

Gaurav Patel
Ph.D. Scholar
School of Water Resources Engineering
Jadavpur University

Table of Contents

Abstract xx

1 Introduction 1

1.1 Background and Motivation 1

1.2 Research Scopes 2

1.3 Research Objectives 3

1.4 Thesis Structure 3

References 4

2 Study Area and Data Utilized 6

2.1 Study Area 6

2.1.1 Kangsabati Basin 6

2.1.2 Keliaghai Basin 6

2.1.3 Silabati Basin 6

2.1.4 Dwarkeswer Basin 6

2.2 Data Used 7

2.2.1 Gridded Temperature Data 7

2.2.2 Gridded Rainfall Data 8

2.2.3 Global Climate Models (GCMs) 8

2.2.4 Data Quality 8

2.2.5 Performance Metrics 8

2.3 Tools and Software 11

References 12

3 Long-Term Rainfall Trend Analysis 13

3.1 Introduction 13

3.2 Methodological Approaches for Long-Term Rainfall Trend Analysis 14

3.2.1 Stationarity and Homogeneity Testing 14

3.2.2 Mann-Kendall Test (MK) 14

3.2.3 Modified Mann-Kendall Test (MMK) 15

3.2.4 Spearman Rank Correlation (SRC) Analysis 15

3.2.5 Şen Slope Estimator (SSE) 16
3.2.6 Innovative Trend Analysis (ITA) 16
3.3 Results and Discussion 16
3.3.1 Stationarity and Homogeneity Tests 16
3.3.2 Mean Annual and Seasonal Rainfall 17
3.3.3 Trend Analysis 19
3.3.4 Annual Trend 22
3.3.5 Summer Trend 22
3.3.6 Monsoon Trend 22
3.3.7 Autumn Trend 23
3.3.8 Winter Trend 23
3.4 Conclusions 24
References 24
4 Decadal Trend Analysis of Temperature Data 26
4.1 Introduction 26
4.2 Results and Discussion 27
4.2.1 Statistical Analysis of Temperatures 27
4.2.2 Annual Temperature Trend 30
4.2.3 Seasonal Temperature Trend 30
4.2.4 Innovative Trend Analysis (ITA) 33
4.2.5 Percentage Changes in Slope of ITA 36
4.2.6 Spatial Variations 37
4.3 Conclusions 40
References 41
5 Ranking of CMIP6 Models Using MCDM 43
5.1 Introduction 43
5.2 Methodology 44
5.2.1 Performance Indicators (PIs) 45
5.2.2 Weight Criteria Techniques 45
5.2.3 Multi-Criteria Decision-Making (MCDM) 45

5.3 Results and Discussion 46
5.3.1 PIs and Weight 46
5.3.2 Ranking of GCMs using Different Parameters 48
5.3.3 MCDM based ranking of GCMs 50
5.3.5 Selection and Ensemble of GCMs for Projection 52
5.4 Conclusions 55
References 56
6 Evaluation of Historical Data Accuracy in CMIP6 Models 57
6.1 Introduction 57
6.2 Study Area 58
6.3 Methodology 60
6.4 Results 61
6.4.1 Assessment Based on Statistics 61
6.4.2 Assessment Based on Climate Classifications 63
6.4.3 Assessment Based on Trend Analysis 65
6.4.4 Assessment Based on the Performance of Individual Parameters 67
6.5 Discussion 70
6.6 Conclusions 71
References 72
7 Multi-Temporal Assessment of CMIP6 Models for Climate Dynamics 73
7.1 Introduction 73
7.2 Goodness-of-Fit 75
7.3 Results and Discussion 76
7.3.1 Descriptive analysis 76
7.3.2 Heat Matrix 78
7.3.3 Compromise Programming 84
7.4 Conclusions 86
References 87
8 Machine Learning for Climate Model Evaluation 89

8.1 Introduction 89
8.2 Study Area and Data Used 91
8.3 Machine Learning Approaches to Evaluation 92
8.3.1 Screening of Best-Performing GCMs 92
8.3.2 ML-Based Ensemble 92
8.3.3 Hyperparameter Tuning 93
8.3.4 Splitting Statistics and Performance Evaluation 93
8.4 Results and Discussion 95
8.4.1 Feature Importance (FI) and Ranking of GCMs 95
8.4.2 Performance and Comparison of ML Algorithms 97
8.4.3 Ensemble of ML Models 99
8.4.4 Performance Evaluation Based on MBE and Residual Analysis 101
8.5 Discussion 103
8.6 Conclusions 105
References 106
9 Projected Precipitation Changes Based on Selective GCMs 108
9.1 Introduction 108
9.2 Empirical and Machine Learning-Based Projections 109
9.2.1 Selection of GCMs 109
9.2.2 Splitting and tuning 109
9.3 Results and Discussion 110
9.4 Conclusions 117
References 117
10 Final Remarks 118
Limitations 121
Future Scopes 122

Abstract

Understanding the dynamics of climate variability is crucial for sustainable development, particularly in Eastern India, which is highly susceptible to climatic variabilities. This thesis presents a comprehensive study of the historical trends and projections of temperature and rainfall, evaluates the accuracy of Global Climate Models (GCMs) from CMIP6, and employs advanced machine learning techniques to enhance climate model evaluation and selection. The study provides a robust framework for understanding climate variability, improving model accuracy, and offering actionable insights for policymakers and stakeholders.

The study begins with analyzing historical rainfall and temperature trends in the Kangsabati, Keliaghai, Silabati, and Dwarkeswer (KKSD) basins, highlighting significant seasonal and annual variations over the decades. The key findings reveal significant rising and declining trends in seasonal rainfall and rising trends in temperatures, with spatial variability observed across the region. Decadal analysis further recognizes temporal periods of increased warming, highlighting the vulnerability of the region to climate extremes. The variability in these climatic parameters has important implications for agriculture, water resources, and disaster management.

To ensure the reliability of climate models, the thesis employs a Multi-Criteria Decision-Making (MCDM) approach to rank CMIP6 models based on multiple performance metrics. This ranking provides a systematic method for selecting models best suited for regional climate studies. The results reveal that certain GCMs consistently outperform others in replicating historical climate data, with canESM5, MIROC-ES2L, IITM-ESM, BCC-CSM2-MR, and EC-Earth3-Veg-LR emerging as top performers across various evaluation criteria. Interestingly, the rankings differ when prioritizing specific metrics, underscoring the importance of a comprehensive evaluation framework. The findings highlight the utility of combining statistical evaluation with MCDM approaches to provide a holistic perspective on model performance. This methodology not only facilitates the identification of optimal GCMs for climate impact studies but also provides a foundation for improving ensemble techniques by utilizing the strengths of individual models.

Further evaluation of the historical accuracy of CMIP6 models across various climatic zones and geographical features, including mountain ranges, reveals biases and variability, emphasizing the need for advanced validation techniques. The accuracy evaluation critically assesses the ability of CMIP6 models to replicate historical maximum temperature data. Statistical metrics were utilized to evaluate model performance. Results reveal substantial variability in model accuracy, with MIROC-ES2L, ACCESS-ESM1-5, and GISS-E2 emerging as top performers in replicating historical patterns for multiple timeframes. Models like INM-CM5-0 and GFDL-ESM4, while moderate in overall accuracy, showed strengths in specific parameters and temporal resolutions. The study demonstrates that such systematic evaluation methods can effectively reduce uncertainty and enhance the reliability of climate predictions.

A unique contribution of this study is the utilization of multiple machine learning (ML) approaches to assess and improve the reliability of climate models. ML and feature importance

analysis revealed that these methods could mitigate individual model biases and produce more reliable outputs. Among the various ML algorithms evaluated, the ensemble-based output performs better, achieving better agreement with observed T_{max}. The findings suggest that integrating machine learning with traditional climate modeling offers a powerful approach to improving prediction accuracy and understanding key drivers of climate variability. The study also explores projected changes across different Shared Socioeconomic Pathways (SSPs) and time durations, providing a better understanding of future climatic scenarios. The projections based on selected CMIP6 models reveal diverse trends under different SSPs. While all scenarios indicate rising temperatures, precipitation trends show significant variability, with increases and decreases projected across different timeframes and scenarios. The analysis highlights the importance of model ensemble techniques to address uncertainties and provide more consistent projections.

Key findings of this study include the identification of historical climate trends, detailed evaluation of CMIP6 model accuracy, development of an innovative model selection framework, and the integration of machine learning for enhanced climate projections. These findings provide a valuable foundation for future research and decision-making, ensuring that climate science continues to inform sustainable development and policy initiatives.

The thesis concludes by providing actionable insights for climate adaptation and mitigation strategies in the KKSD basins. By integrating advanced statistical methods, MCDM approaches, and ML, the research offers a comprehensive framework for evaluating and utilizing climate models effectively. This framework can be adapted to other regions, contributing to global initiatives to mitigate climate change and strengthen vulnerable populations.

Chapter 1
Introduction

1.1. Background and Motivation

Understanding the climate system has become very important due to challenges such as climate change, global warming, and extreme weather events. Climatology, a key branch of atmospheric sciences, serves as the foundation for this understanding. By analyzing the long-term atmospheric state and the processes that govern it, it provides insights into past, present, and future climate behavior. This field not only examines climatic trends and variability but also investigates the underlying causes, such as atmospheric circulation, ocean-atmosphere interactions, and anthropogenic influences. These insights are essential for addressing the uncertainties inherent in predicting future climate conditions and their implications for ecosystems, economies, and human societies.

Climatology includes various components and subfields that gives a complete understanding of the climate system. The fundamental components contain:

1. **Physical Climatology**: Focuses on energy exchanges and the physical processes driving the climate of the Earth. This includes the study of solar radiation, heat balance, and atmospheric thermodynamics.
2. **Dynamic Climatology**: Explores the role of atmospheric motions, such as winds, jet streams, and cyclones, in shaping climate patterns. It highlights the dynamic interactions between the atmosphere and other elements of the Earth system.
3. **Synoptic Climatology**: Examines weather patterns and their influence on regional climates, using observational and statistical techniques to link large-scale atmospheric phenomena with local climate variations.
4. **Paleoclimatology**: Investigates historical climates through proxy data such as ice cores, tree rings, and sediment records, offering insights into natural variability and long-term climate trends.
5. **Applied Climatology**: Focuses on the practical application of climate knowledge to sectors such as agriculture, urban planning, water resource management, and disaster mitigation.

These components highlight the interdisciplinary nature of climatology, bridging atmospheric science with fields like geology, hydrology, and ecology. Understanding atmospheric circulation requires complex models capable of predicting global patterns based on dynamic conditions. These complex models are frequently employed at the planetary scale because the behavior of atmospheric components is naturally continuous, indicating that processes in one region can influence conditions elsewhere. These models are collectively known as Global Climate Models (GCMs). All GCMs and weather forecasting models rely on seven fundamental equations to understand and predict atmospheric flow and behavior. These

include the Navier-Stokes equations of motion, the thermodynamic energy equation, the moisture conservation equation, the continuity equation, and the equation of state.

Over the years, several studies have focused on developing methods to visualize, analyze, and predict the dynamics, interactions, and patterns of climatic variables, leading to significant progress (Anandhi and Nanjundiah 2015, Raju et al. 2017, Ruan et al. 2018, Zamani and Berndtsson 2019, Shiru and Chung 2021, Deepthi and Sivakumar 2022, Jose and Dwarakish 2022). However, relatively few studies have concentrated on the critical task of selecting appropriate GCMs (Jose et al. 2022, Fu et al. 2023, Shetty et al. 2023, Wang et al. 2023). The proper selection of GCMs is therefore essential for accurate climate data analysis and projections. In conclusion, selecting suitable GCMs using approaches that integrate various temporal scales, Multi-Criteria Decision-Making (MCDM), and machine learning techniques is crucial for improving the understanding of climatic variables.

Analyzing historically observed climatic parameters is essential for establishing a baseline to understand the selection and projections based on GCMs. Over the years, numerous studies have examined rainfall and temperature trends using diverse methodologies. Malik et al. (2019) employed the Mann-Kendall (MK), Modified MK, and Kendall Rank Correlation to analyze spatial and temporal patterns of trends in the Himalayan region of Uttarakhand, India. Similarly, Salehi et al. (2020) explored rainfall trends in Iran using MK and Sequential MK techniques. Ashraf et al. (2021) applied MK, Spearman's Rho, and ITA to examine streamflow trends over the Indus basin.

In the context of temperature trends, Sonali and Kumar (2013) utilized a collection of trend detection techniques to analyze extreme temperature patterns across India and its seven homogeneous regions, using three distinct temporal datasets. Moharji et al. (2017) incorporated ITA and multi-duration trend analysis to study global temperature trends. These studies highlight the application of multiple methods to detect rainfall and temperature trends. However, the study of an ideal trend analysis method, particularly in combination with decadal analysis, remains unexplored, leaving a gap in the standardization and comparability of trend detection techniques.

1.2. Research Scopes

This thesis focuses on analyzing temperature and rainfall variability in the perspective of climate change, with specific importance on Eastern India. The research combines analysis of historical temperature and rainfall data, assessment of outputs from multiple GCMs, and machine learning techniques to provide a comprehensive understanding of past, present, and future temperature and rainfall trends.

The scope of the study includes:

- **Historical Analysis:** Investigating historical patterns to identify trends that inform the baseline for future projections.
- **GCM Evaluation:** Evaluating CMIP6 GCM's ability to understand temperature and rainfall trends under different Shared Socioeconomic Pathways (SSPs).
- **Machine Learning Integration:** Employing ensemble methods to address GCM uncertainties and improve projection reliability.

- **Scenario-Based Projections:** Analyzing changes across near-term, mid-term, and far-term timeframes under SSP126, SSP245, SSP370, and SSP585 scenarios.
- **Regional Focus:** Providing region-specific insights for Eastern India, with a focus on suggestions for effective climate adaptation strategies.

By integrating traditional and advanced modeling approaches, this research aims to overcome the limitations of individual GCMs and deliver smooth projections for regional climate planning.

1.3. Research Objectives

The primary objective of this work is to enhance the understanding of temperature and rainfall variability and future trends in context of climate change, with a specific focus on Kangsabati, Keliaghai, Silabati, and Dwarkeswer (KKSD) river basins. The study seeks to achieve the following specific objectives:

- To analyze historical trends over KKSD basins in West Bengal, identifying significant patterns that serve as a baseline for future projections.
- To evaluate multiple CMIP6 GCMs in demonstrating historical and future temperature and rainfall under different SSP scenarios.
- To address the uncertainties in GCM outputs by employing machine learning techniques and MCDM, including ensemble methods and analysis, to refine projections.
- To assess scenario-based changes in rainfall across near-term, mid-term, and far-term timeframes, highlighting implications for water resources and climate adaptation.
- To identify the most influential GCMs in predicting temperature and rainfall outcomes using feature analysis, providing guidance for future climate modeling efforts.
- To develop actionable insights for policymakers and stakeholders by translating model outputs into practical recommendations for water resources management and climate resilience.

1.4. Thesis Structure

The dissertation has been organized into ten chapters, each concentrating on a different component of the research to provide a comprehensive overview of climatic dynamics in West Bengal.

Chapter 1: Introduction

The opening chapter introduces the thesis by defining its background and motivation, research scope, objectives, and organization of the study. It highlights the critical importance of understanding rainfall and temperature variability.

Chapter 2: Study Area and Data Utilized

This chapter describes the geographical characteristics of study area and provides a detailed account of the datasets used. It includes observational data, GCM outputs, machine learning inputs, and spatial data, along with the preprocessing techniques employed for analysis.

Chapter 3: Long-Term Rainfall Trends Analysis
In this chapter, long-term rainfall trends are analyzed using statistical methods. The study identifies significant patterns in historical rainfall data, providing insights into the climatic behavior of the region over several decades.

Chapter 4: Decadal Trend Analysis of Temperature Data
This chapter concentrates on the decadal analysis of temperature trends, investigating minimum and maximum temperatures. It highlights seasonal and spatial variability, with implications for agriculture, water resources, and climate adaptation strategies.

Chapter 5: Ranking of CMIP6 Models Using MCDM
In this chapter, a Multi-Criteria Decision-Making (MCDM) mechanism along with individual performance parameters are applied to rank CMIP6 models based on their performance. The chapter discusses the methodology, criteria, and results, highlighting the importance of selecting reliable models for climate studies.

Chapter 6: Evaluation of Historical Data Accuracy in CMIP6 Models
This chapter evaluates the accuracy of CMIP6 models in replicating historical climatic conditions. The analysis compares GCM outputs against observational data, identifying biases and strengths in individual models.

Chapter 7: Multi-Temporal Assessment of CMIP6 Models for Climate Dynamics
A detailed assessment of CMIP6 models is presented in this chapter, focusing on their ability to simulate climate dynamics across multiple time periods and scenarios. The results provide a deeper understanding of model performance and variability.

Chapter 8: Machine Learning for Climate Model Evaluation
This chapter introduces machine learning techniques to enhance the evaluation of climate models. It demonstrates how ensemble methods and feature importance analyses can improve the reliability of projections and identify the most influential models.

Chapter 9: Projected Precipitation Changes Based on Selective GCMs
Focusing on future climate scenarios, this chapter examines projected precipitation changes using selective GCMs. It explores trends across different SSP scenarios and time periods, providing valuable insights for policymakers and stakeholders.

Chapter 10: Final Remarks
The concluding chapter summarizes the principal findings of the study, considers their implications and limitations, and outlines prospective areas for future research.

References

Anandhi, A. and Nanjundiah, R.S. (2015). Performance evaluation of AR4 Climate Models in simulating daily precipitation over the Indian region using skill scores. Theor. Appl. Climatol., 119(3–4), 551–566.

Ashraf, M.S., Ahmad, I., Khan, N.M., Zhang, F., Bilal, A. and Guo, J. (2021). Streamflow variations in monthly, seasonal, annual and extreme values using Mann-Kendall, Spearmen's rho and innovative trend analysis. Water Resour. Manag., 35(1), 243–261.

Deepthi, B. and Sivakumar, B. (2022). Performance assessment of general circulation models:

application of compromise programming method and global performance indicator technique. Stoch. Environ. Res. Risk Assess., 36(6), 1761–1778.

Fu, Y., Zhuang, H., Shen, X. and Li, W. (2023). Assessment and prediction of regional climate based on multimodel ensemble machine learning method. Clim. Dyn., 61(9–10), 4139–4158.

Jose, D.M. and Dwarakish, G.S. (2022). Ranking of downscaled CMIP5 and CMIP6 GCMs at a basin scale: case study of a tropical river basin on the South West coast of India. Arab. J. Geosci., 15(1), 120.

Jose, D.M., Vincent, A.M. and Dwarakish, G.S. (2022). Improving multiple model ensemble predictions of daily precipitation and temperature through machine learning techniques. Sci. Rep., 12(1), 4678.

Malik, A., Kumar, A., Guhathakurta, P. and Kisi, O. (2019). Spatial-temporal trend analysis of seasonal and annual rainfall (1966–2015) using innovative trend analysis method with significance test. Arab J. Geosci., 12(10), 328.

Mohorji, A.M., Şen, Z. and Almazroui, M. (2017). Trend Analyses Revision and Global Monthly Temperature Innovative Multi-Duration Analysis. Earth Syst. Environ., 1(1), 9.

Raju, K.S., Sonali, P. and Kumar, D.N. (2017). Ranking of CMIP5-based global climate models for India using compromise programming. Theor. Appl. Climatol., 128(3–4), 563–574.

Ruan, Y., Yao, Z., Wang, R. and Liu, Z. (2018). Ranking of CMIP5 GCM skills in simulating observed precipitation over the Lower Mekong Basin, using an improved score-based method. Water, 10(12), 1868.

Salehi, S., Dehghani, M., Mortazavi, S.M. and Singh, V.P. (2020). Trend analysis and change point detection of seasonal and annual precipitation in Iran. Int. J. Climatol., 40(1), 308–323.

Shetty, S., Umesh, P. and Shetty, A. (2023). The effectiveness of machine learning-based multi-model ensemble predictions of CMIP6 in Western Ghats of India. Int. J. Climatol., 43(11), 5029–5054.

Shiru, M.S. and Chung, E.S. (2021). Performance evaluation of CMIP6 global climate models for selecting models for climate projection over Nigeria. Theor. Appl. Climatol., 146(1–2), 599–615.

Singh, R., Sah, S., Das, B., Potekar, S., Chaudhary, A. and Pathak, H. (2021). Innovative trend analysis of spatio-temporal variations of rainfall in India during 1901–2019. Theor. Appl. Climatol., 145(1–2), 821–838.

Sonali, P. and Kumar, D.N. (2013). Review of trend detection methods and their application to detect temperature changes in India. J. Hydrol., 476, 212–227.

Wang, D., Liu, J., Luan et al. (2023). Projection of future precipitation change using CMIP6 multimodel ensemble based on fusion of multiple machine learning algorithms: A case in Hanjiang River Basin, China. Meteorol. Appl., 30(5), e2144.

Zamani, R. and Berndtsson, R. (2019). Evaluation of CMIP5 models for west and southwest Iran using TOPSIS-based method. Theor. Appl. Climatol., 137(1–2), 533–543.

Chapter 2

Study Area and Data Utilized

2.1. Study Area

The study area consists of four major basins in West Bengal: Kangsabati, Keliaghai, Silabati, and Dwarkeswer, collectively referred to as the KKSD Basins.

2.1.1. Kangsabati Basin

The Kangsabati River basin is situated within the lower Ganga basin and represents its final tributary in India. It is situated within the coordinates of 87°32' E to 85°57' E and 22°18' N to 23°28' N. The Kangsabati River begins in the Chhota Nagpur Plateau in the Purulia district and flows southeast, where it meets its primary tributary, the Kumari River, at Mukutmanipur in the Bankura district. The Kangsabati River stretches approximately 465 km in length, and its sub-basin has a catchment area of 5,385 km^2.

2.1.2. Keliaghai Basin

The Keliaghai River begins its journey at Dudhkundi in the Jhargram area of Paschim Medinipur district, flowing in a south-easterly direction through Purba Medinipur before joining the New Cossye, which is another branch of the Kangsabati, to create the Haldi River. Along its path, it receives water from several tributaries, including the Kapaleswari, Baghai, and Chandia. Spanning a length of 121 km, the river has a basin area of 1,432 km^2. It has a significant influence in causing floods in the Sabang region of Paschim Medinipur district.

2.1.3. Silabati Basin

The Silabati River, also referred to as Silai originates from the hilly regions of the Chhota Nagpur Plateau in the Purulia district. It flows southeast through Bankura and Paschim Medinipur districts before joining the Dwarkeswar River to create the Rupnarayan River. Key tributaries of the Silabati include the Joyponda, Ketia, Donai, Kubai, and Parang rivers. A small barrage has been built at Kadamdeuli in Bankura district as part of the Kangsabati Reservoir Project. The area for this basin spans 5,040 km^2.

2.1.4. Dwarkeswar Basin

The Dwarkeswar River, also referred to as Dhalkishore, is a significant river located in the western region of West Bengal. It begins its journey from the Tilboni hill in the Chhota Nagpur Plateau, situated in Purulia district, and flows into Bankura district near Chatna. The river primarily moves in a south-easterly direction and, upon reaching the Hooghly district, it shifts southward near the town of Arambag. One of its key tributaries, the Gandheswari, which originates in Bankura district, converges with Dwarkeswar close to Bankura town. The river

also collects water from several smaller tributaries, including Arkasha, Berai, and Shankari, before it ultimately merges with the Silabati River at Bandar, near Ghatal town in Paschim Medinipur district, forming the Rupnarayan River. The catchment area of this sub-basin spans 3,500 km^2. Particularly, the Dwarkeswar River, which stretches 200.5 km, exhibits a unique combination of characteristics, experiencing flash floods in its upper reaches, monsoonal flooding in the middle section, and tidal influences at its lower confluence.

This study examines these four key river basins- Kangsabati, Keliaghai, Silabati, and Dwarkeswar-collectively abbreviated as KKSD, as depicted in Fig. 2.1. The selected region spans an area of 15,358 km^2, which constitutes approximately 17.3% of the total geographical area of West Bengal.

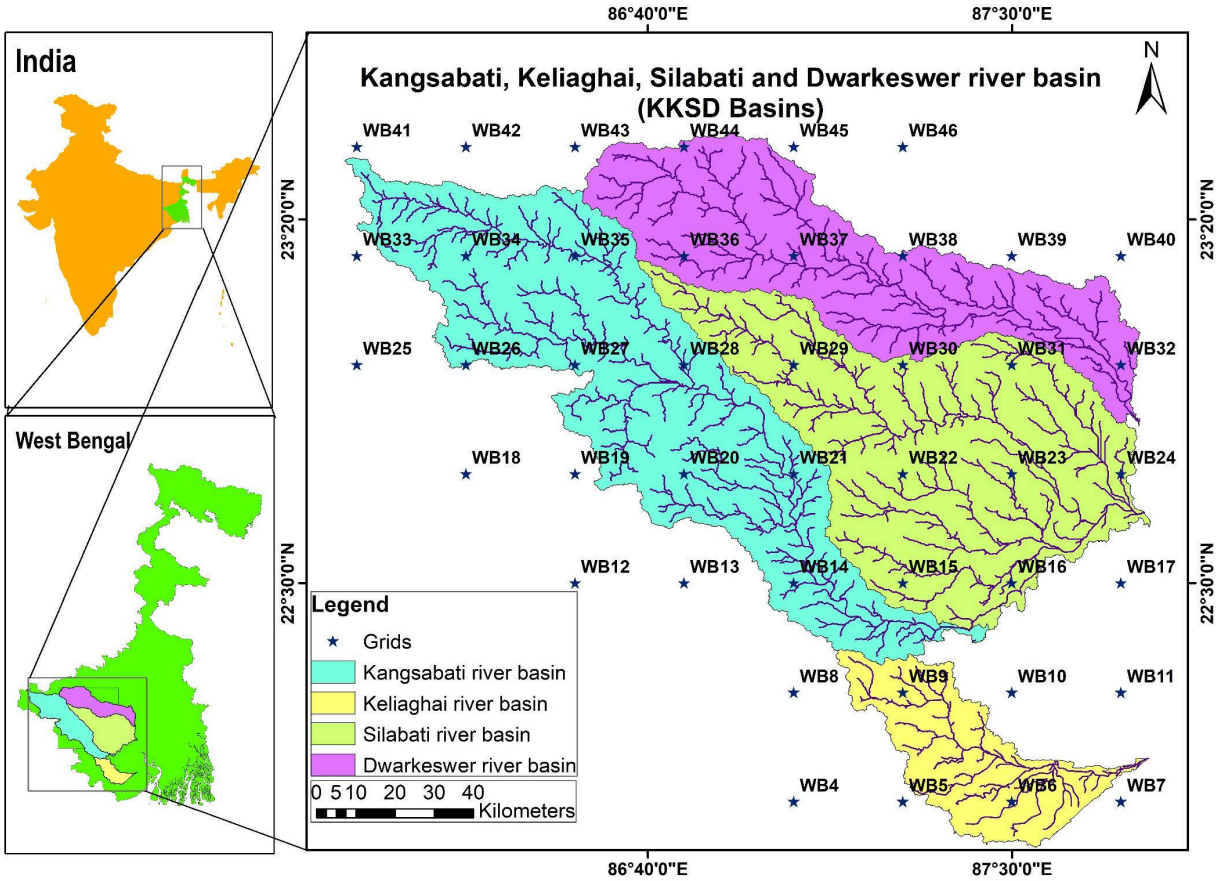

Fig. 2.1. A comprehensive overview of the study area.

2.2. Data Used

This research utilizes a combination of gridded meteorological data and outputs from GCMs to examine temperature and rainfall trends. The datasets, covering the period from 1901 to 2023, offer a strong basis for assessing both seasonal and annual patterns, along with the effects of climatic variability on regional ecosystems and water resources.

2.2.1. Gridded Temperature Data

Temperature data for daily maximum (T_{max}) and minimum (T_{min}) over a span of 70 years (1951-2020) have been acquired from the India Meteorological Department (IMD), Pune. The datasets were produced at a spatial resolution of 1° × 1° grids, as given by Srivastava et al.

(2009). Analyses were performed on a seasonal and annual basis, utilizing the following Indian climatic seasons: Summer (March-May), Monsoon (June-September), Autumn (October-November), and Winter (December-February) (WBPCB 2016). The dataset go through comprehensive quality control measures to ensure both spatial and temporal consistency and was validated against other high-resolution datasets (Pai et al. 2014).

2.2.2. Gridded Rainfall Data

Daily rainfall data covering a period of 123 years (from 1901 to 2023) was obtained from the IMD, featuring a high spatial resolution of $0.25^{\circ} \times 0.25^{\circ}$ grids. The dataset was created using the distance-weighted interpolation method proposed by Sheppard (1968) and was validated by comparing it with five independent datasets. It shows a correlation of over 95% with these datasets, highlighting their reliability (Pai et al. 2014). This detailed rainfall data has been extensively utilized in hydrological studies, helping in the analysis of historical rainfall patterns and assessing the impact of climate variability on water resources, agriculture, and ecosystems (Mishra et al. 2020, Patel et al. 2023, Patel et al. 2024).

2.2.3. Global Climate Models (GCMs)

The climate model data utilized in this study was provided by NASA Earth Exchange Global Daily Downscaled Projections (NEX-GDDP). These are statistically downscaled and bias-corrected datasets from the Coupled Model Intercomparison Project Phase 6 (CMIP6). The NEX-GDDP data features a spatial resolution of $0.25^{\circ} \times 0.25^{\circ}$ and includes both historical and future climate scenarios based on shared socioeconomic pathways (SSP1-2.6, SSP2-4.5, SSP3-7.0, SSP5-8.5). These datasets were chosen for their capability to reflect topographical influences and deliver detailed climatic information (Thrasher et al. 2022). A total of 24 Global Climate Models (GCMs) were utilized, as detailed in Table 2.1, to study historical and projected changes in precipitation and temperature.

2.2.4. Data Quality

All datasets were subjected to detailed quality evaluations, which included verifying geographical location accuracy, coding precision, consistency across space and time, and addressing any missing values.

2.2.5. Performance Metrics

To understand the climatic impacts and evaluate the efficiency of the models, a variety of derived metrics were used. These metrics were crucial for determining the suitability of the models in relation to regional adaptation and mitigation strategies (Maity 2022). A comprehensive overview of the metrics utilized are presented in Table 2.2.

Table 2.1. Details of the 24 CMIP6 GCMs.

Model No.	Model Name	Variant	Country	Resolution (km)
M1	ACCESS CM2	r1i1p1f1	Australia	250
M2	ACCESS ESM1-5	r1i1p1f1	Australia	250
M3	IITM-ESM*	r1i1p1f1	India	250
M4	BCC-CSM2-MR	r1i1p1f1	China	100
M5	CMCC-CM2	r1i1p1f1	Italy	100
M6	CMCC-ESM2	r1i1p1f1	Italy	100
M7	CNRM-CM6-1	r1i1p1f2	France	250
M8	CNRM-ESM2-1	r1i1p1f2	France	250
M9	canESM5*	r1i1p1f1	Canada	500
M10	EC-Earth3-Veg-LR	r1i1p1f1	Europe	100
M11	EC-Earth3	r1i1p1f1	Europe	100
M12	GFDL-ESM4	r1i1p1f1	USA	100
M13	GISS-E2-1-G	r1i1p1f2	USA	250
M14	INM-CM4-8	r1i1p1f1	Russia	100
M15	INM-CM5	r1i1p1f1	Russia	100
M16	IPSL-CM6A-LR	r1i1p1f1	France	250
M17	MIROC6	r1i1p1f1	Japan	250
M18	MIROC-ES2L	r1i1p1f2	Japan	500
M19	MPI-ESM1-2-HR	r1i1p1f1	Germany	100
M20	MPI-ESM1-2-LR	r1i1p1f1	Germany	250
M21	MRI-ESM2-0	r1i1p1f1	Japan	100
M22	NorESM2-LM	r1i1p1f1	Norway	250
M23	NorESM2-MM	r1i1p1f1	Norway	100
M24	TaiESM-1	r1i1p1f1	Taiwan	100

*Represents the excluded models in the temperature projection due to non-availability of scenarios; r: realization; i: initialization; p: physics; f: forcing

Table 2.2. Mathematical representations of performance metrics.

Name	Mathematical Expressions	Best Value
Correlation Coefficient (CC)	$\frac{\sum_{i=1}^{N}(o_i-\overline{o})(s_i-\overline{s})}{(N-1)\sigma_o\sigma_s}$	1
Skill Score (SS)	$\frac{1}{N}\sum_{i=1}^{nb}\min(f_s,f_o)$	1
Root Mean Square Error (RMSE)	$\sqrt{\frac{1}{N}\sum_{i=1}^{N}(o_i-s_i)^2}$	0
Coefficient of Determination	$\frac{\sum_{i=1}^{N}(o_i-\overline{o})(s_i-\overline{s})}{\sqrt{\sum_{i=1}^{N}(o_i-\overline{o})^2\sum_{i=1}^{N}(s_i-\overline{s})^2}}$	1
Kling Gupta Efficiency (KGE)	$1-\sqrt{(CC-1)^2+(\sigma_r-1)^2+(\gamma-1)^2}$	1
Percentage Bias (PBIAS)	$\left[\frac{\sum_{i=1}^{N}(o_i-s_i)}{\sum_{i=1}^{N}o_i}\right]\times 100$	0
Taylor Skill Score (TSS)	$\frac{4(1+r)}{\left(\sigma_r+\frac{1}{\sigma_r}\right)^2(1+r_o)}$	1
Modified Taylor Skill Score (MTSS)	$\frac{4(1+r)^4}{\left(\sigma_r+\frac{1}{\sigma_r}\right)(1+r_o)^4}$	1
Sum of Square Error (SSE)	$\sum_{i=1}^{N}(s_i-o_i)^2$	0
Index of Agreement (IoA)	$1-\frac{\sum_{i=1}^{N}(o_i-s_i)^2}{\sum_{i=1}^{N}\left(\lvert o_i-\overline{o}\rvert+\lvert s_i-\overline{o}\rvert\right)^2}$	1
Mean Absolute Error (MAE)	$\frac{1}{N}\sum_{i=1}^{N}\lvert s_i-o_i\rvert$	0

Nash–Sutcliffe Efficiency (NSE)	$1-\frac{\sum_{i=1}^{N}(o_i-s_i)^2}{\sum_{i=1}^{N}(o_i-\overline{o})^2}$	1
Standard Deviation (SD)	$\sqrt{\frac{\sum_{i=1}^{N}(o_i-\overline{o})^2}{N}}$	0
Kolmogorov–Smirnov Test (KST)	$\max_{o}\left\{\left\|F^s(o)-F^o(o)\right\|\right\}$	1
Normalized Root Mean Square Error (NRMSE)	$\frac{RMSE}{\overline{o}}$	0

Note: where o_i and s_i are the observed and simulated data, $\bar{o}$ and $\bar{s}$ are the averages of observed and simulated data for N number of observations, σ_o and σ_s are the SDs of o_i and s_i. F^s and F^o are the cumulative distribution functions of the model simulations and observations. r and σ_r are the Pearson CC and ratio of SD between simulated and observed data and r_o is referred to as the maximum attainable value of CC which is 1. f_s and f_o are the frequency of values in the given bin from the selected GCM and observed data; nb is the number of bins used to calculate the probability density function for a given region. γ is the ratio of mean between simulated and observed data.

2.3. Tools and Software

A variety of tools and software were utilized in this research to facilitate detailed data analysis, and visualization. The selection of each tool was conducted by its specific functionality and its alignment with the objectives of the study. The primary tools and software used are as follows:

a) ArcGIS

ArcGIS was employed for analyzing and visualizing spatial data from gridded datasets. With its powerful geoprocessing features, it allowed for the development of thematic maps and spatial interpolation, making it easy to compare different data resolutions, such as 1° × 1° and 0.5° × 0.5° grids. Furthermore, it supported the merging of geospatial layers to examine climatic variability across various regions.

b) RStudio

RStudio served as a primary environment for statistical analysis, trend detection, and data management. Key packages such as `ggplot2`, `modifiedmk`, and `trendchange` were used to perform regression analysis, compute trend lengths and slopes, and generate insightful plots.

c) Python

Python was employed for machine learning (ML) applications, hyperparameter optimization, and advanced data processing. Libraries such as `pandas`, `numpy`, and `scikit-learn` were used for data handling, while `matplotlib` and `seaborn` were used for visualizations.

Ensemble modeling and climate model evaluation were implemented using various ML models.

d) Microsoft Office

Microsoft Excel and Word were crucial for organizing data, performing basic computations, and drafting content. Excel was useful for preliminary data exploration and tabular representations, while Word facilitated the seamless documentation of findings.

e) Panoply

Panoply was used to visualize and analyze Network Common Data Form (NetCDF) climate model outputs. Its user-friendly interface allows the inspection of gridded data.

References

Maity, R. (2022). Basic Statistical Properties of Data. In: Statistical Methods in Hydrology and Hydroclimatology. Springer Transactions in Civil and Environmental Engineering. Springer, Singapore.

Mishra, V., Bhatia, U. and Tiwari, A.D. (2020). Bias-corrected climate projections for South Asia from Coupled Model Intercomparison Project-6. Sci. Data, 7(1), 338.

Pai, D.S., Rajeevan, M., Sreejith, O.P., Mukhopadhyay, B. and Satbha, N.S. (2014). Development of a new high spatial resolution (0.25° × 0.25°) long period (1901-2010) daily gridded rainfall data set over India and its comparison with existing data sets over the region. Mausam, 65(1), 1–18.

Patel, G., Das, S. and Das, R. (2024). Determine the best method for analyzing long-term (120 years) annual and seasonal rainfall trends in four East India river basins. J. Earth Syst. Sci., 133(2), 70.

Patel, G., Das, R. and Das, S. (2023). Is the extreme temperature trend changed in last two decades compared to last seven decades? Case Study from Eastern India. J. Earth Syst. Sci., 132(3), 140.

Shepard, D. (1968). A two-dimensional interpolation function for irregularly-spaced data. In Proceedings of 1968 23rd ACM national conference (ACM'68), 517–524.

Srivastava, A.K, Rajeevan, M. and Kshirsagar, S.R. (2009). Development of a high resolution daily gridded temperature data set (1969-2005) for the Indian region. Atmos. Sci. Lett., 10(4), 249–254.

Thrasher, B., Wang, W., Michaelis, A., Melton, F., Lee, T. and Nemani, R. (2022). NASA Global Daily Downscaled Projections, CMIP6. Sci. Data, 9(1), 262.

WBPCB (2016). State of Environment Report-West Bengal. West Bengal Pollution Control Board (WBPCB) W.B., India.

Chapter 3

Long-Term Rainfall Trend Analysis

"Patel, G., Das, S. and Das, R. (2024). Determine the best method for analysing long-term (120 years) annual and seasonal rainfall trends in four east India river basins. J. Earth Syst. Sci., 133(2), 70. https://doi.org/10.1007/s12040-024-02282-7"

3.1. Introduction

Climate change driven by human activities, along with greater variability in climate, has especially changed global rainfall patterns and trends (IPCC 2018). These changes in rainfall are quite diverse and often distinct at the regional level which requires proper approaches for their analysis. To understand these specific regional patterns, researchers typically utilize various statistical tests to identify trends in hydro-meteorological data. Some of the widely utilized methods include the Mann-Kendall test (MK) (Kendall 1938, Mann 1945), the modified Mann-Kendall test (MMK) (Hamed and Rao 1998, Yue and Wang 2004), Spearman's rank correlation (SRC) (Spearman 1904), Sen's slope estimator (SSE), and the innovative trend analysis (ITA) (Şen 2012). Each of these methods has its specific uses and limitations, which can affect their effectiveness based on the characteristics of the data, including factors like autocorrelation.

The MK test is widely utilizing approach for analyzing trends in meteorological research, especially suited for datasets that are non-normally distributed, independent, and lack autocorrelation (Dash and Maity 2019). However, many studies in this field tend to apply the MK test without first checking for autocorrelation or other distributional properties that might require a more robust analytical method. Previous studies by Sonali and Kumar (2013) and Malik et al. (2019) highlight the necessity of carefully choosing statistical techniques based on the characteristics of the data. Ignoring these aspects can result in misleading trend detection, particularly since autocorrelation can be imprecise or alter trends when using the MK and other methods.

Recently, many studies have been investigating various alternative techniques, such as SRC, SSE, and MMK, to analyze spatial and temporal patterns in hydro-meteorological data (Singh et al. 2021). Furthermore, the ITA, introduced by Şen (2012), offers a graphical and distribution-free method for trend detection, which can discover significant patterns that traditional approaches might fail to detect. Kisi (2015) showed that ITA is effective in identifying trends in data influenced by autocorrelation, a challenge for MK and similar tests. The global use of ITA, with studies conducted in North America, Africa, Europe, and Asia, has demonstrated its adaptability in analyzing trends in rainfall, discharge, air temperature, and other variables (Caloiero et al. 2020, Patel et al. 2023).

An investigation of the existing research shows that many hydro-meteorological trend analyses primarily rely on single methods, with only a few studies making an effort to compare various trend analysis techniques comprehensively (Patel et al. 2023).

This chapter explores long-term annual and seasonal rainfall patterns and variability across four major river basins in Eastern India. By analyzing regional-scale data, the study seeks to capture rainfall patterns and variability that might be unnoticed at a global scale. Using an extensive hydro-meteorological dataset spanning from 1901 to 2020, the study analyzes trends in annual, monsoon, autumn, summer, and winter rainfall. The primary objective of this investigation is to evaluate is to evaluate the MK, MMK, SRC, SSE, and ITA to provide insights into long-term rainfall trends in Eastern India. Significantly, the methodological approach demonstrates the sensitivity of the ITA method in detecting subtle positive trends across all seasons, setting it apart from other conventional methods. This methodological refinement contributes to a more accurate and sensitive trend detection framework, offering valuable insights with significant implications for future research and practical applications in regional climate assessments.

3.2. Methodological Approaches for Long-Term Rainfall Trend Analysis

Identifying and measuring trends in rainfall data is crucial to understanding long-term hydrological and climatic patterns, particularly in regions sensitive to climate variability. This study incorporates multiple non-parametric trend detection techniques each with its unique advantages and limitations to capture potential shifts and assess the consistency of observed trends. These methods include the MK, MMK, SRC, SSE, and ITA. The effectiveness of each method is enhanced by conducting preliminary tests for stationarity and homogeneity, which are crucial for ensuring accurate trend detection (Maity 2022).

3.2.1. Stationarity and Homogeneity Testing

To ensure the effectiveness of trend analysis techniques, it is essential to first evaluate the stationarity and homogeneity of the time series data. For testing stationarity, two conventional methods were utilized: the Augmented Dickey-Fuller (ADF) Test (Dickey and Fuller 1979) and the Kwiatkowski–Phillips–Schmidt–Shin (KPSS) Test (Kwiatkowski et al. 1992). The ADF test looks for unit roots, which suggest non-stationarity, by analyzing level stationarity. On the other hand, the KPSS test examines both trend and level stationarity, offering a deeper understanding of the stability of data over time.

For the homogeneity testing, the Standard Normal Homogeneity Test (SNHT) (Alexandersson 1986) and the Pettitt Test (Pettitt 1979) were applied at a 5% significance level. These tests are effective in detecting any structural changes or shifts in the data, which helps to maintain the consistency of the data across the study period.

3.2.2. Mann-Kendall Test (MK)

The MK is a commonly utilized nonparametric method for detecting trends in hydrometeorological data, making it suitable for analyzing rainfall patterns (Patel et al. 2023). The MK does not require the normally distributed data and is particularly suited for data without strong autocorrelation. The test statistic, S (Eq. 3.1), is calculated as follows:

$$S = \sum_{p=1}^{n-1} \sum_{q=p+1}^{n} \operatorname{sign}(x_q - x_p) \tag{3.1}$$

where n is the number of observations, x_p and x_q are data values at time points p and q, respectively. The sign function assigns values of -1, 0, or +1 based on whether $(x_p - x_q)$ is negative, zero, or positive.

For larger datasets ($n \geq 10$), S approximates a normal distribution with a zero mean, and its variance $Var(S)$ is expressed as in Eq. (3.2):

$$Var(S) = \frac{(n^2 - n)(2n + 5) - \sum_{u=1}^{U} t_u(t_u - 1)(2t_u + 5)}{18} \tag{3.2}$$

where U denotes the number of unique groups in the data, and t_u represents the frequency of each group. A normalized test statistic, Z_{MK}, is then computed to determine the direction and significance of the trend given in Eq. (3.3).

$$Z_{MK} = \begin{bmatrix} \frac{S-1}{\sqrt{Var(S)}} \text{ for } S > 0 \\ 0 \text{ for } S = 0 \\ \frac{S+1}{\sqrt{Var(S)}} \text{ for } S < 0 \end{bmatrix} \tag{3.3}$$

3.2.3. Modified Mann-Kendall Test (MMK)

The MMK was developed to address the potential bias introduced by autocorrelation in the time series. This study applies the versions proposed by Hamed and Rao (1998) and Yue and Wang (2004), denoted as MMK1998 and MMK2004, respectively. While MMK1998 focuses on significant lags, MMK2004 considers all autocorrelation lags, providing a robust approach to adjust for serial correlation effects.

The adjusted variance, $Var^*(S)$, is computed using correction factors as given in Eqs. (3.4-3.6):

$$Var^*(S) = C_{fac} \times Var(S) \tag{3.4}$$

$$C_{fac_1} = 1 + \frac{2}{(n^2 - n)(n-2)} \sum_{p=1}^{n-1} (n-p)(n-p-1)(n-p-2)\rho_p \tag{3.5}$$

$$C_{fac_2} = 1 + 2 \sum_{p=1}^{n-1} \left(1 - \frac{p}{n}\right)\rho_p \tag{3.6}$$

where C_{fac1} and C_{fac2} are correction factors for MMK1998 and MMK2004, respectively, and ρ_p is the normalized autocorrelation coefficient.

3.2.4. Spearman Rank Correlation (SRC) Analysis

SRC provides a nonparametric approach to detect trends by examining the correlation between ranked data. This method is particularly useful for identifying monotonic trends within hydro-

climatic time series (Gautheir 2001). The coefficient ρ (Eq. 3.7) and the standardized test statistic Z_{SRC} (Eq. 3.8) is calculated as follows:

$$\rho = 1 - \frac{6\sum_{rank=1}^{n} d_{rank}^2}{n^3 - n} \tag{3.7}$$

$$Z_{SRC} = \rho\sqrt{(n-1)} \tag{3.8}$$

where d_{rank} is the rank difference, and n represents the number of observations. A standardized test statistic, Z_{SRC}, is derived to assess the direction and magnitude of the trend.

3.2.5. Şen Slope Estimator (SSE)

Developed by Şen (1968), the SSE calculates the magnitude of the trend through pairwise comparisons in the time series. The slope S_s is given by Eq. (3.9):

$$S_i = \frac{x_p - x_q}{p - q},\ i = 1, 2, 3, \ldots N \text{ for } p > q \tag{3.9}$$

where x_p and x_q are values at times p and q, respectively.

3.2.6. Innovative Trend Analysis (ITA)

The ITA (Şen 2012) provides a novel approach by graphically analyzing trends without assumptions of data distribution or autocorrelation. ITA divides the time series into two halves, plots them on Cartesian coordinates, and examines the alignment relative to a 1:1 line. Pairs above the 1:1 line indicate a positive trend, while those below indicate a negative trend.

The trend slope S is calculated as Eq. (3.10):

$$S = \frac{2(M_{2h} - M_{1h})}{n} \tag{3.10}$$

where M_{1h} and M_{2h} are the means of the first and second halves, and n represents the number of observations. The slope of standard deviation (Eq. 3.11) and confidence intervals (Eq. 3.12) around this slope are defined as:

$$\sigma_{Std} = \frac{2\sqrt{2}}{n\sqrt{n}}\sigma\sqrt{1 - \rho_{\bar{y}_1 \bar{y}_2}} \tag{3.11}$$

$$C_{(1-\alpha)} = 0 \pm S_{cri}\sigma_{std} \tag{3.12}$$

where S_{cri} is the critical value for the standard normal distribution. This study utilizes an α as 5% significance level to evaluate trends across annual and seasonal rainfall data for a comprehensive understanding of rainfall variability.

3.3. Results and Discussion

3.3.1. Stationarity and Homogeneity Tests

The ADF and KPSS tests are conducted to assess the stationarity of the rainfall time series. For the ADF test, the null hypothesis H_o assumes that the series has a unit root, indicating it is non-stationary. On the other hand, the alternative hypothesis H_a suggests that the series has no unit root and is stationary. In the KPSS test, H_o assumes that the series is stationary, while H_a assumes non-stationarity. For the daily rainfall data across all grids, both tests indicate significant stationarity at the 5% significance level, suggesting that the series lacks unit roots and is stationary according to both methods.

To analyze homogeneity, the Pettit test and SNHT are applied. In these tests, the null hypothesis H_o suggests that the data are homogeneous, while the alternative hypothesis H_a indicates a change point in the data, suggesting non-homogeneity. Both tests, at a 5% significance level, reject the null hypothesis, concluding that the daily rainfall time series is not homogeneous. This non-homogeneity indicates a discontinuity or shift in the trend within the time series, pointing to a structural change in rainfall patterns over time.

3.3.2. Mean Annual and Seasonal Rainfall

From 1901 to 2020, the average annual rainfall across the four selected river basins was observed to be approximately 1430 mm. This study categorizes the distribution of mean annual rainfall across seasons as follows: about 12% falls during the three-month summer season, with average rainfall of 180 mm; approximately 76% occurs in the monsoon season, spanning four months with an average rainfall of 1090 mm; roughly 8% falls during the two-month autumn season, averaging 120 mm; and the remaining 4% is distributed over the three-month winter season, with an average of 40 mm.

Table 3.1 provides detailed statistics on annual and seasonal rainfall for 25 specific grid points and Fig. 3.1 shows spatial gridded locations.

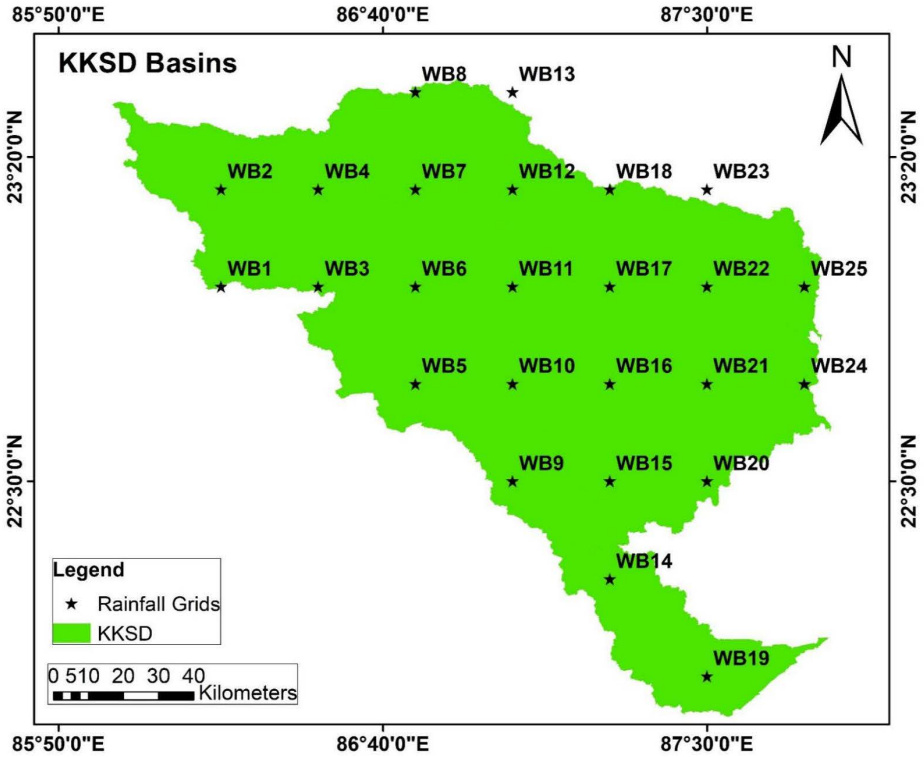

Fig. 3.1. Description of grids for rainfall analysis.

Table 3.1. Annual and seasonal rainfall mean (mm) and standard deviation (σ, mm) for the KKSD basins during 1901-2020.

Grids	Latitude	Longitude	Annual		Summer (MAM)		Monsoon (JJAS)		Autumn (ON)		Winter (DJF)	
			Mean	σ	Mean	σ	Mean	σ	Mean	σ	Mean	σ
WB1	23.00	86.25	1333.3	263.7	40.6	19.1	267.8	59.7	48.6	38.1	14.2	13.3
WB2	23.25	86.25	1338.6	236.5	40.0	18.5	267.7	52.5	51.7	39.8	14.7	13.0
WB3	23.00	86.50	1343.5	281.5	48.0	21.5	262.6	59.6	52.7	42.8	14.4	15.5
WB4	23.25	86.50	1343.0	279.3	45.0	21.1	266.1	60.6	50.5	38.7	14.1	15.2
WB5	22.75	86.75	1419.3	273.7	58.0	25.4	273.0	58.5	54.9	43.7	14.3	13.5
WB6	23.00	86.75	1437.2	394.1	54.4	26.8	280.2	85.8	54.9	43.3	14.3	15.7
WB7	23.25	86.75	1433.0	359.6	51.7	27.2	279.8	74.1	55.2	41.8	15.8	19.2
WB8	23.50	86.75	1321.9	249.4	43.6	20.6	262.2	53.9	51.5	40.8	12.9	12.7
WB9	22.50	87.00	1498.4	283.7	66.3	31.3	283.3	60.6	60.9	46.1	14.6	13.2
WB10	22.75	87.00	1438.1	255.4	61.5	26.4	274.4	54.6	56.8	41.2	13.9	12.3
WB11	23.00	87.00	1374.0	261.8	54.8	24.2	264.3	55.0	55.2	38.1	13.8	12.8
WB12	23.25	87.00	1318.9	243.7	51.3	23.8	254.6	50.6	52.9	38.1	13.4	13.1
WB13	23.50	87.00	1274.1	280.0	48.8	24.6	246.4	58.4	51.9	42.9	12.6	12.7
WB14	22.25	87.25	1574.2	285.4	70.2	31.2	291.4	60.3	76.0	53.1	15.2	12.9
WB15	22.50	87.25	1552.0	290.6	72.3	32.3	289.5	62.9	66.1	47.9	14.8	12.8
WB16	22.75	87.25	1449.5	275.6	67.8	31.0	270.8	56.8	61.0	44.2	13.5	12.3
WB17	23.00	87.25	1361.5	261.4	58.1	29.2	258.6	56.7	56.6	42.5	13.0	12.7
WB18	23.25	87.25	1321.9	245.9	55.0	23.7	251.9	53.6	54.7	42.2	13.1	12.7
WB19	22.00	87.50	1683.1	307.5	69.0	35.4	308.2	61.5	97.7	69.3	15.8	13.9
WB20	22.50	87.50	1574.4	321.7	70.6	33.8	294.3	69.1	69.6	48.1	15.2	13.6
WB21	22.75	87.50	1498.8	331.4	70.9	33.4	278.7	68.6	65.0	47.4	13.6	12.8
WB22	23.00	87.50	1415.5	276.6	65.4	30.5	263.8	58.0	61.7	44.8	13.4	12.3
WB23	23.25	87.50	1449.3	301.3	65.4	30.0	272.4	64.3	59.4	46.0	14.8	15.0
WB24	22.75	87.75	1531.4	327.4	70.7	33.4	283.2	67.6	71.0	50.1	14.7	13.0
WB25	23.00	87.75	1455.8	296.7	70.4	30.3	268.0	63.1	64.4	45.6	14.5	13.6

The mean annual rainfall ranges from 1274 mm at grid point WB13 to 1683 mm at grid point WB19. The standard deviation ranges from 236 mm (WB2) to 394 mm (WB6), indicating variability in rainfall across different locations within the basins.

The spatial distribution map in Fig. 3.2 illustrates a general trend of decreasing rainfall from southeast to northwest across the basins, indicating potential influences of topographical and climatic factors on the rainfall distribution across these regions.

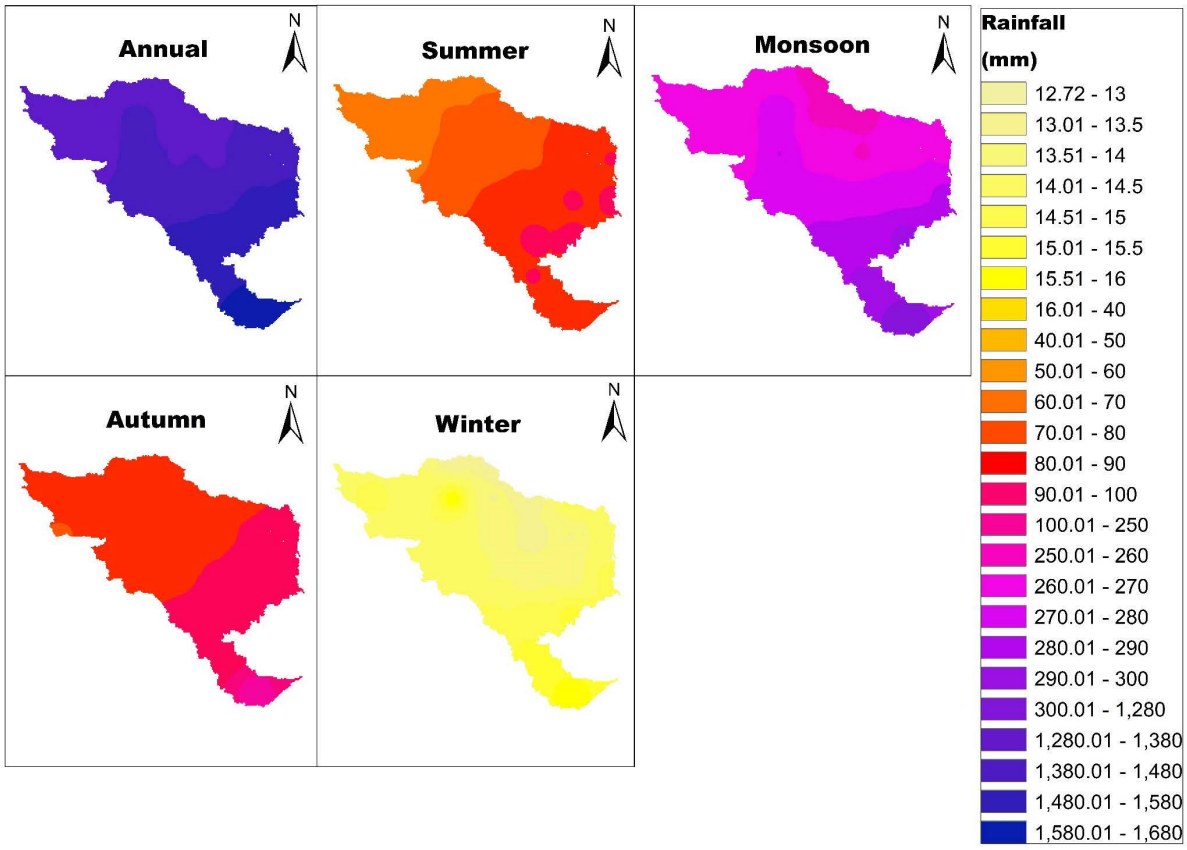

Fig. 3.2. Spatial distribution of average rainfall over KKSD basins annually and in four seasons during 1901-2020.

3.3.3. Trend Analysis

A trend analysis was carried out employing six methods to assess the significance and direction of rainfall trends across 25 grid points from 1901 to 2020. The MK and MMK were evaluated, with Z statistics (Z_{c1998} and Z_{c2004}) calculated at a 5% significance level. The results are summarized in Table 3.2, providing insights into significant trends (positive or negative) that were detected in the time series.

The ITA was further applied, with the results for annual and seasonal rainfall trends presented in Table 3.3. To broaden the analysis, three additional methods - SSE, SRC, and ITA were included. The combined outcomes of these methods are compiled in a similar table, offering a more comprehensive view of rainfall trends.

Figure 3.3 illustrates the spatial distribution of trends in rainfall across the KKSD basins, visualizing both the magnitude and direction of trends over time, which highlights areas with noticeable positive or negative trends across different seasons and annually.

Table 3.2. Mann–Kendall statistic Z and modified Mann–Kendall statistics Z_{c1998} and Z_{c2004} for annual and seasonal rainfall trends in the KKSD basins from 1901 to 2020.

Grids	Annual			Summer			Monsoon			Autumn			Winter		
	Z	Z_{c1998}	Z_{c2004}	Z	Z_{c1998}	Z_{c2004}	Z	Z_{c1998}	Z_{c2004}	Z	Z_{c1998}	Z_{c2004}	Z	Z_{c1998}	Z_{c2004}
WB1	0	0	0	0.57	0.70	1.20	0.13	0.15	0.35	-0.10	-0.10	-0.29	-1.18	-1.05	**-2.00**
WB2	0.14	0.12	0.30	1.60	1.60	**2.53**	0.03	0.03	0.07	0.26	0.26	0.87	-1.21	-1.21	**-2.02**
WB3	1.93	1.79	**3.16**	1.87	1.87	**3.05**	1.68	1.68	**3.08**	0.71	0.84	**2.42**	-0.24	-0.21	-0.47
WB4	**2.69**	**2.05**	**3.36**	**2.78**	**2.78**	**3.04**	**2.06**	**2.30**	**3.16**	1.24	1.24	**5.50**	0.01	0.01	0.03
WB5	**2.29**	1.88	**3.98**	**2.46**	**2.46**	**3.83**	**2.24**	**2.30**	**5.00**	0.81	1.38	**2.94**	-0.69	-0.93	-0.94
WB6	**2.12**	**1.99**	**3.48**	**2.19**	**2.19**	**5.76**	1.95	1.73	**2.90**	1.09	1.09	**3.18**	-0.14	-0.16	-0.31
WB7	1.88	1.63	**2.65**	**2.50**	1.95	**2.90**	1.4	1.39	**2.23**	0.95	0.95	**3.51**	-0.10	-0.10	-0.22
WB8	**2.60**	**2.96**	**4.13**	**2.25**	1.90	**3.11**	**2.08**	**2.08**	**4.00**	0.97	0.94	**3.74**	-0.11	-0.12	-0.21
WB9	**3.35**	**3.35**	**10.36**	**2.73**	1.95	**3.53**	**2.36**	**2.36**	**8.57**	1.08	1.32	**3.76**	-0.77	-1.52	-1.76
WB10	**2.93**	**2.73**	**6.67**	**3.02**	**3.36**	**4.24**	**2.54**	**3.03**	**7.85**	1.09	1.09	**3.92**	-0.28	-0.32	-0.52
WB11	1.65	1.65	**3.75**	1.47	1.47	**2.22**	1.62	1.62	**4.62**	0.61	0.61	1.95	-0.43	-0.39	-0.88
WB12	1.48	1.31	**2.50**	1.01	0.76	1.20	1.67	**1.99**	**4.12**	0.26	0.26	1.01	-0.34	-0.34	-0.59
WB13	1.09	1.09	1.89	1.37	1.06	1.82	1.03	1.09	**2.37**	0.32	0.41	1.38	-0.53	-0.53	-0.87
WB14	0.97	0.97	**2.69**	0.28	0.28	0.46	1.2	1.46	**3.64**	-0.70	-0.70	-1.90	-0.90	-0.90	**-2.32**
WB15	1.30	1.66	**3.35**	0.17	0.15	0.32	1.17	1.89	**4.15**	0.37	0.5	1.15	-0.49	-0.49	-1.46
WB16	1.41	1.24	**2.83**	0.84	0.8	1.47	1.44	**2.34**	**3.77**	0.51	0.69	1.62	-0.23	-0.24	-0.50
WB17	-0.69	-0.47	-0.80	-0.21	-0.16	-0.19	-0.31	-0.33	-0.54	0.76	1.04	**3.01**	-0.10	-0.11	-0.17
WB18	0.17	0.21	0.41	-0.05	-0.04	-0.05	0.53	0.53	1.55	0.65	0.65	**2.40**	-0.17	-0.17	-0.29
WB19	**2.25**	**2.25**	**7.55**	-0.32	-0.32	-0.51	1.64	1.64	**4.60**	1.82	**2.31**	**3.86**	-1.24	-1.73	**-4.90**
WB20	-0.20	-0.20	-0.65	-1.74	**-2.13**	**-6.32**	0.10	0.13	0.37	0.5	0.48	1.25	-0.84	-0.90	**-2.24**
WB21	-0.34	-0.34	-1.12	-1.32	-1.23	**-4.99**	-0.08	-0.07	-0.24	0.33	0.32	0.94	-0.70	-0.74	-1.67
WB22	-0.39	-0.52	-0.81	-0.58	-0.54	-1.05	-0.12	-0.13	-0.33	0.38	0.46	1.22	-0.63	-0.67	-1.63
WB23	-1.74	-1.74	**-5.40**	**-2.42**	**-2.30**	**-3.12**	-1.09	-1.09	**-3.11**	0.07	0.08	0.32	-0.79	-0.83	-1.58
WB24	-0.83	-1.13	**-2.20**	-0.91	-0.99	**-2.57**	-0.73	-0.95	-1.48	0.60	0.60	1.56	-1.07	-1.15	**-3.90**
WB25	-0.81	-0.81	-1.63	-1.33	-1.33	**-2.85**	-0.98	-1.04	-1.65	0.67	0.69	**1.96**	-0.64	-0.67	**-1.98**

Note: The bold tabulations are a significant positive or negative trend in average rainfall.

Table 3.3. Şen slope estimator (SSE), Spearman Z statistic value (Z_{SRC}), and slope of innovative trend analysis (SITA) for annual and seasonal rainfall over the KKSD basins from 1901 to 2020.

Grids	Annual			Summer			Monsoon			Autumn			Winter		
	SSE	Z_{SRC}	SITA	SSE	Z_{SRC}	SITA	SSE	Z_{SRC}	SITA	SSE	Z_{SRC}	SITA	SSE	Z_{SRC}	SITA
WB1	0.003	0.00	-0.55*	0.030	0.60	0.04*	0.017	0.11	-0.09*	-0.010	-0.03	-0.07*	-0.028	-1.22	-0.06*
WB2	0.102	0.29	-0.32*	0.074	1.63	0.09*	0.004	0.07	-0.10*	0.028	0.17	-0.02	-0.031	-1.33	-0.05*
WB3	1.408	2.01*	2.16*	0.103	1.98*	0.13*	0.284	1.81	0.41*	0.063	0.76	0.05*	-0.005	-0.29	0.01
WB4	1.891	2.76*	2.28*	0.160	3.07*	0.17*	0.303	2.13*	0.37*	0.111	1.15	0.10*	0.000	-0.03	0.02*
WB5	1.762	2.53*	2.45*	0.164	2.52*	0.18*	0.340	2.43*	0.47*	0.073	0.83	0.07*	-0.017	-0.65	-0.03*
WB6	1.847	2.21*	0.12	0.138	2.33*	0.08*	0.382	1.88	-0.04	0.101	1.17	0.01*	-0.002	-0.17	0.01
WB7	1.614	1.86	2.52*	0.177	2.66*	0.17*	0.247	1.41	0.43*	0.086	0.89	0.09*	-0.002	-0.14	0.03
WB8	1.778	2.73*	1.99*	0.137	2.28*	0.15*	0.295	2.13*	0.37*	0.077	0.92	0.05*	-0.002	-0.14	-0.02*
WB9	2.473	3.43*	2.74*	0.204	2.96*	0.29*	0.380	2.39*	0.45*	0.114	1.01	0.07*	-0.021	-0.75	-0.03*
WB10	2.041	3.11*	2.27*	0.202	3.07*	0.23*	0.357	2.66*	0.36*	0.097	1.11	0.09*	-0.007	-0.27	-0.02*
WB11	1.129	1.73	0.72*	0.089	1.48	0.05*	0.237	1.67	0.15*	0.057	0.62	0.02*	-0.006	-0.49	-0.02*
WB12	0.994	1.58	1.09*	0.070	1.04	0.07*	0.218	1.71	0.22*	0.024	0.24	0.05*	-0.006	-0.32	-0.02*
WB13	0.810	1.13	1.23*	0.084	1.31	0.09*	0.155	1.01	0.24*	0.029	0.34	0.05*	-0.010	-0.47	-0.03*
WB14	0.745	0.92	0.87*	0.028	0.27	0.05*	0.174	1.20	0.29*	-0.083	-0.59	-0.19*	-0.026	-0.94	-0.02*
WB15	0.962	1.29	0.97*	0.018	0.21	0.02	0.200	1.12	0.24*	0.047	0.45	-0.02	-0.013	-0.45	-0.01*
WB16	1.073	1.58	1.62*	0.068	0.85	0.09*	0.225	1.54	0.33*	0.054	0.53	0.04*	-0.007	-0.21	-0.02*
WB17	-0.568	-0.66	0.17	-0.013	-0.39	-0.01	-0.050	-0.32	0.05*	0.075	0.83	0.04*	-0.001	-0.24	-0.02*
WB18	0.119	0.10	0.38*	-0.002	-0.09	-0.01	0.080	0.45	0.12*	0.061	0.66	0.01	-0.003	-0.22	-0.03*
WB19	1.790	2.33*	1.14*	-0.033	-0.33	-0.04*	0.260	1.68	0.25*	0.290	1.80	0.17*	-0.034	-1.25	-0.02*
WB20	-0.170	-0.30	-0.68*	-0.150	-1.75	-0.18*	0.013	0.00	-0.01	0.050	0.52	-0.03*	-0.020	-0.83	-0.01*
WB21	-0.286	-0.41	-0.17	-0.103	-1.31	-0.14*	-0.013	-0.12	0.06*	0.041	0.34	0.04*	-0.018	-0.71	-0.03*
WB22	-0.308	-0.28	0.28*	-0.046	-0.59	-0.01	-0.021	-0.12	0.09*	0.040	0.39	0.00	-0.013	-0.65	-0.01*
WB23	-1.396	-1.68	-0.77*	-0.181	-2.40*	-0.16*	-0.199	-1.10	-0.02	0.010	0.17	-0.05	-0.017	-0.75	-0.03*
WB24	-0.745	-0.85	-1.01*	-0.065	-0.91	-0.10*	-0.128	-0.81	-0.18*	0.079	0.63	0.02*	-0.029	-1.12	-0.02*
WB25	-0.685	-0.79	-0.40*	-0.098	-1.32	-0.08*	-0.165	-1.03	-0.05*	0.077	0.64	0.04*	-0.016	-0.60	-0.02*

** significant trend at 5% level*

Figure 3.4 provides a summary of the percentage of grid points exhibiting statistically significant positive or negative trends across annual and seasonal rainfall datasets, as detected by each of the six methods.

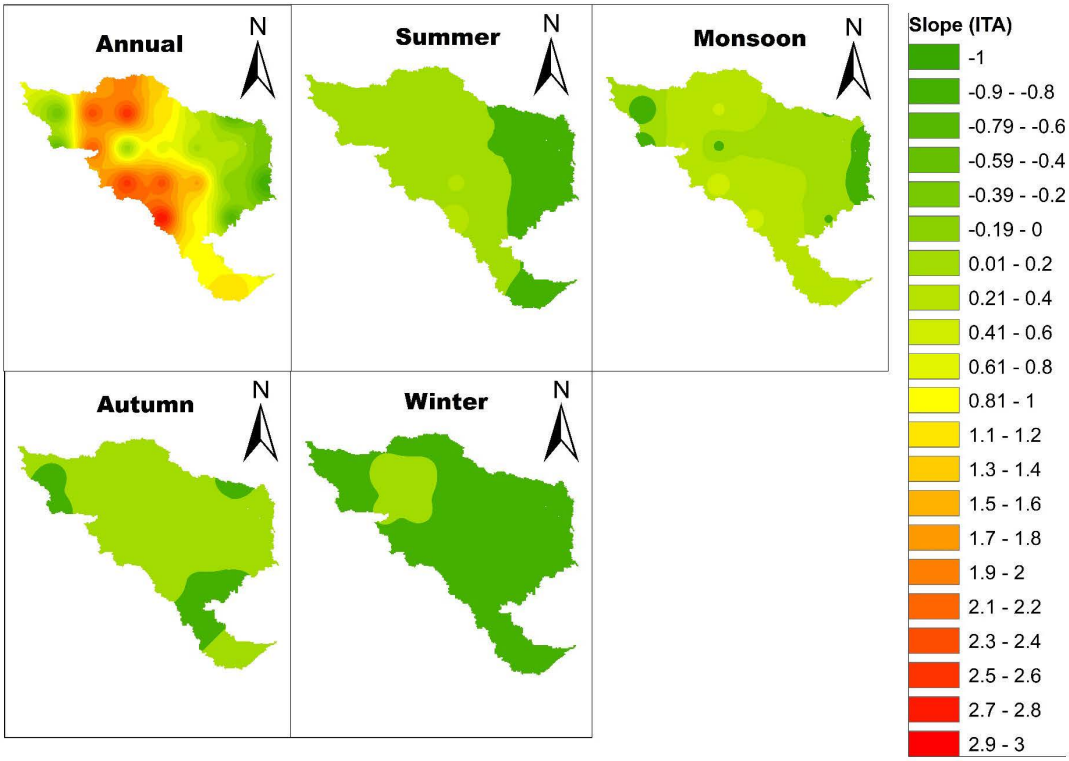

Fig. 3.3. Spatial distribution of ITA slope for annual and seasonal trends.

3.3.4. Annual Trend

Tables 3.2 and 3.3 present an analysis of annual rainfall patterns across 25 IMD grid points, utilizing statistical techniques like MK, MMK, SRC, SSE, and ITA. Among these, 18 grid points exhibit a positive trend, while seven (WB17, WB20, WB21, WB22, WB23, WB24, WB25) display a negative trend according to the MK, MMK, SRC, and SSE analyses. The MK, MMK1998, and MMK2004 methods identify significant increasing trends in 28%, 24%, and 60% of the grid points, respectively. Furthermore, Table 3.3 from the ITA assessment indicates that six grid points have significant negative trends, 17 show significant positive trends, and two have no detectable trends, all assessed at a 5% significance level.

3.3.5. Summer Trend

The analysis of summer rainfall trends from 1901 to 2020 indicates that 16 out of 25 grid points (WB1 to WB16) demonstrate notable positive trends, while the other points (WB17 to WB25) reflect negative trends according to MK, MMK, SRC, and SSE methods. In Table 3.3, the ITA slope shows that 84% of the grid points have statistically significant positive trends. Figure 3.4 illustrates that ITA and MMK2004 produce significant findings at 84% and 60%, respectively. However, it is important to note that 36% of the grid reveals a statistically significant negative trend when using ITA, highlighting its ability to detect trends that other methods, like MMK, might miss, particularly several significant negative trends.

3.3.6. Monsoon Trend

During the monsoon season, an upward trend in rainfall has been observed at 19 grid points, as reported by MK, MMK, SSE, and SRC. Particularly, MK, MMK1998, and MMK2004 show significant trends in 20%, 28%, and 64% of instances, respectively. The ITA findings for monsoon rainfall (Table 3.3 and Fig. 3.4) indicate both notable increases and decreases, affecting 84% of the grid points. While 24% of the grids show a non-significant decline based on Z statistics, ITA highlights a statistically significant 28% negative trend at the 5% level, demonstrating its ability to detect subtle variations.

3.3.7. Autumn Trend

Analysis of autumn rainfall trends across 25 grid points (Table 3.2) indicates that 92% of these points show an increasing trend according to the MK, MMK, SSE, and SRC methods. The results for autumn trends are further elaborated in Table 3.3 and Fig. 3.4, revealing that 76% of the values are positive and 84% are statistically significant. The Z statistics indicate that only two grid points exhibit a downward trend, but this is not statistically significant at the 5% level. On the other hand, the ITA method identifies a 24% significant downward trend, which reinforces its ability to detect subtle changes in trend direction.

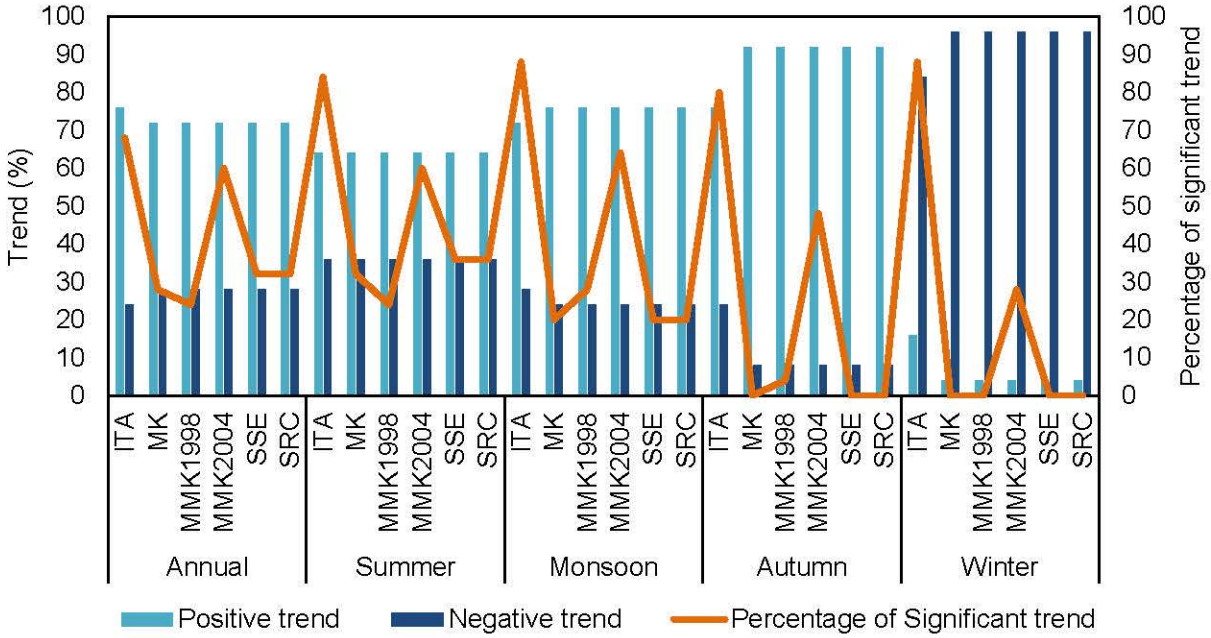

Fig. 3.4. Percentages of 25 grid points showing positive and negative annual and seasonal trends at a 5% significance level and probability of significance using MK, MMK1998, MMK2004, SSE, SRC, and ITA methods.

3.3.8. Winter Trend

Winter rainfall trends from 1901 to 2020 show a downward trajectory across 24 grid points, as analyzed using MK, MMK, SSE, and SRC methods. Particularly, 24% of these trends are significant according to MMK2004. As shown in Table 3.3, MK, MMK1998, and MMK2004 reveal a negative trend in 96% of the grid points, while ITA results indicate an 84% decrease

in trends. The Z statistics identify just one grid point with a slight upward trend, which is not statistically significant. Nevertheless, ITA does find a 16% significant positive trend at the 5% level. Figure 3.3 spatially represents the ITA slope, showing consistent seasonal patterns, with the main variability found in the magnitude of the slope. This stability, along with Fig. 3.4 summarizing positive seasonal trends across all seasons (except winter), underscores the capability of ITA to reveal significant seasonal variations. In summary, the spatial and trend analyses conducted through ITA offer deeper insights into both positive and negative seasonal trends, consistently demonstrating a stronger trend across seasons compared to traditional approaches. Figure 3.3 depicts the stable underlying pattern, while Fig. 3.4 highlights the important positive trends observed throughout the seasons, especially when evaluated using ITA. These findings support further exploration and informed decision-making regarding seasonal rainfall dynamics.

3.4. Conclusions

This study assesses and determines the most efficient methods for trend analysis, specifically MK, MMK1998, MMK2004, SSE, SRC, and ITA, by examining 120 years of rainfall data from 1901 to 2020 across four river basins in Eastern India. The study includes both seasonal and annual rainfall trends, utilizing 25 IMD grid points to effectively represent the geographical area under investigation.

The results demonstrate that the MMK method consistently detects more significant trends than MK, SRC, and SSE, particularly for annual, summer, and monsoon rainfall, where MMK shows trend significance levels at least 30% higher than MK. For winter rainfall trends, MMK and ITA exhibit comparable significance levels, while for autumn, ITA detects trends with 40% higher significance than MK. Particularly, ITA surpasses all other methods, identifying trends with 80% greater significance than those detected by MK, MMK, SRC, and SSE combined.

This study highlights ITA and MMK as the most effective methods for capturing both increasing and decreasing trends in rainfall across seasons. The ability of ITA to detect subtle and significant trends underscores its methodological robustness, making it essential for precise trend analysis and informed decision-making. These findings underscore the importance of selecting appropriate methods for statistical trend analysis, with ITA demonstrating significant potential for broader applications in various research and policy domains.

The insight obtained from this research serves as a basis for further research into regional-scale seasonal rainfall patterns and offers valuable guidance for global researchers aiming to enhance trend analysis outcomes. Additionally, these results support the development of targeted mitigation strategies for extreme rainfall events, aiding in the effective planning and management of water resources and climate adaptation projects.

References

Alexandersson, H. (1986). A homogeneity test applied to precipitation data. J. Climatol., 6(6), 661-675.

Caloiero, T., Coscarelli, R. and Ferrari, E. (2020). Assessment of seasonal and annual rainfall trend in Calabria (southern Italy) with the ITA method. J. Hydroinformatics, 22(4), 738–748.

Dash, S. and Maity, R. (2019) Temporal evolution of precipitation-based climate change indices across India: contrast between pre- and post-1975 features. Theor. Appl. Climatol., 138(3–4), 1667–1678.

Dickey, D.A. and Fuller, W.A. (1979). Distribution of the estimators for autoregressive time series with a unit root. J. Am. Stat. Assoc., 74(366), 427–431.

Gautheir, T.D. (2001). Detecting Trends Using Spearman's Rank Correlation Coefficient. Environ. Forensics, 2(4), 359-362.

Hamed, K.H. and Rao, A.R. (1998). A modified Mann-Kendall trend test for autocorrelated data. J. Hydrol., 204(1–4), 182–196.

IPCC (2018). Global warming of 1.5°C. An IPCC Special Report on the impacts of global warming of 1.5°C above pre-industrial levels and related global greenhouse gas emission pathways, in the context of strengthening the global response to the threat of climate change. In Press.

Kendall, M.G. (1938). A New Measure of Rank Correlation. Biometrika, 30(1/2), 81–89.

Kisi, O. (2015). An innovative method for trend analysis of monthly pan evaporations. J. Hydrol., 527, 1123–1129.

Kwiatkowski, D., Phillips, P.C., Schmidt, P. and Shin, Y. (1992). Testing the null hypothesis of stationarity against the alternative of a unit root. J. Econom., 54(1–3), 159–178.

Maity, R. (2022). Hypothesis Testing and Non-parametric Test. In: Statistical Methods in Hydrology and Hydroclimatology. Springer Transactions in Civil and Environmental Engineering. Springer, Singapore.

Malik, A., Kumar, A., Guhathakurta, P. and Kisi, O. (2019). Spatial-temporal trend analysis of seasonal and annual rainfall (1966–2015) using innovative trend analysis method with significance test. Arab J. Geosci., 12(10), 328.

Mann, H.B. (1945). Nonparametric Tests Against Trend. Econometrica, 13(3), 245–259.

Patel, G., Das, R. and Das, S. (2023). Is the extreme temperature trend changed in the last two decades compared to last seven decades? Case Study from Eastern India. J. Earth Syst. Sci., 132(3), 140.

Pettitt, A.N. (1979). A non-parametric approach to the change-point problem. J. R. Stat. Soc. Ser. C. Appl. Stat., 28(2), 126–135.

Şen, Z. (2012). Innovative trend analysis methodology. J. Hydrol. Eng., 17(9), 1042–1046.

Singh, R., Sah, S., Das, B., Potekar, S., Chaudhary, A. and Pathak, H. (2021). Innovative trend analysis of spatio-temporal variations of rainfall in India during 1901–2019. Theor. Appl. Climatol., 145(1–2), 821–838.

Spearman, C. (1904). The proof and measurement of association between two things. Am. J. Psychol., 15(1), 72.

Sonali, P. and Kumar, D.N. (2013). Review of trend detection methods and their application to detect temperature changes in India. J. Hydrol., 476, 212–227.

Yue, S. and Wang, C.Y. (2004). The Mann-Kendall Test Modified by Effective Sample Size to Detect Trend in Serially Correlated Hydrological Series. Water Resour. Manag., 18(3), 201–218.

Chapter 4

Decadal Trend Analysis of Temperature Data

"Patel, G., Das, R. and Das, S. (2023). Is the extreme temperature trend changed in last two decades compared to last seven decades? Case Study from Eastern India. J. Earth Syst. Sci., 132(3), 140. https://doi.org/10.1007/s12040-023-02158-2"

4.1. Introduction

Global warming, primarily driven by rising levels of greenhouse gas (GHG) concentrations, stands as one of the most vital issues facing today. This warming negatively impacts the hydrological cycle, which is critical for sustaining life on Earth (Jose and Dwarakish 2022). The global pattern of atmospheric warming stimulates significant climate change phenomena, with spatial and temporal variations that require comprehensive research. Studies indicate that the climate of Earth has been changing at an unprecedented rate in recent history (IPCC 2021), with remarkable increases in surface and air temperatures documented since the 1950s (IPCC 2018). Furthermore, temperature extremes have been intensifying at a faster rate than average temperatures, making it essential to study these extremes to understand the warming cycle.

Several studies have looked into global temperature patterns (Cui et al. 2017, Mohorji et al. 2017). In India, Ross et al. (2018) focused on temperature trends over decades and found a significant increase in maximum surface temperatures during the pre-monsoon months of April and May from the 1950s to the 2010s. Long-term assessments indicate an increase in surface air temperatures in India from 1901 to 2010 (Srivastava et al. 2017). Particularly, Eastern India experienced a temperature rise of 0.3 °C from 1981 to 2010 and an even greater increase of 0.9 °C from 2001 to 2010 (Gogoi et al. 2019). Extreme temperatures have a greater impact on urban areas, affecting health, the economy, and overall quality of life (Sera et al. 2019). To effectively understand and address these climate change effects, especially regarding regional water resources and vulnerability management, robust trend analysis methods are essential.

Various trend analysis methods, such as the Mann-Kendall (MK) test, modified Mann-Kendall (MMK) test (Singh et al. 2021, Patel et al. 2024), linear regression (Biswas et al. 2019), and Theil-Sen approach (Meshram et al. 2017), have been applied to analyze climatic variables over time. Recently, the Innovative Trend Analysis (ITA) by Şen (2012) has proven useful for detecting trends in hydrological and meteorological variables, as it allows for trend identification in different subcategories without any distribution assumptions. Marak et al. (2020) demonstrated that ITA outperforms the MK test in trend detection for rainfall levels in Meghalaya, India. Şen further developed a significance test for ITA, making it easier to analyze complex data (Şen 2017), and several studies have since applied ITA for trend analysis (Güçlü 2018, Ali et al. 2019, Patel et al. 2024). Radhakrishnan et al. (2017) highlighted recent seasonal temperature increases but noted a lack of detailed explanations, underscoring the need for focused trend analysis on annual and seasonal temperature extremes.

Particularly, no detailed studies have yet used ITA to analyze decadal changes in extreme temperatures, which would offer a better understanding of current warming trends. Analyzing the changes across various timeframes that show historical shifts and recent warming trends is crucial for adapting to regional climate changes. Thus, this study utilizes ITA to examine extreme temperature patterns across different periods. The benefits of ITA, such as its non-reliance on serial correlation, non-normality, and sample size assumptions, make it particularly valuable for identifying hydrological and meteorological trends.

Most trend analyses typically look at large areas like countries or states, but it is essential to conduct basin-specific temperature trend analyses for effective hydrological studies and development planning. This research focuses on the KKSD basins, which include four river basins in Eastern India that are prone to extreme events. Understanding temperature trends in this context is important for managing these events and supporting regional development. By utilizing ITA, this study seeks to explore the spatial and temporal changes in extreme temperatures over recent decades. The results are anticipated to help policymakers make well-informed decisions and take practical steps to address future climate challenges.

4.2. Results and Discussion

4.2.1. Statistical Analysis of Temperatures

The study was carried out for 11 selected grid points across the KKSD basins as shown in Fig. 4.1. This investigation primarily focused on analyzing the maximum temperature (T_{max}) and minimum temperature (T_{min}) on both seasonal and annual scales.

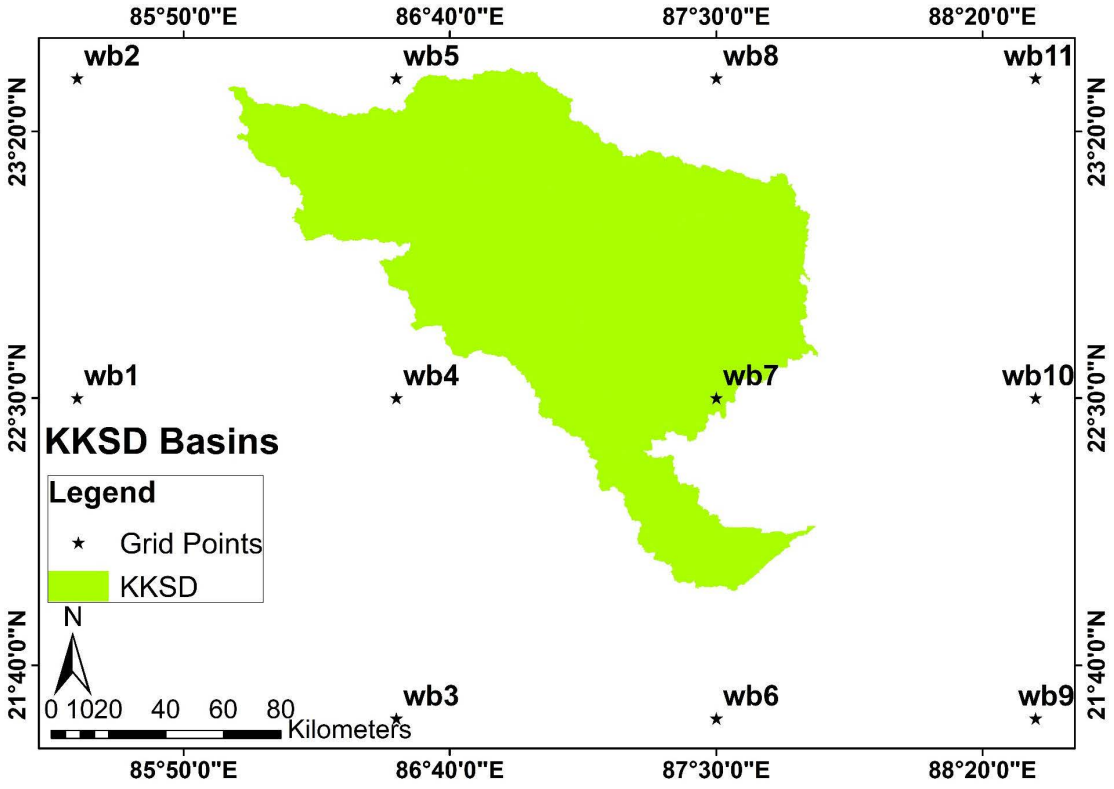

Fig. 4.1. Description of grids utilized for temperature analysis.

For the analysis, we utilized gridded daily temperature data covering 70 years, starting from 1951 to 2020. This dataset was generated by the India Meteorological Department (IMD), Pune, and is based on a grid size of 1° latitude by 1° longitude. This long-term dataset enabled a comprehensive assessment of temperature trends and variations across the selected grid points in KKSD basins. The T_{max} and T_{min} data have been collected to analyze the mean values for each grid. These values are presented in Table 4.1.

Table 4.1. Statistical summary of annual and seasonal temperatures in the KKSD basins for 1951 to 2020.

			T_{max} (°C)				
Stations	**Latitude**	**Longitude**	**Annual**	**Summer**	**Monsoon**	**Autumn**	**Winter**
WB1	22.5	85.5	31.32	36.52	31.93	29.44	26.55
WB2	23.5	85.5	31.16	36.27	32.15	29.39	25.92
WB3	21.5	86.5	31.43	34.20	32.47	30.54	27.85
WB4	22.5	86.5	31.68	35.28	32.93	30.42	27.26
WB5	23.5	86.5	31.81	36.60	32.96	30.28	26.52
WB6	21.5	87.5	30.72	32.57	32.13	30.46	27.18
WB7	22.5	87.5	31.15	33.45	32.70	30.65	27.12
WB8	23.5	87.5	31.75	34.91	33.38	30.93	26.94
WB9	21.5	88.5	30.42	31.94	32.04	30.38	26.78
WB10	22.5	88.5	30.80	32.46	32.42	30.68	27.04
WB11	23.5	88.5	31.55	34.14	33.21	31.00	27.12
			T_{min} (°C)				
WB1	22.5	85.5	19.65	22.09	24.30	18.02	12.08
WB2	23.5	85.5	19.27	21.61	24.23	17.64	11.39
WB3	21.5	86.5	21.39	23.63	25.28	20.27	14.69
WB4	22.5	86.5	20.91	23.20	25.38	19.61	13.52
WB5	23.5	86.5	19.96	22.16	24.75	18.69	12.19
WB6	21.5	87.5	22.43	24.56	26.12	21.59	15.94
WB7	22.5	87.5	21.88	24.10	26.08	21.01	14.65
WB8	23.5	87.5	20.27	22.27	24.97	19.46	12.56
WB9	21.5	88.5	22.69	24.78	26.45	22.08	15.99
WB10	22.5	88.5	22.04	24.13	26.12	21.45	14.90
WB11	23.5	88.5	21.30	23.21	25.75	20.81	13.77

The study examines variations in T_{max} and T_{min} across different dimensions, including latitude, longitude, and seasons such as annual, summer, monsoon, autumn, and winter. The highest recorded T_{max} over the KKSD basins is 46.42°C, observed in May 1972, while the lowest recorded T_{min} is 1.56°C, observed in January 1955. The annual and seasonal mean values of T_{max} and T_{min} for the entire period from 1951 to 2020 have been plotted over the KKSD basins to understand their spatial distribution. These spatial distributions are shown in Figs. 4.2 and 4.3, respectively.

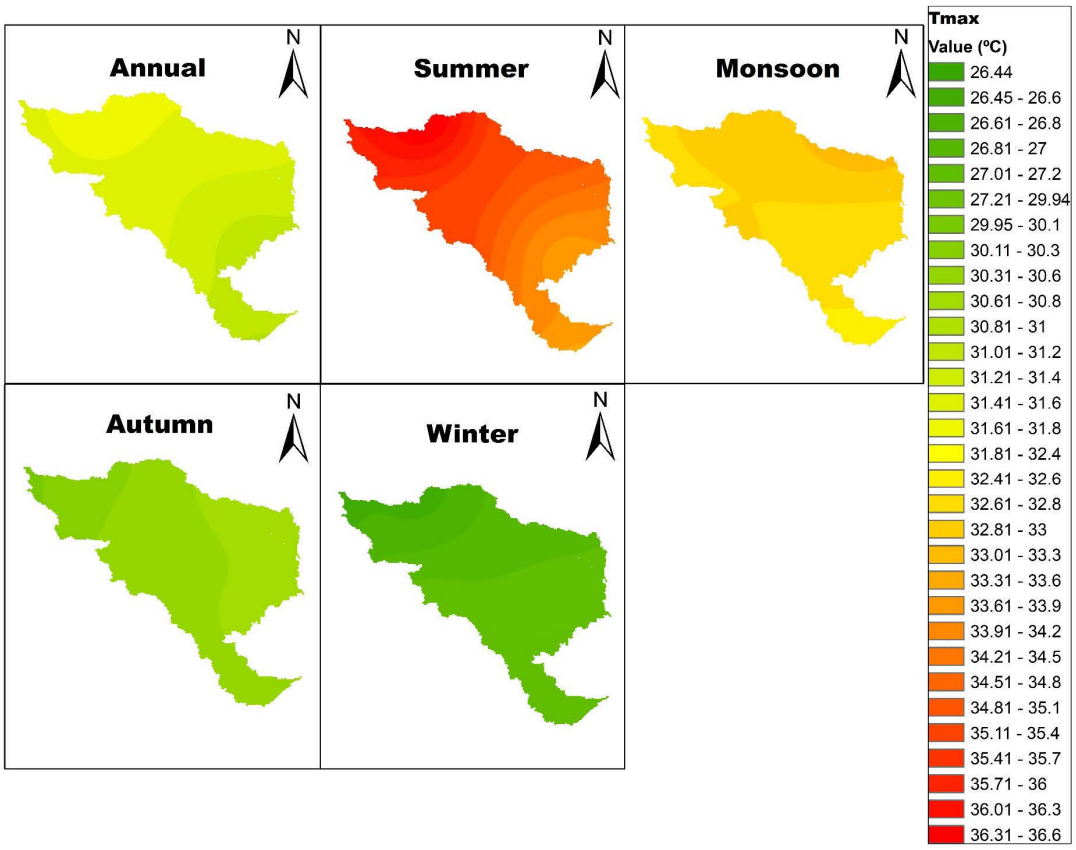

Fig. 4.2. Spatial distributions of T_{max} over the KKSD basins.

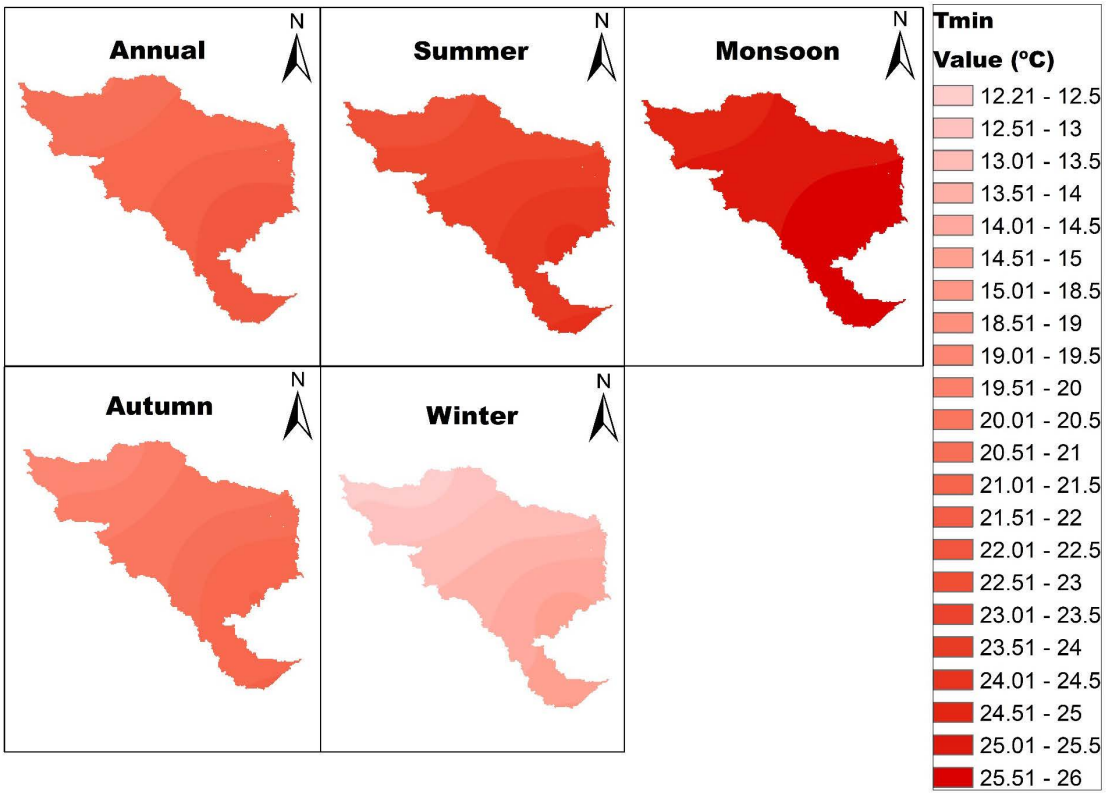

Fig. 4.3. Spatial distributions of T_{min} over the KKSD basins.

The spatial distribution of T_{max} over the KKSD basins reveals significant variability across different seasons. It is evident that the annual and summer T_{max} distributions share similar patterns. Specifically, the southeastern part of the basins consistently shows the lowest T_{max} values, whereas the northwestern part exhibits the highest T_{max} values.

However, for other seasons, the variability is different. During the monsoon period, the northern part of the basins experiences the highest T_{max} values. In contrast, autumn and winter seasons show patterns that are the opposite of those observed during the annual and summer seasons. Similarly, the spatial distribution of T_{min} across the KKSD basins shows a similar pattern for different seasons. There is an upward trend in T_{min} values moving from the southeastern part of the basins towards the northwestern part. This consistent pattern highlights the spatial variation of T_{min} across the basin over different seasonal periods.

4.2.2. Annual Temperature Trend

The annual trend analysis of T_{max} and T_{min} over the past 70 years across the basins has been carried out by dividing the dataset into two distinct periods: 1951-2000 and 2001-2020. This division enables a comparative understanding of how temperature trends have evolved over these two intervals. The analysis reveals significant changes in the slope patterns of temperature trends for both T_{max} and T_{min} during these periods. Figure 4.4 provides a visualization of the historical temperature trends, offering insights into long-term changes over multiple decades. In contrast, Fig. 4.5 focuses on the trends observed during the most recent decade, highlighting more recent variations and shifts in temperature patterns.

For the first period, from 1951 to 2000, the mean values of T_{max} and T_{min} exhibit a clear and consistent long-term declining trend. This suggests a gradual decrease in temperatures over this extended time frame. However, during the more recent period of 2001-2020, the slope patterns undergo an abrupt shift. Instead of continuing the previous decreasing trend, both T_{max} and T_{min} show an increasing trend. This indicates that temperatures have started rising in the past two decades. Furthermore, the rate of increase in T_{max} is especially faster compared to that of T_{min} during this recent period. This differential rate of warming highlights the complex nature of temperature changes and suggests that T_{max} is responding more dynamically to recent climatic factors compared to T_{min}.

4.2.3. Seasonal Temperature Trend

The seasonal trend analysis over the study period of 1951-2020 reveals distinct patterns for T_{max} and T_{min} across different seasons, with distinguished variations between the earlier period (1951-2000) and the more recent two decades (2001-2020). Each season demonstrates unique temperature trends that highlight the dynamic nature of climatic changes in the region.

During the summer season, the long-term analysis shows a decreasing slope for both T_{max} and T_{min} over the entire study period. However, there are clear differences in the magnitude of these slopes between the two distinct periods. From 1951 to 2000, both T_{max} and T_{min} exhibited significantly negative slopes, indicating a steady decline in summer temperatures during this time. Similarly, the recent two decades (2001-2020) show a negative trend, where the slope of T_{min} becomes steeper compared to T_{max}, suggesting that minimum temperatures are falling at

a slightly faster rate. This change reflects a shift in the thermal regime of the summer season, with T_{min} experiencing greater variability.

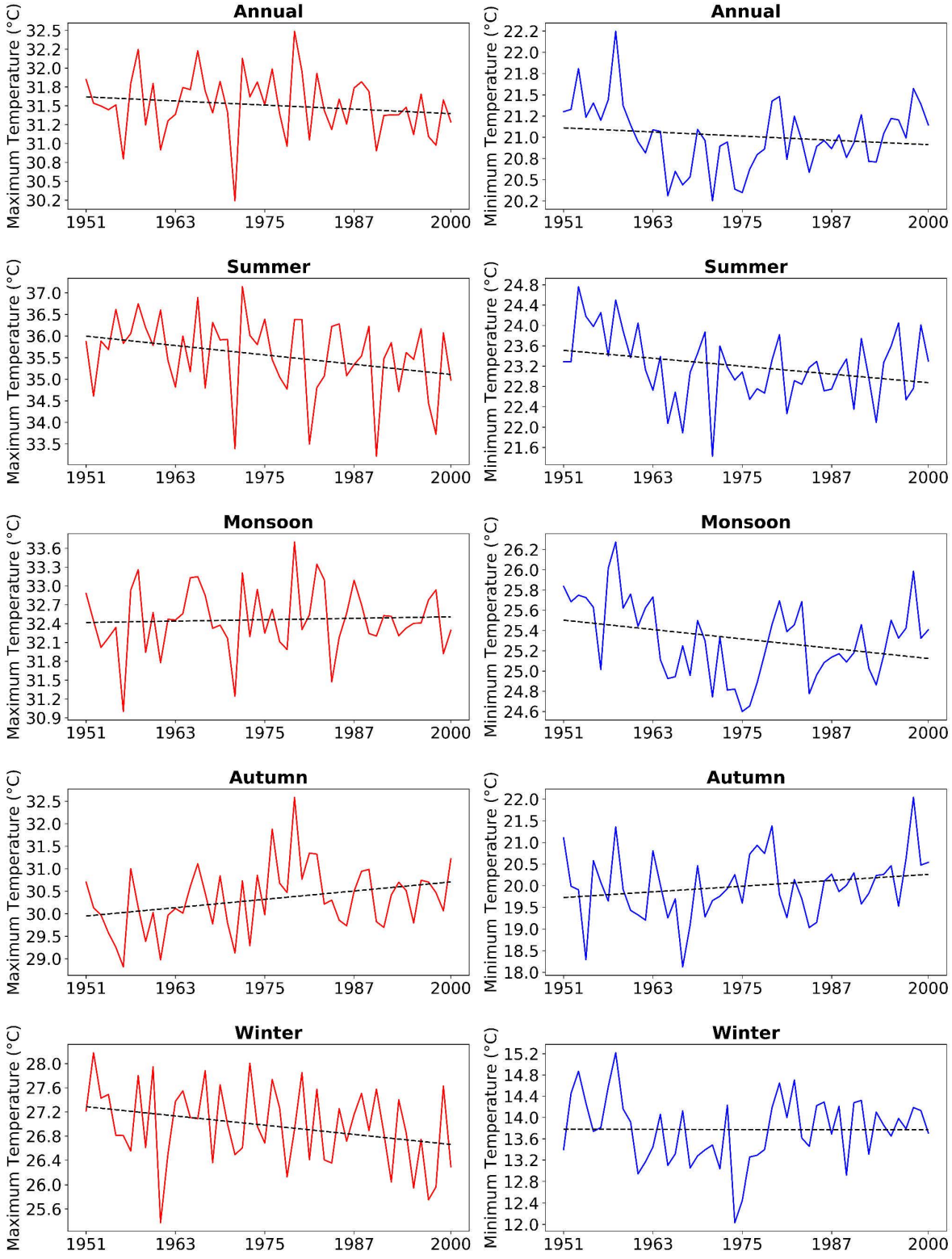

Fig. 4.4. Historical (1951-2000) trends of T_{max} and T_{min} over the KKSD basins.

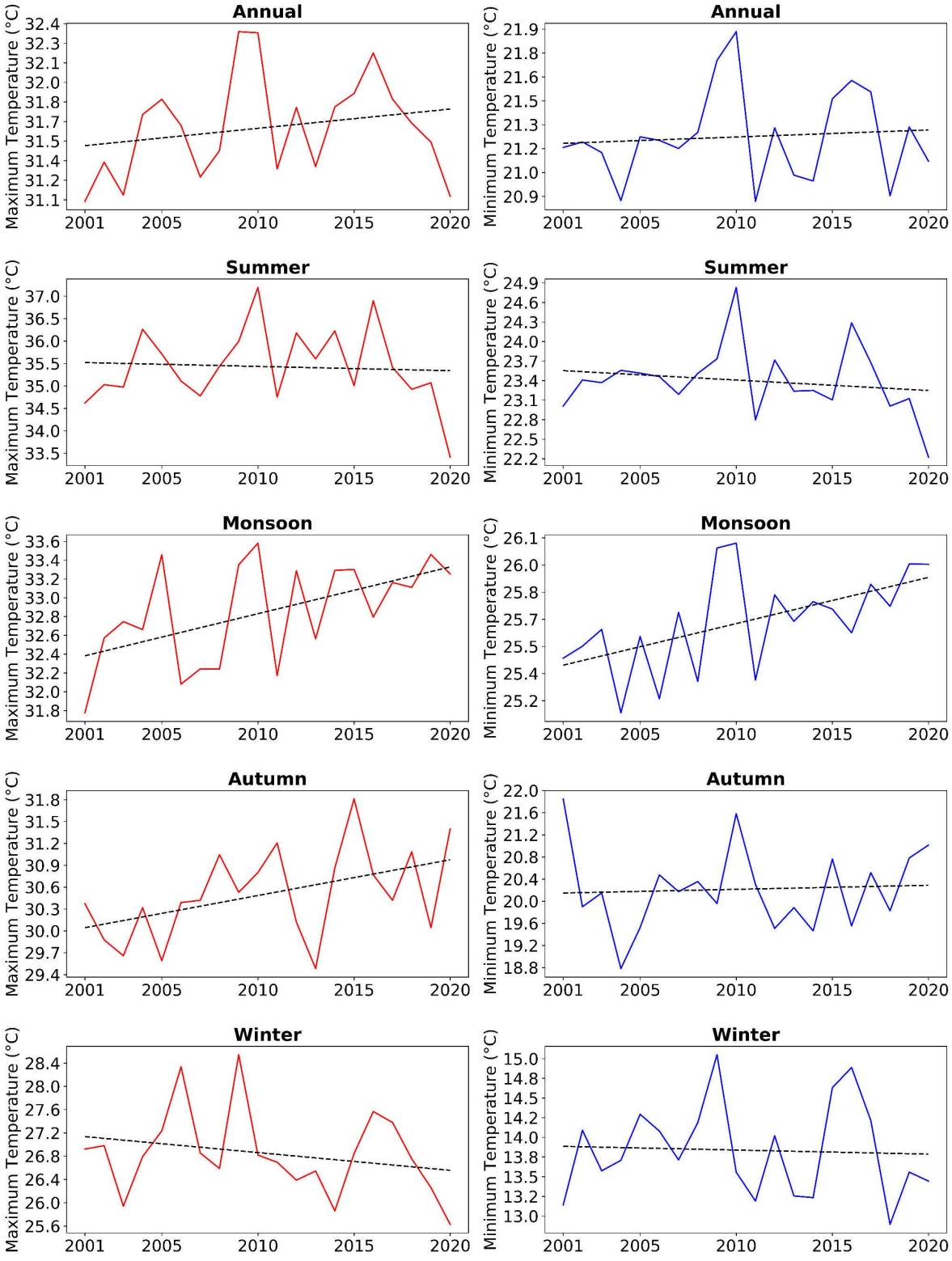

Fig. 4.5. Recent decade (2001-2020) trends of T_{max} and T_{min} over the KKSD basins.

In the monsoon season, the trends for T_{max} and T_{min} also show clear differences between the two time periods. Over the earlier period from 1951 to 2000, T_{max} demonstrates a stable trend, while T_{min} displays a negative trend, indicating a slight decrease in minimum temperatures during the monsoon. However, the trends in the recent two decades (2001-2020)

contrast sharply with this earlier pattern. Both T_{max} and T_{min} exhibit strong upward trends during this period, with higher magnitudes compared to earlier decades. This indicates a visible warming trend during the monsoon season in the last 20 years, suggesting that both maximum and minimum temperatures are rising consistently.

The autumn season shows consistent patterns for both T_{max} and T_{min}. From 1951 to 2000, both trends during autumn exhibits a positive slope, indicating a gradual increase in temperatures over this period. In the recent period (2001-2020), however, the T_{min} trend shows minimal change, continuing its near-zero slope, while T_{max} trends show positive variation. This stability in autumn T_{min} trends contrasts with the more dynamic patterns observed in other seasons.

In the winter season, trends for T_{max} and T_{min} also vary significantly across the two time periods. From 1951 to 2000, T_{max} trends show a declining slope, indicating that maximum temperatures during winter were gradually decreasing over this period. In contrast, T_{min} exhibits no visible trend during the same time frame, suggesting that minimum temperatures remained relatively stable in winter. However, the trends shift in the 2001-2020 period, where both T_{max} and T_{min} exhibit negative slopes. This indicates that both maximum and minimum temperatures during winter are now decreasing, highlighting a cooling trend that contrasts with the warming observed in other seasons such as monsoon and summer.

Overall, the seasonal analysis illustrates diverse and evolving temperature trends for T_{max} and T_{min}. While some seasons, like monsoon, show a clear warming trend in recent decades, others, like winter, reveal a cooling pattern. These seasonal variations underscore the diverse nature of climate change, with different drivers and localized impacts influencing temperature trends across seasons. Such findings emphasize the importance of considering both seasonal and long-term perspectives when assessing regional climate dynamics.

4.2.4. Innovative Trend Analysis (ITA)

The ITA method was applied to evaluate temperature trends and slope magnitudes for annual and seasonal maximum (T_{max}) and minimum (T_{min}) temperatures over two periods, 1951-2020 and 2001-2020, across 11 grid points in the KKSD basins. The results are presented in Tables 4.2 and 4.3 and visually illustrated in Figs. 4.6 and 4.7, reveal significant variations in slope (Eq. 3.10) magnitudes across the grids.

For the historical period (1951-2020), the ITA indicates that T_{max} slopes range between -0.198°C/decade and 0.097°C/decade, while T_{min} slopes range from -0.065°C/decade to 0.185°C/decade. In the more recent period (2001-2020), wider variations are observed, with T_{max} slopes ranging from -0.662°C/decade to 0.715°C/decade and T_{min} slopes from -0.500°C/decade to 0.345°C/decade. These variations highlight distinct regional differences in warming trends over time.

Table 4.2. ITA slope of annual and seasonal extreme temperatures in the KKSD basins from 1951 to 2020.

Grids	Annual		Summer		Monsoon		Autumn		Winter	
	T_{max}	T_{min}	T_{max}	T_{min}	T_{max}	T_{min}	T_{max}	T_{min}	T_{max}	T_{min}
WB1	0.018	-0.038	-0.071	-0.063	0.043	-0.041	0.077	0.024	0.034	-0.051
WB2	-0.010	-0.022	-0.108	-0.065	0.033	-0.017	0.058	0.037	-0.017	-0.024

WB3	0.023	-0.001	-0.024	-0.019	0.068	0.000	0.060	0.049	-0.015	-0.016
WB4	-0.024	0.015	-0.127	-0.015	0.059	0.020	0.036	0.079	-0.073	-0.004
WB5	-0.047	0.049	-0.172	0.005	0.051	0.060	0.033	0.115	-0.105	0.037
WB6	0.019	0.047	-0.039	0.026	0.088	0.045	0.069	0.095	-0.050	0.040
WB7	-0.023	0.090	-0.108	0.061	0.077	0.087	0.039	0.152	-0.113	0.081
WB8	-0.064	0.078	-0.198	0.035	0.052	0.072	0.027	0.151	-0.147	0.081
WB9	0.004	0.056	-0.068	0.025	0.085	0.056	0.065	0.104	-0.071	0.055
WB10	-0.012	0.104	-0.106	0.071	0.097	0.096	0.064	0.161	-0.112	0.111
WB11	-0.045	0.117	-0.176	0.079	0.083	0.105	0.049	0.185	-0.149	0.125

Table 4.3. ITA slope of annual and seasonal extreme temperatures in the KKSD basins from 2001 to 2020.

Grids	Annual		Summer		Monsoon		Autumn		Winter	
	T_{max}	T_{min}	T_{max}	T_{min}	T_{max}	T_{min}	T_{max}	T_{min}	T_{max}	T_{min}
WB1	-0.208	0.236	-0.369	-0.019	0.055	0.0345	0.102	0.319	-0.603	0.290
WB2	-0.156	0.104	-0.365	-0.110	0.091	0.0270	0.265	0.072	-0.557	0.120
WB3	-0.070	-0.148	-0.221	-0.368	0.231	0.0040	0.249	-0.138	-0.533	-0.186
WB4	-0.047	-0.060	-0.213	-0.308	0.335	0.0235	0.359	-0.110	-0.662	-0.172
WB5	0.229	-0.118	-0.046	-0.378	0.557	0.0210	0.715	-0.213	-0.257	-0.232
WB6	0.075	-0.255	0.000	-0.475	0.349	0.0016	0.424	-0.259	-0.448	-0.395
WB7	0.084	-0.133	-0.140	-0.370	0.487	0.0188	0.492	-0.153	-0.502	-0.312
WB8	0.103	-0.089	-0.145	-0.284	0.493	0.0215	0.589	-0.164	-0.491	-0.249
WB9	0.113	-0.265	-0.008	-0.500	0.458	0.0040	0.447	-0.269	-0.446	-0.433
WB10	0.053	-0.144	-0.149	-0.351	0.492	0.0149	0.441	-0.136	-0.591	-0.333
WB11	0.103	-0.150	-0.117	-0.319	0.511	0.0167	0.536	-0.199	-0.511	-0.373

a) Annual ITA Trend

The annual ITA analysis for the periods 1951-2020 and 2001-2020 reveals significant changes in T_{max} and T_{min} trends across the KKSD basins, highlighting the importance of decade based analysis for detecting trends (Mohorji et al. 2017). The results demonstrate trend stability over time, with distinct variations in the number of positive and negative trends observed across the 11 grid points.

For T_{max}, four grids (WB1, WB3, WB6, and WB9) exhibited positive trends during the historical period (1951-2020), while the recent period (2001-2020) shows an increase to seven grids (WB5, WB6, WB7, WB8, WB9, WB10, and WB11) with positive trends. On the other hand, T_{min} trends display greater variability and magnitude. During the historical period, three grids (WB1, WB2, and WB3) show negative trends, whereas, in the recent period, two grids (WB1 and WB2) shift to positive trends, and the remaining show negative trends.

This variability underscores the dynamic nature of temperature trends across the basins and emphasizes the value of examining trends over multiple timeframes for a comprehensive understanding of climate dynamics in the region.

b) Seasonal ITA Trend

The ITA analysis for different seasons across two time periods, 1951-2020 (historical) and 2001-2020 (recent), reveals significant variations in temperature trends for multiple grid points in the KKSD basins.

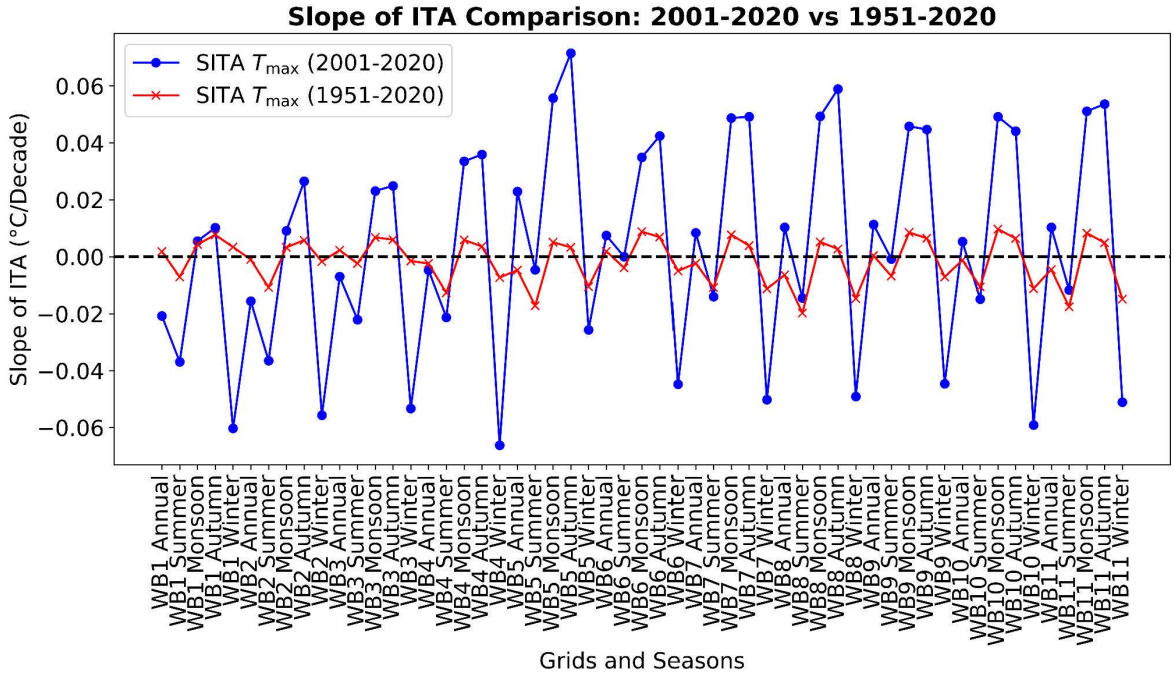

Fig. 4.6. Comparison of slopes of ITA (SITA) for T_{max} over the KKSD basins.

In the summer season, T_{max} exhibits a 100% negative trend across the basins in both periods. For T_{min}, the historical period shows negative trends for four grids (WB1, WB2, WB3, and WB4), while the recent period indicates a 100% negative trend across all grids. For the monsoon season, T_{max} consistently shows a 100% positive trend in both periods. However, T_{min} trends vary; in the historical period, three grids (WB1, WB2, and WB3) show negative trends, while the recent period displays a 100% positive trend across the basins.

During the autumn season, T_{max} exhibits a 100% positive trend in both periods across all grids. T_{min} shows a contrasting pattern, with only two grids (WB1 and WB2) displaying positive trends in the recent period, while the historical period reflects a 100% positive trend. In winter, T_{max} trends are predominantly negative across both periods, except for WB1, which shows a positive trend in the recent period. T_{min} trends diverge significantly; the historical period shows 36% negative trends (WB1-WB4), whereas the recent period reports nine grids (WB3-WB11) with negative trends.

A comparison of the two periods highlights distinct seasonal variations. In the recent period, monsoon and autumn seasons indicate a rising trend in T_{max}, while T_{min} shows a significant increasing trend only during the monsoon. For other seasons and the annual scale, T_{min} predominantly exhibits a decreasing trend, except in a few grids. In contrast, the historical period demonstrates inconsistent trends, with neither the magnitude nor the direction of T_{max} and T_{min} showing an absolute pattern. These results demonstrate the temporal and spatial complexities of temperature trends in the KKSD basins.

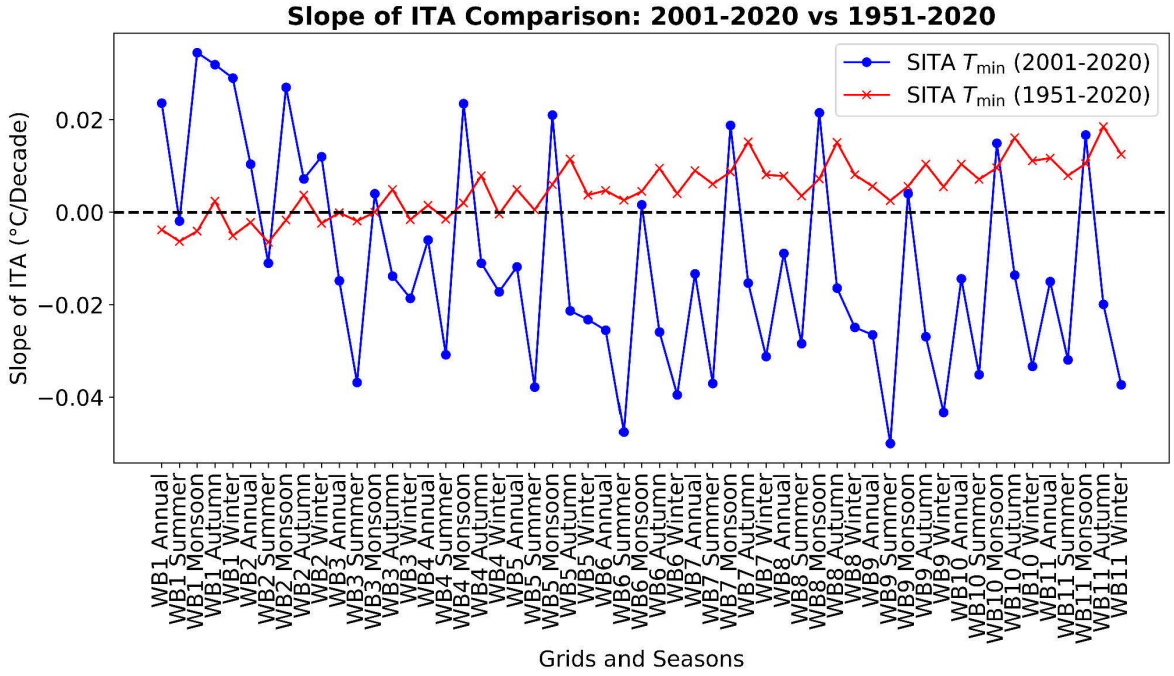

Fig. 4.7. Comparison of slopes of ITA (SITA) for T_{min} over the KKSD basins.

4.2.5. Percentage Changes in Slope of ITA

The relative percentage changes in SITA between the historical period (1951-2020) and the recent period (2001-2020) are illustrated in Fig. 4.8. The analysis reveals a consistent pattern of positive changes in T_{max} and negative changes in T_{min} across all seasons. Abrupt changes are observed in T_{max} for the annual, monsoon, autumn, and winter seasons, while T_{min} shows prominent changes during the summer season.

These findings partially align with Sonali and Kumar (2013), who analyzed extreme temperatures over three distinct periods: 1901-2003, 1948-2003, and 1971-2003, employing various trend detection techniques. Their study reported significant and consistent relative percentage changes in T_{min} in the northeast region, particularly a decline during the monsoon season that is reflected similarly to the observations of this study. However, differences in the overall study duration and analyzed timeframes result in variations in the observed seasonal trends, underscoring the importance of temporal context in climate trend analysis.

Mall et al. (2021) investigated changes in the diurnal temperature range (DTR) across agro-climatic zones and found a shift from increasing DTR in the historical period to decreasing DTR in the recent period. These DTR variations suggest corresponding changes in T_{min}, validating the observed patterns of the current study. Figure 4.9 compares these relative percentage changes over the northeast region, highlighting the influence of spatial and temporal scales on climate trends.

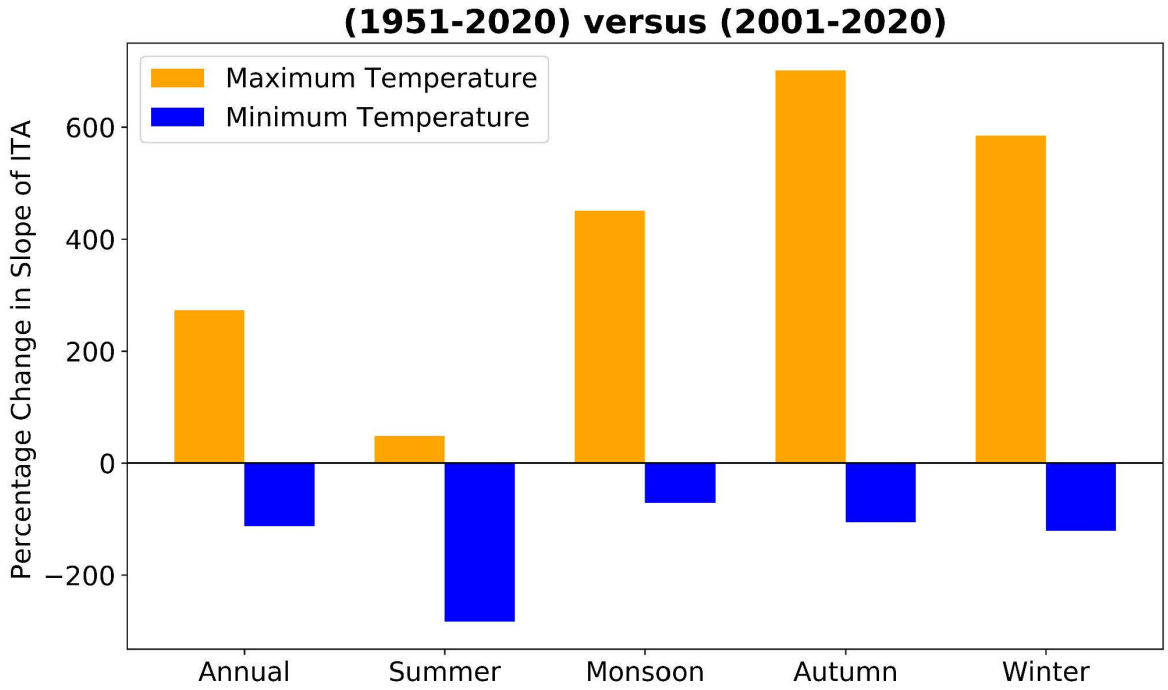

Fig. 4.8. Relative percentage changes from the historical decade to the recent decade in SITA over the KKSD basins.

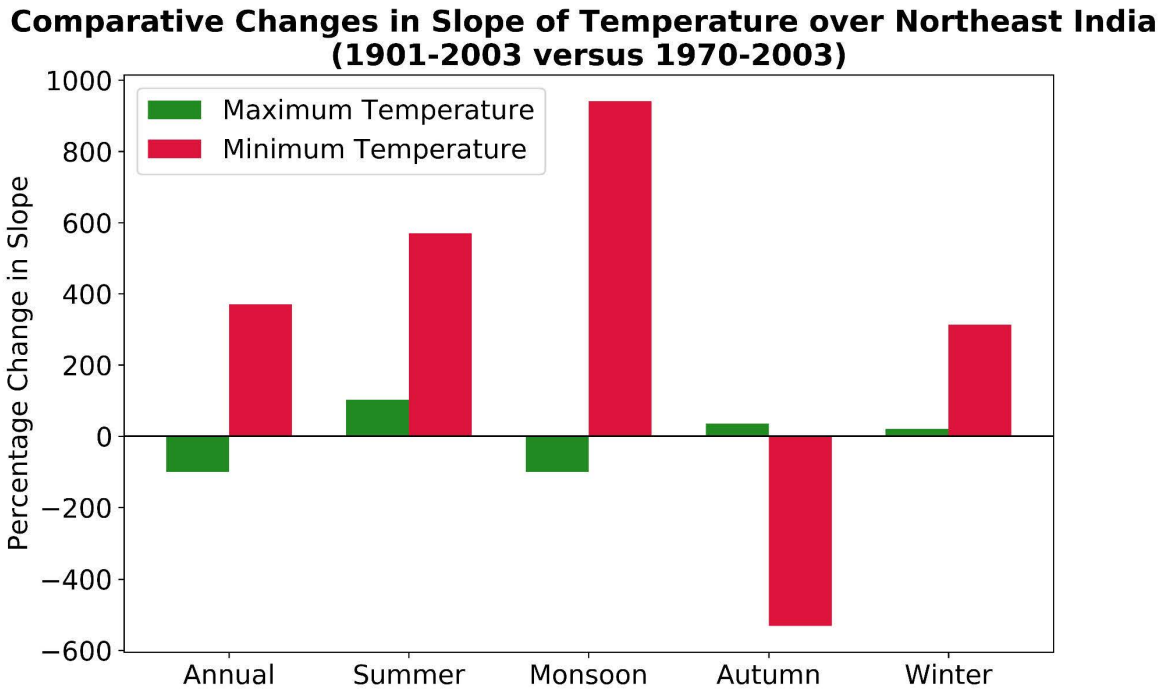

Fig. 4.9. Relative percentage changes from the historical decade 1901-2003 to the recent decade 1970-2003 in Slope over Northeast India (Sonali and Kumar 2013).

4.2.6. Spatial Variation

The spatial variation of the ITA slopes for different seasons, decades, and grid points are illustrated in Figs. 4.10–4.13. Specifically, Figs. 4.10 and 4.11 represent the spatial distribution

of SITA for T_{max} during the historical and recent decades, while Figs. 4.12 and 4.13 represent the SITA for T_{min}.

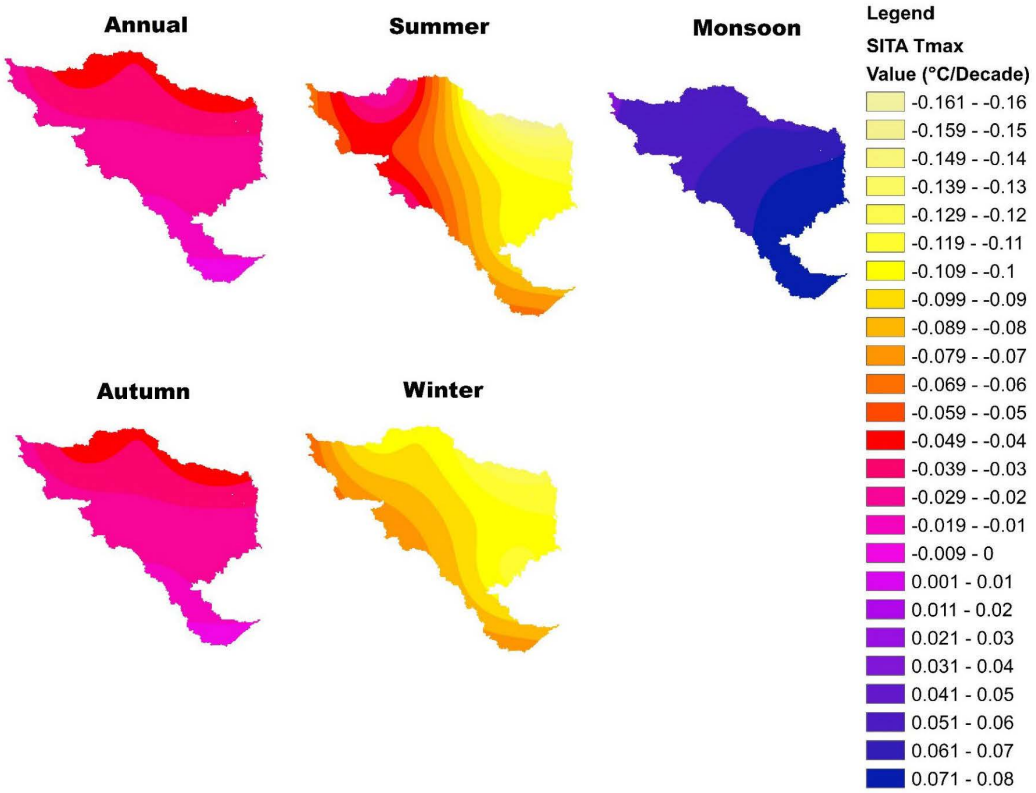

Fig. 4.10. Spatial distributions of SITA of T_{max} from 1951 to 2020 for different seasons.

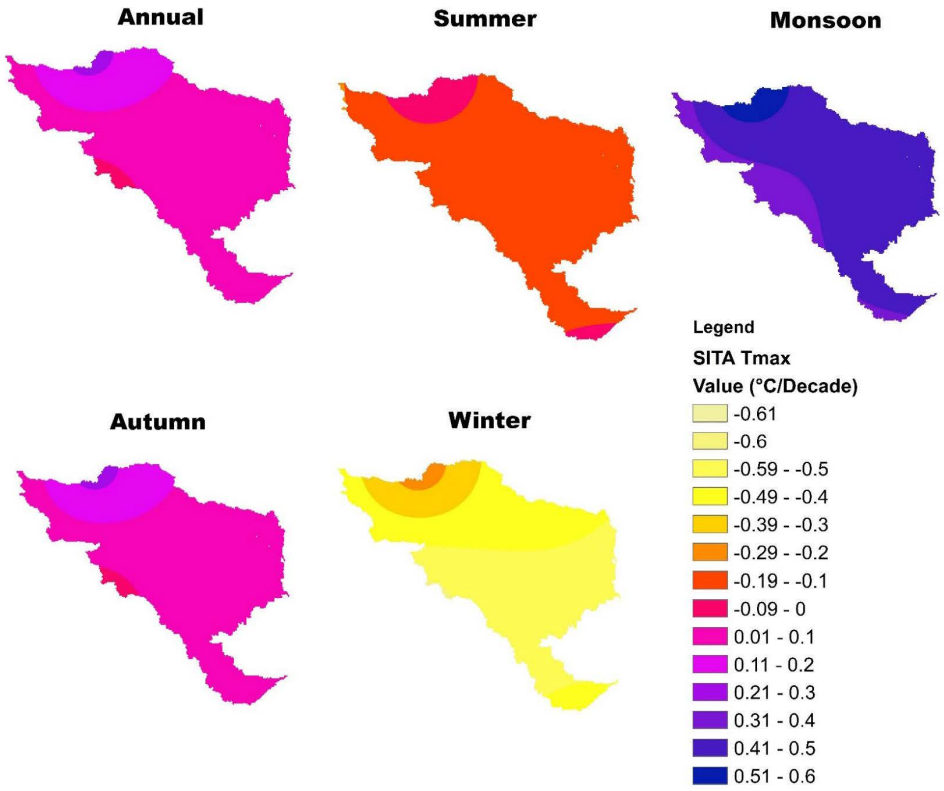

Fig. 4.11. Spatial distributions of SITA of T_{max} from 2001 to 2020 for different seasons.

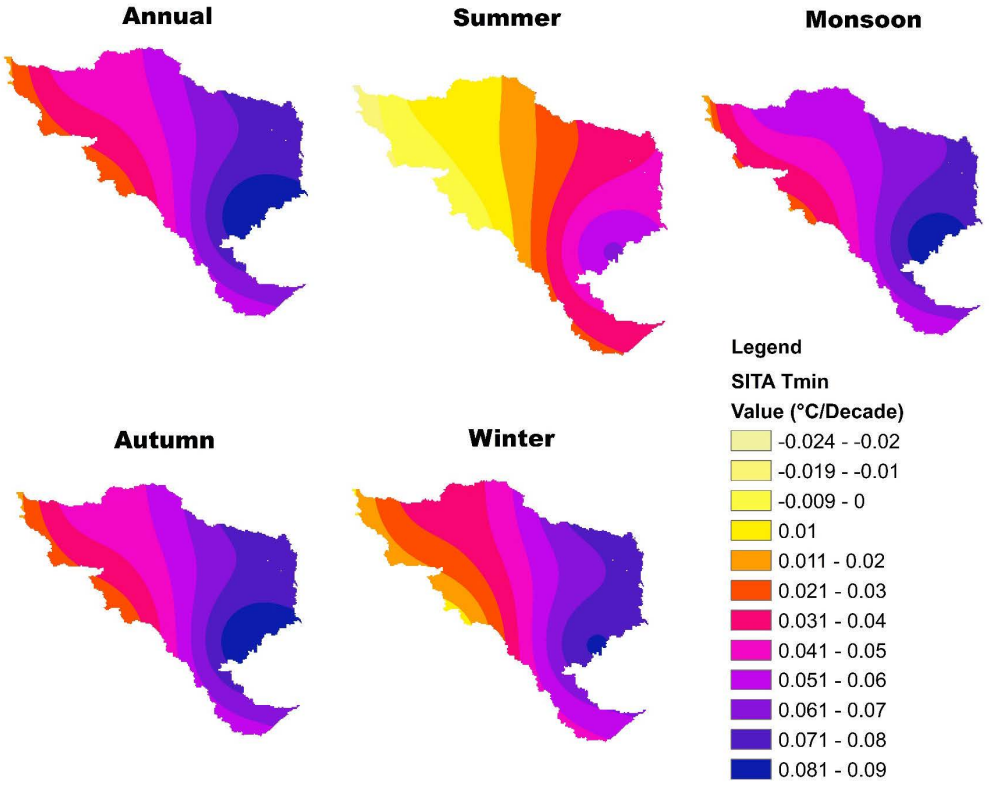

Fig. 4.12. Spatial distributions of SITA of T_{min} from 1951 to 2020 for different seasons.

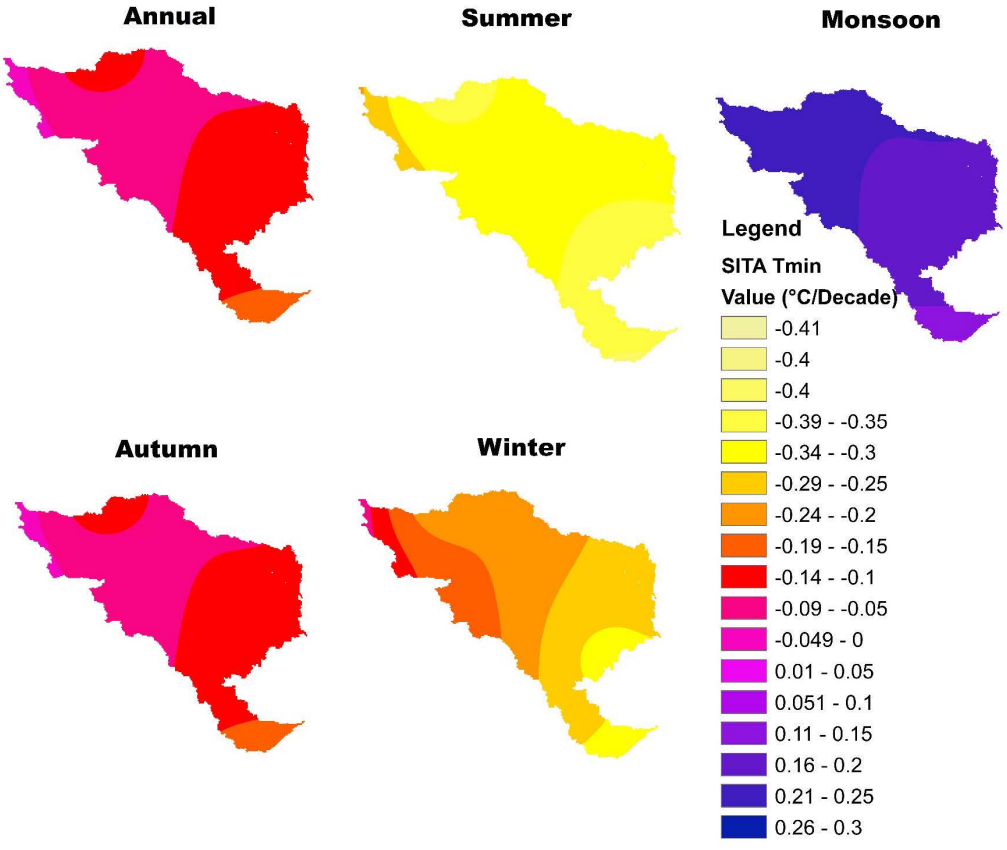

Fig. 4.13. Spatial distributions of SITA of T_{min} from 2001 to 2020 for different seasons.

From the spatial distribution of SITA for T_{max} during the historical decade, it is evident that all seasons, except the monsoon, follow a similar pattern. Higher magnitudes of SITA are observed in grids WB3, WB4, WB6, WB7, WB9, and WB10 within the KKSD basins. Grids WB1-WB4, WB7, and WB9 exhibit the highest magnitudes for the monsoon season. This indicates that the southern part of the basins experienced greater changes in the magnitude of SITA during the historical decade.

In contrast, during the recent decade, all seasons show a consistent pattern, with grid WB5 exhibiting the highest SITA magnitudes across the basins. This shift suggests that the northern part of the basins has experienced more significant changes in recent decades.

For T_{min}, the historical decade shows a consistent trend across all seasons, with the eastern part of the basins displaying greater SITA magnitudes. However, the recent decade reveals contradictory results, where the western part of the basins shows higher SITA values. Across both decades, the monsoon season has the highest SITA magnitudes for both T_{min} and T_{max}.

4.3. Conclusions

This study examines seasonal and annual extreme temperatures across the KKSD basins using the ITA method from 1951 to 2020. For analysis, the study period is divided into two timeframes: (a) a historical decade from 1951 to 2000, and (b) a recent decade from 2001 to 2020, with comparative assessments conducted between these time frames to capture changes in temperature extremes.

Upon examining extreme temperatures across these periods, the basin grids display both increasing and decreasing trends across seasons, with distinct patterns emerging between the two-time frames. The ITA results exhibit robust performance, offering reliability across varied data distributions, automatic integration, and flexible data length, which makes it more sensitive for trend detection than traditional methods like the MK and MMK.

Key findings from ITA include:

- T_{max} for 1951-2020: During the monsoon and autumn seasons, approximately 100% of the grids show positive trends, while winter, summer, and annual periods display decreasing trends across 80% of grids.
- T_{max} for 2001-2020: Annual, monsoon, and autumn seasons reveal positive trends across about 64% of grids, while summer and winter show negative slopes at around 90% of grids with prominent magnitudes.
- T_{min} for 1951-2020: All seasons exhibit increasing trends across more than 80% of grids.
- T_{min} for 2001-2020: Apart from the monsoon season, which shows a positive trend with significant magnitude across 100% of grids, all other seasons demonstrate negative slopes across more than 82% of grids.

The observed shifts in ITA slopes across these two decades highlight significant changes in T_{max} and T_{min} across different seasons, pointing to a shifting climate pattern in recent decades. These findings provide essential information for water resource management and may support the development of climate adaptation strategies, especially about extreme events. Furthermore, the observed decadal shifts in temperature extremes may hold relevance

for assessing climate impacts on agriculture in Eastern India, contributing valuable knowledge for climate-resilient agricultural planning.

References

Ali, R., Kuriqi, A., Abubaker, S. and Kisi, O. (2019). Long-Term Trends and Seasonality Detection of the Observed Flow in Yangtze River Using Mann-Kendall and Sen's Innovative Trend Method. Water, 11(9), 1855.

Biswas, B., Jadhav, R.S. and Tikone, N. (2019). Rainfall Distribution and Trend Analysis for Upper Godavari Basin, India, from 100 Years Record (1911–2010). J. Indian Soc. Remote Sens., 47(10), 1781-1792.

Cui, L., Wang, L., Lai, Z., Tian, Q., Liu, W. and Li, J. (2017). Innovative trend analysis of annual and seasonal air temperature and rainfall in the Yangtze River Basin, China during 1960–2015. J. Atmos. Sol.-Terr. Phys., 164, 48–59.

Gogoi, P.P., Vinoj, V., Swain, D., Roberts, G., Dash, J. and Tripathy, S. (2019). Land use and land cover change effect on surface temperature over Eastern India. Sci. Rep., 9, 8859.

Güçlü, Y.S. (2018). Multiple Şen-innovative trend analyses and partial Mann-Kendall test. J. Hydrol., 566, 685–704.

IPCC (2018). Global Warming of 1.5°C. An IPCC Special Report on the impacts of global warming of 1.5°C above pre-industrial levels and related global greenhouse gas emission pathways, in the context of strengthening the global response to the threat of climate change, sustainable development, and efforts to eradicate poverty [Masson-Delmotte V, Zhai P, Pörtner H O, Roberts D, Skea J, Shukla P R, Pirani A, Moufouma-Okia W, Péan C, Pidcock R, Connors S, Matthews J B R, Chen Y, Zhou X, Gomis M I, Lonnoy E, Maycock T, Tignor M and Waterfield T (eds.)] Cambridge University Press

IPCC (2021). Summary for Policymakers. In: Climate Change 2021: The Physical Science Basis. Contribution of Working Group I to the Sixth Assessment Report of the Intergovernmental Panel on Climate Change [Masson-Delmotte V, Zhai P, Pirani A, Connors S L, Péan C, Berger S, Caud N, Chen Y, Goldfarb L, Gomis M I, Huang M, Leitzell K, Lonnoy E, Matthews J B R, Maycock T K, Waterfield T, Yelekçi O, Yu R and Zhou B (eds.)] Cambridge University Press

Jose, D.M. and Dwarakish, G.S. (2022). Bias Correction and Trend Analysis of Temperature Data by a High-Resolution CMIP6 Model over a Tropical River Basin. Asia-Pac. J. Atmos. Sci., 58(1), 97–115.

Mall, R.K., Chaturvedi, M., Singh, N., Bhatla, R., Singh, R.S., Gupta, A. and Niyogi, D. (2021). Evidence of asymmetric change in diurnal temperature range in recent decades over different agro-climatic zones of India. Int. J. Climatol., 41(4), 2597–2610.

Marak, J.D.K., Sarma, A.K. and Bhattacharjya, R.K. (2020). Innovative trend analysis of spatial and temporal rainfall variations in Umiam and Umtru watersheds in Meghalaya, India. Theor. Appl. Climatol., 142(3–4), 1397–1412.

Meshram, S.G., Singh, V.P. and Meshram, C. (2017). Long-term trend and variability of precipitation in Chhattisgarh State, India. Theor. Appl. Climatol., 129(3–4), 729–744.

Mohorji, A.M., Şen, Z. and Almazroui, M. (2017). Trend Analyses Revision and Global Monthly Temperature Innovative Multi-Duration Analysis. Earth Syst. Environ., 1(1), 1–13.

Patel, G., Das, S. and Das, R. (2024). Determine the best method for analysing long-term (120 years) annual and seasonal rainfall trends in four east India river basins. J. Earth Syst. Sci., 133(2), 70.

Radhakrishnan, K., Sivaraman, I., Jena, S.K., Sarkar, S. and Adhikari, S. (2017). A Climate Trend Analysis of Temperature and Rainfall in India. Clim. Chang. Environ. Sustain., 5(2), 146.

Ross, R.S., Krishnamurti, T.N., Pattnaik, S. and Pai, D.S. (2018). Decadal surface temperature trends in India based on a new high-resolution data set. Sci. Rep., 8, 7452.

Şen, Z. (2012). Innovative Trend Analysis Methodology. J. Hydrol. Eng., 17(9), 1042–1046.

Şen, Z. (2017). Innovative trend significance test and applications. Theor. Appl. Climatol., 127(3–4), 939–947.

Sera, F., Armstrong, B., Tobias, A. et al. (2019). How urban characteristics affect vulnerability to heat and cold: a multi-country analysis. Int. J. Epidemiol., 48(4), 1101–1112.

Serencam, U. (2019). Innovative trend analysis of total annual rainfall and temperature variability case study: Yesilirmak region, Turkey. Arab. J. Geosci., 12(23), 704.

Singh, R., Sah, S., Das, B., Vishnoi, L. and Pathak, H. (2021). Spatio-temporal trends and variability of rainfall in Maharashtra, India: Analysis of 118 years. Theor. Appl. Climatol., 143(3–4), 883–900.

Sonali, P. and Kumar, D.N. (2013). Review of trend detection methods and their application to detect temperature changes in India. J. Hydrol., 476, 212-227.

Srivastava, A.K., Kothawale, D.R. and Rajeevan, M.N. (2017). Variability and Long-Term Changes in Surface Air Temperatures Over the Indian Subcontinent. In: Rajeevan M and Nayak S (eds) Observed Climate Variability and Change over the Indian Region. Springer Geology, Springer Singapore.

Ranking of CMIP6 Models Using MCDM

"Patel, G., Das, S. and Das, R. (2023). Identification of Best CMIP6 Global Climate Model for Rainfall by Ensemble Implementation of MCDM Methods and Statistical Inference. Water Resour. Manag., 37(13), 5147–5170. https://doi.org/10.1007/s11269-023-03599-6"

5.1. Introduction

Climate change has emerged as a significant environmental issue due to its potentially adverse impacts on ecosystems, economic conditions, and public health. A key challenge linked to climate variability is the change in water resources, which influences irrigation, urban water supply, and industrial needs (Deepthi and Sivakumar 2022). Rainfall is an essential climate factor that significantly influences various aspects of our environment. Changes in rainfall patterns can alter hydrological processes and affect ecological balance, which in turn can have intense effects on socioeconomic growth and public health (Ruan et al. 2018). Anticipating future climate trends is essential for implementing effective adaptation and mitigation strategies. In this regard, Global Climate Models (GCMs) serve as primary tools, providing simulations based on atmospheric, oceanic, and land surface processes governed by physical laws and empirical relationships. Over the past decades, advancements in GCM development have enhanced their resolution and incorporated additional variables, leading to improved simulation accuracy. However, GCM outputs remain susceptible to uncertainties restricted by factors like model resolution, assumptions, and calibration, limiting their accuracy at regional scales.

Selecting an appropriate GCM for specific regions and scales is challenging due to inherent uncertainties in model responses and accuracy. As the variety of available GCMs increases, careful evaluation of their performance becomes essential. The Coupled Model Intercomparison Project (CMIP) organizes GCM simulations into phases, with the latest being CMIP6. CMIP6 has improved upon previous phases (e.g., CMIP5) by addressing limitations such as biases in seasonal and annual rainfall patterns (Gusain et al. 2020). Therefore, a lot of studies has concentrated on selecting and evaluating GCMs based on their ability to accurately reflect observed climatology. This assessment process often relies on performance indicators (PIs) like the skill score (SS), Taylor diagram, pattern correlation, index of agreement (IoA), and others (Anandhi and Nanjundiah 2015, Jose and Dwarakish 2022, Paul and Maity 2023).

Most existing studies in GCM selection emphasize either error-based or skill-based PIs, often without assigning weights to specific PIs. Since each PI provides unique insights, it is crucial to evaluate how the selection of PIs influences model ranking. Previous studies, including the work of Jose and Dwarakish (2022), have employed correlations, errors, and SS in the selection of PIs. However, these approaches may lead to biases that favor specific categories of PIs. Multi-criteria decision-making (MCDM) methods have also been employed in GCM evaluation, using methods like Vlse Kriterijumska Optimizacija Kompromisno

Resenje (VIKOR), technique for order-preference by similarity to an ideal solution (TOPSIS), and compromise programming (CP) (Zamani and Berndtsson 2019, Shiru and Chung 2021). Despite the benefits of MCDM techniques, many studies rely on a single approach, which may produce biased or exaggeratedly simplified results.

Given the limited research on CMIP6 GCMs ranking, particularly in India, this study aims to comprehensively evaluate and rank CMIP6 GCMs for the Kangsabati, Keliaghai, Silabati, and Dwarkeswer basins in West Bengal. This research systematically integrates five widely recognized Multi-Criteria Decision-Making (MCDM) techniques: MOORA (Multi-Objective Optimization by Ratio Analysis), SAW (Simple Additive Weighting), TOPSIS (Technique for Order of Preference by Similarity to Ideal Solution), VIKOR (Vlse Kriterijumska Optimizacija Kompromisno Resenje), and CP (Compromise Programming), to facilitate a comprehensive evaluation framework. These MCDM methods are combined with three distinct weighting methodologies to refine the decision-making process and enhance the robustness of rankings. The weighting methods employed are: (i) the entropy method, which quantifies the inherent importance of criteria based on data variability; (ii) the Criteria Importance Through the Inter-Criteria Correlation (CRITIC) approach, which accounts for the intensity of relationships among criteria to assign weights; and (iii) the equal weightage method, which ensures a balanced consideration of all criteria without bias.

The integration of these weighting techniques with the selected MCDM methods is strategically designed to minimize the influence of subjective biases and uncertainty in the evaluation process. This approach not only improves the reliability of the ranking outcomes but also provides a more transparent and strong decision-making framework. By utilizing the complementary strengths of these methods, this study seeks to offer a robust mechanism for addressing complex multi-criteria decision-making challenges, ensuring that the resulting rankings are reliable.

To conduct this study, the National Aeronautics and Space Administration (NASA) Earth Exchange Global Daily Downscaled Projections (NEX-GDDP) dataset, a high-resolution, statistically downscaled, and bias-corrected CMIP6 dataset is utilized, alongside India Meteorological Department (IMD) gridded daily rainfall data as a reference. By applying 17 distinct PIs, this study ranks a selection of 24 CMIP6 GCMs based on their rainfall simulation performance. This approach allows for ensemble modeling, capturing a broad range of potential climate outcomes and identifying consistent trends across models. The best-performing GCMs identified in this study could serve as valuable tools for climate adaptation and mitigation in climate-vulnerable regions.

5.2. Methodology

This study evaluates the effectiveness of 24 GCMs within the KKSD basins over a historical timeframe of 64 years, spanning from 1950 to 2014. Table 2.1 provides a complete overview of the 24 GCMs used in this analysis. The results from these models are compared against actual rainfall data sourced from the gridded IMD dataset. To evaluate how accurately each GCM replicates real-world data, PIs are utilized to rank the models. In total, 17 PIs are incorporated into this study, examining various aspects such as efficiency, bias, and error. To enhance data reliability and reduce redundancy, these PIs are normalized using the vector

technique. The weighting factors for each PI are determined through three distinct methods, and MCDM techniques are employed to identify the top-performing GCMs.

5.2.1. Performance Indicators (PIs)

Performance indicators (PIs) are essential for evaluating the effectiveness of GCMs. A range of 17 PIs, including correlation coefficient (CC), root mean square error (RMSE), coefficient of determination (R^2), PBIAS, sum of squared error (SSE), mean absolute error (MAE), mean absolute percentage error (MAPE), mean bias error (MBE), normalized RMSE (NRMSE), standard deviation (SD), Nash-Sutcliffe Efficiency (NSE), Kling-Gupta Efficiency (KGE), Taylor Skill Score (TSS), modified TSS (MTSS), Kolmogorov-Smirnov test (KST), Index of Agreement (IoA), and Skill Score (SS), are used to assess the performance of each model. These indicators are selected for their ability to highlight different aspects of model performance. To maintain consistency in the results, a comprehensive set of PIs is used, with similar results grouped into clusters and treated as unified entities. A detailed list of the selected PIs can be found in Table 2.2.

5.2.2. Weight Criteria Technique

The weighting of the PIs is crucial for determining their importance in the final ranking. Three distinct weighting techniques are applied: entropy, CRITIC, and equal weightage.

- Entropy Method: This technique calculates the weights based on the amount of information provided by each PI.
- CRITIC Method: This objective method computes weights by considering the degree of contrast and conflict between the PIs. It uses correlation analysis to assess how distinct the PIs are from one another, and it incorporates the standard deviation of normalized criterion values. CRITIC is a more sophisticated approach as it accounts for the interaction between criteria, unlike the entropy method which solely focuses on the information content of the PIs.
- Equal Weightage: This approach assigns equal importance to all PIs, simplifying the analysis by eliminating potential bias introduced through subjective weight assignments. It ensures that no single PI disproportionately influences the ranking.

5.2.3. Multi-Criteria Decision-Making (MCDM)

To calculate the rankings of the GCMs, five different MCDM techniques are used: SAW, TOPSIS, VIKOR, MOORA, and CP. Each method has its unique advantages and challenges, which is why they are employed to ensure robustness and consistency in the results.

- Simple Additive Weighting (SAW): SAW is one of the most widely used decision-making techniques, valued for its simplicity and ease of implementation. It works by aggregating the weighted scores across all criteria.
- Technique for Order of Preference by Similarity to Ideal Solution (TOPSIS): TOPSIS evaluates alternatives by comparing their distance to an ideal solution, aiming to select the alternative that is closest to the ideal and farthest from the worst. This method

assumes that the attributes are independent, which may not always be the case in complex systems.

- Vlse Kriterijumska Optimizacija Kompromisno Resenje (VIKOR): VIKOR focuses on finding a compromise solution in situations where multiple conflicting criteria must be balanced. While it is effective at handling such conflicts, VIKOR requires careful attention to the subjective weighting of criteria, which can introduce uncertainty in its outcomes.
- Multi-Objective Optimization based Ratio Analysis (MOORA): MOORA uses a ratio-based approach that compares the performance of alternatives using squared responses. It is especially effective at considering the relationships between alternatives and criteria comprehensively, though it requires non-zero and non-negative data, which could limit its applicability in some situations.
- Compromise Programming (CP): CP is a straightforward multi-objective optimization technique that does not require preference data but can accommodate it. It aims to identify a highly efficient compromise.

In this study, employing multiple MCDM methods ensures that the results are both robust and consistent. This diversity in approaches helps account for different model behaviors and biases, enhancing the reliability of the final rankings of GCMs.

5.3. Results and Discussion

A range of PIs is employed to compare rainfall data generated by the NEX-GDDP GCMs with IMD gridded observations. 17 PIs are used to evaluate efficiency, error, and biases. Following this, three distinct methods are applied to calculate the weights for each PI, aiming to assess the variations in weighting techniques that influence performance outcomes. Subsequently, individual GCMs are ranked using various MCDM methods based on different PIs.

Annual rainfall variations and the ensemble mean of 24 CMIP6 GCMs over the 64-year baseline period are displayed in Fig. 5.1. The annual rainfall ranges from 994 mm in 2010 to 2029 mm in 1971. Outputs from the 24 CMIP6 models are represented in grey, the CMIP6 ensemble means in red and observed IMD values in blue. The results show that using the direct ensemble mean of GCMs may not be advisable due to the reduced fluctuation in outcomes. While the average rainfall matches closely with IMD observations, the variation in the ensemble mean does not align with the IMD data. Therefore, it is recommended to rank the models first and then create an ensemble based on their rankings for better accuracy.

5.3.1. PIs and Weight

PIs are used to evaluate the accuracy of GCMs replicating observed data. For the entire basin, PIs are calculated monthly, with their ranges detailed in Table 5.1. To ensure no single PI dominates the calculation of weights due to its broader range, a vector normalization technique is applied. This technique, recommended for specific weight computation and MCDM methods, is utilized to minimize discrepancies in results. Table 5.1 presents the extreme value of PIs for rainfall from the NEX-GDDP dataset, along with their corresponding weights. The variability in PI weights across different methods highlights the need to investigate each ranking approach with its specific weighting technique.

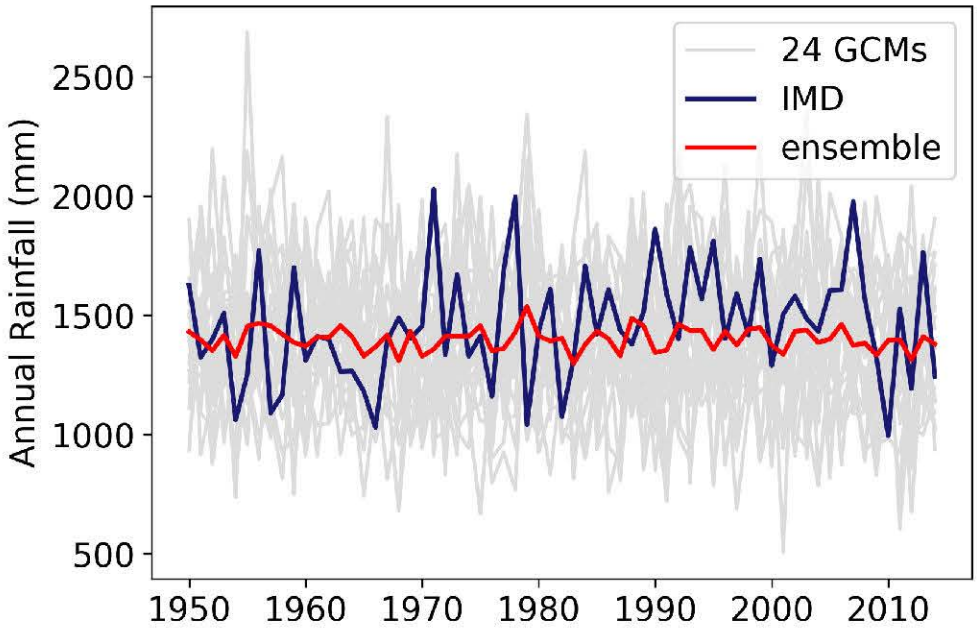

Fig. 5.1. Annual rainfall from 24 CMIP6 GCMs compared with IMD data and the ensemble of CMIP6 GCMs for the baseline period (1950-2014).

In the weight analysis, higher-percentage (important) weights are marked in red. For the entropy method, critical PIs include CC, R^2, NSE, KGE, TSS, MTSS, KST, IoA, and SS. In contrast, the CRITIC method identifies PBIAS, MBE, KGE, SD, TSS, MTSS, KST, IoA, and SS as significant PIs. Common PIs between these methods are KGE, TSS, MTSS, KST, IoA, and SS. However, entropy also emphasizes efficiency-related PIs such as CC, R^2, and NSE, while CRITIC highlights bias-related PIs like PBIAS, MBE, and SD. Particularly, SS is the most influential PI under the CRITIC method. Based on these findings, combining all effective PIs is recommended for a more robust ranking calculation.

Table 5.1. Range and weight of PIs.

PIs	Min	Max	Entropy	CRITIC	Equal Weight
CC	0.679	0.788	0.092 (9%)	0.021 (2%)	0.058
RMSE	2.859	3.77	0.023 (2%)	0.030 (3%)	0.058
R^2	0.461	0.621	0.091 (9%)	0.030 (3%)	0.058
NSE	0.254	0.572	0.090 (9%)	0.030 (3%)	0.058
PBIAS	0.910	7.492	0.016 (2%)	0.075 (8%)	0.058
SSE	6377.14	11122.88	0.022 (2%)	0.047 (5%)	0.058
MAE	1.830	2.340	0.023 (2%)	0.049 (5%)	0.058
MAPE	1.830	2.340	0.023 (2%)	0.049 (5%)	0.058
MBE	-0.296	-0.036	0.016 (2%)	0.081 (8%)	0.058
NRMSE	0.722	0.954	0.023 (2%)	0.045 (5%)	0.058
KGE	0.651	0.785	0.092 (9%)	0.066 (7%)	0.058
SD	4.408	4.963	0.023 (2%)	0.069 (7%)	0.058
TSS	0.826	0.894	0.092 (9%)	0.070 (7%)	0.058
MTSS	0.489	0.639	0.091 (9%)	0.070 (7%)	0.058
KST	0.196	0.219	0.092 (9%)	0.094 (9%)	0.058
IoA	0.811	0.884	0.092 (9%)	0.068 (7%)	0.058

SS	0.920	0.977	0.092 (9%)	0.097 (10%)	0.058

Note: Red color represents the effective PI

5.3.2. Ranking of GCMs Using Different Parameters

Ranking GCMs based on various parameters is crucial due to the differing weightage of these metrics. To address this, rankings were calculated for individual parameters, offering critical insights into the accuracy of GCMs in replicating observed climate behaviours (Fig. 5.2). Models that rank highly by exhibiting minimal bias and robust efficiency metrics are considered to perform better.

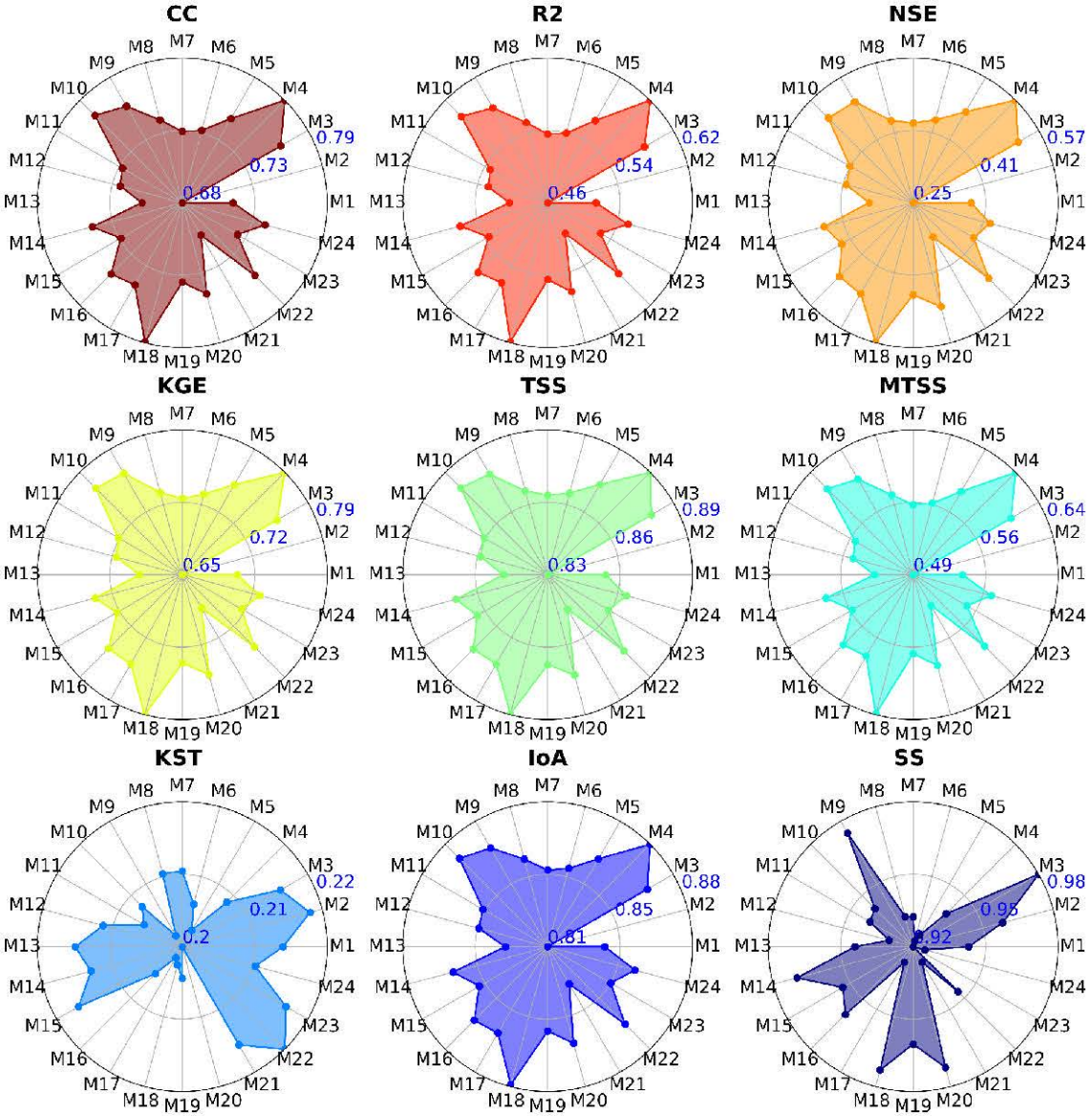

Fig. 5.2. Radar graphs represent the efficiency-based PIs with points near the outer periphery considered to be ideal.

However, no single metric can fully evaluate GCM performance. A comprehensive assessment requires combining multiple metrics to provide a holistic evaluation.

From Fig.5.2, it is evident that for efficiency-based PIs, points located near the outer edges of the radar plots indicate optimal performance. In contrast, for error and bias-based PIs, points situated closer to the centre of the radar plots are considered most desirable, as shown in Fig. 5.3.

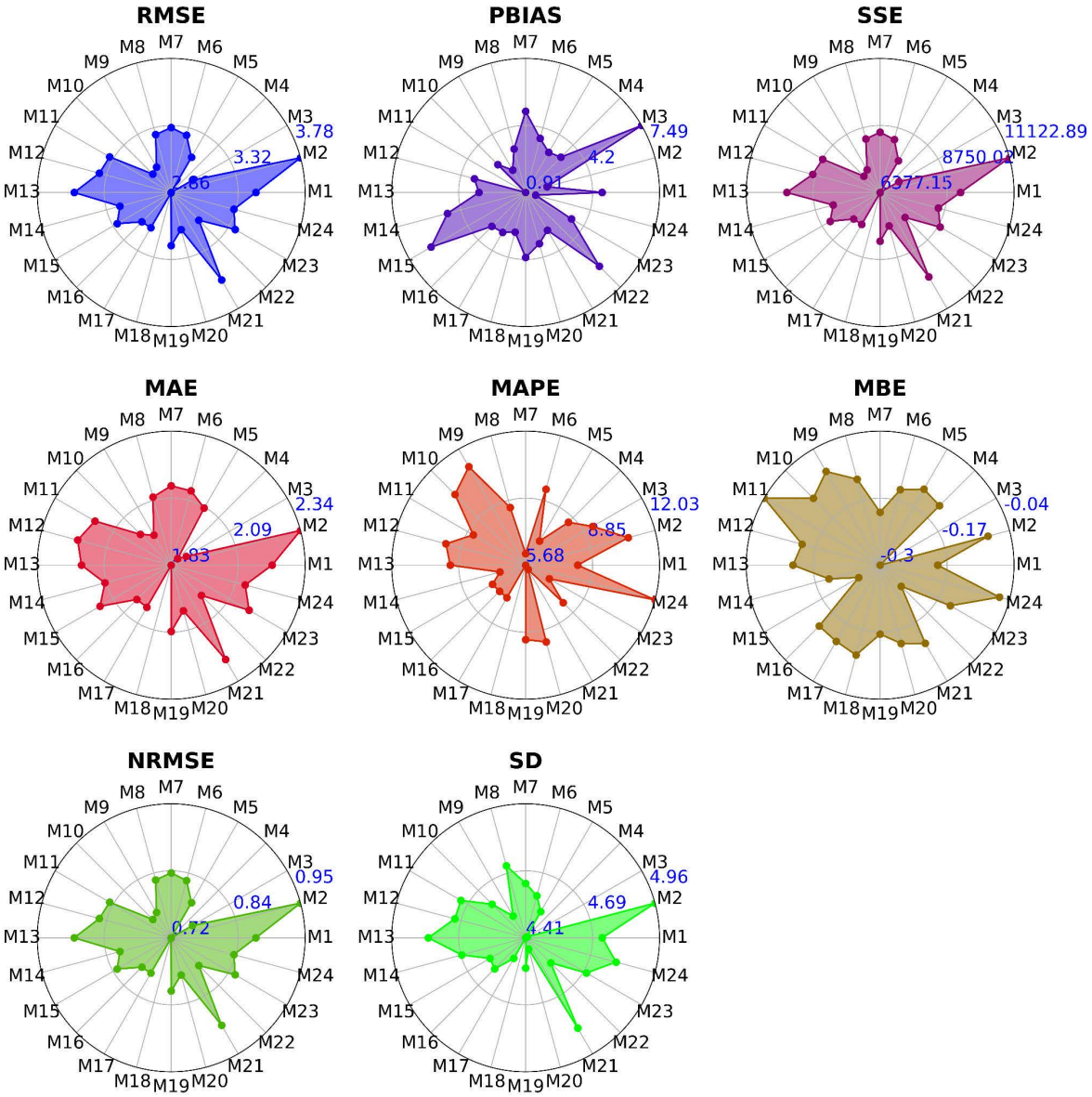

Fig. 5.3. Radar graphs represent the error-based PIs with points near the centre of the plot considered to be ideal.

The plots reveal consistent ranking patterns for PIs such as CC, R^2, KGE, TSS, IoA, MTSS, and NSE, while metrics like NRMSE, SSE, and RMSE also show similar trends. Furthermore, the rankings for MAE, SD, MBE, and MAPE are inconsistent. Given these patterns, it is advisable to use a single representative PI for groups of similar metrics to simplify the evaluation process.

After normalizing all PIs to maintain consistency in analysis, the average value for each GCM was calculated. This average was used to determine the top-performing models. As shown in Fig. 5.4, the top five GCMs are M18, M4, M11, M9, and M10. These rankings serve

as a foundation for applying five different MCDM techniques, which use the top five GCMs as references. This approach enables the determination of a final combined ranking for the CMIP6 GCMs.

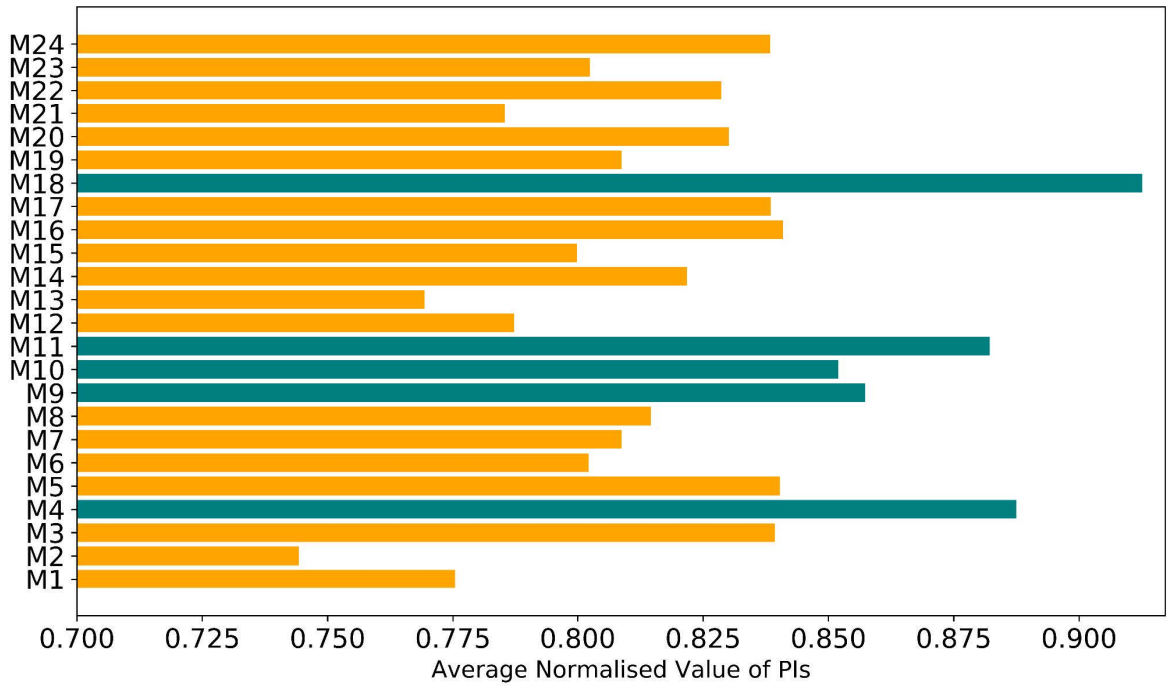

Fig. 5.4. Ranking of GCMs based on PIs (green color represents the top five best GCMs).

5.3.3. MCDM based ranking of GCMs

The ranking of GCMs for rainfall over the KKSD basins is determined using five MCDM techniques: SAW, TOPSIS, VIKOR, MOORA, and CP, with each technique applying three different weighting methods. The rankings for each method, shown in Table 5.2, illustrate that MOORA, CP, and SAW produce consistent results across all weight methods, while the remaining methods yield varying results. When comparing the MCDM rankings with those based on individual parameter rankings, it becomes clear that VIKOR does not provide consistent rankings and is therefore not recommended. MOORA, CP, and SAW, however, show around 80% consistency with the individual parameter-based rankings. TOPSIS, on the other hand, only delivers desirable results with the equal weight method.

Based on the rankings from the different MCDMs, VIKOR and TOPSIS are not recommended for ranking CMIP6 models for rainfall over eastern India. According to MOORA, the top five GCMs across all weight methods are M18, M4, M10, M9, and M3, with each model developed by a different modeling centre: M3 (India), M4 (China), M9 (Canada), M10 (Europe), and M18 (Japan). For VIKOR, the best-ranked model is M2 (Australia) for two weight methods, but the rankings vary for other methods. For SAW, M11 (Europe) and M3 (India) are the top two models, with the remaining models aligning with the ranking of MOORA.

Table 5.2. Ranking of CMIP6 models based on MCDM with different weight techniques (different bold colors show the top five models based on PIs).

Rank	MOORA			VIKOR			SAW			TOPSIS			CP		
	Entropy	Equal	CRITIC	Entropy	Equal	CRITIC	Entropy	Equal	CRITIC	Entropy	Equal	CRITIC	Entropy	Equal	CRITIC
1	**M18**	**M18**	**C18**	M2	M2	M23	**M18**	**M18**	**M11**	M3	M19	M19	**M9**	**M9**	M24
2	**M4**	**M4**	**M4**	M21	M23	M21	**M4**	**M4**	**M18**	**M9**	M16	M15	**M18**	M24	**M11**
3	**M10**	M3	M3	M23	**M11**	M6	**M10**	**M11**	**M4**	**M18**	**M11**	M16	**M10**	**M11**	**M9**
4	**M9**	**M9**	**M9**	M6	M21	M2	M3	**M9**	**M9**	M20	M15	**M11**	**M4**	**M18**	**M10**
5	M3	**M10**	**M10**	M24	M6	M24	**M9**	**M10**	M24	M14	M22	M14	M24	**M10**	**M18**
6	M20	M20	M20	M12	M24	**M11**	M22	M24	**M10**	M2	M14	M22	M17	M17	M17
7	M16	M16	M16	M13	M20	M12	M16	M3	M3	M16	M13	M2	M5	**M4**	M5
8	M17	M17	M17	M20	M12	M5	M20	M16	M16	M19	**M18**	M20	M16	M5	M8
9	M5	M22	M22	M17	M17	M20	M5	M20	M20	M15	M20	M13	**M11**	M16	M2
10	M22	M5	M5	M5	M5	M17	M17	M17	M17	**M4**	M1	**M10**	M20	M8	M16
11	M14	M19	M19	M7	M3	M7	M14	M5	M5	M22	**M10**	**M18**	M8	M20	**M4**
12	M19	M14	M14	M1	M13	M8	M24	M22	M22	**M10**	**M9**	M24	M6	M6	M20
13	M8	M8	M6	M8	M1	**M9**	**M11**	M8	M8	**M11**	M24	M1	M19	M23	M21
14	M6	M6	M8	**M11**	M7	M19	M19	M14	M14	M1	M2	**M4**	M23	M12	M13
15	M24	M24	M15	M19	**M9**	M13	M8	M19	M19	M17	**M4**	**M9**	M12	M21	M23
16	M15	M15	M7	**M9**	M15	M1	M6	M6	M6	M8	M8	M3	M14	M13	M12
17	M7	M7	M24	M16	M8	M16	M15	M7	M23	M5	M3	M8	M13	M2	M6
18	**M11**	**M11**	**M11**	M15	M19	M15	M7	M15	M12	M13	M21	M7	M21	M19	M19
19	M12	M12	M12	**M18**	M22	**M18**	M23	M23	M7	M7	M7	M21	M7	M14	M1
20	M23	M23	M23	**M10**	**M18**	M3	M12	M12	M15	M24	M12	M12	M1	M1	M14
21	M1	M1	M1	M22	M16	**M10**	M1	M1	M13	M12	M17	M17	M22	M7	M7
22	M13	M13	M13	**M4**	M10	M22	M13	M13	M21	M6	M5	M5	M2	M22	M22
23	M21	M21	M21	M14	M14	**M4**	M21	M21	M2	M23	M6	M6	M15	M15	M15
24	M2	M2	M2	M3	**M4**	M14	M2	M2	M1	M21	M23	M23	M3	M3	M3

TOPSIS shows different best GCMs depending on the weight method used: M3 (India) for entropy weight and M19 (Germany) for the other weight criteria.

When comparing this study to similar studies, such as Raju et al. (2017), who ranked CMIP5-based GCMs for India, it is observed that while they used CMIP5 models and several parameters, the ranking process remains similar. Raju et al. (2017) found MIROC5 to be the best model for maximum temperature and CESM1-CAM5 the best for minimum temperature in the northeastern region. This study has addressed several gaps in previous research, leading to improved results and more refined ranking methodologies.

5.3.4. Selection and Ensemble of GCMs for Projection

The final ranking of various GCMs for simulating observed rainfall, derived through multiple MCDM techniques, is presented in Table 5.2. Combined individual parameter-based rankings of the GCMs are illustrated in Fig. 5.4. The top five ranked GCMs identified using MCDM for rainfall simulation are M9, M18, M11, M4, and M10, whereas the top-ranked models for individual parameters include M18, M4, CM11, M9, and M10. However, when MCDM rankings are integrated with individual parameter performances, the rankings adjust to M9, M18, M3, M4, and M10 (Fig. 5.5).

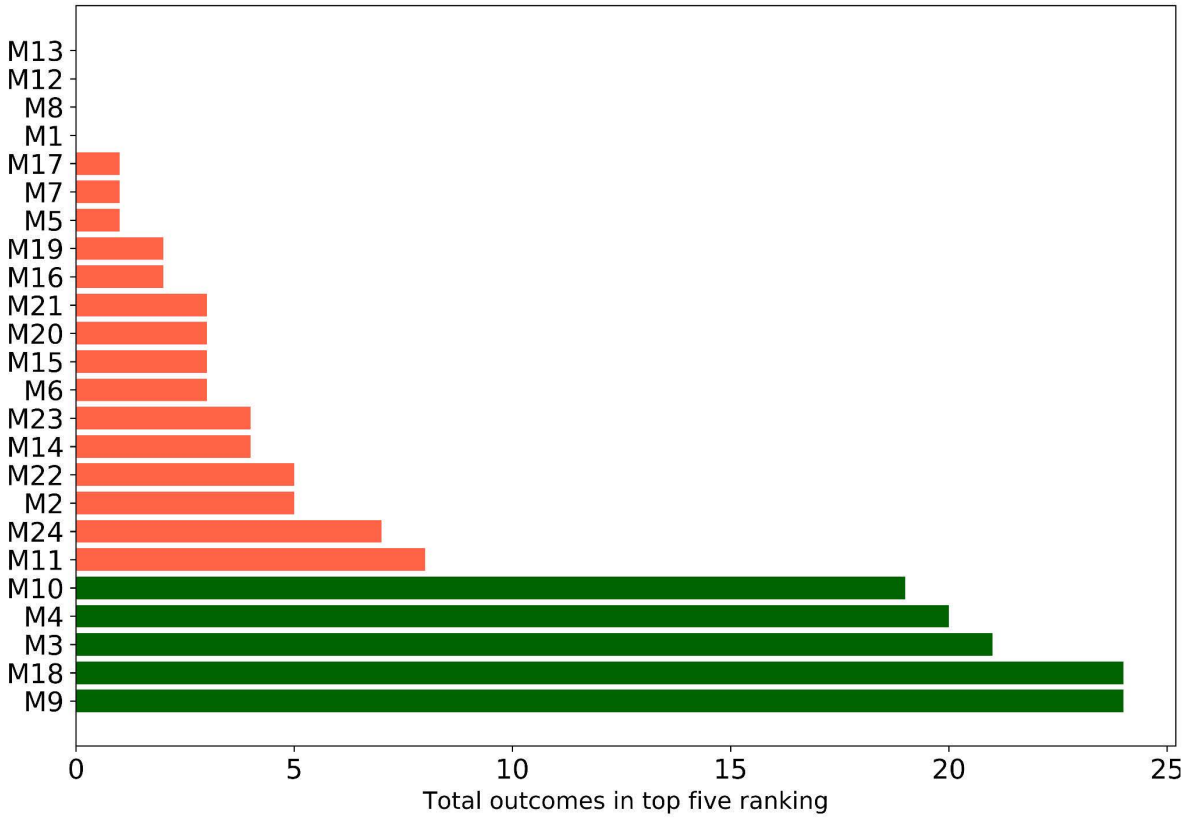

Fig. 5.5. Visualization of GCM rankings achieved through the combined impact of MCDM and PIs.

Particularly, M11, despite appearing frequently in the top five rankings, is excluded from the final ensemble recommendations due to its outputs showing minimal PBIAS, which may lead to an imbalance in the combined evaluation. The rankings were determined based on the frequency of a GCM appearing among the top five models across all methods. To ensure

robust projections, an ensemble approach comprising the highest-ranked GCMs is encouraged. Ensembles, being weighted by ranked frequencies, were observed to provide outputs closely resembling the observed data.

The weighted contributions for the top five models, calculated based on their relative frequency in the top rankings, were 22%, 22%, 19%, 19%, and 18%. This weighting method underscores the reliability of the ensemble by highlighting consistent model performance. Figure 5.5 displays the outcomes of different GCMs appearing among the top-ranked models, while Fig. 5.6 illustrates that almost all top-ranked models yield outputs that closely align with the observed data trends.

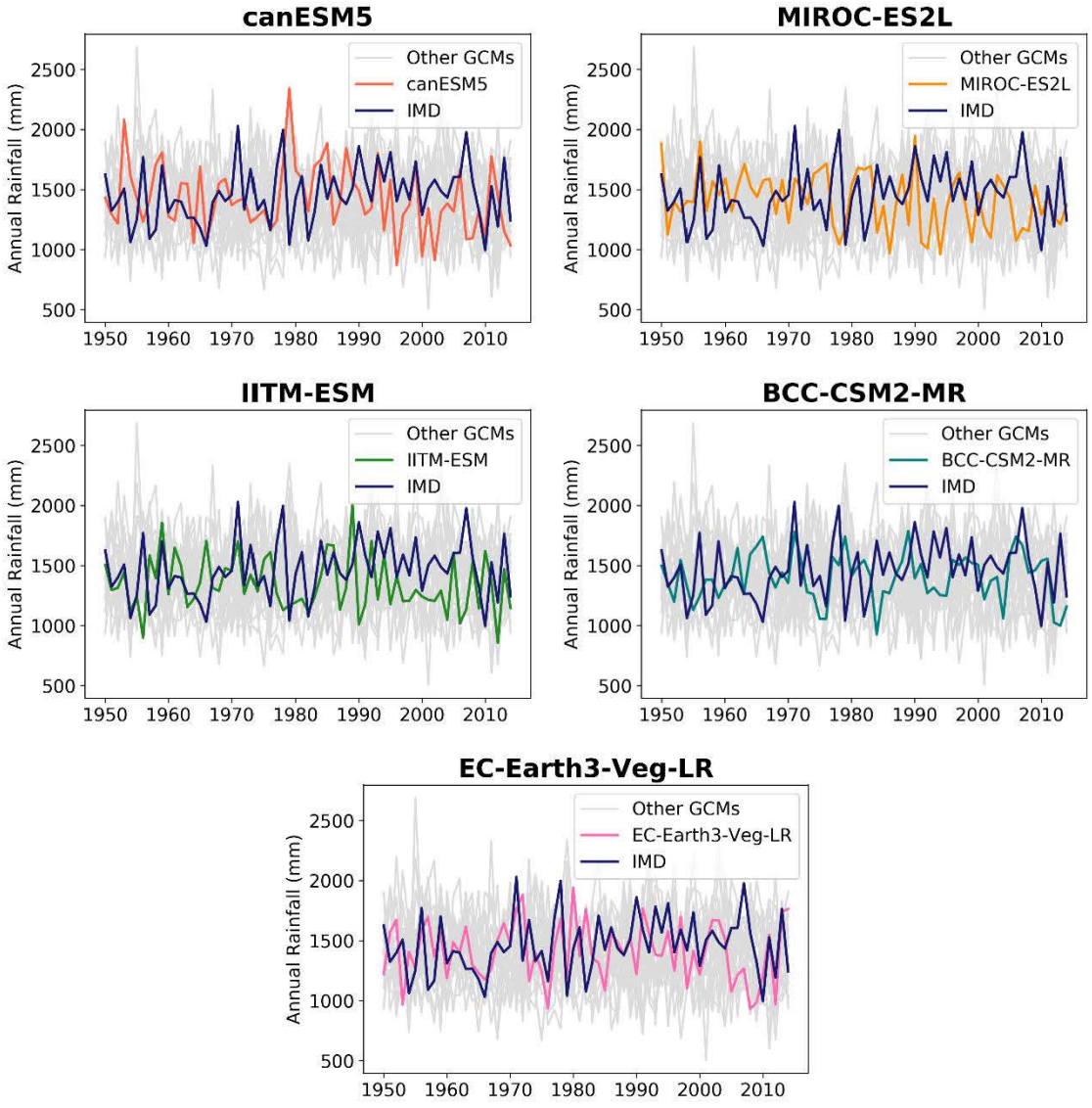

Fig. 5.6. Representation of individual model historical projection of top five rank models with IMD.

M9 (canESM5) emerged as the best-performing GCM due to its consistent appearance in the top five rankings (24 times), followed by M18 (MIROC-ES2L), which also appeared 24 times in 160 iterations. Other high-performing models, including M3 (IITM-ESM), M4 (BCC-

CSM2-MR), and M10 (EC-Earth3-Veg-LR), appeared 19, 19, and 18 times, respectively, in the top five rankings.

When prioritizing PIs as a performance criterion, M18 (MIROC-ES2L) was identified as the best GCM. The outcomes emphasize the importance of selecting models that exhibit robust historical performance for projecting future climate. While individual GCMs display unique characteristics and variability in performance, none of the models achieved a perfect replication of observed rainfall patterns, supporting the necessity of ensemble approaches.

The ensemble methodology adopted in this study utilized a simple weighted mean. Four ensemble combinations were tested to identify the ideal solution, as presented in Fig. 5.7. The results demonstrate that the distortion from individual models reduces as more top performing models are included in the ensemble approaches. The best ensemble was identified as the one that closely matched the observed data, which included five top-ranked GCMs. While the ensemble improved the overall simulation accuracy, an important limitation was its incapability to replicate the intensity of rainfall peaks observed in historical data.

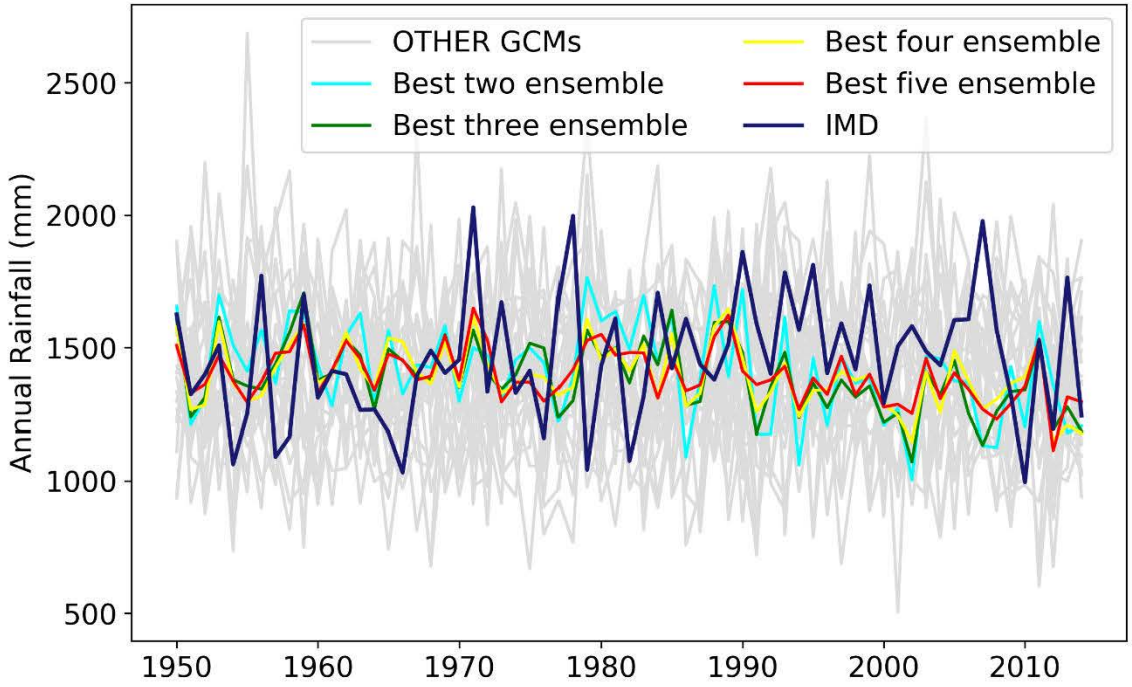

Fig. 5.7. Representation of ensemble top-rank models with IMD as reference data.

Among individual models, M18 and M4 captured the rainfall peak better than others, though the peaks did not align perfectly with observed data. The ensemble results underscore the potential for enhancing projections by integrating machine learning models for weighted ranking and peak intensity estimation. The disparities among GCMs are attributed to differences in model physics, spatial and temporal resolutions, forcing scenarios, initial conditions, feedback mechanisms, and tuning processes.

The superior rankings of certain GCMs reflect their alignment with historical climatology, capacity to simulate observed trends, and consistency with current climate understanding. Previous studies evaluating CMIP6 GCMs, such as Reddy and Saravanan (2023), support these findings, highlighting the strong performance of EC-Earth3, EC-Earth3-Veg, and MIROC models in projecting rainfall and extreme precipitation indices over India. These

results are validated by the present study, which also identified EC-Earth3-Veg-LR as a high-performing GCM for Eastern India.

The reliability of the findings of this study was strengthened through the application of robust statistical techniques to mitigate outliers, cross-validation to ensure consistency and an exhaustive review of existing methodologies. Despite the robustness of the results, limitations include the inherent subjectivity in assigning weights to performance criteria and uncertainties in model outputs and observational data. Findings from the research contribute valuable insights for climate researchers and policymakers, highlighting the importance of ensemble modeling for improved climate projections and adaptation strategies.

5.4. Conclusions

This study aimed to replicate the rainfall characteristics across the KKSD basins by evaluating the performance of 24 CMIP6 GCMs using 17 statistical PIs and five MCDM techniques, coupled with three different weighting criteria methods. The following are the main findings from the analysis:

- **Variability in GCM Performance:** The performance of GCMs varies significantly across different PIs, highlighting the need to account for multiple factors when evaluating models. Each performance indicator gives a different perspective on model accuracy, suggesting that a holistic approach is required for model evaluation.
- **Weighting Approaches:** The study demonstrated that different weighting methods assign varying importance to the PIs, which in turn results in differing rankings of the GCMs. The discrepancies in the weight distributions emphasize the importance of considering the weighting methodology when selecting GCMs for climate projections.
- **Top-Performing GCMs:** For rainfall simulations, M9 (canESM5) and M18 (MIROC-ES2L) were identified as the best-performing models for the KKSD basins based on the cumulative ranking from all evaluation methods. The other top-ranked models include M3 (IITM-ESM), M4 (BCC-CSM2-MR), and M10 (EC-Earth3-Veg-LR).
- **Ensemble Models:** Several combinations of ensemble models performed better than individual GCMs, demonstrating the potential advantages of integrating multiple models. However, traditional ensemble methods did not adequately capture the peak values of the time series, indicating the need for more advanced ensemble techniques.
- **Recommendations for Future Work:** The results suggest that conventional ensemble methods may not be sufficient for accurate peak prediction in rainfall data. Future research could benefit from machine learning-based ensemble techniques, which could incorporate top-ranked GCMs as foundational models to improve predictive accuracy. Additionally, the methodology established in this study can be extended to assess climatic impacts across other regions and watersheds, offering a universal framework for GCM selection.
- **Application for Future Projections:** Given the robust and consistent ranking of GCMs for the KKSD basins, the study recommends the use of the top-ranked models for future climate projections under various SSPs (Shared Socioeconomic Pathways). This approach ensures that future climate assessments in the region are based on

models that have shown the most reliable performance in replicating observed rainfall patterns.

Overall, this study highlights the importance of selecting appropriate GCMs using a comprehensive evaluation approach that considers multiple performance indicators, weighting schemes, and model combinations. The findings provide valuable insights for improving future climate projections and enhancing the understanding of climatic impacts in the KKSD basins.

References

Anandhi, A. and Nanjundiah, R.S. (2015). Performance evaluation of AR4 Climate Models in simulating daily precipitation over the Indian region using skill scores. Theor. Appl. Climatol., 119(3–4), 551–566.

Deepthi, B. and Sivakumar, B. (2022). Performance assessment of general circulation models: application of compromise programming method and global performance indicator technique. Stoch. Environ. Res. Risk Assess., 36(6), 1761–1778.

Gusain, A., Ghosh, S. and Karmakar, S. (2020). Added value of CMIP6 over CMIP5 models in simulating Indian summer monsoon rainfall. Atmos. Res., 232,104680.

Jose, D.M. and Dwarakish, G.S. (2022). Ranking of downscaled CMIP5 and CMIP6 GCMs at a basin scale: case study of a tropical river basin on the South West coast of India. Arab. J. Geosci., 15(1), 1–23.

Paul, A.R. and Maity, R. (2023). Future projection of climate extremes across contiguous northeast India and Bangladesh. Sci. Rep., 13(1), 15616.

Raju, K.S., Sonali, P. and Kumar, D.N. (2017). Ranking of CMIP5-based global climate models for India using compromise programming. Theor. Appl Climatol., 128(3–4), 563–574.

Reddy, N.M. and Saravanan, S. (2023). Extreme precipitation indices over India using CMIP6: a special emphasis on the SSP585 scenario. Environ. Sci. Pollut. Res., 30(16), 47119–47143.

Ruan, Y., Yao, Z., Wang, R. and Liu, Z. (2018). Ranking of CMIP5 GCM skills in simulating observed precipitation over the Lower Mekong Basin, using an improved score-based method. Water, 10(12), 1868.

Shiru, M.S. and Chung, E.S. (2021). Performance evaluation of CMIP6 global climate models for selecting models for climate projection over Nigeria. Theor. Appl. Climatol., 146(1–2), 599–615.

Zamani, R. and Berndtsson, R. (2019). Evaluation of CMIP5 models for west and southwest Iran using TOPSIS-based method. Theor. Appl. Climatol., 137(1–2), 533–543.

Evaluation of Data Accuracy in CMIP6 Models

"Patel, G., Das, S. and Das, R. (2024). Accuracy of historical precipitation from CMIP6 global climate models under diversified climatic features over India. Environ. Dev., 50, 100998. https://doi.org/10.1016/j.envdev.2024.100998"

6.1. Introduction

Climate change is a significant global concern that affects many critical industries, including water supply, healthcare, energy production, and agriculture. Its impact is especially severe in regions that are vulnerable to environmental changes, where even slight shifts in climate can lead to major disruptions in both industries and ecosystems. Greenhouse gas (GHG) emissions play a crucial role in this situation, causing important alterations in the climatic system. To better understand and predict these effects, Global Climate Models (GCMs) have become vital resources. These models are broadly used to analyze past climate trends and forecast future conditions based on different GHG concentration scenarios, laying the groundwork for effective climate adaptation and mitigation efforts.

One of the major strengths of GCMs is their capability to forecast future climate changes based on different levels of greenhouse gas concentrations in the atmosphere. Through the Coupled Model Intercomparison Project (CMIP), these models are made available to the public, enabling researchers and the global community to study and comprehend the potential effects of climate change. However, it is important to recognize that many GCMs still face significant challenges, especially in accurately representing the physical processes that influence climate systems (Alizadeh 2022). This limitation is particularly noticeable when it comes to modeling regional climate events, where higher-resolution models are essential for effectively capturing the complexities of local climate dynamics (Hamed et al. 2022).

The evolution of CMIP models, starting from CMIP1 and concluding in the latest CMIP6, has focused on overcoming previous limitations. The CMIP6 models portray an improved realistic depiction of the physical processes of the Earth and incorporate projections based on the Shared Socioeconomic Pathways (SSPs). These updated models consider recent socioeconomic trends, technological progress, and environmental shifts like land use, creating a more precise framework for evaluating the effects of climate change policies. However, despite these improvements, GCMs continue to face challenges in accurately forecasting precipitation patterns, especially regarding regional and seasonal differences.

Previous studies have shown notable differences in the outputs of GCMs, where certain models either overpredict or underpredict actual precipitation levels, especially in areas with complicated topography (Yazdandoost et al. 2021, Sarkar and Maity 2022, Sekar and Gumus 2022, Wang et al. 2023). These issues highlight the importance of ongoing enhancements in GCMs to better reflect the variations in regional precipitation and other climate-related factors.

This study investigates the historical assessment of CMIP6 GCMs, specifically in the Indian region along with KKSD basins. The main objective is to evaluate how well these models reflect actual climate data and to examine their performance across various climatic zones and geographical features, including mountain ranges. By analyzing the model outputs against observed data, the research seeks to uncover any biases and identify areas where GCMs could be improved.

This research stands out due to its thorough evaluation of the historical performance of CMIP6 GCMs specifically in the Indian region. It offers a detailed analysis that highlights regional climate features and the real-world impacts of GCM performance. The outcomes of this study could play an important role in shaping future model development, especially in enhancing GCM accuracy across various climatic zones and in mountainous areas, where climate variability tends to be more significant. Additionally, these findings may aid in climate change mitigation efforts by delivering more precise forecasts of future climate events, which are vital for effective planning and decision-making in sectors sensitive to climate change.

6.2. Study Area

This study concentrates on evaluating precipitation from the CMIP6 models over India, a nation strongly influenced by climate dynamics and variability. India experiences an average annual precipitation of approximately 1200 mm, with significant regional heterogeneity. Northeastern India, for instance, receives more than 4000 mm of annual precipitation, highlighting the spatial variability of rainfall patterns. Climatic zones of India are shown in Fig. 6.1, prepared using data from Beck et al. (2018).

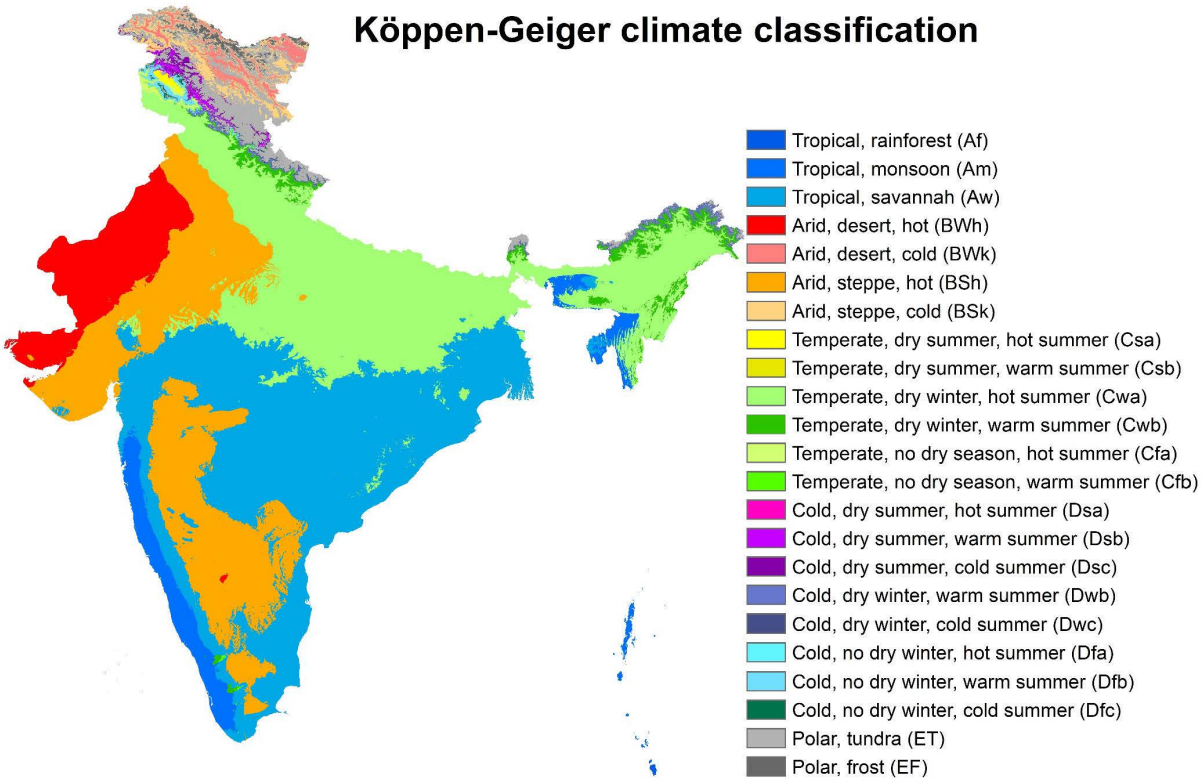

Fig. 6.1. Climate zones in India according to the Köppen-Geiger climate classification.

In this study, various districts and KKSD basins across India were selected for analysis, representing diverse climatic zones based on the Köppen-Geiger climate classification system. A detailed explanation of the Köppen climate symbols and their defining criteria can be found in Peel et al. (2007). Table 6.1 presents the Köppen climate symbols utilized in this study. A total of 44 districts and KKSD basins across India were randomly selected for analysis to identify regions where precipitation estimation errors are most evident.

Table 6.1. Details of Köppen climate indications (Peel et al. 2007).

1st	2nd	3rd	Symbol
A (Tropical)	f (Rainforest) m (Monsoon) w (Savanna, Dry Winter) s (Savanna, Dry Summer)		Af Am Aw As
B (Dry)	W (Arid Dessert) S (Semi-Arid or Steppe)	h (Hot) k (Cold)	BWh, BWk, BSh, BSk
C (Temperate)	w (Dry Winter) f (No Dry Season) s (Dry Summer)	a (Hot Summer) b (Warm Summer) c (Cold Summer)	Cwa, Cwb, Cwc, Cfa, Cfb, Cfc, Csa, Csb, Csc
D (Continental)	w (Dry Winter) f (No Dry Season) s (Dry Summer)	a (Hot Summer) b (Warm Summer) c (Cold Summer) d (Very Cold Winter)	Dwa, Dwb, Dwc, Dwd, Dfa, Dfb, Dfc, Dfd, Dsa, Dsb, Dsc, Dsd
E (Polar)		T (Tundra) F (Frost)	ET, EF

The selection of districts was guided by the diverse climatic conditions across the country, ensuring representation from each state. We have listed all the chosen locations in Table 6.2 and Fig 6.2. The districts were selected randomly, and during our analysis, we noticed that the northern districts of West Bengal and all the districts of Sikkim exhibit similar characteristics. Based on this similarity we decided to combine these districts into one group.

Table 6.2. Details of locations selected throughout India.

Location Code	Location	State	Location Code	Location	State
D1	Kurung Kumey	Arunachal Pradesh	D14	Varanasi	Uttar Pradesh
D2	Mangan Namchi Pakyong Soreng Gangtok Geyzing	Sikkim	D15	Barmer	Rajasthan
			D16	Kolasib	Mizoram
			D17	Banas Kantha	Gujrat
			D18	Gajapati	Orissa
			D19	West Godavari	Andhra Pradesh
			D20	Korba	Chhattisgarh
D3	Chamoli	Uttarakhand	D21	Deogarh	Odisha
D4	Udupi	Karnataka	D22	Kancheepuram	Tamil Nadu
D5	Ratnagiri	Maharashtra	D23	Dhanbad	Jharkhand
D6	Kullu	Himachal Pradesh	D24	Warangal	Telangana
D7	Chandel	Manipur	D25	South Tripura	Tripura
D8	Dimapur	Nagaland	D26	Nalanda	Bihar
D9	Pulwama	Jammu and Kashmir	D27	Jhunjhunun	Rajasthan

D10	Tirap	Arunachal Pradesh	D28	Sonipat	Haryana
D11	Alipurduar Darjeeling Jalpaiguri Kalimpong Koch Bihar	North West Bengal	D29 D30 D31 D32 D33	Narmada Nagpur Amritsar Gwalior Trivandrum	Gujarat Maharashtra Punjab Madhya Pradesh Kerala
D12	East Khasi Hill	Meghalaya	D34	Coimbatore	Tamil Nadu
D13	Dibrugarh	Assam	D35	Nizamabad	Telangana
			KKSD	Kangsabati Keliaghai Silabati Dwarkeswer	West Bengal

Figure 6.2 illustrates the geographical positions of the chosen districts, surrounding a diverse range of climatic zones, topographies, and annual precipitation levels across India.

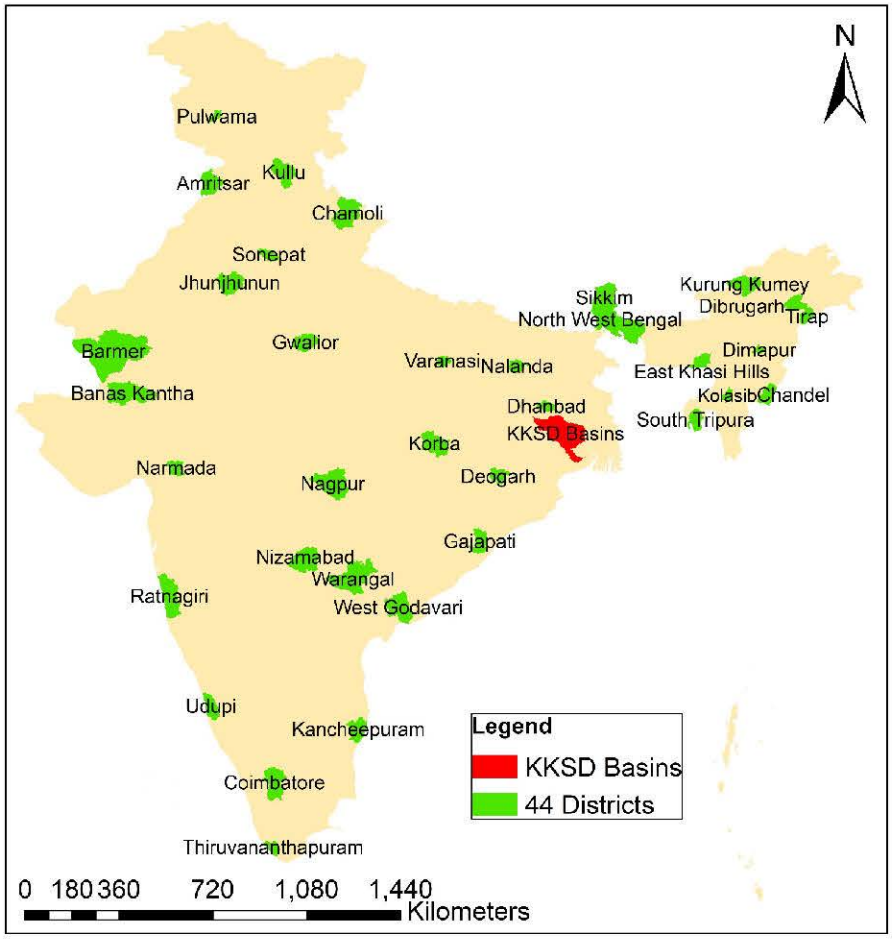

Fig. 6.2. Demarcation of locations utilized for study.

6.3. Methodology

This study, conducted across randomly selected locations and KKSD basins in India, aims to evaluate the accuracy of climate models in simulating historical precipitation patterns using data from 24 CMIP6 models compared to India Meteorological Department (IMD) data

spanning from 1950 to 2014. By focusing on the assessment of CMIP6 models in capturing these patterns, the study provides insights into climate model accuracy and reliability, contributing valuable information for climate-related decision-making.

The IMD gridded dataset serves as the reference for assessing model data error, with a resolution of 0.25 degrees standardized across both observed and model datasets. Four performance metrics Modified Taylor Skill Score (MTSS), Refined Index of Agreement (RIoA), correlation coefficient (CC), and percentage bias (PBIAS) are used to evaluate model performance based on three categories: bias, correlation, and efficiency. Additionally, the study compares model performance based on Köppen-Geiger climate classifications and topographical features, particularly hilly areas, to better understand how well the models reflect regional climate variations, ultimately guiding effective climate adaptation and mitigation strategies. Table 6.3 represents the locations with absolute PBIAS along with average annual precipitation.

Table 6.3. Absolute PBIAS and annual average precipitation of different locations.

Location Code	Absolute PBIAS (%)	Avg. Annual Precipitation (mm)	Location Code	Absolute PBIAS (%)	Avg. Annual Precipitation (mm)
D1	52.4	2959.8	D19	12.2	1139.1
D2	43.3	2826.2	D20	12.0	1351.8
D3	42.3	1359.3	D21	11.8	1456.6
D4	41.4	4032.3	D22	10.9	1163.4
D5	36.1	2826.2	D23	9.6	1317
D6	34.3	1103.6	D24	9.2	1050.1
D7	28.3*	1522.2	D25	5.9*	2369.7
D8	27.3*	1587.4	D26	5.5	1016.6
D9	25.8	980	D27	5.1	466.9
D10	24.2	2462.5	D28	4.5*	630.8
D11	23.8	3216.7	D29	3.8*	1009.6
D12	19.1*	3487.4	D30	3.0	1119.4
D13	18.5	2437.8	D31	2.3	701.1
D14	18.3	954.7	D32	1.9	808.3
D15	16.4	303.5	D33	1.7*	1624.2
D16	15.6*	2579.8	D34	1.6*	1188.7
D17	15.5	593.6	D35	0.3*	975.9
D18	15.1	1244.5	KKSD	7.45	1450

*shows positive PBIAS

6.4. Results and Discussion

6.4.1. Assessment Based on Statistics

The study utilized observed data alongside CMIP6 model simulations to generate graphical representations of precipitation patterns on annual and monthly scales. Kurung Kumey (Arunachal Pradesh), exhibiting the largest PBIAS value, and Nizamabad (Telangana), with the smallest PBIAS value, were selected as case studies to illustrate the extremes of model performance (Fig. 6.3). These graphical representations help identify potential limitations in

the models, particularly in capturing extreme precipitation events or specific seasonal fluctuations. For Kurung Kumey, where PBIAS is highest, the discrepancies highlight significant challenges in accurately simulating precipitation.

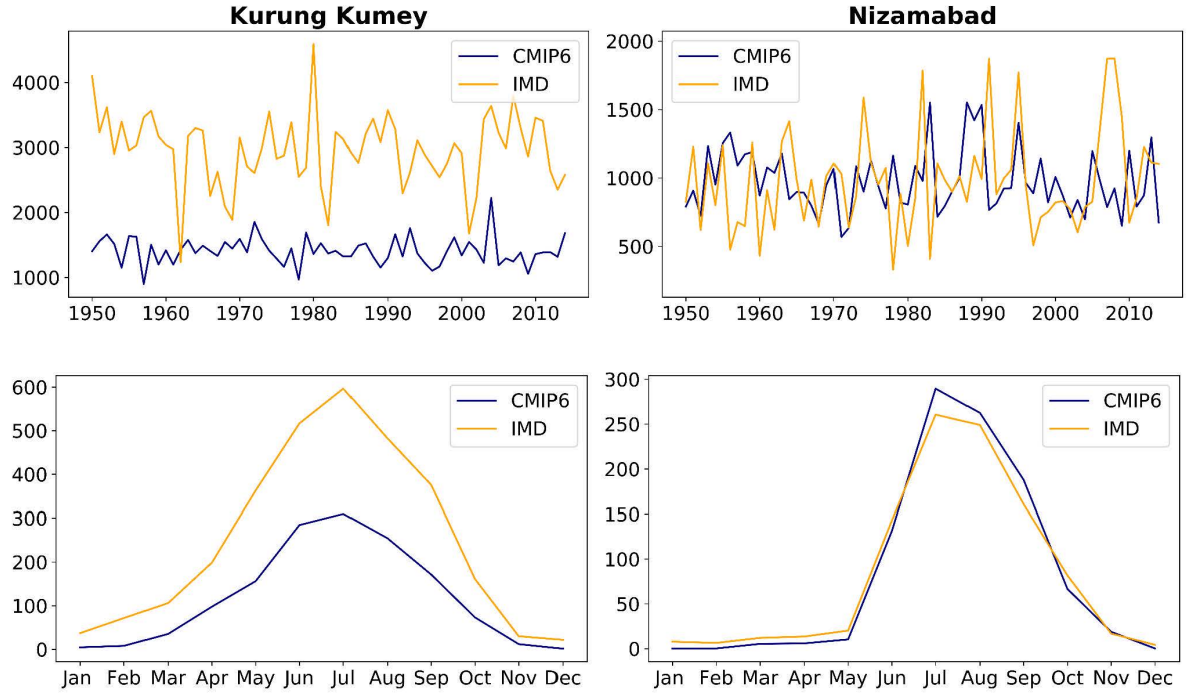

Fig. 6.3. IMD and ensemble CMIP6 long-term (1950-2014) annual and monthly average precipitation series observations for Kurung Kumey and Nizamabad.

Figure 6.3 indicates that the average annual precipitation for Kurung Kumey, an area with high PBIAS, is approximately 3000 mm based on observed data. In comparison, the CMIP6 models predict an average of only 1500 mm. Furthermore, the monthly estimates reveal significant deviations between the model simulations and observed data. However, in the case of Nizamabad, which has the lowest PBIAS, the precipitation estimates of models are closely aligned with the observed data, indicating better performance in capturing the precipitation patterns.

During the analysis of PBIAS across all locations, it was observed that the values varied significantly, ranging from 0% to 52%. Based on these variations, the PBIAS values were categorized into two zones: below 20% and above 20%. In Fig. 6.4, the overall distribution of the districts is shown, with regions exhibiting PBIAS below 20% highlighted in green and those with PBIAS above 20% marked in red. The analysis combined various hilly regions, including the Sivalik, Eastern Ghats, Western Ghats, and Naga Hills, to illustrate the diverse outcomes across different geographical areas. This selection effectively highlighted the spatial differences in data estimation accuracy.

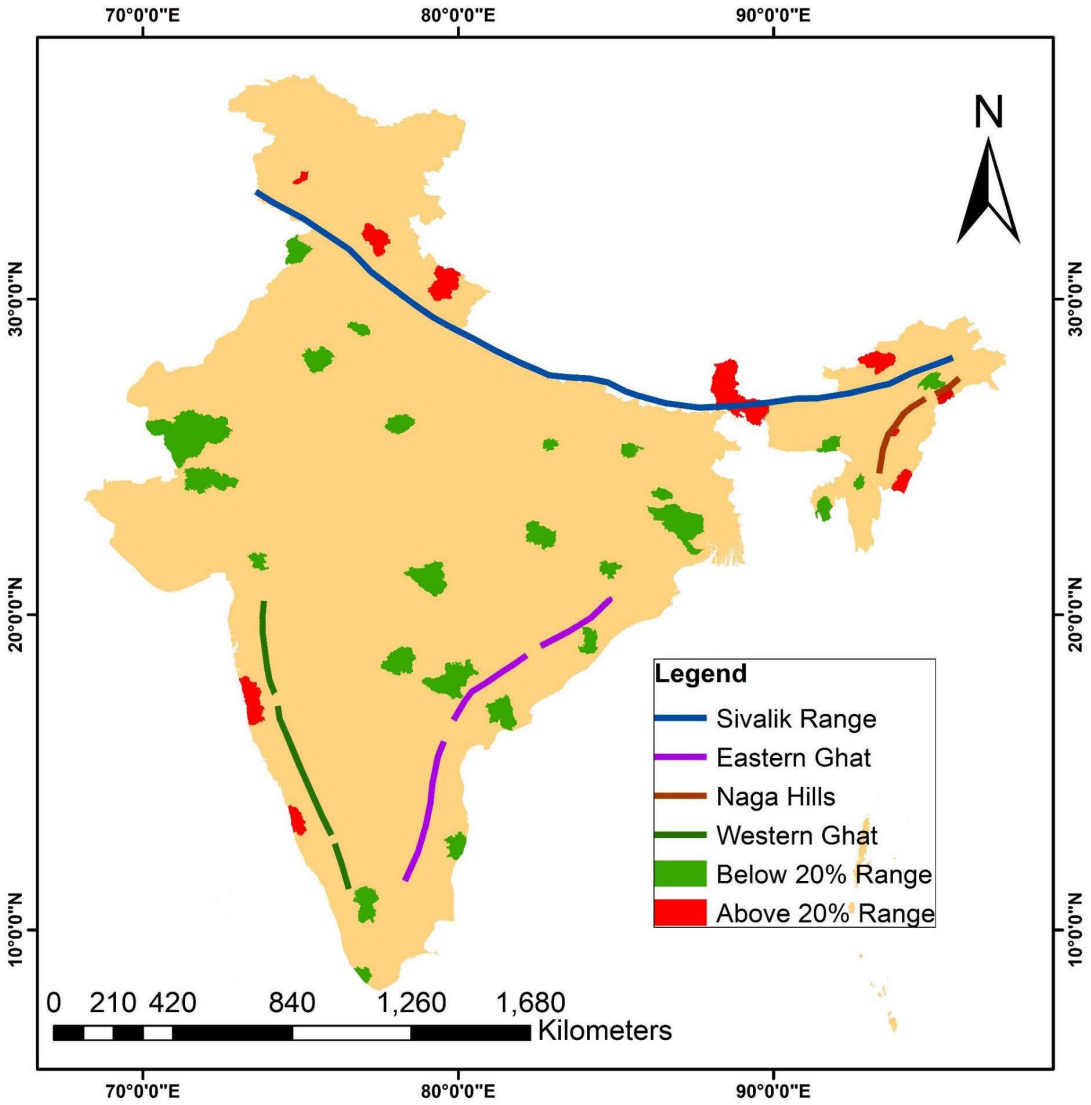

Fig. 6.4. Overall representation of estimated precipitation along with different ranges.

The plotted data provided valuable information into the precipitation patterns and trends within each region, contributing to a more extensively understanding of overall findings of the study. In the vicinity of the Sivalik range, the analysis revealed significant inconsistencies, where precipitation estimates were either overestimated or underestimated. Similarly, the Eastern Ghats and Naga Hills showed a PBIAS above 20%, indicating substantial estimation bias. These discrepancies could be attributed to the differences in altitude among the regions, which may influence data collection and analysis. However, identifying the precise causes of these discrepancies would require a more in-depth analysis.

6.4.2. Assessment Based on Climate Classifications

A comprehensive analysis of the climatic conditions within the study area is crucial for understanding the behavior of different locations with PBIAS. The study identified 36 distinct locations and categorized them according to the Köppen-Geiger climate classification, taking into account their specific PBIAS ranges. In Fig. 6.5, the distribution of locations is spread out across different climate zones.

As shown in Fig. 6.5, various locations display distinct climatic zones when PBIAS exceeds 20%. This observation suggests that the unique climatic conditions of these locations significantly influence the accuracy and performance of models. Variations in PBIAS across these zones may be attributed to factors such as regional topography, and local weather patterns, all of which impact hydrological processes and the predictive capabilities of the models. This analysis underscores the importance of accounting for local climatic contexts when evaluating PBIAS results.

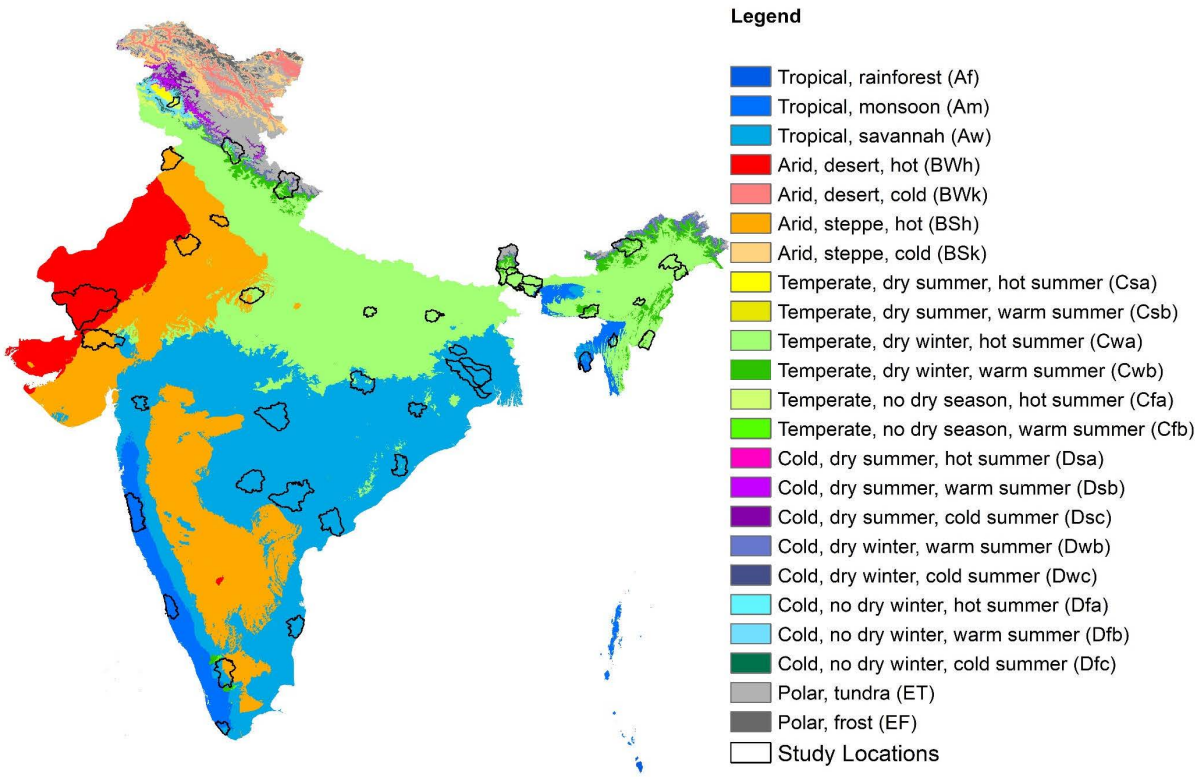

Fig. 6.5. Different locations based on climatic classifications.

Northern India, particularly in districts like Pulwama, Kullu, and Chamoli, experiences a combination of polar tundra (ET), temperate (Csa, Cwa, Cwb), and cold (Dsa, Dsb) climates. These climatic conditions intensely affect hydrological processes, agricultural practices, and overall environmental dynamics. Moving westward, districts such as Ratnagiri and Udupi are characterized by a Tropical Monsoon (Am) climate, noticeable by seasonal rainfall and high humidity. This monsoonal influence plays a critical role in agricultural productivity and water availability.

In northeastern India, regions such as Sikkim, North West Bengal, Kurung Kumey, Tirap, Dimapur, and Chandel, a combination of polar tundra (ET) and temperate (Cwa, Cwb) climatic zones is evident. These climates significantly shape the biodiversity, vegetation, and water resources of the area. An advanced understanding of these diverse climatic zones is crucial for effective water resource management, sustainable agricultural practices, and climate change adaptation strategies.

Figure 6.5 also shows several districts that fall within the 10% to 20% PBIAS range, encompassing a variety of climate zones. These include arid zones (BWh, BSh) in western India, tropical monsoon (Am), and temperate (Cwa, Cwb) zones in northeastern India. Central

and southeastern India predominantly feature Tropical Savannah (Aw) and temperate (Cwa) climatic classifications. The differences in PBIAS values across these zones highlight the significant influence of local climatic factors on hydrological processes and water resource availability.

Yazdandoost et al. (2021) conducted an evaluation of CMIP6 precipitation data across various climatic zones in Iran, revealing significant variations in the performance of CMIP6 models across these zones. Their findings demonstrated that the accuracy and reliability of CMIP6 models varied substantially depending on the regional climatic characteristics. Interestingly, our results align with these findings, showing comparable patterns of variation in model performance across diverse climatic zones. This consistency underscores the critical importance of understanding both the strengths and limitations of CMIP6 models in capturing precipitation trends across distinct regions. Such insights contribute to more accurate climate projections and support better-informed decision-making processes.

6.4.3. Assessment Based on Trend Analysis

The evaluation of model accuracy requires the correlation between climate classifications and the PBIAS. Moreover, a comprehensive analysis of trend patterns across various regions with PBIAS is also crucial for better understanding. To explore these trends, three methodologies were utilized: Mann-Kendall (MK), Modified Mann-Kendall (MMK), and Sen's Slope (SS).

The MMK test accounts for potential serial correlations in the data, improving its reliability in hydrological time series analysis. The MK test is effective in detecting monotonic trends, while SS provides robust estimates of trend magnitude, making it particularly valuable for understanding changes in hydrological parameters. Regular trend studies are essential to monitor hydrological shifts, especially in the perspective of climate change.

The analysis of the collected data reveals no distinct pattern of trends between the IMD data and CMIP6 model simulations. This indicates a lack of clear correlations between the two datasets. For both CMIP6 and IMD data, the MMK analysis produced a wide range of Z statistics. CMIP6 Z statistics range from 6.94 to -6.14, reflecting significant variations in patterns across regions. Similarly, the IMD Z statistics range from 4.33 to -15.41 (Fig. 6.6a).

Sen's Slope analysis also shows significant variations in trend magnitudes. For CMIP6 data, SS ranges from 4.18 mm/year to -3.29 mm/year, indicating both positive and negative precipitation trends (Fig. 6.6b). For IMD data, the slopes range from 13.64 mm/year to -9.47 mm/year, further highlighting differences between the two datasets.

In comparison, the MK test results show a narrower range of Z statistics, suggesting more consistent trend patterns. The Z statistics for CMIP6 data range from 1.93 to -1.89, while those for IMD data range from 2.36 to -3.66 (Fig. 6.6c). Despite this narrower range, the MK test might not fully understand the level of complexity, and variability inherent in the datasets.

The lack of identifiable patterns or correlations between CMIP6 and IMD data highlights the challenges in simulating climate and hydrological systems. This variability underscores the need for ongoing research and advancements in understanding precipitation trends, as well as their suggestions for water resource management and climate change adaptation.

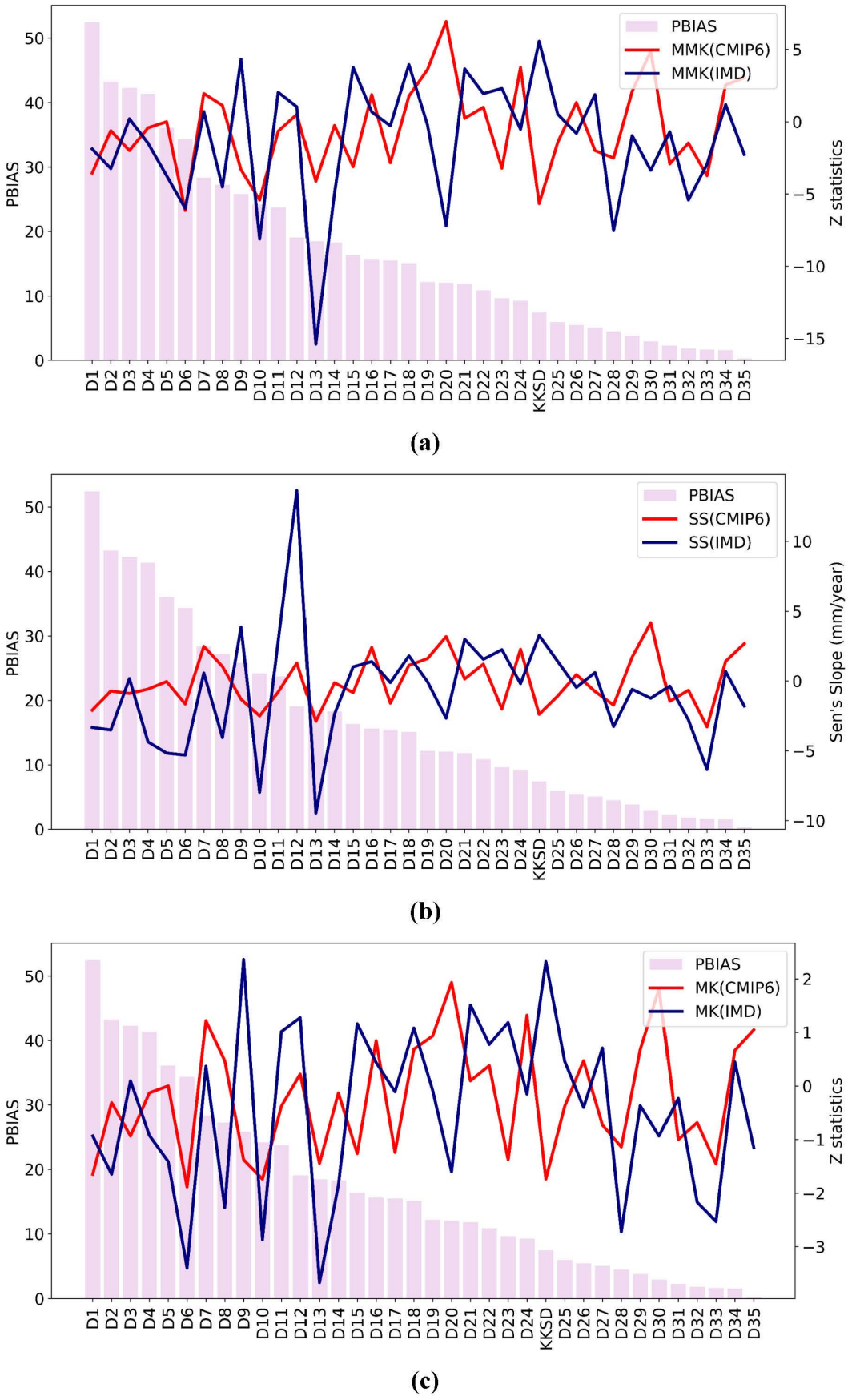

Fig. 6.6. Trend analysis patterns based on different methodologies (a) modified Mann Kendall (MMK) (b) Sen's Slope (SS) (c) Mann Kendall (MK).

6.4.4. Assessment Based on the Performance of Individual Parameters

- **Modified Taylor Skill Score**

The MTSS and PBIAS are crucial parameters for evaluating the performance of predictive models across diverse applications, including weather forecasting, climate modeling, and hydrological simulations. An important trend is evident in the plot illustrating the relationship between MTSS and PBIAS. As PBIAS decreases, MTSS consistently increases, signifying a strong positive correlation between the two metrics.

The results illustrated in Fig. 6.7 offer valuable insights into the behavior of MTSS under varying levels of bias within the data. A declining PBIAS reflects reduced systematic error, indicating that the predictions of the model align more closely with observed values. Consequently, the MTSS, which assesses the ability of models to capture patterns and variability, improves as bias reduces. Understanding the interaction between MTSS and PBIAS provides a foundation for refining predictive models. This relationship highlights the importance of minimizing bias to enhance model performance, thereby enabling more accurate and reliable projections.

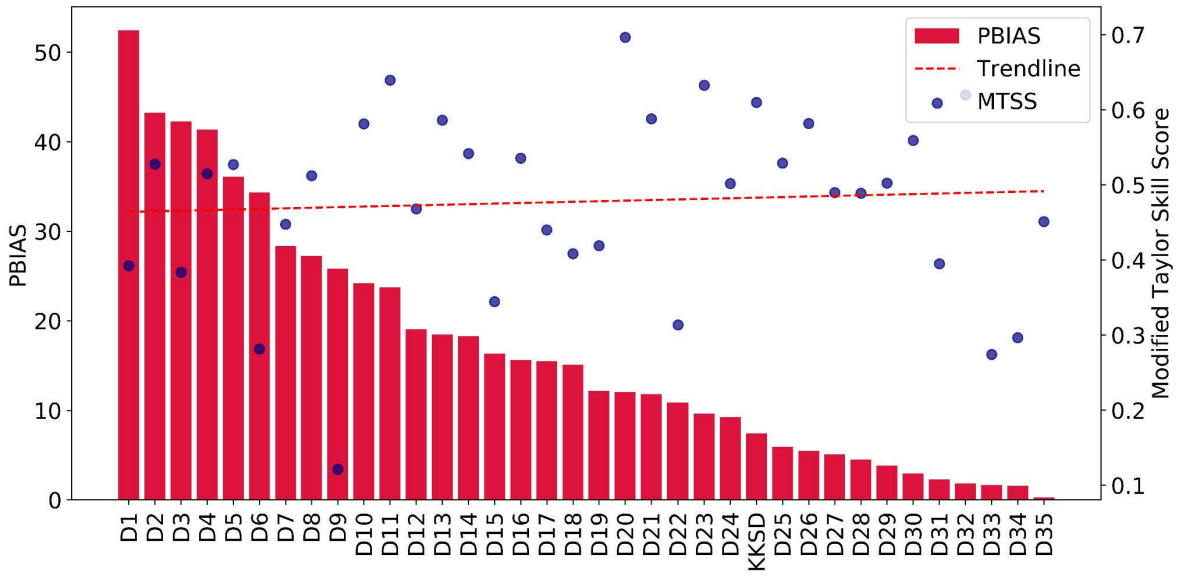

Fig. 6.7. Variation of PBIAS with modified Taylor skill score.

- **Refined Index of Agreement**

The consideration of the correlation between RIoA and PBIAS is required to assess the variations in RIoA values across various PBIAS. The findings were surprising, as they indicated that even with a decrease in PBIAS, there were no significant variations in the RIoA values. This relationship is illustrated in Fig. 6.8, where a linear trend line highlights the index behavior across varying PBIAS.

An increase in RIoA values would typically be associated with a decrease in PBIAS, which indicates that the model predicts and follows more accurate methods. However, the observed stability of RIoA despite decreasing PBIAS raises interesting questions about the performance evaluation of GCMs in replicating precipitation patterns.

This unexpected outcome permits careful analysis to identify potential factors influencing the observed trends. It is essential to understand why RIoA remains relatively stable despite variations in PBIAS, as this could reveal limitations in the sensitivity of RIoA to subtle performance improvements related to PBIAS.

The findings suggest the need for further investigation, including exploring alternative evaluation metrics that might provide a more advanced understanding of model performance. Such investigation is crucial for accurately assessing the ability of GCM to replicate observed precipitation patterns and improving model evaluation frameworks.

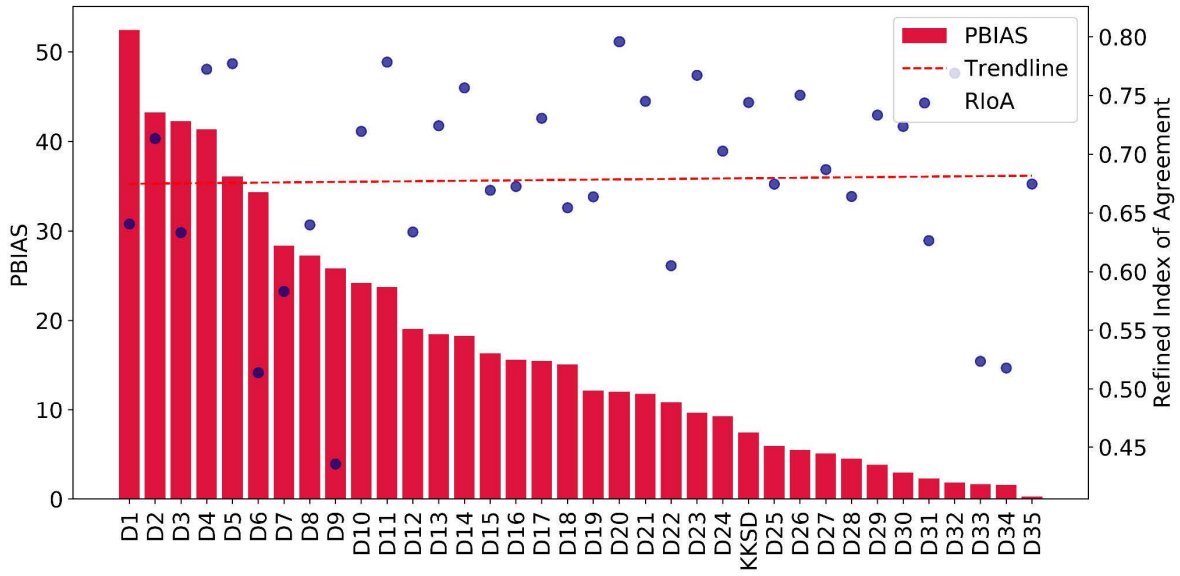

Fig. 6.8. Variation in PBIAS with Refined Index of Agreement.

- **Correlation Coefficient**

The correlation coefficient analysis produced unexpected results, indicating that the relationship between the CC and PBIAS decreases as PBIAS decreases. Typically, CC is to improve as the bias in data reduces, reflecting a closer alignment between model predictions and observed values. However, the findings of this study suggest an absence of a clear positive relationship between these two variables.

Figure 6.9 visually represents this trend, with a slightly negative slope observed in the analysis. This negative slope implies that as PBIAS decreases, the CC tends to decline marginally rather than increase. Such an outcome challenges the conventional assumption that reducing bias would inherently lead to stronger correlations between model outputs and observed data. These findings prompt critical questions regarding the relationship between the accuracy of GCMs and their capacity to replicate observed precipitation patterns. Insights gained from such assessment could inform the development of more comprehensive evaluation methods, improving the reliability of GCMs in representing hydrological processes.

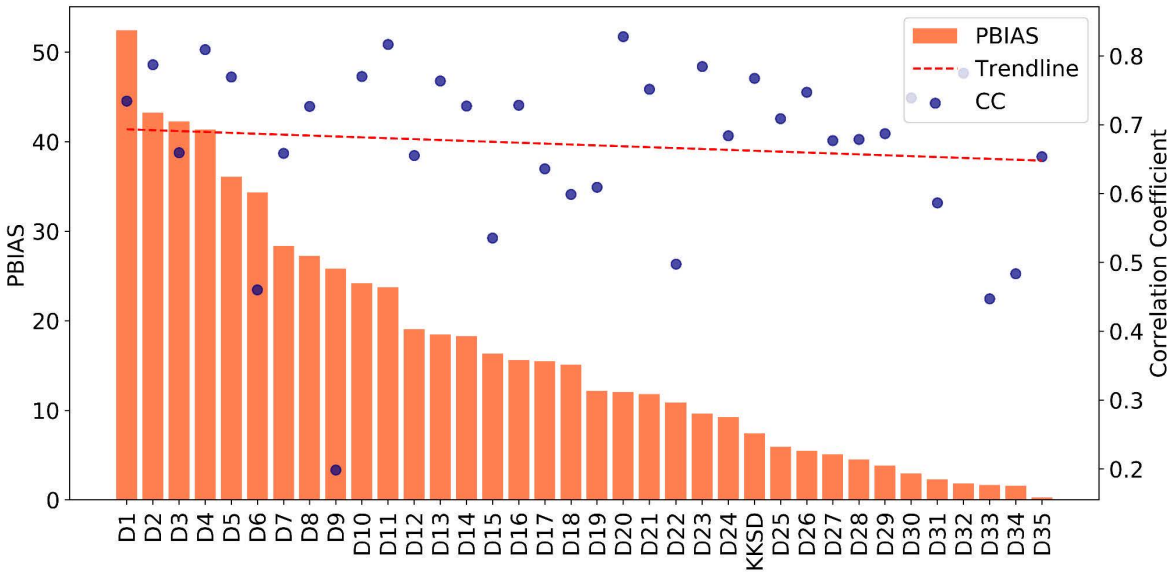

Fig. 6.9. PBIAS trend with varying correlation coefficient.

- **Mean Absolute Error**

In climate model simulations, bias and error are typically expected to exhibit a parallel relationship: as bias decreases, overall error should also decline. The results of this study align with this expectation, revealing a remarkable trend where lower PBIAS values correspond to reduced MAE. Figure 6.10 visually represents this relationship, depicting the variation of MAE concerning PBIAS values.

A remarkable finding is the strongly negative slope of the MAE plot. This indicates that as PBIAS decreases, reflecting better agreement between observed data and model outputs, the magnitude of MAE reduces significantly. This result underscores the critical connection between reduced bias and overall model accuracy. It also highlights the importance of minimizing PBIAS to improve climate model predictions.

The implications of such a negative slope suggest that achieving low bias in climate models leads to substantial reductions in overall error, reinforcing the need to prioritize bias minimization during model development and evaluation. This observation also emphasizes the complexity of assessing model performance in climate simulations, where refined interactions between error metrics can provide valuable insights.

Further investigation into the underlying mechanisms driving this relationship is essential. A deeper understanding could enhance climate modeling techniques, contributing to more reliable and accurate future projections, and supporting informed decision-making in the aspect of climate change.

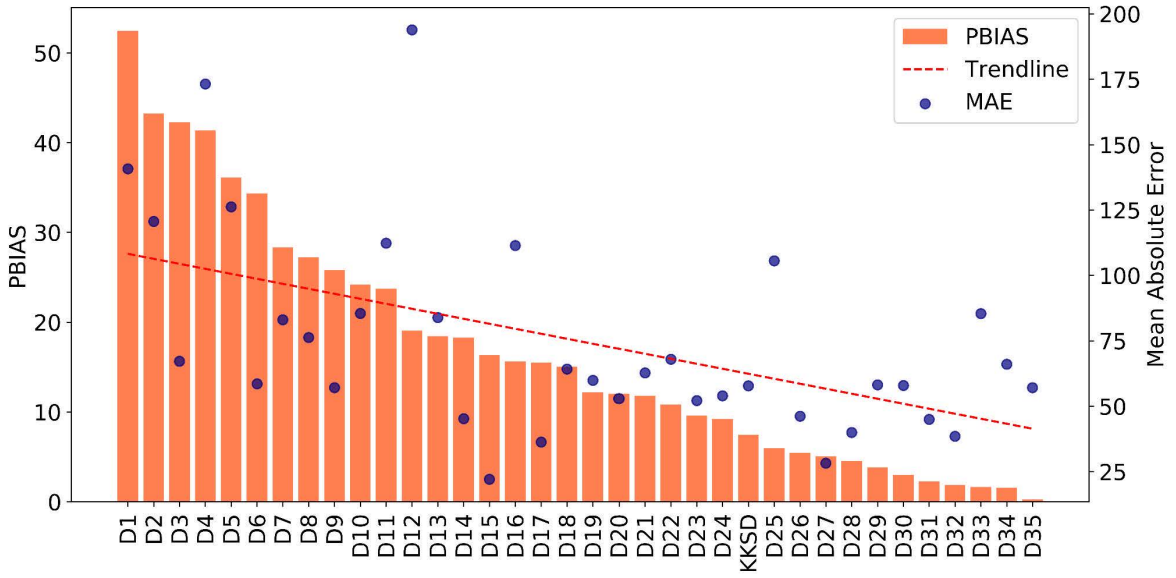

Fig. 6.10. PBIAS changing with mean absolute error.

6.5. Discussion

This study aimed to assess the accuracy and reliability of the 24 GCMs from CMIP6 in reproducing historical precipitation patterns, as compared to the observational data. To achieve this, various critical performance metrics were employed. The comprehensive evaluation revealed significant findings related to trend analysis methods and model performance (Jose and Dwarakish 2022, Li et al. 2023). Despite employing different methodologies and performance indicators, the analysis did not establish robust relationships between the metrics across diverse climatic conditions. This lack of strong correlation emphasizes the inherent complexity of climate dynamics and highlights the challenges in understanding and including the outputs of various trend analysis approaches. The results underscore the requirement for further research to recognize the complicated relationships between trend analysis methods, performance metrics, and climatic factors (Yazdandoost et al. 2021, Hamed et al. 2023).

The study further identified biases in precipitation patterns across different regions of India when comparing CMIP6 model data with observed data. These biases displayed overestimations or underestimations of precipitation in specific regions, influenced by Köppen-Geiger climate classifications and regional topography, particularly mountain ranges. By analyzing these discrepancies, the study aimed to provide a better comprehension of these biased regions and the potential causes, ultimately helping the improvement of climate projections for more accurate, region-specific outcomes. Regions with PBIAS exceeding 20% predominantly correspond to four climate classifications: polar tundra (ET), temperate (Csa, Cwa, Cwb), cold (Dsa, Dsb), and tropical monsoon (Am). Notably, these areas are typically located at higher altitudes, underscoring the challenges faced by GCMs in accurately simulating precipitation dynamics in such environments.

Locations with PBIAS ranging between 10% and 20% were primarily associated with arid (BWh, BSh), temperate (Cwa, Cwb), and tropical (Am, Aw) climates. A significant finding is the clustering of overestimated or underestimated locations accounting for more than 20%

of total discrepancies around three major mountain ranges: the Sivalik, Naga Hills, and Western Ghats. This observation highlights persistent limitations in CMIP6 GCMs in capturing the discrepancies of precipitation patterns in mountainous regions. Despite advancements, these models have not demonstrated significant improvements in representing the complex interplay between topography and climatic factors in such regions. These insights into the relationships between model biases, altitude, and climate classifications provide valuable guidance for enhancing the accuracy of climate projections. Additionally, they underscore the importance of model improvements to address specific regional and topographical challenges, ultimately contributing to more reliable and actionable climate predictions (Lalande et al. 2021).

6.6. Conclusions

This study estimated an assessment of 24 CMIP6 GCMs in India, offering significant insights into their ability to reproduce historical precipitation patterns accurately and reliably. By systematically analyzing the biases and trends across diverse climatic and topographical conditions, the study identified critical limitations in the current models and highlighted areas for improvement.

- **Bias Across Climate Classifications:** Regions with specific climate classifications such as polar tundra (ET), temperate (Csa, Cwa, Cwb), cold (Dsa, Dsb), and tropical monsoon (Am) exhibited PBIAS values exceeding 20%, indicating important discrepancies in model outputs.
- **Impact of Mountain Ranges:** Locations near the Sivalik, Naga Hills, and Western Ghats regions were prone to substantial biases, with PBIAS values also exceeding 20%, underscoring challenges in simulating precipitation dynamics in complex terrains.
- **Crucial Factors in Climate Modeling:** Altitude, climate classification, and proximity to mountain ranges were identified as key determinants influencing model performance and precipitation projections.
- **Performance Parameter Relationships:** The study found no significant relationship between trend analysis and PBIAS, suggesting that bias alone does not predict trends in precipitation. Minimal changes in the MTSS and RIoA with varying PBIAS suggest their limited sensitivity in capturing subtle performance improvements. MAE showed better alignment with PBIAS, making them more reliable metrics for evaluating GCM performance. However, CC does not portray the expected results and recommends comprehensive metric analysis required.

Developing GCMs that account for regional complexities, including altitude and topographical influences, is crucial for enhancing accuracy. Before analysis, individual GCMs and their data-estimation capabilities should be thoroughly evaluated to avoid compounding inaccuracies. Enhancing GCMs with region-specific data and parameters will provide more precise and actionable climate projections. A multi-factor approach combining performance metrics and trend analyses is recommended to capture the multifaceted nature of climate dynamics.

Facilitating efficient allocation and planning of water resources under changing climatic conditions. Enhancing crop planning and yield predictions to support food security. Informing preparedness strategies for floods, droughts, and other climate-induced hazards. Supporting climate-resilient development and long-term sustainability of infrastructure projects. Assisting policymakers in developing effective adaptation strategies that are customized for specific regions. This study underscores the importance of ongoing refinement of GCMs understanding to achieve a more reliable climate study.

References

Alizadeh, O. (2022). Advances and challenges in climate modeling. Clim. Change, 170(1–2), 18.

Beck, H.E., Zimmermann, N.E. and McVicar et al. (2018). Present and future Köppen-Geiger climate classification maps at 1-km resolution. Sci. Data, 5, 180214.

Hamed, M. M., Nashwan, M. S., Shahid et al. (2022). Inconsistency in historical simulations and future projections of temperature and Precipitation: A comparison of CMIP5 and CMIP6 models over Southeast Asia. Atmos. Res., 265, 105927.

Hamed, M. M., Nashwan, M. S., Shahid et al. (2023). Future Köppen-Geiger climate zones over Southeast Asia using CMIP6 Multimodel Ensemble. Atmos. Res., 283, 106560.

Jose, D.M. and Dwarakish, G.S. (2022). Bias Correction and Trend Analysis of Temperature Data by a High-Resolution CMIP6 Model over a Tropical River Basin. Asia-Pacific J. Atmos. Sci., 58(1), 97–115.

Lalande, M., Ménégoz, M., Krinner, G., Naegeli, K. and Wunderle, S. (2021). Climate change in the High Mountain Asia in CMIP6. Earth Syst. Dyn., 12(4), 1061–1098,

Li, X., Fang, G., Wei et al. (2023). Evaluation and projection of precipitation and temperature in a coastal climatic transitional zone in China based on CMIP6 GCMs. Clim. Dyn., 61(7–8), 3911–3933.

Peel, M. C., Finlayson, B. L. and McMahon, T. A. (2007). Updated world map of the Köppen-Geiger climate classification. Hydrol. Earth Syst. Sci., 11(5), 1633-1644.

Sarkar, S., and Maity, R. (2022). Future characteristics of extreme precipitation indicate the dominance of frequency over intensity: A multi-model assessment from CMIP6 across India. J. Geophys. Res. Atmos., 127, e2021JD035539.

Sekar, M. and Gumus, V. (2022). Projection of temperature and precipitation in the Mediterranean region through multi-model ensemble from CMIP6. Atmos. Res., 280, 106440.

Wang, G., He, Y., Zhang et al. (2023). Historical evaluation and projection of precipitation phase changes in the cold season over the Tibetan Plateau based on CMIP6 multimodels. Atmos. Res., 281, 106494.

Yazdandoost, F., Moradian, S., Izadi, A. and Aghakouchak, A. (2021). Evaluation of CMIP6 precipitation simulations across different climatic zones: uncertainty and model intercomparison. Atmos. Res., 250, 105369.

Chapter 7

Multi-Temporal Assessment of CMIP6 Models for Climate Dynamics

"Patel, G. and Das, S. (2025). Multi-Temporal Evaluation of CMIP6 Models for Maximum Temperature in East India: Improving Climate Dynamics Understanding. (Stochastic Environmental Research and Risk Assessment-2nd Revision)"

7.1. Introduction

Global variations in temperature and precipitation patterns have become a critical challenge, driving the complexity and frequency of extreme hydrological events. These changes pose significant risks to human populations and ecosystems. Therefore, understanding future variations in these climatic parameters is critical for identifying efficient approaches to mitigate the consequences of climate change and adapt to the strengthening of extreme events.

Global Climate Models (GCMs) are extensively utilized as an effective tool for predicting future climate change and understanding complex climate systems. While they remain the most robust numerical models for studying future climates, GCMs have inherent limitations that require careful consideration. These include errors in the modeling process, uncertainties in input data, and challenges in accurately predicting global climate events. Addressing these limitations is vital to enhancing the precision and reliability of GCM-based climate projections. The field of science plays a pivotal role in advancing these models and delivering timely, accurate insights into the dynamic evolution of climate extremes.

GCMs have been employed to investigate historical and projected changes in various climate parameters (Zhang et al. 2023). These models offer invaluable insights, aiding stakeholders in developing resilient, sustainable, and effective policies (Ayugi et al. 2021, Salehie et al. 2022). According to the 6th Assessment Report of the Intergovernmental Panel on Climate Change (IPCC), there is a greater than 50% probability that global temperatures will rise by 1.5 °C (2.7 °F) between 2021 and 2040, depending on different scenarios. This projection, coupled with heatwave conditions, underscores the demanding need to address climate change, as such temperature increases could significantly impact ecosystems and societies (IPCC 2021, Anvari and Moghaddasi 2023, Domeisen et al. 2023).

GCMs also play an essential role in advancing the scientific understanding of climatic systems and improving simulation capabilities (Yang et al. 2019). However, significant discrepancies remain between GCM outputs and observational data. These discrepancies arise from constraints such as limited computational resources, inadequate information on climate response mechanisms, model simplifications, uncertainties in parameterization, and unrealistic assessments of natural forcing factors (Scafetta et al. 2021).

According to Balaji (2022), GCMs are essential tools for climate research, yet they exhibit inherent structural flaws and uncertainties. These limitations can be mitigated by adopting

higher-resolution models and incorporating machine learning techniques. Yang et al. (2019) highlighted substantial uncertainties and biases in GCMs, particularly in replicating precipitation and temperature patterns in arid and semi-arid regions of China. Such findings underscore the critical need to enhance model accuracy, especially in climate-sensitive regions. Karmalkar et al. (2019) stress the importance of utilizing diverse GCMs in regional climate studies. A variety of models not only provide a range of projections but also help balance computational demands, enabling more precise assessments. The reliability of a GCM largely depends on its capacity to replicate essential climate features, evaluating GCM performance as a foundation of climate change research.

Despite their importance, selecting appropriate GCMs remains a complex challenge. Currently, no universally accepted assessment framework exists, and temporal assessments of GCMs are often unnoticed. Sonali and Kumar (2013) demonstrated that decadal trends can deviate significantly from overall trends, underscoring the necessity of temporal analysis for a deeper understanding of model behavior. Recent advancements have introduced innovative methods for evaluating GCM performance. For instance, statistical test-based methodologies now assess how well GCMs replicate observed responses to external radiative forcing (Raju et al. 2017, Carmen et al. 2021). These approaches offer interesting observations into the reliability and limitations of GCMs, paving the way for more robust climate modeling practices.

A distinct investigation introduced a score-based system to analyze the outcomes of GCMs in simulating regional temperature and precipitation patterns (Shi et al. 2018). This approach considers multiple criteria to assess how effectively the models capture regional climate dynamics. Despite their utility, GCMs exhibit significant uncertainties, with each model varying in its ability to represent climatological variables. These variations arise from differences in external forcing, the scale of internal variability, and the unique climatic sensitivity of each model (Wu et al. 2021, Patel et al. 2024).

To tackle these challenges, Patel et al. (2023a) used a multi-criteria decision-making methodology to determine the most appropriate GCM for precipitation. This approach assesses individual performance indicators while also taking into account their combined ensemble effects, providing a thorough framework for selecting the most suitable GCM. The comprehensive evaluations of GCMs have provided critical insights into their strengths and weaknesses. These assessments form a foundation for enhancing model accuracy and improving the reliability of future climate projections.

Temporal assessment of goodness-of-fit (GoF) metrics is essential in evaluating and ranking climate models, as the selection of the best-performing models can vary significantly depending on the evaluation indicators employed. Rankings derived from one indicator often differ from those based on others, presenting challenges in identifying an optimal model. To address this, the present study employs a multi-metric temporal analysis, providing an objective framework for model selection while mitigating uncertainties in climatic projections and hydrological applications.

A comprehensive evaluation of GCMs, particularly through temporal analysis, is essential for accurately assessing their overall performance. Despite its importance, the temporal evaluation of GCMs concerning climatic parameters remains unexplored in existing studies. Significantly, no prior research has assessed the temporal performance of GCMs using GoF

metrics. This study is unique because of its methodology, which bridges this critical research gap by introducing a robust approach to temporal analysis for GCM evaluation. This innovative framework enhances the reliability of model assessments, contributing to improved climate modeling and more precise future projections.

Previous investigations primarily evaluated models at a resolution of (1° × 1°), which is well-suited for continental or global analyses. However, such resolutions may lack the precision necessary for regional or hydrological basin-scale studies. To address this, our study employs a finer resolution of (0.25° × 0.25°) to enhance the representativeness of climate series.

The main goal of this research is to conduct a temporal assessment of maximum temperature projections from various GCMs in Eastern India. This region is particularly significant due to its distinct climate dynamics, the escalating impacts of climate change on heat extremes, the vulnerability of temperature variability to the agricultural sector, and the critical need for effective disaster preparedness to mitigate heatwave risks.

Temporal evaluation aligns with the strengths of CMIP models, which are optimized to capture long-term climate trends rather than short-term daily weather patterns. By focusing on temporal variations, this approach enables a more accurate assessment of regional temperature variability over time, providing essential insights for long-term climate adaptation strategies and informed policy-making.

7.2. Goodness-of-Fit

A variety of GoF metrics are independently employed to assess the ability of GCMs to replicate the climatology of maximum temperature, using data from the India Meteorological Department (IMD) for the period 1951-2014. The selection of 12 GoF metrics is due to their extensive use in prior studies, reflecting their effectiveness in assessing model performance across diverse criteria such as association, error, variability, and efficiency (Muhammad et al. 2019, Jose and Dwarakish 2022, Patel et al. 2023a; Shetty et al. 2023).

These metrics provide a robust framework for evaluating the effectiveness and applicability of GCMs. Through a comprehensive analysis of the selected metrics, the study identifies the most appropriate GCMs that effectively address the specific challenges and requirements of regional climate modeling. Table 2.2 provides a detailed overview of the GoF metrics utilized in this study. These metrics are designed to assess statistical equivalence between observed and predicted values, offering a complex evaluation of model performance.

- **Correlation Coefficient**: This shows both the direction and strength of the linear relationship between actual and predicted values.
- **Mean Absolute Error**: Reflects the average magnitude of errors, providing insight into overall prediction accuracy.
- **Mean Bias Error**: Highlights the average tendency of predictions to be systematically too high or too low.
- **Refined Index of Agreement**: Enhances model assessment by reducing sensitivity to outliers.
- **Nash-Sutcliffe Efficiency**: Measures how well the model predicts relative to the mean of the observed values.

- **Akaike Information Criterion**: Balances model fit against complexity to assess overall model quality.
- **Theil's Coefficient of Inequality**: Evaluates prediction accuracy by comparing predicted values to observations.
- **Modified Kling-Gupta Efficiency**: Combines correlation, bias, and variability to provide a complete evaluation of model efficiency.
- **Skill Score**: Quantifies the performance of models relative to a benchmark, highlighting relative improvements.
- **Modified Taylor Skill Score**: Incorporates correlation, standard deviation, and error to focus on error reduction and pattern alignment.
- **Percentage Bias**: Measures the average inclination of predictions to systematically deviate from observed values.
- **Normalized Mean Square Error**: Adjusts the mean square error by observed variance to evaluate predictive reliability.

These metrics collectively ensure a robust evaluation of GCMs, allowing a detailed assessment of their effectiveness in replicating observed climate patterns. These GoF tests employ diverse approaches to assess equivalence, making them sensitive to various inherent characteristics of the analyzed data, such as its distribution and the presence of outliers. Consequently, multiple statistical measures are typically utilized for a comprehensive assessment of model performance.

In this study, the GoF calculations are conducted across multiple temporal durations to capture variations in performance. Specifically, four temporal scales are considered: daily, monthly, seasonal, and decadal.

- **Daily Analysis**: Examines model performance at the finest temporal resolution, capturing day-to-day variations.
- **Monthly Analysis**: Considers the average of month-wise data over an extended period, providing insights into recurring monthly patterns.
- **Seasonal Analysis**: Calculates the average for each season over a long-term period, reflecting seasonal trends and variability.
- **Decadal Analysis**: Aggregates daily data over a decade, enabling the evaluation of long-term trends and patterns.

The selection of these temporal characteristics is driven by the need for a detailed understanding of the data and its temporal behavior. By analyzing data across these durations, the study ensures a robust evaluation of GCM performance, tailored to various time scales critical for climate studies.

7.3. Results and Discussion

7.3.1. Descriptive analysis

The daily variation in maximum temperature for the study locations is shown in Fig. 7.1, providing a clear visualization of individual model performance over the KKSD basins. Complementing this, Table 7.1 presents the descriptive statistics for maximum temperature

based on daily data. These statistics offer a detailed quantitative assessment, enabling a comprehensive insight into the statistical performance of models. Together, Fig. 7.1 and Table 7.1 provide valuable understanding into the accuracy and reliability of the evaluated models. It is evident that none of the models closely align with the IMD data. Among the GCMs, EC-Earth3-Veg-LR exhibits the highest mean value for daily maximum temperature, whereas GFDL-ESM4 shows the lowest.

Table 7.1 highlights an important discrepancy in the upper limit of daily maximum temperature between IMD data and model projections, with most models tending to overestimate this upper limit. In contrast, the lower limit of daily maximum temperature shows better agreement with IMD data, indicating stronger model performance in predicting lower temperature extremes. This trend suggests that while the models excel in capturing the lower bounds of temperature extremes, they struggle with overestimating the upper bounds.

The mean maximum temperature estimates of model range from 31.8°C to 32°C, demonstrating a consistent tendency to overestimate compared to IMD observations. However, the lowest maximum temperature estimates from the models, spanning 13.5°C to 19.3°C, exhibit close alignment with observed values, indicating good predictive performance in this aspect.

Table 7.1. Descriptive statistics of daily maximum temperature over the KKSD basins.

Models	Mean (°C)	Min (°C)	Max (°C)	SD (°C)
IMD	31.703	17.666	44.129	4.074
ACCESS CM2	31.983	16.638	49.997	4.220
ACCESS ESM1-5	32.004	14.672	46.691	4.145
BCC-CSM2-MR	31.975	17.791	47.420	4.371
CMCC-CM2	32.006	18.175	49.161	4.285
CMCC-ESM2	31.928	13.951	48.750	4.284
CNRM-CM6	31.967	17.769	47.763	4.294
CNRM-ESM2	31.976	18.172	48.598	4.292
EC-Earth3	31.890	15.844	51.626	4.305
EC-Earth3-Veg-LR	32.026	16.745	49.536	4.372
GFDL-ESM4	31.935	13.562	49.154	4.359
GISS-E2	31.986	18.299	47.252	4.166
INM-C4-8	31.992	19.287	50.187	4.209
INM-CM5-0	31.980	15.520	47.337	4.266
IPSL-CM6A-LR	31.934	17.719	46.490	4.257
MIROC6	32.018	14.751	49.305	4.300
MIROC-ES2L	31.923	19.228	48.566	4.160
MPI-ESM1-2-HR	31.987	16.165	49.819	4.296
MPI-ESM1-2-LR	31.980	15.178	48.791	4.255
MRI-ESM2	31.956	16.066	46.889	4.337
NorESM2-LM	32.011	17.185	50.634	4.209
NorESM2-MM	31.953	16.063	51.561	4.295
TaiESM1	31.966	18.098	48.206	4.265

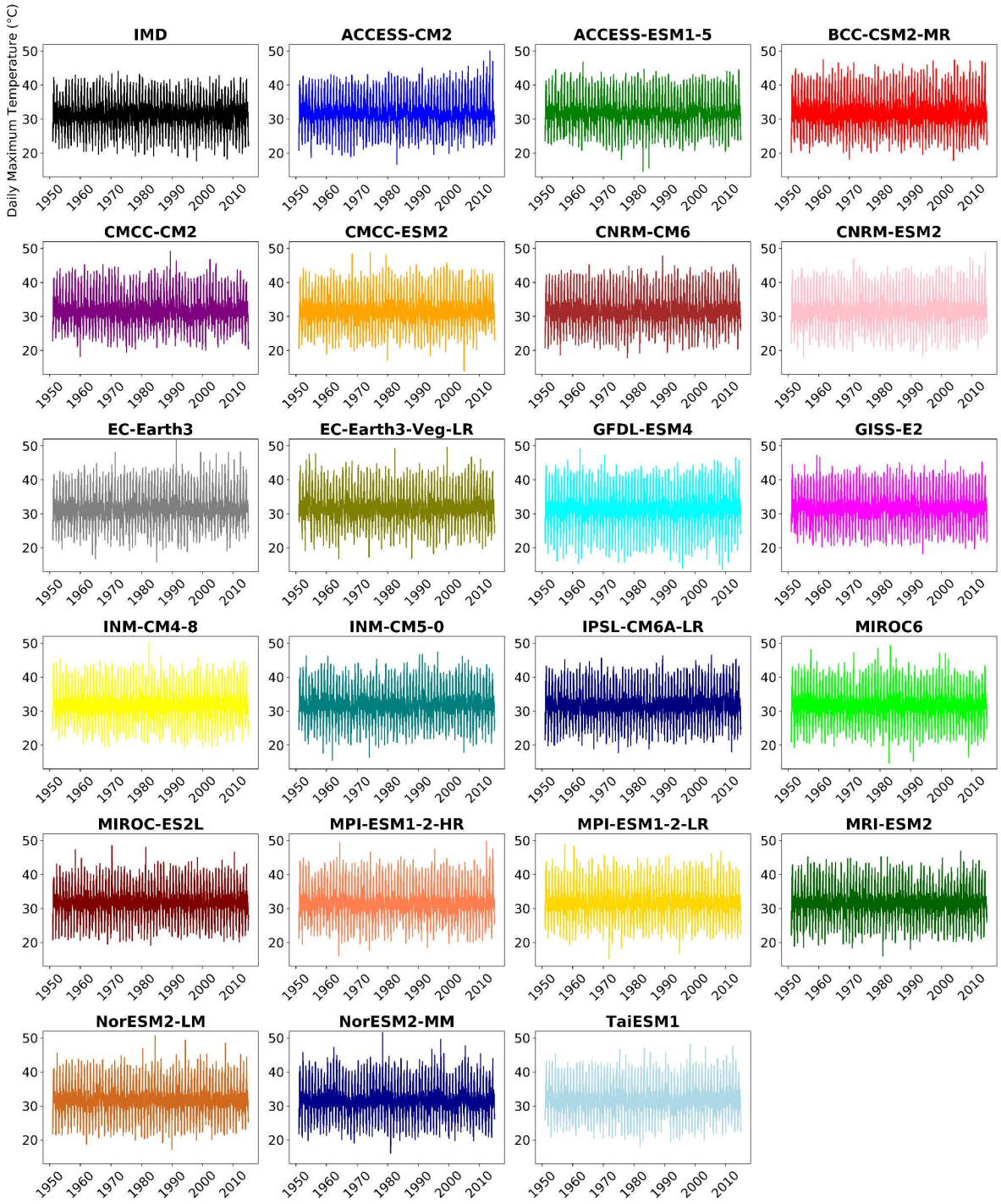

Fig. 7.1. Visualization of individual model performance over the KKSD basins.

7.3.2. Heat matrix

A heat matrix is employed to represent the distribution of values across multiple GoF metrics, providing a clear visual framework for overall inter-comparison among models. This approach enables the performance evaluation of specific models relative to reference models, as well as comparisons among multiple models. Detailed heat matrix representations for modified Taylor Skill Score values are shown in Figs. 7.2-7.5. Figure 7.2 illustrates the heat matrix for modified Taylor Skill Score values corresponding to daily maximum temperature during the period

1951-2014. The visualization reveals that three models MIROC-ES2L, ACCESS-ESM1-5, and GISS-E2 demonstrate greater performance compared to the other 19 models among the 22 GCMs analyzed. The remaining heat matrix sections display the performance of additional CMIP6 GCMs, which could be considered for inclusion in the ensemble.

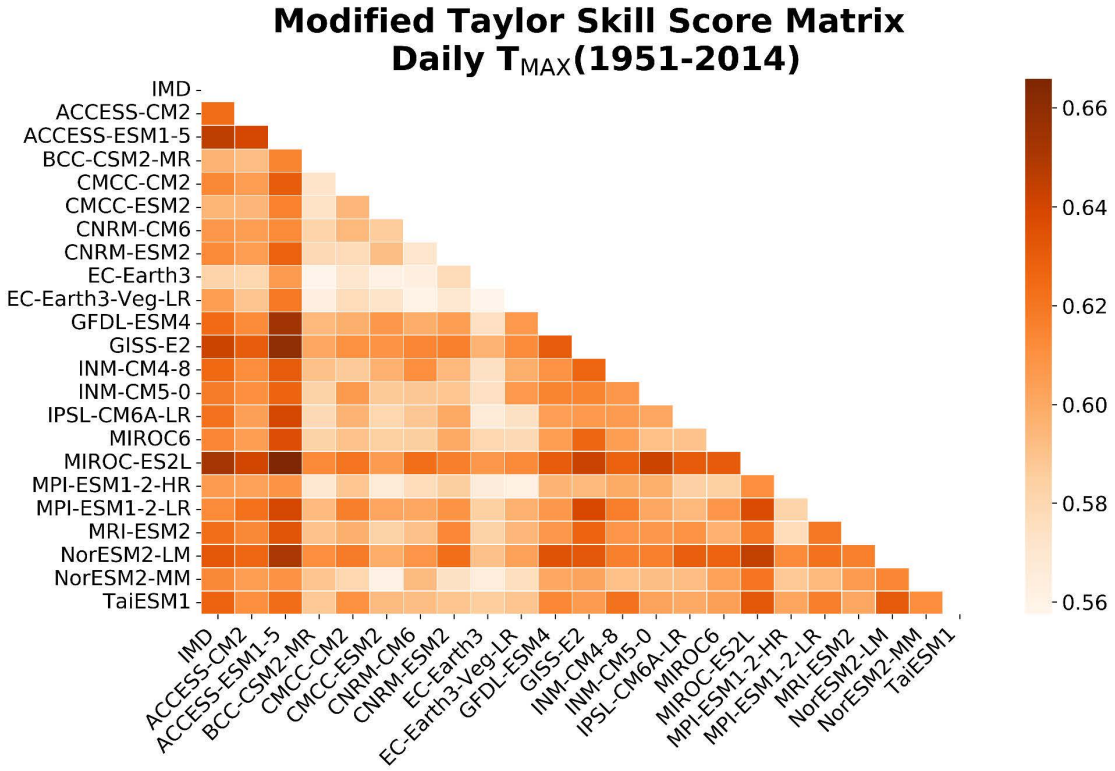

Fig. 7.2. Heat matrix of modified Taylor Skill Score for daily maximum temperature.

This heat matrix serves as a useful tool for identifying high-performing models while excluding those with suboptimal performance, thereby facilitating the selection process for model ensembles. This study employed multiple time scales to evaluate GoF metrics and identify the best-performing GCMs. The next phase of the analysis focuses on the month-wise evaluation for the period 1951-2014. Figure 7.3 presents the heat matrix for this period. The findings confirm that GISS-E2 and MIROC-ES2L remain the top-performing models among the 22 GCMs evaluated.

While the results for daily and month-wise maximum temperatures exhibit important similarities, the remaining sections of the heat matrix highlight discrepancies among other CMIP6 GCMs. These differences indicate some level of disagreement in the temporal analysis across models. Particularly, the month-wise heat matrix reveals a stronger agreement between GISS-E2 and MIROC-ES2L.

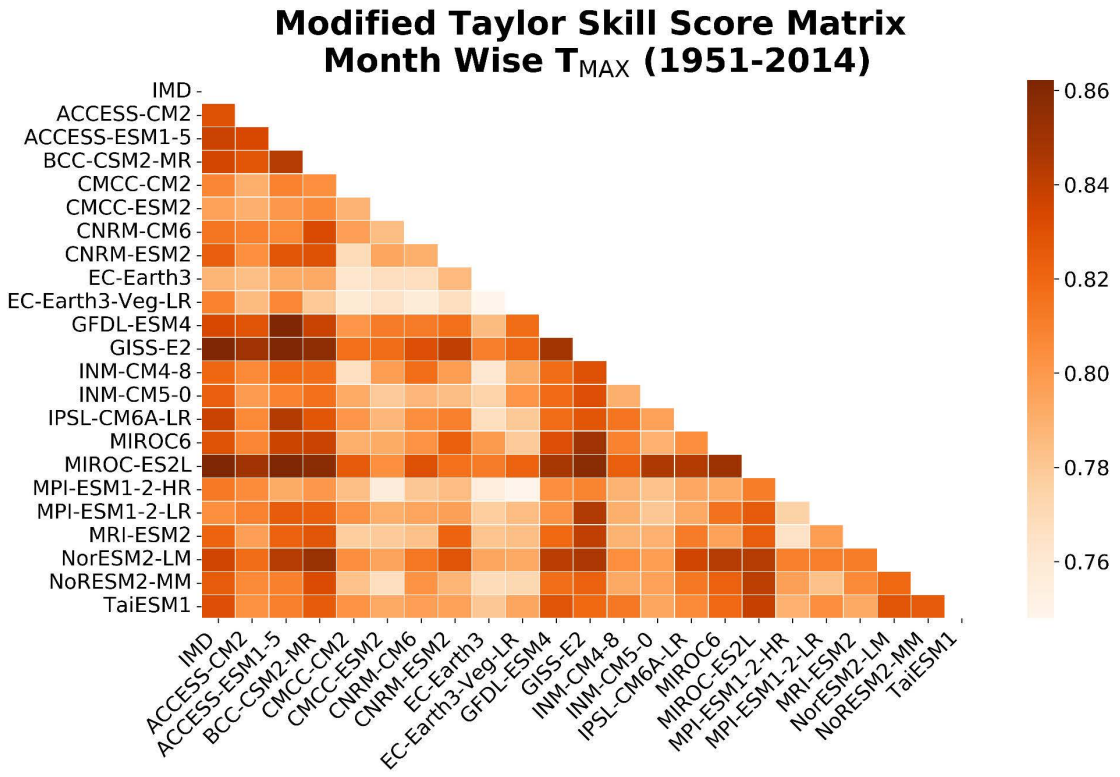

Fig. 7.3. Heat matrix of modified Taylor Skill Score for month-wise average maximum temperature.

This observed agreement suggests that combining these models into an ensemble could be beneficial. Such an ensemble approach could effectively mitigate individual model uncertainties and yield more robust and reliable projections, especially for applications requiring high confidence in climatic assessments. The season-wise performance of GCMs has been analyzed to further enhance the model selection process. Figure 7.4 presents the heat matrix for the season-wise evaluation period. The findings confirm that GISS-E2 and MIROC-ES2L remain the top-performing GCMs.

The season-wise analysis reveals performance variations similar to those observed in the month-wise analysis. However, a notable difference lies in the magnitude of the performance indicators, which suggests a better agreement during this evaluation period. The heat matrix also highlights several other GCMs that could be valuable for ensemble modeling. In particular, apart from the three leading GCMs, INM-CM5-0, and GFDL-ESM4 emerge as important contributors to a potential ensemble.

To enhance the seasonal understanding, individual seasonal performance was also analyzed. However, due to the limited data availability over the combined 64-year period, the results were not as robust as desired.

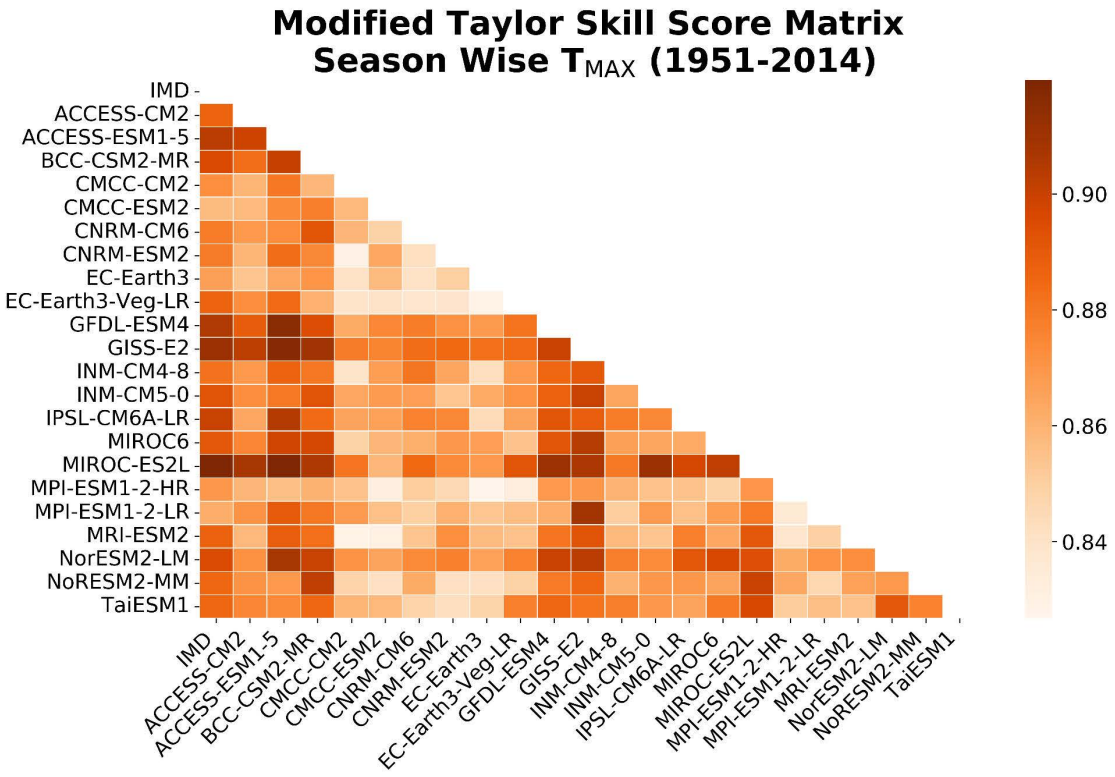

Fig. 7.4. Heat matrix of modified Taylor Skill Score for season-wise average maximum temperature.

This study further explores the decade-wise performance of GCMs, categorizing the six decades from 1951 to 2010, as illustrated in Fig. 7.5. The results demonstrate a broad range of performance across the GCMs. Particularly, the first decade shows that MIROC-ES2L provides the strongest match, while in the second decade, GISS-E2 outperforms the other models.

However, the following two decades (2001-2010) do not show promising results, as none of the GCMs demonstrated outstanding performance. A potential reason for this decline could be the variability in the representation of key climatic phenomena, such as monsoonal patterns, in the GCMs during these decades. GCMs may have had limited capabilities in accurately capturing these processes, leading to discrepancies in performance when analyzed on a decadal scale (Jose and Dwarakish 2020).

For the decade 1991-2000, the results are consistent with those observed in the daily and month-wise analyses. The last decade (2011-2020) also indicates that MIROC-ES2L remains the best-performing model among all the GCMs.

Overall, the performances of GCMs across months and seasons show greater consistency compared to other periods. These outcomes align with expectations, as aggregating daily variabilities into monthly and seasonal means inherently reduces noise and variability, leading to a smoother dataset. This smoothing process allows the modeled data to better align with the IMD observational dataset, especially when large-scale trends dominate over short-term daily fluctuations.

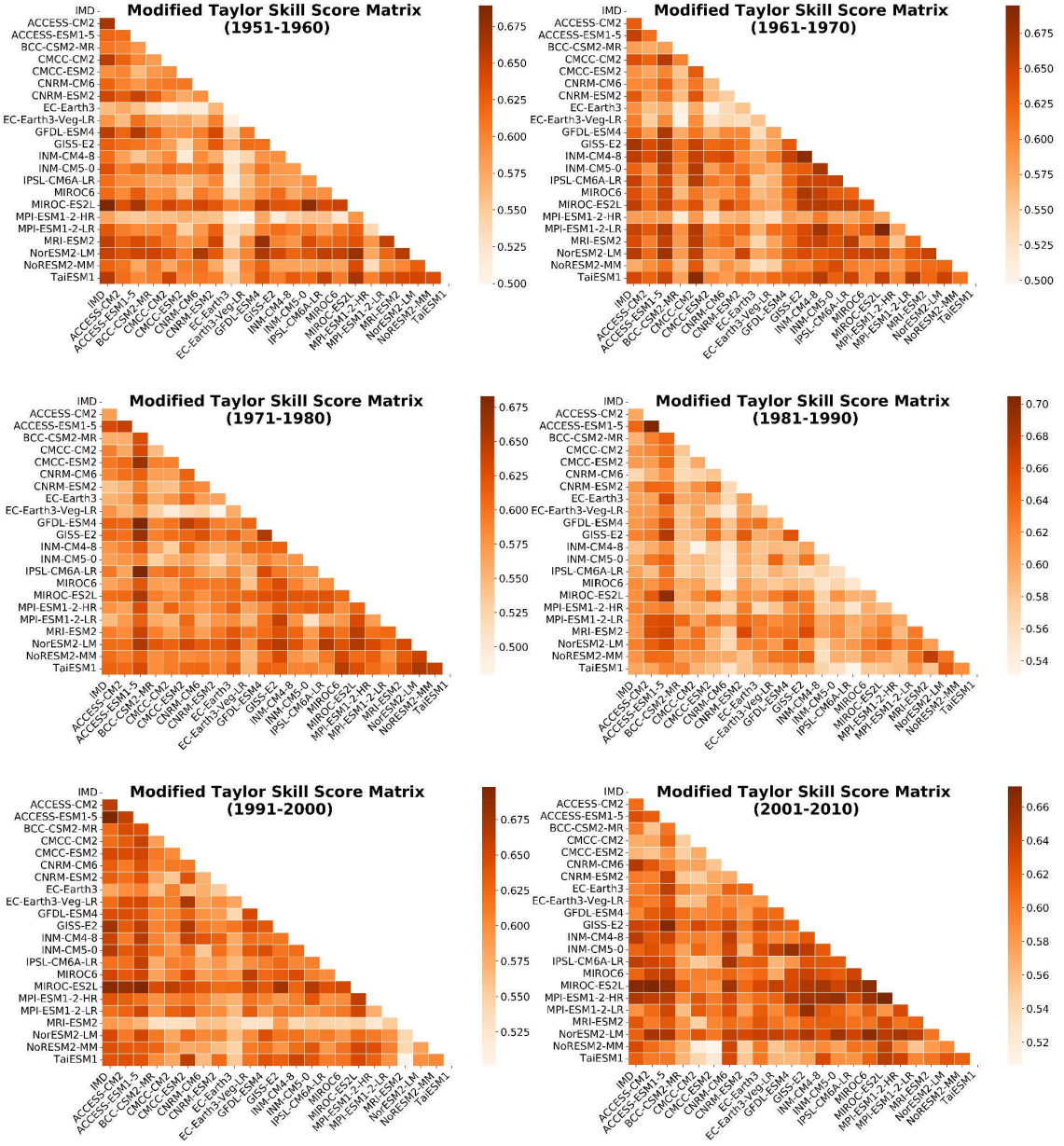

Fig. 7.5. Decade-wise (daily) heat matrix of modified Taylor Skill Score.

Additionally, we have plotted the overall performance of all the GoF metrics used in this study. The plot takes the form of a double-range heat matrix, where the upper portion represents the efficiency performance, and the lower portion represents the error performance of the GoF metrics. The performance values span from 0 to 1, with a value of 1 indicating a better match for efficiency and a value of 0 representing error. Figure 7.6 illustrates the heat matrix for all the GoF metrics utilized across different temporal durations.

A general selection of GCMs based on the upper matrix suggests that MIROC-ES2L, GISS-E2, and ACCESS-ESM1-5 are the best-performing GCMs, excluding the SS. The results shown by SS are highly diverse, indicating that none of the models performed consistently well across different durations, with each model showing varying results.

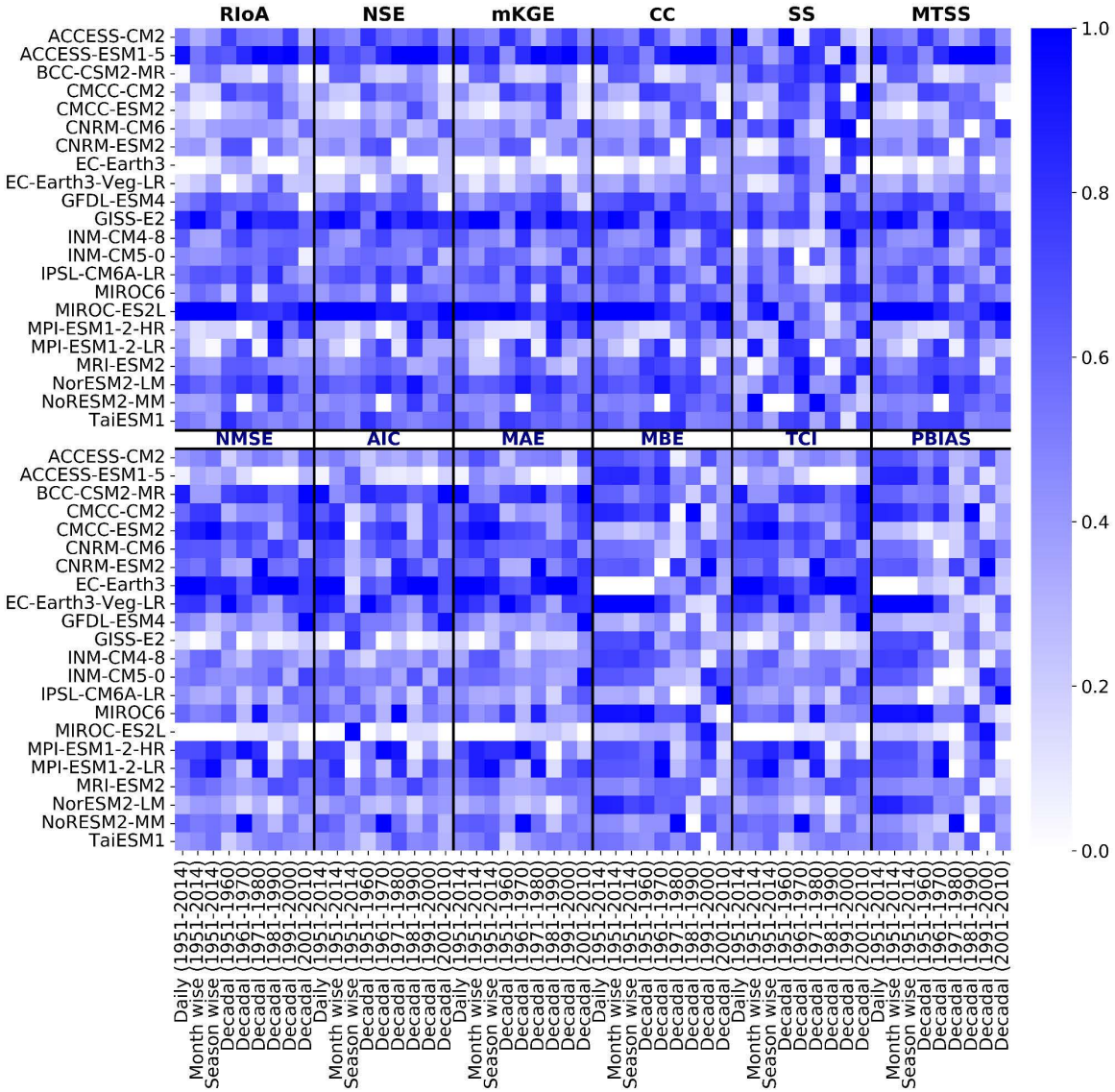

Fig. 7.6. Heat matrix of all GoF metrics used in the study with different time intervals (upper matrix for performance GoF and lower matrix for error GoF).

Similarly, the error-based GoF metrics also reveal a similar pattern, with MIROC-ES2L, GISS-E2, and ACCESS-ESM1-5 emerging as the best-performing models. However, two error-based metrics, PBIAS and MBE, indicate that EC-Earth3 performs better for certain durations. This highlights the varied performance across different models, with some outshining in specific durations according to particular error metrics.

When comparing the multi-temporal outcomes, we observed a consistent pattern of results for both types of GoF metrics from the 1960s to the 2000s. This suggests that the unanimity between CMIP6 GCMs and observed data during this period is as strong as for other durations, with no significant variation in magnitude. However, different GCMs were identified as the ideal models for different decades within this period. As a result, we do not rely on individual GCMs for overall performance but recommend ensemble models that may provide more robust results. This recommendation aligns with similar suggestions by McSweeney et al. (2015), supporting the findings of the current study.

7.3.3. Compromise Programming

A distinct ranking pattern emerges for different GoF metrics. For example, EC-Earth3 ranks the best based on PBIAS, while ACCESS CM2 performs the best based on SS. However, other GoF metrics suggest that MIROC-ES2L is the top-performing model.

Due to the inconsistency in the ranking of GCMs across multiple metrics and temporal periods, the CRI is employed to calculate the cumulative effect of all equal weighted GoF metrics used in the study. The CRI provides a comprehensive ranking that accounts for all GoF metrics and their respective temporal resolutions given in Table 7.2. The CRI values are calculated separately for each temporal resolution, and the combined overall ranking based on CRI suggests that MIROC-ES2L, GISS-E2, and ACCESS-ESM1-5 are the top three best-performing GCMs for maximum temperature in the eastern region of India.

The individual ranking based on CRI for daily maximum temperature spans from 0.33 to 0.76, with the lowest CRI value indicating the best model. In this category, MIROC-ES2L ranks as the top model. For the month-wise duration, the CRI range is from 0.30 to 0.83, with MIROC-ES2L again emerging as the best model.

In the decade 1951-1960, the CRI values ranged from 0.32 to 0.83, with TaiESM1 being the best-performing GCM. For the decade 1961-1970, the CRI range was from 0.30 to 0.84, with MIROC-ES2L leading. In the decade 1971-1980, the CRI values ranged from 0.30 to 0.87, and ACCESS-ESM1-5 was the top model. For the decade 1981-1990, the CRI values ranged from 0.32 to 0.80, and NorESM2-LM performed the best. The decade 1991-2000 saw CRI values ranging from 0.29 to 0.84, with 2M250 as the top model. For the decade 2001-2010, the CRI ranged from 0.30 to 0.79, and MPI-ESM1-2-HR emerged as the best model.

Overall, the CRI values range from 0.33 to 0.76, indicating that EC-Earth3 and EC-Earth3-Veg-LR consistently perform the worst across most time frames. The overall rank across all temporal resolutions is based on the average CRI value.

Individual rankings derived from different temporal resolutions indicate variability in the results, making it inadvisable to rely on individual GCMs for climate projections. Instead, creating ensembles of multiple GCMs, selected based on their rankings across various periods, would likely yield more robust climate projections. Iqbal et al. (2021) proposed an optimized algorithm for the classification of GCMs, which could be valuable for the ensemble process to strengthen the accuracy and reliability of projections.

The inconsistencies observed in GCM results can be attributed to factors such as spatial and temporal resolutions, initial conditions, and model tuning. The ranking of certain models higher than others is a result of their better agreement with IMD historical data and their ability to simulate observed changes. MIROC-ES2L outperforms other models due to its superior individual performance in GoF metrics, which ultimately influences its overall ranking when the CRI is used for cumulative evaluation.

Due to the limited number of studies that integrate both methodological (temporal analysis) and regional aspects, a direct comparison of our findings with previous research is challenging. Temporal analysis plays a critical role in this context, as emphasized by Sonali and Kumar (2013), who noted that decadal trends can differ significantly from overall trends.

Table 7.2. Ranking of GCMs based on CRI of daily, month-wise, season-wise and decade-wise maximum temperatures.

GCMs	Daily (1951-2014)		Month wise (1951-2014)		Season wise (1951-2014)		Daily (1951-1960)		Daily (1961-1970)		Daily (1971-1980)		Daily (1981-1990)		Daily (1991-2000)		Daily (2001-2010)		Average CRI	Overall rank
	CRI	Rank	CRI	Rank	CRI	Rank	CRI	Rank	CRI	Rank	CRI	Rank	CRI	Rank	CRI	Rank	CRI	Rank		
ACCESS CM2	0.44	5	0.54	12	0.54	10	0.33	**2**	0.51	15	0.51	11	0.44	11	0.44	9	0.60	13	0.48	8
ACCESS ESM1-5	0.40	**3**	0.45	6	0.40	6	0.48	13	0.39	10	0.30	**1**	0.39	6	0.29	**1**	0.44	6	0.39	**3**
BCC-CSM2-MR	0.77	21	0.43	5	0.40	5	0.61	18	0.70	20	0.71	18	0.49	14	0.58	16	0.79	22	0.61	18
CMCC-CM2	0.57	14	0.72	19	0.76	18	0.36	5	0.45	13	0.42	7	0.50	16	0.60	19	0.73	19	0.57	14
CMCC-ESM2	0.68	19	0.80	21	0.89	21	0.60	17	0.64	18	0.52	13	0.40	8	0.47	10	0.75	20	0.64	20
CNRM-CM6	0.61	17	0.60	15	0.60	14	0.48	12	0.60	16	0.52	12	0.68	21	0.59	17	0.47	9	0.57	15
CNRM-ESM2	0.57	13	0.58	14	0.69	17	0.38	6	0.38	7	0.87	22	0.52	18	0.57	15	0.61	14	0.57	16
EC-Earth3	0.83	22	0.83	22	0.77	19	0.71	21	0.60	17	0.77	20	0.80	22	0.84	22	0.66	16	0.76	22
EC-Earth3-Veg-LR	0.74	20	0.77	20	0.66	16	0.83	22	0.65	19	0.53	15	0.35	**3**	0.62	20	0.63	15	0.64	21
GFDL-ESM4	0.45	6	0.41	4	0.29	**3**	0.36	4	0.42	12	0.36	**2**	0.43	10	0.42	7	0.78	21	0.43	5
GISS-E2	0.37	**2**	0.36	**3**	0.28	**2**	0.49	14	0.31	**3**	0.39	4	0.37	5	0.31	**2**	0.36	**3**	0.36	**2**
INM-C4-8	0.51	10	0.56	13	0.65	15	0.54	16	0.39	8	0.54	16	0.53	19	0.35	**3**	0.38	4	0.49	9
INM-CM5-0	0.53	11	0.53	11	0.48	8	0.42	9	0.50	14	0.52	14	0.50	17	0.42	8	0.67	18	0.51	11
IPSL-CM6A-LR	0.46	7	0.36	**2**	0.34	4	0.44	10	0.38	6	0.46	9	0.42	9	0.54	14	0.57	12	0.44	6
MIROC6	0.59	16	0.49	10	0.54	9	0.62	19	0.39	9	0.76	19	0.45	12	0.37	4	0.44	7	0.52	12
MIROC-ES2L	0.36	**1**	0.30	**1**	0.07	**1**	0.34	**3**	0.31	**1**	0.39	**3**	0.46	13	0.42	6	0.34	**2**	0.33	**1**
MPI-ESM1-2-HR	0.62	18	0.68	17	0.78	20	0.69	20	0.84	22	0.60	17	0.40	7	0.52	12	0.29	**1**	0.60	17
MPI-ESM1-2-LR	0.58	15	0.70	18	0.89	22	0.46	11	0.42	11	0.82	21	0.36	4	0.59	18	0.67	17	0.61	19
MRI-ESM2	0.46	8	0.61	16	0.57	12	0.38	7	0.37	5	0.43	8	0.59	20	0.63	21	0.43	5	0.50	10
NorESM2-LM	0.46	9	0.48	8	0.43	7	0.41	8	0.31	**2**	0.40	5	0.32	**1**	0.40	5	0.52	11	0.41	4
NorESM2-MM	0.55	12	0.49	9	0.58	13	0.51	15	0.84	21	0.50	10	0.33	**2**	0.53	13	0.45	8	0.53	13
TaiESM1	0.42	4	0.45	7	0.56	11	0.32	**1**	0.36	4	0.42	6	0.50	15	0.48	11	0.47	10	0.44	7

*Bold represents the top three ranked GCMs

Our study addresses this by conducting a detailed temporal analysis using CMIP6 data. As a result, we compared our findings with research conducted in other regions and studies focused on single temporal analyses. The outcomes of our study contradict those obtained from CMIP6 GCMs for the Western Ghats region (Jose and Dwarakish 2022), where MPI-ESM1-2-HR was identified as the best-performing GCM. The variation in GCM selection is influenced by differences in gridded datasets, resolutions, and, crucially, the study location. Moreover, the ability of each GCM to simulate temperature and precipitation varies across regions, making it essential to assess the performance of each model individually for each climate variable.

Previous research highlights that the performance of models in one region may not necessarily apply to other regions, likely due to the diverse climatic conditions in each area (Zamani and Berndtsson 2019). This study, which primarily focuses on temporal analysis using specific observational datasets alongside a statistically downscaled CMIP6 dataset particularly emphasizing T_{max} variability acknowledges its limitations. These include the exclusion of dynamically downscaled data and other climate variables such as T_{min} and precipitation.

Future research should aim to address these gaps by incorporating dynamically downscaled data, conducting more comprehensive temporal evaluations, employing multi-model ensemble strategies, and applying advanced bias-correction methods to enhance the accuracy of regional climate projections and improve the robustness of decision-making processes.

7.4. Conclusions

This investigation assessed the performance of 22 CMIP6 GCMs in predicting maximum temperature for Eastern India. The assessment was based on individual GoF metrics and the combined performance using the CRI. The results indicate that the top-performing models across various temporal durations, based on both GoF and CRI, are MIROC-ES2L, GISS-E2, and ACCESS-ESM1-5. The key findings from this research are as follows:

- The majority of models tend to overestimate the upper limit of daily maximum temperature.
- Most models accurately represent the lower limit of daily maximum temperature.
- Individual assessments based on GoF metrics show similarities in outcomes.
- The results from SS, MBE, and PBIAS metrics exhibit inconsistencies.
- MIROC-ES2L, GISS-E2, and ACCESS-ESM1-5 are identified as the best-performing models based on both GoF and CRI across various temporal durations.
- Models with the least performance are not recommended for inclusion in ensemble modeling for maximum temperature projections.

The rankings for multi-duration comparisons are largely consistent, except for the 1981-1990 decade. This highlights the importance of the GCM selection process for climate impact assessments, as it significantly influences the overall ranking of GCMs. Therefore, future research could benefit from developing a machine learning-based ensemble of GCMs for the basin, incorporating the top-ranked models identified in this study. Such an approach would

allow for the evaluation of the temporal impact on climatic variables across the entire basin, based on the careful selection of GCMs. By focusing on GCMs that are not influenced by location, this approach can be applied universally to other regions as well. Given the consistent ranking of GCMs in our study area, it is recommended that these same models be used for future climate projections under various SSPs, ensuring consistent results in future projections.

References

Anvari, S. and Moghaddasi, M. (2023). Historical changes of extreme temperature in relation to soil moisture over different climatic zones of Iran. Stoch. Environ. Res. Risk Assess., 38(1), 157-173.

Ayugi, B., Ngoma, H., Babaousmail et al. (2021). Evaluation and projection of mean surface temperature using CMIP6 models over East Africa. J. Afr. Earth Sci., 181, 104226.

Carmen, M.A.A., Estrada, F. and Gay-García, C. (2021). A new method for assessing the performance of general circulation models based on their ability to simulate the response to observed forcing. J. Clim., 34(13), 5385-5402.

Cherchi, A., Fogli, P.G., Lovato et al. (2019). Global mean climate and main patterns of variability in the CMCC-CM2 coupled model. J. Adv. Model. Earth Syst., 11(1), 185–209.

IPCC (2021) Summary for Policymakers. In: Climate Change 2021: The Physical Science Basis. Contribution of Working Group I to the Sixth Assessment Report of the Intergovernmental Panel on Climate Change [Masson-Delmotte V, P. Zhai, A. Pirani, S.L. Connors, C. Péan, S. Berger, N. Caud, Y. Chen, L. Goldfarb, M.I. Gomis, M. Huang, K. Leitzell, E. Lonnoy, J.B.R. Matthews, T.K. Maycock, T. Waterfield, O. Yelekçi, R. Yu, and B. Zhou (eds.)]. In Press.

Jose, D.M. and Dwarakish, G.S. (2022). Ranking of downscaled CMIP5 and CMIP6 GCMs at a basin scale: case study of a tropical river basin on the South West coast of India. Arab. J. Geosci., 15(1), 120.

Patel, G., Das, S. and Das, R. (2024). Accuracy of historical precipitation from CMIP6 global climate models under diversified climatic features over India. Environ. Dev., 50, 100998.

Patel, G., Das, S. and Das, R. (2023a). Identification of Best CMIP6 Global Climate Model for Rainfall by Ensemble Implementation of MCDM Methods and Statistical Inference. Water Resour. Manag., 37(13), 5147–5170.

Patel, G., Das, R. and Das, S. (2023b). Is the extreme temperature trend changed in last two decades compared to last seven decades? Case study from Eastern India. J. Earth Syst. Sci., 132(3), 140.

Raju, K.S., Sonali, P. and Kumar, D.N. (2017). Ranking of CMIP5-based global climate models for India using compromise programming. Theor. Appl. Climatol., 128(3–4), 563–574.

Scafetta, N. (2021). Testing the CMIP6 GCM Simulations versus Surface Temperature Records from 1980–1990 to 2011–2021: High ECS Is Not Supported. Climate, 9(11), 161.

Shi, F., Wang, Z., Qi, L. and Chen, R. (2018). An assessment of GCM performance at a regional scale using a score-based method. Adv. Meteorol., 2018(1), 7641019.

Srivastava, A.K., Rajeevan, M. and Kshirsagar, S.R. (2009). Development of a high resolution daily gridded temperature data set (1969–2005) for the Indian region. Atmos. Sci. Lett. 10(4), 249–254.

Thrasher, B., Wang, W., Michaelis et al. (2022). NASA Global Daily Downscaled Projections, CMIP6. Sci. Data, 9(1), 262.

Zelany, M. (1974). A concept of compromise solutions and the method of the displaced ideal. Comput. Oper. Res., 1(3–4), 479–496.

Machine Learning for Climate Model Evaluation

"Patel, G., Das, S. and Das, R. (2024). A comparative approach to understand the performance of CMIP6 models for maximum temperature near Tropic of Cancer using multiple machine learning ensembles. Water Resources Management (in review)"

8.1. Introduction

Climate change on a global scale has become a significant concern, with rising temperatures and shifting precipitation patterns severely impacting the water sector and causing complex hydrological events. These changes pose significant risks to public health, food security, flood management, water security, and environmental sustainability (Wang et al. 2023). Temperature, as a fundamental component of the climatic system, plays a pivotal role in the occurrence of extreme events such as heatwaves and severe wildfires. Therefore, achieving a comprehensive understanding and accurate projection of temperature variations is vital for mitigating these extreme hydrological and climatic events.

Global Climate Models (GCMs) are essential tools for understanding the complex climate system of Earth and its responses to both anthropogenic and natural forcings. The Coupled Model Intercomparison Project Phase 6 (CMIP6) provides a comprehensive ensemble of climate models, each contributing unique projections of future climate conditions (Eyring et al. 2016). However, the performance of these models varies considerably, introducing uncertainty into their predictions (Jose and Dwarakish 2020). To address these uncertainties, several approaches have been proposed, including downscaling techniques, bias correction, multimodel ensemble approaches, and the application of advanced machine learning methodologies.

As policymakers and researchers increasingly rely on climate models for informed decision-making, the need for a robust framework to rank and evaluate the credibility of these models has become critical. To address uncertainties associated with GCMs, many researchers have adopted the widely used Multi-Model Ensemble (MME) approach. This method combines the most reliable GCMs from various sources, utilizing systematic bias correction techniques to enhance accuracy (Ahmed et al. 2020, Jose et al. 2022). However, the performance of both individual models and MMEs is often constrained by the inherent randomness, nonlinearity, and methodological complexities involved in climate modeling (Fu et al. 2023, Wang et al. 2023).

In the last few years, machine learning (ML) algorithms have become crucial in tackling diverse challenges in climate change research and prediction (Shetty et al. 2023). The unique climate dynamics of the Indian subcontinent, particularly the Indian monsoon and the high solar radiation near the Tropic of Cancer (TOC) play a pivotal role in influencing maximum temperature (T_{max}) projections. The Indian monsoon, marked by complex atmospheric interactions, results in significant variability in precipitation patterns and temperature

extremes. These complexities pose challenges for accurately forecasting T_{max}, as traditional models often struggle to capture the refined relationships between atmospheric parameters and temperature fluctuations. Furthermore, the proximity of the area to the TOC causes strong sun radiation, which greatly influences T_{max} values. This solar radiation interacts with local topography, land use, and other climatic factors, creating localized temperature anomalies that are challenging to predict using conventional methods. The complex interplay of these factors underscores the limitations of traditional approaches in capturing the intricate dynamics of T_{max} variability.

To address these challenges, employing advanced machine learning (ML) techniques and ensemble approaches becomes essential. These techniques highlight combining several datasets, identifying nonlinear correlations, and considering the geographical and temporal fluctuations inherent in the climatic system of the region. By utilizing such advanced techniques, researchers can significantly enhance the accuracy of T_{max} predictions. This, in turn, provides more reliable information for evolving effective climate adaptation and mitigation strategies tailored to the unique climatic dynamics of the region. In recent years, several studies have utilized ML ensembles of GCMs to predict precipitation and temperature, demonstrating the potential of advanced techniques in improving climate projections (Ahmed et al. 2020, Dey et al. 2022, Jose et al. 2022, Fu et al. 2023, Shetty et al. 2023, Wang et al. 2023).

Ahmed et al. (2020) compared the effectiveness of various ML algorithms, including Artificial Neural Network (ANN), K-Nearest Neighbor (KNN), Support Vector Machine (SVM), and Relevance Vector Machine (RVM), for predicting precipitation and temperature in Pakistan. Their results indicated that KNN and RVM outperformed SVM and ANN in terms of accuracy.

Shetty et al. (2023) evaluated seven ML ensembles for climate predictions in the Western Ghats of India, finding that Extreme Gradient Boosting Regressor (XGBR) and Random Forest Regressor (RFR) delivered superior results compared to other methods.

Wang et al. (2023) examined six MME techniques, including Random Forest (RF), KNN, Extreme Tree (ET), Gradient Boosting Decision Tree (GBDT), a fusion of all ML methods, and the simple mean for MME. Their study concluded that the fusion of all ML methods provided better agreement than individual models or the mean MME approach.

Dey et al. (2022) employed an MME framework using ANN, RF, SVM, and Simple Arithmetic Mean (SAM) for simulating precipitation and temperature. The results indicated that RF and SVM outperformed the other methods in their analysis. Fu et al. (2023) assessed the performance of nine ML techniques for predicting precipitation, radiation, and temperature. Based on individual performance, the top three models Light Gradient Boosting Machine (LGBM), Gradient Boosting Regressor (GBR), and RF were selected for stacking. The stacked model demonstrated superior agreement compared to individual methods.

Jose et al. (2022) evaluated MME performance using six methods: SVM, Multiple Linear Regression (MLR), ET, RF, Long Short-Term Memory (LSTM), and simple mean. Their findings revealed that LSTM significantly outperformed other ML methods in predicting precipitation. As highlighted above, machine learning-based algorithms often outperform individual models when used in ensemble approaches. While previous studies have primarily focused on individual ML models or limited ensembles to showcase their advantages, the

complexities of climate-driven complicated interactions and diverse statistical properties demand a more refined modeling approach. Recent research has begun to address these complexities by employing integrated ensemble techniques.

However, critical aspects such as the selection of ML models, performance evaluation criteria, ranking methods for GCM selection, and the methodologies for integrating ensembles remain unexplored. These factors are pivotal for utilizing the full potential of machine learning in climate studies. A comprehensive framework that incorporates these elements is likely to enhance the selection and performance of ensembles, offering more accurate and reliable climate projections than those achieved with earlier methods.

The aim of this research is to establish a systematic framework for ranking CMIP6 climate models and their ensembles based on predictive accuracy using ML and ensembles of top-performing ML models. By evaluating and comparing the performance of diverse ML algorithms within an integrated ensemble framework, this research aims to address the critical challenge of quantifying model reliability and enhancing confidence in climate projections. The ultimate goal is to provide the scientific community with a robust, methodologically sound tool for identifying models that excel in replicating observed climate data, thereby contributing to more accurate and reliable climate predictions.

In this study, 14 ML algorithms, along with four multi-ML ensembles (MMLEs) widely applied across various fields, are utilized to evaluate the robustness of different climate models. The novelty of this study lies in utilizing the most reliable techniques for ranking and integrating ensemble methods to achieve superior performance. The objectives of the investigation are to: (i) develop a systematic ranking approach for CMIP6 climate models, (ii) evaluate the performance of 14 ML algorithms within an integrated ensemble framework, (iii) explore feature importance techniques for model ranking, and (iv) investigate the optimal number of GCMs and ML algorithms required for enhanced predictive accuracy. The findings are expected to be highly relevant to climate scientists, policymakers, and stakeholders engaged in climate impact assessment and adaptation planning, particularly in the domain of water resource management.

8.2. Study Area and Data Used

The selection of the study area was guided by its proximity to the TOC. Regions near the TOC typically experience intense solar radiation, which significantly affects temperature patterns, making them ideal for climatic studies and the evaluation of climate change impacts. This study focuses on two key areas: (i) four major river basins in eastern India, analyzed as a single entity, and (ii) one district in northern India (Fig. 8.1). The study focuses on four river basins: Kangsabati, Keliaghai, Silabati, and Dwarkeswer (KKSD). These basins are located between the geographical coordinates of 21°53′ to 23°31′ N latitude and 85°58′ to 87°48′ E longitude, collectively covering an area of about 15,358 km². These basins are prone to frequent flooding, particularly in their extensive floodplains during the monsoon season (Patel et al. 2023). The district of Ujjain, which spans approximately 6100 km², is located in Madhya Pradesh, India, about 1200 km away from the river basins. Both the river basins and the Ujjain district fall under the tropical savanna climate (Aw) as per the Köppen climate classification. The 22 GCMs selected for this study were taken from Table 7.1.

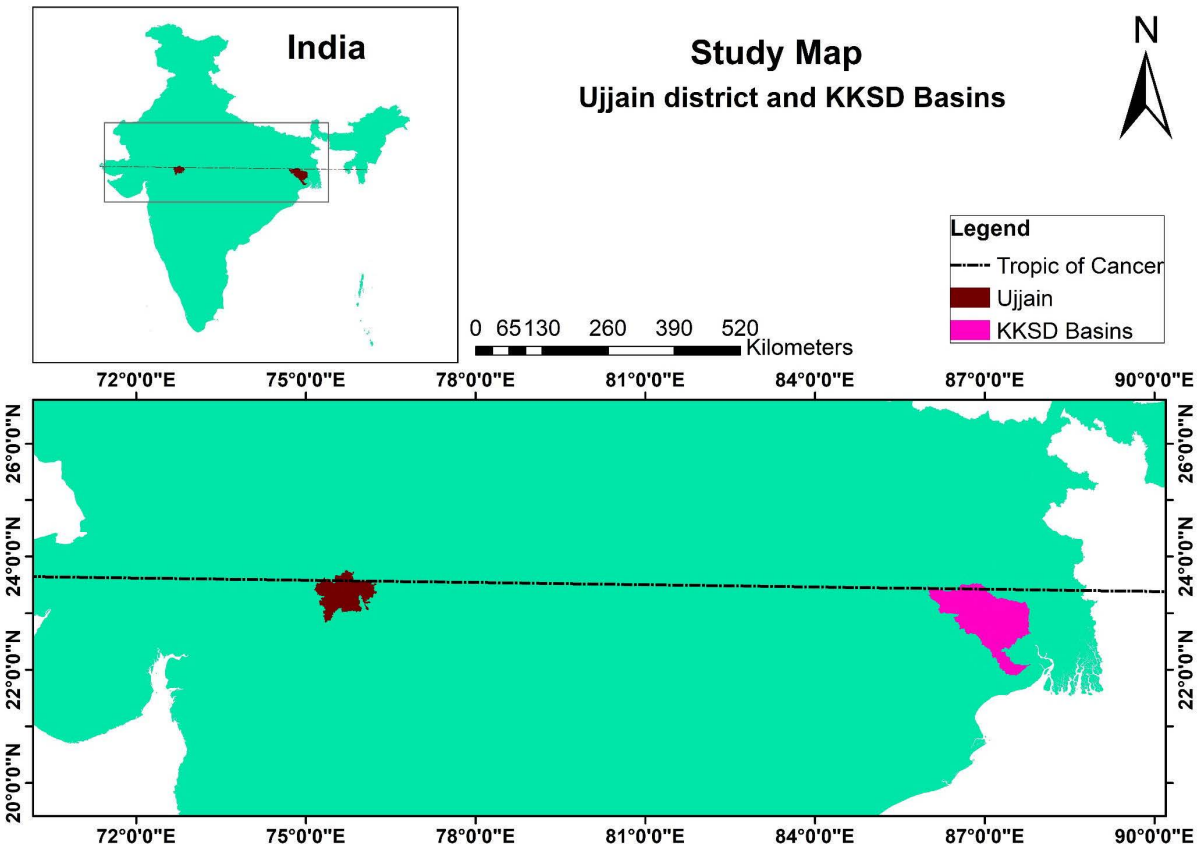

Fig. 8.1. Demarcation of locations utilized for study.

8.3. Machine Learning Approaches to Evaluation

8.3.1. Screening of Best-Performing GCMs

Feature Importance (FI) is an important aspect to understand the effectiveness of different GCMs for predicting T_{max}. In this study, tree-based machine learning models are utilized to calculate FI, focusing on individual features (GCM) that contribute to reducing impurity within the ensemble of decision trees. Impurity reduction is quantified using metrics such as Gini impurity, which measures the effectiveness of a feature in splitting data across the decision trees.

A higher FI value indicates greater significance of a particular GCM in accurately predicting T_{max}. By ranking GCMs based on their FI values, the study identifies the most relevant models for subsequent analysis. This systematic approach ensures the selection of the best-performing GCMs and ML algorithms, enhancing the accuracy and reliability of the prediction framework for climate studies.

8.3.2. ML-Based Ensemble

In this study, a total of 18 techniques are utilized to construct an MME for predicting maximum temperature (T_{max}) at both study locations. These techniques are based on the top-ranked GCMs, identified using FI criteria. The ensemble combines 14 ML algorithms and four MMLE methods, aiming to enhance the overall predictive performance of the framework.
The 14 ML algorithms employed in this study include:

- Random Forest (RF)
- Least Angle Regression (LAR)
- Extreme Gradient Boosting (XGB)
- LightGBM (LGB)
- CatBoost (CB)
- AdaBoost (AB)
- Extra Trees Regressor (ETR)
- Gradient Boosting (GB)
- Support Vector Regression (SVR)
- K-Nearest Neighbors (KNN)
- Histogram-Based Gradient Boosting (HGB)
- Multi-Layer Perceptron (MLP)
- Linear Regression (LR)
- Multivariate Adaptive Regression Splines (MARS)

Additionally, the four MMLE techniques include:

- Stacking
- Bagging
- Voting
- Blending

These algorithms are used to integrate the top-performing GCMs into a robust multi-model ensemble, designed to minimize uncertainty and improve the precision of T_{max} projections. Each algorithm within the ensemble is accurately tuned through a systematic hyperparameter optimization process, ensuring peak efficiency and reliable outputs.

8.3.3. Hyperparameter Tuning

For each ML algorithm, hyperparameters are systematically optimized to achieve peak efficiency and enhance model performance. Grid search is employed as the preferred method for hyperparameter optimization in this study. This method systematically explores a predefined parameter grid, ensuring an exhaustive search for the best hyperparameters for each model. Grid search is particularly advantageous in scenarios where the parameter space is small and well-defined, providing a reliable framework for model tuning.

The primary objective of utilizing these 18 techniques is to address the uncertainty inherent in climate model simulations. By combining the strengths of individual models with advanced ensemble methods, the study seeks to enhance the precision of T_{max} predictions, thereby improving the reliability of climate change projections for the study regions.

The success of this methodology hinges on the ability of these models to effectively capture and generalize climate patterns. By providing more accurate and actionable insights, the approach aims to support climate adaptation and mitigation strategies, offering a robust tool for policymakers and stakeholders involved in managing climate impacts.

8.3.4. Split Statistics and Performance Evaluation

Traditional methods of splitting data based solely on time periods can unintentionally create training datasets that fail to adequately represent more recent temperature trends. This mismatch poses a risk of introducing bias in the evaluation process, as the ability of models to generalize to current or future climates may be compromised.

This issue becomes especially pertinent when the phenomena under study are influenced by gradual climate changes. To address this challenge, advanced data-splitting techniques that account for long-term trends are essential. These techniques ensure that the training datasets reflect the evolving nature of climate patterns, enhancing the reliability of the models in predicting temperature variability under changing climatic conditions.

To address this problem, random splitting is employed as a more robust method. Random splitting mitigates the bias caused by time-based data partitioning by balancing the distribution of values across both the training and validation sets. This approach ensures that both extremes and trends over time are adequately represented, allowing the model to train on a broader, more representative sample.

Additionally, to further enhance fairness in data splitting, the study explored the use of sampling based on quantiles or binning by temperature ranges. These techniques ensure that each subset of data contains a fair representation of the temperature spectrum. By incorporating a comprehensive distribution of temperature values in both training and validation datasets, these methods enable the model to generalize effectively across potential future climate scenarios.

An optimal split ratio is also critical for the performance of models. Traditional ratios like 70-30 or 80-20 are often used in machine learning studies. However, through empirical testing, we found that an 80-20 split (80% training data and 20% validation data) yields better performance for our climate data, allowing the models to capture sufficient variability in both the training and validation phases.

To enhance the performance and robustness of our climate models, hyperparameter tuning and cross-validation are crucial steps in the modeling process. These steps ensure that the models are optimized for predictive accuracy and generalization, particularly when dealing with complex and diverse climate datasets.

We have used Grid Search Cross-Validation (GSCV) to fine-tune the hyperparameters of each machine learning algorithm and ensemble method. GSCV involves systematically searching through a predefined set of hyperparameters to identify the optimal configuration for each model.

Cross-validation further enhances the robustness of the model by partitioning the data into multiple subsets, allowing each subset to be used as both training and validation data at different stages. This iterative approach reduces the risk of overfitting and ensures that the performance of models is consistent across various data splits.

By employing GSCV and cross-validation, the study ensures that each machine learning algorithm and the ensemble approach are customized to the unique features of the climate data. This rigorous optimization process significantly contributes to reducing uncertainty in T_{max} predictions and improving the reliability of climate projections for the study regions.

The performance evaluation metrics (R^2, MBE, RMSE, IoA) offer a comprehensive valuation of model accuracy and reliability, ensuring that the selected models are optimized for climate projections and can generalize well across various future scenarios.

8.4. Results and Discussion

8.4.1. Feature Importance (FI) and Ranking of GCMs

The performance of individual GCMs was evaluated using various ML algorithms, as shown in Fig. 8.2. Among these, the R^2 values for KNN, ETR, and RF were higher for both the KKSD basins and Ujjain locations, indicating strong model performance for these algorithms.

In this study, FI was utilized to rank the GCMs based on their contribution to the prediction of the models. FI is an important concept in machine learning as it quantifies the influence of each feature on the output of the models, providing insight into which GCMs are most informative for climate projections. While determining FI in algorithms like KNN is complex due to its non-parametric, instance-based nature, it is more straightforward in model-based methods like decision trees and linear regression. Therefore, we chose ETR to analyze the FI values of the GCMs, given its ability to handle feature importance effectively.

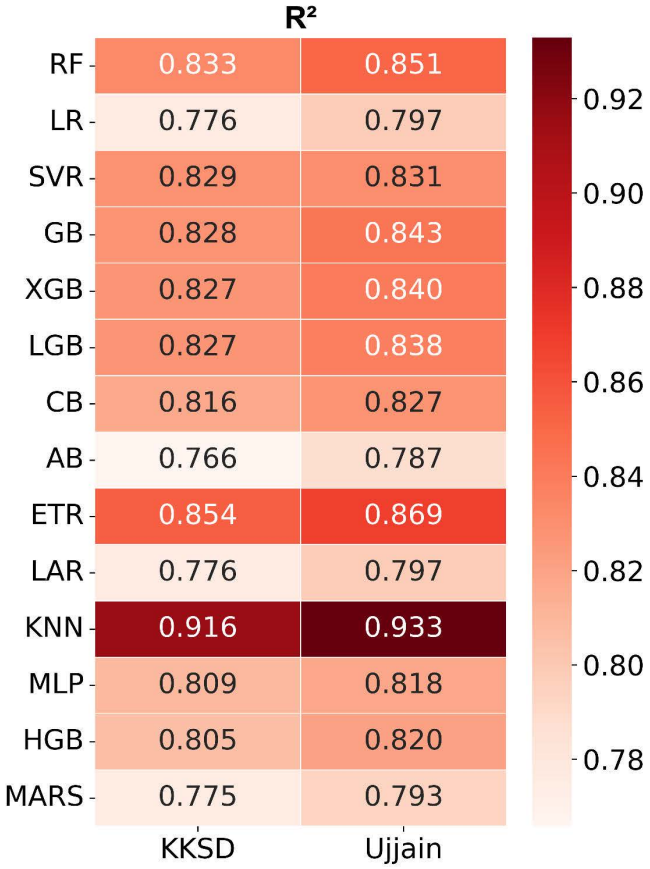

Fig. 8.2. Performance of individual ML for KKSD basins and Ujjain district.

According to the FI results, the top three GCMs for KKSD basins were MIROC-ES2L, GISS-E2, and ACCESS-ESM1-5. For Ujjain, the top three GCMs were INM-CM4-8, MRI-ESM2, and MIROC-ES2L. These rankings reflect the varying contributions of different models to the climate projections in each location.

Figure 8.3 presents the complete ranking of the 22 GCMs for both KKSD basins and Ujjain. Particularly, the least contributing GCMs were EC-Earth3 for KKSD basins and GISS-

E2 for Ujjain. Despite these differences in GCM rankings between the two locations, MIROC-ES2L consistently appeared as one of the top contributing models in both regions.

The observed differences in the rankings of GCMs between KKSD basins and Ujjain may be attributed to several factors. First, regional climate dynamics including local topography and atmospheric circulation patterns, can influence how climate variables respond to broader climate drivers. These regional characteristics may cause different sensitivity levels to GCM projections, making certain models more accurate or relevant for one location over another. Additionally, inter-model variability plays a role. Each GCM operates under distinct assumptions and parameterizations, leading to differences in how each simulates specific climate responses. Such variability can make certain GCMs align better with the historical climate data of one region, contributing to discrepancies in the rankings between locations.

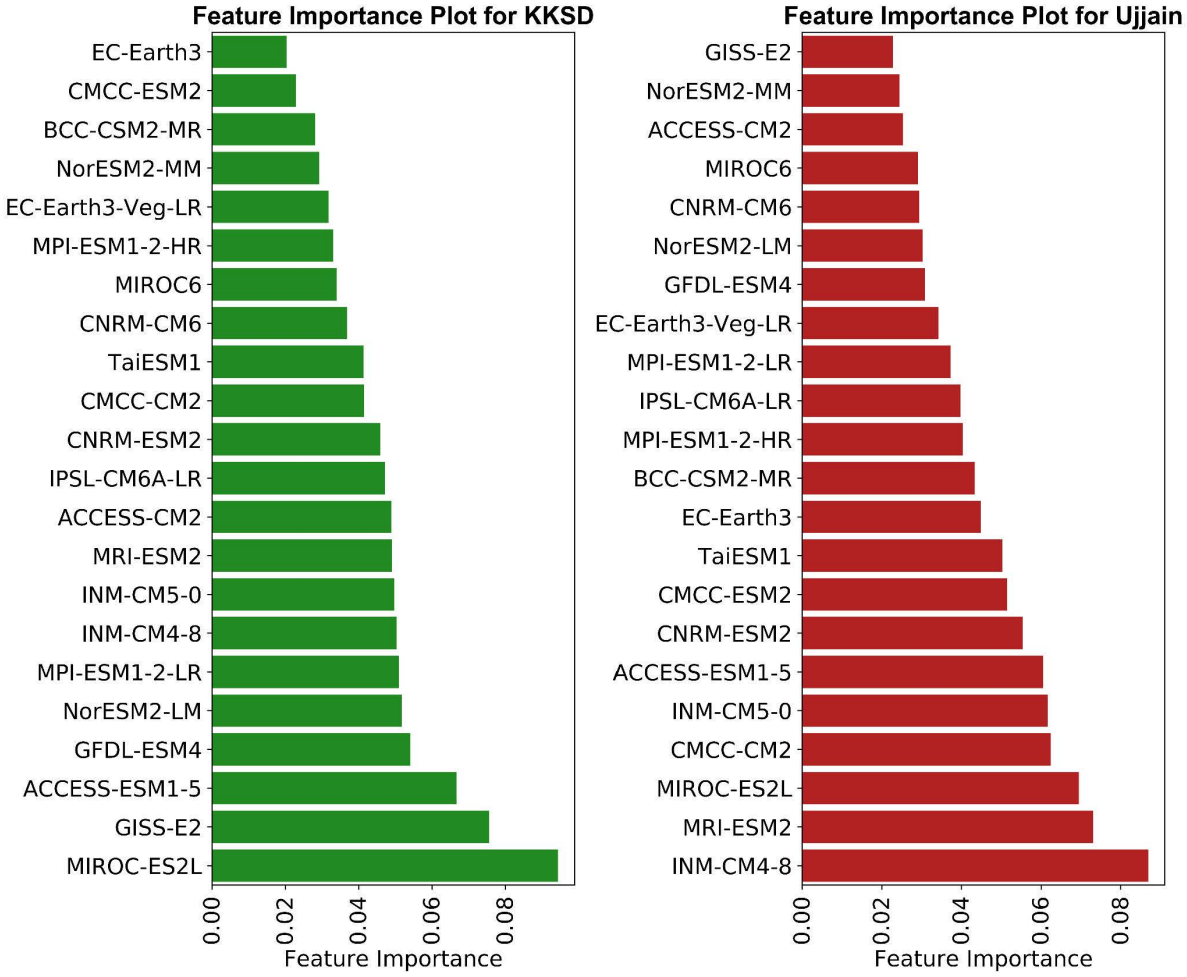

Fig. 8.3. FI plots for ETR over KKSD basins and Ujjain district.

Furthermore, we also analyzed the contribution of these GCMs when used in an ensemble approach. Our findings revealed that the performance of model improves as the number of GCMs included in the ensemble increases. Therefore, it was concluded that selecting only the top-ranked GCMs, as often suggested in the literature, might not always yield the best results. This is because the diversity of the ensemble contributes to better performance by capturing a wider range of model behavior.

Figure 8.4 illustrates the performance of the selected ML algorithms based on the ranked GCMs according to their FI values. As shown, the inclusion of all 22 GCMs in the ensemble provided improved results. Hence, we opted to consider all 22 GCMs in the ensemble for this study, supporting the idea that incorporating a broad range of models enhances the overall predictive accuracy.

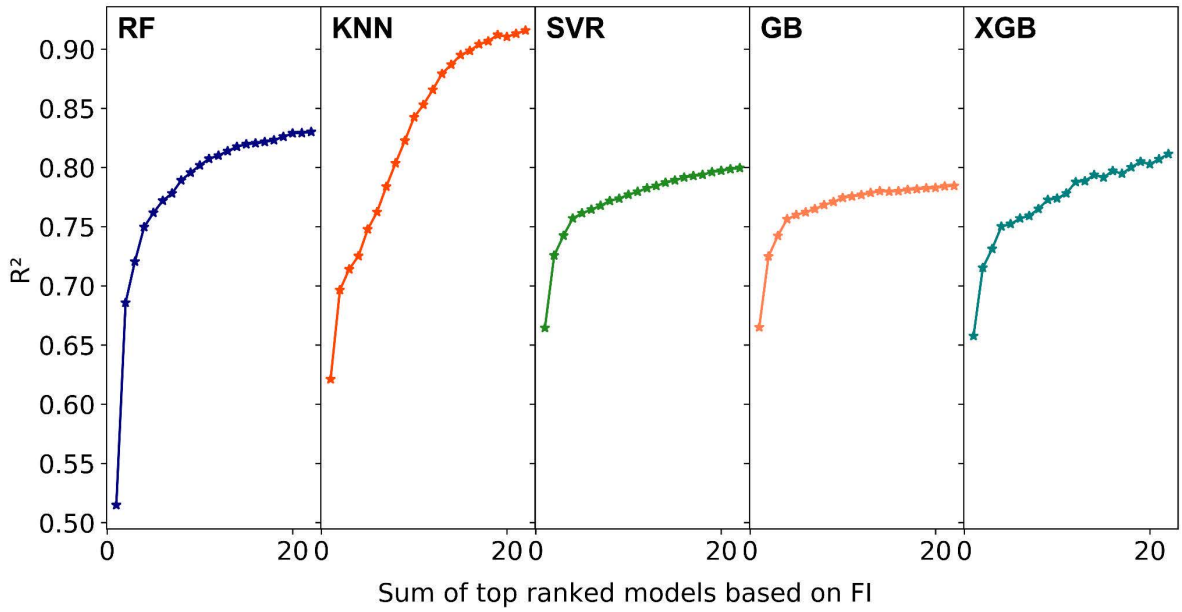

Fig. 8.4. Performance of selective ML algorithms based on collective ranked GCMs.

The analysis of GCM performance in this study highlights the importance of ensemble-based approaches that integrate multiple GCMs, as they allow for better generalization and improved climate predictions.

8.4.2. Performance and Comparison of ML Algorithms

In this study, a total of 14 ML algorithms were chosen to create an ensemble of GCMs, and four performance metrics were used to assess the overall ability of the ML models. The outcomes of the evaluation are presented in Figs. 8.5(a) and 8.5(b). The comparison reveals that the R^2 values between the models and observed data are significantly higher for the ML ensemble compared to the individual GCMs for both KKSD basins and Ujjain district. The R^2 values for all the individual GCMs are below 0.583, while the ML ensemble yields R^2 values exceeding 0.775, highlighting the superior predictive accuracy of the ensemble approach.

The MBE ranges from -0.747 to 0.323, with the MBE values for the ML ensemble being closer to zero, indicating more balanced predictions. The ensemble effectively integrates the outputs of the individual models, except for AB, which shows some deviation. Particularly, there is a negative MBE for Ujjain district and a positive MBE for KKSD basins, suggesting that the ensemble model handles the biases differently across the two locations, but remains efficient in managing these variations within an acceptable range.

The RMSE ranges from 1.184 to 3.336, with individual GCMs showing higher RMSE values. In contrast, the ML ensemble achieves a reduced range of 1.184 to 2.218, further

supporting the conclusion that the ML ensemble provides a more accurate and robust evaluation of the climate data.

Finally, the IoA follows a similar trend to the R^2 results, with the individual GCMs lagging behind the ML ensemble. This reinforces the conclusion that the ensemble method offers a superior fit to the observed data, both in terms of accuracy and consistency.

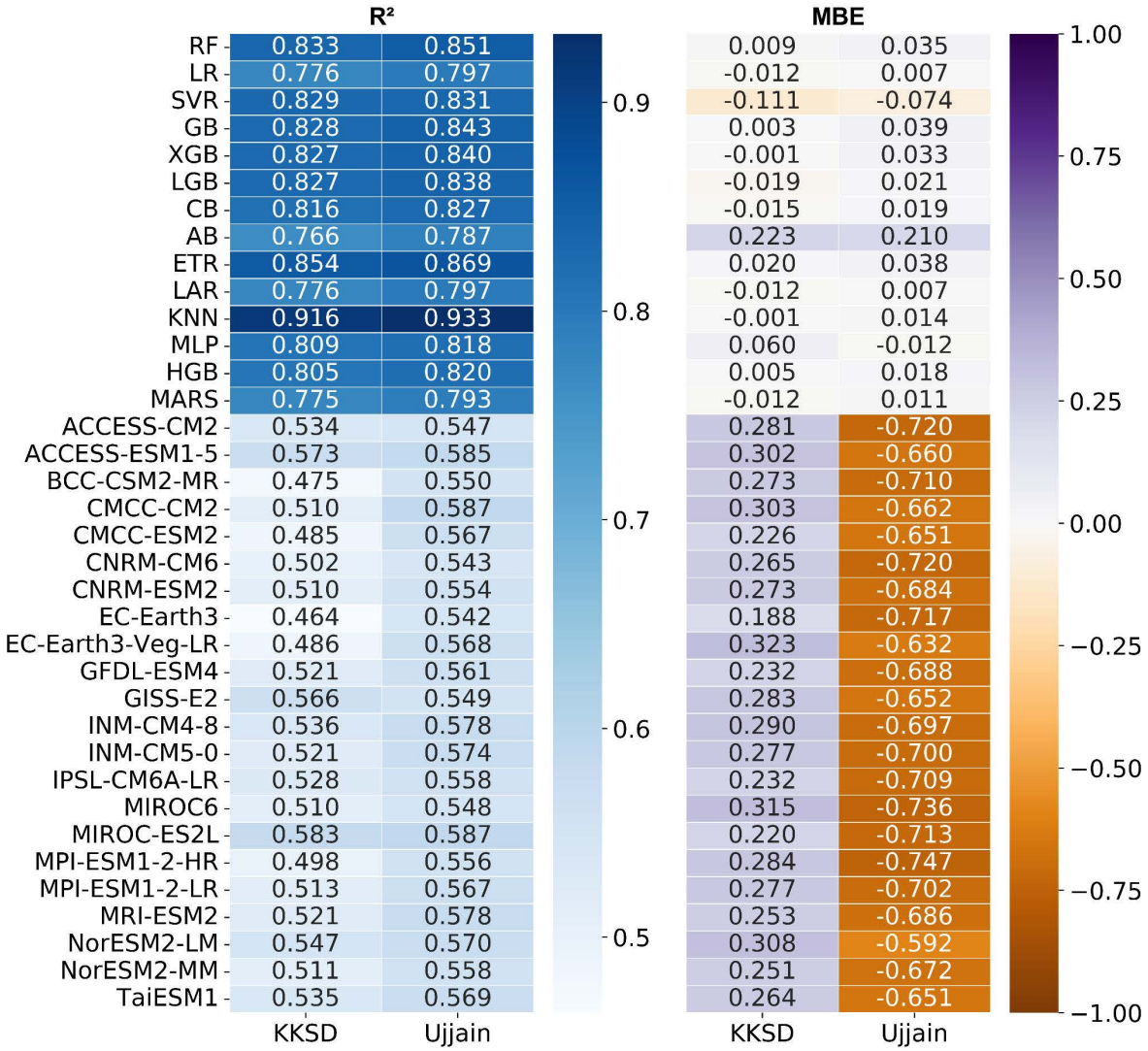

Fig. 8.5. (a) Individual GCMs and ML metric performance for KKSD basins and Ujjain district.

To enhance understanding of the outputs, we represented the performance of the individual metrics visually. For MBE, lighter shades indicate better representation, including both positive and negative biases, whereas, for RMSE, R^2, and IoA, darker shades denote better results. In conclusion, the results demonstrate that the MME, developed using various ML methods, performs significantly better than the individual GCMs, providing a more reliable and accurate model for climate predictions. The performance improvement observed in the ensemble approach highlights the value of integrating multiple machine learning algorithms to enhance the predictive capacity and robustness of climate models.

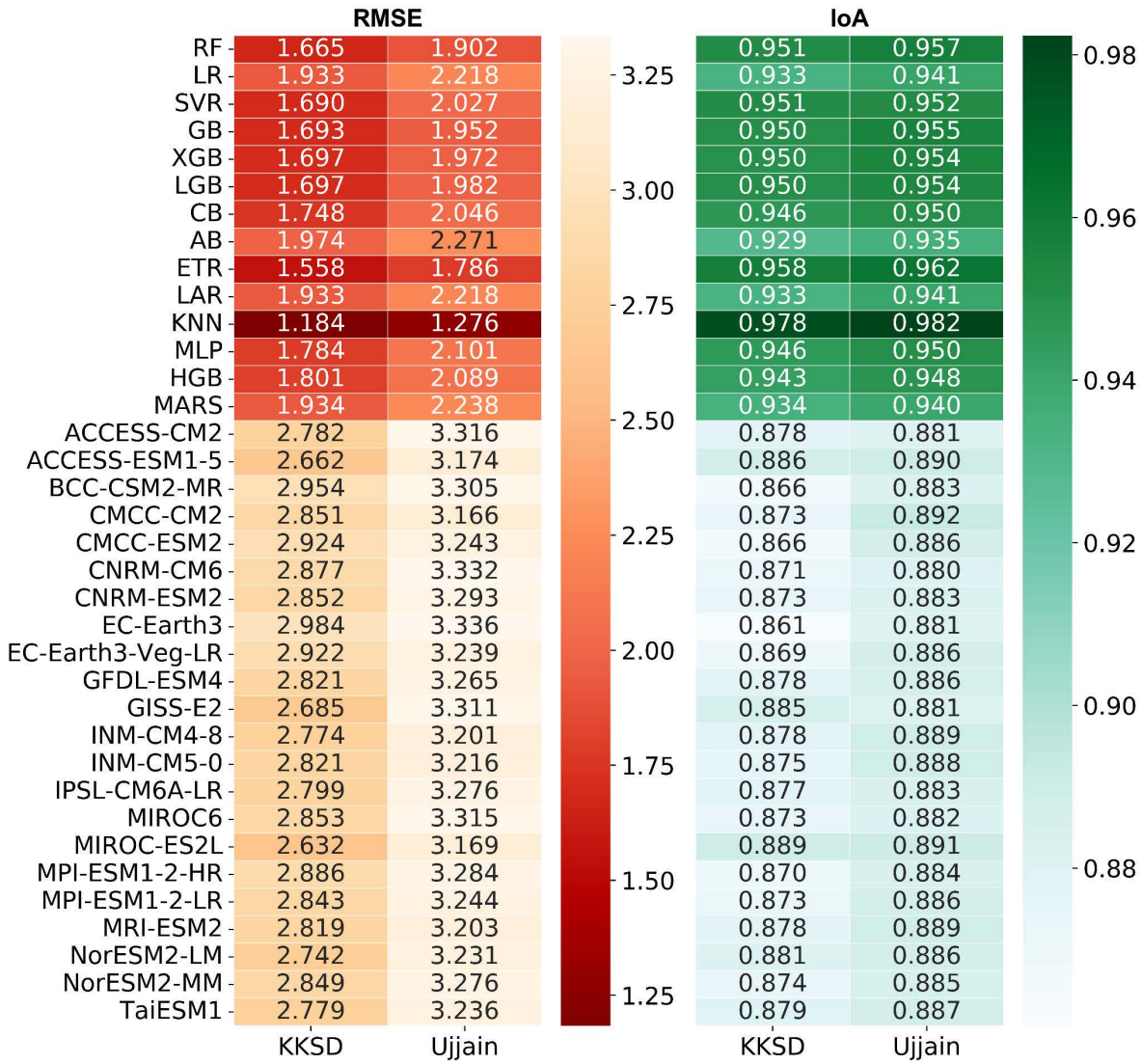

Fig. 8.5. (b) Individual GCMs and ML metric performance for KKSD basins and Ujjain district.

8.4.3. Ensemble of ML Models

In this study, an MME was developed using 22 CMIP6 GCMs and 14 ML algorithms. The performance of the ML ensemble consistently outperformed that of individual GCMs. To refine the results further, we employed MMLE that combined the outputs of multiple ML models, using four widely adopted approaches: bagging, blending, stacking, and voting. These methods were chosen because they effectively harness the collective predictive power of various ML models, enhancing the overall accuracy and reliability of the predictions beyond what individual models could achieve.

While it is possible to ensemble all models collectively, the approach of combining models based on their performance rankings provides a more refined analysis. By utilizing the strengths of each ML model according to their ranking, we ensured a more effective and robust combination, improving predictive accuracy. Based on the R^2 rankings shown in Fig. 8.2, the top-performing ML algorithms for both KKSD basins and Ujjain district were KNN, ETR, and RF. Additionally, SVR performed well for KKSD basins, and GB shined for the Ujjain

district. Despite variations across locations, many of the models demonstrated comparable performance.

To organize the analysis, we grouped the ML algorithms into three categories based on their performance ranks: Top 14, Top 5, and Top 3. The results of fusing multiple ML algorithms are illustrated in Figs. 8.6(a) and 8.6(b). The ensemble combinations based on R^2 values showed that 12 of the ensemble combinations outperformed individual ML models, except for KNN. The R^2 values for the ensemble methods ranged from 0.775 to 0.934, demonstrating significant improvement over individual model performance.

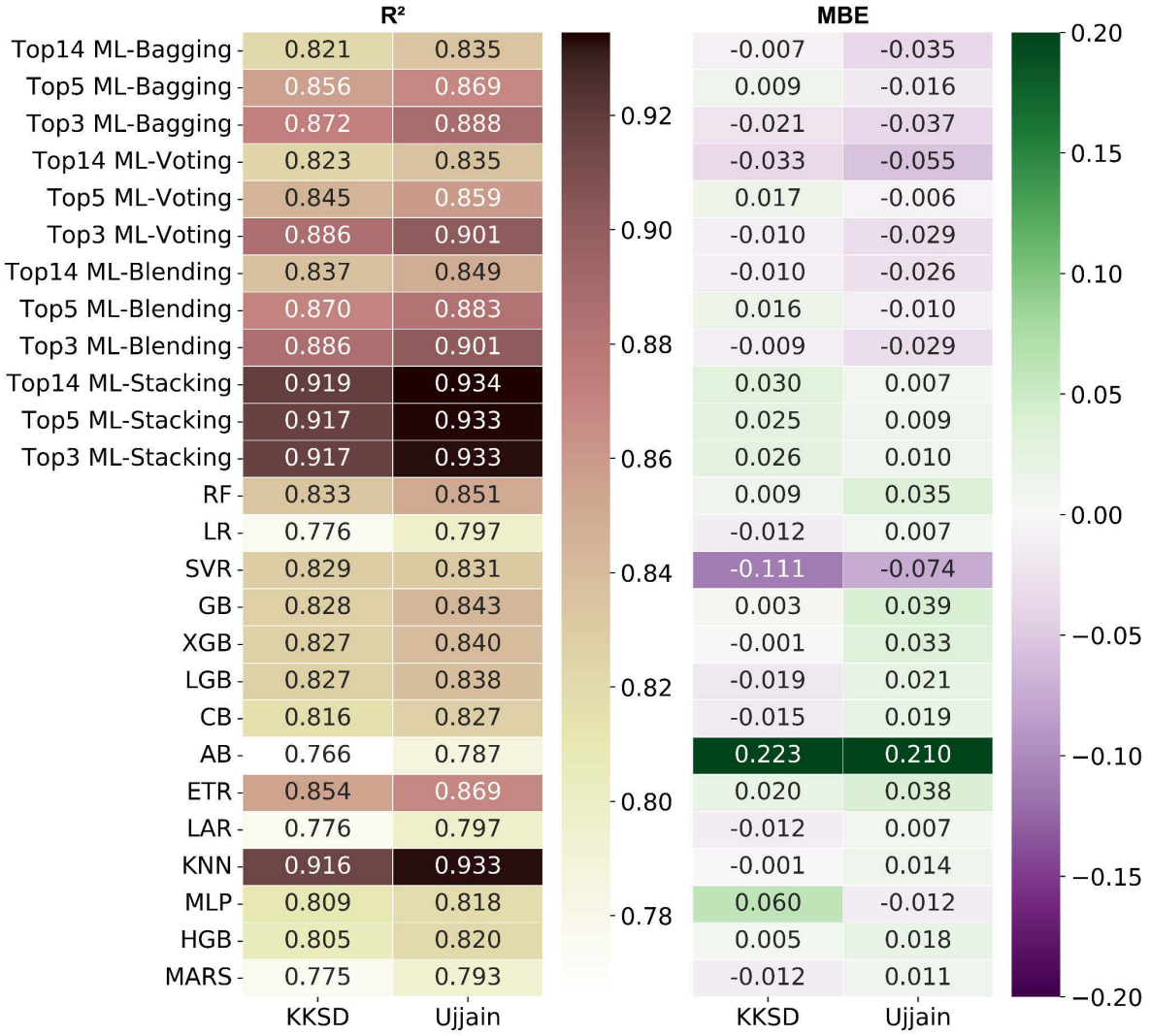

Fig. 8.6. (a) Metric performance of individual ML and ensemble ML for KKSD basins and Ujjain district.

For both the KKSD basins and the Ujjain district, the performance of KNN was found to be comparable to that of the stacking approach. The stacking of the top 14 ML models yielded substantial improvements, and the output from stacking did not show significant changes as the number of base models increased. In contrast, the performance of other ensemble approaches improved as the number of base learners decreased, suggesting that ensembles composed of the best-performing ML models yielded superior results.

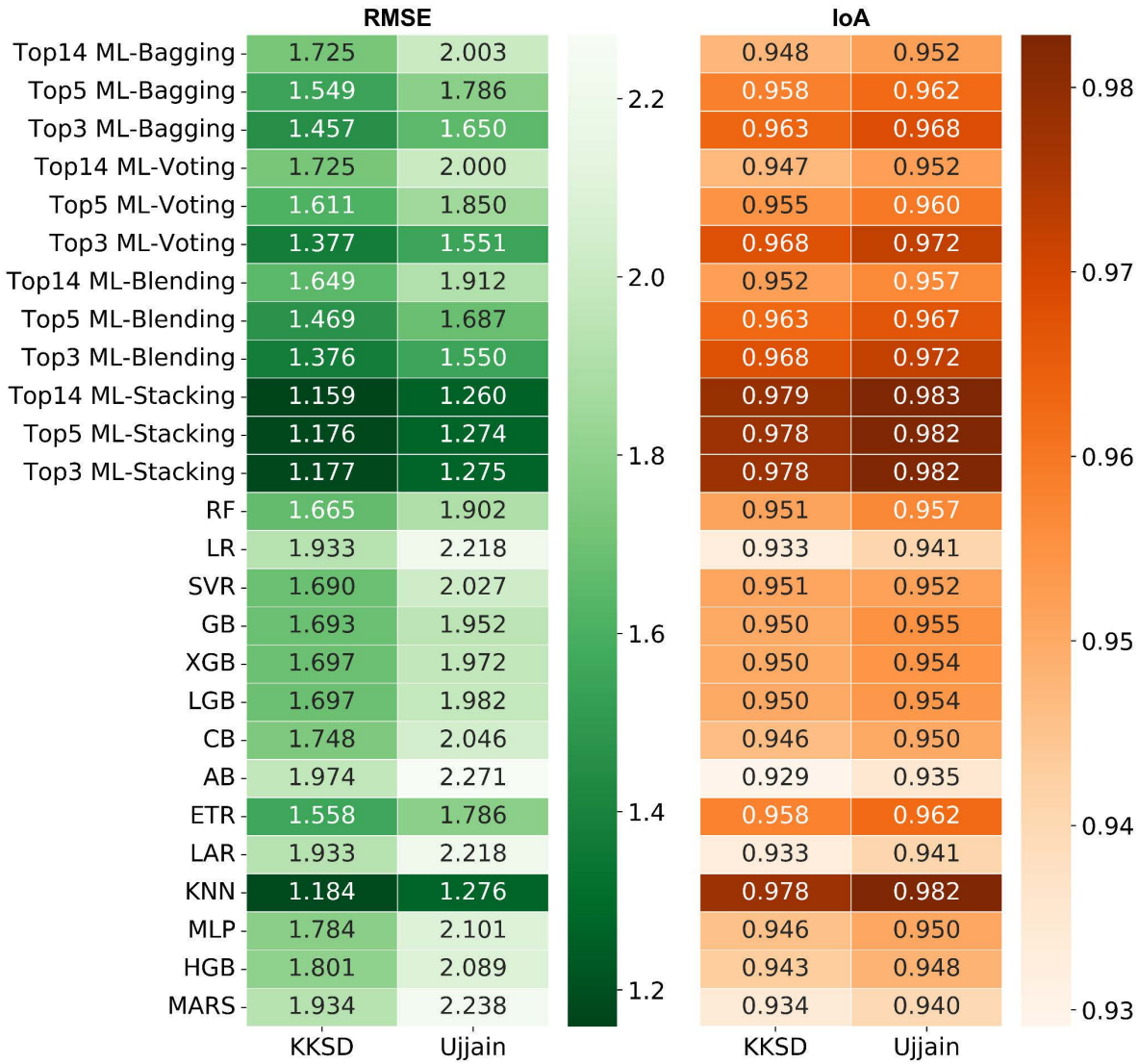

Fig. 8.6. (b) Metric performance of individual ML and ensemble ML for KKSD basins and Ujjain district.

Comparing the performance of the top 3 ML ensembles against the individual ML models further emphasized the effectiveness of the ensemble approach, with the ensemble models consistently delivering better results, except for KNN.

In summary, the results identify that the ensemble of ML significantly enhances predictive performance, offering more accurate and reliable climate projections compared to individual GCMs. This approach of combining multiple algorithms based on their performance rankings allows for a more refined and effective integration of various model strengths, making it a powerful tool for improving climate model predictions.

8.4.4. Performance Evaluation Based on MBE and Residual Analysis

The performance evaluation of individual ML models and ensemble approaches, using the MBE, revealed that most models demonstrated better results, with their MBE values closer to zero. However, AB and SVR showed relatively higher bias, with AB being particularly prone to overfitting, which may explain the increased bias in its predictions. The remaining

performance indices, such as R^2, RMSE, and IoA, demonstrated similar patterns to R^2, with stacking and KNN outperforming the other methods in terms of predictive accuracy.

For a more comprehensive evaluation, we analyzed the projected values against observed values using scatter plots and residual plots. Ideally, the scatter plot should show points closely aligned along a 45-degree line, representing a good correlation between observed and predicted values. The residual plot should display residuals randomly distributed around zero, with no discernible patterns, ensuring the model is not suffering from systematic issues. Combined plots for KKSD basins and Ujjain district allowed for a comparison of model performance across these two locations, highlighting any discrepancies or location-specific patterns in the performance of the models.

Figure 8.7 illustrates the scatter and residual plots. Upon visual inspection, it appears that individual models slightly outperform the stacked ensemble of the top three ML algorithms, with KNN providing a closer simulation of the observed temperature patterns. Specifically, KNN achieved higher R^2 values across both locations, indicating its better overall performance. The scatter plot, however, does not show significant differences in prediction accuracy between the individual and stacked models. The residuals are clustered near the zero line, indicating that both the KNN and stacked ensemble models are adequately capturing the observed temperature patterns. While the residuals show a slight spread, this may be attributed to local climate anomalies or minor factors not fully captured by the models.

In summary, the results indicate that ML and ensemble-based approaches consistently outperform the individual GCM simulations in terms of predictive performance. This is significant for climate change analysis and projections, demonstrating that these models are more effective in understanding and predicting regional climate dynamics than traditional single-GCM approaches. The ability of ML and ensemble models to better simulate observed temperature patterns suggests they hold great promise for improving climate modeling and forecasting, especially when applied to regional-scale studies. The findings highlight the value of using advanced ML techniques, including stacking and KNN, for more accurate climate predictions, which is essential for developing effective strategies for climate adaptation and mitigation.

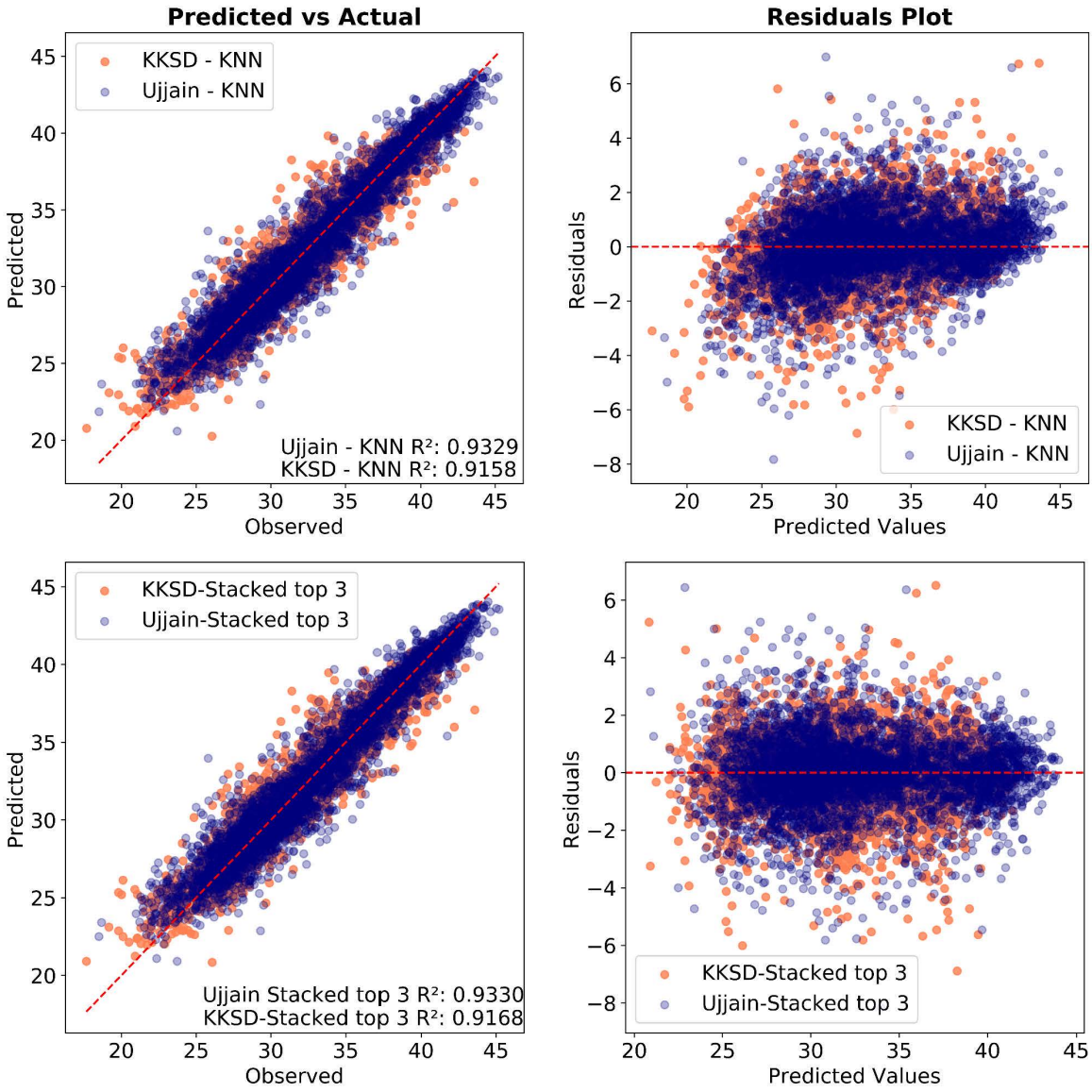

Fig. 8.7. Scattered and residual plot for KNN and stacked ensemble of top 3 ML for KKSD basins and Ujjain district.

8.5. Discussion

This study introduces a framework for identifying and utilizing the most effective individual ML models and ensembles, to accurately replicate observed temperature datasets. The evaluation of the performance of individual ML models and ensembles, constructed using CMIP6 GCMs, revealed significant biases in the historical simulations of individual GCMs, rendering them insufficient for accurate climate analysis. To address these shortcomings, an MME approach was adopted, and the results demonstrated that individual ML models were successful in improving the performance of GCMs. However, the effectiveness of individual GCMs varied between the two locations, influenced by the local climate regimes (Zamani and Berndtsson 2019). The variability in GCM performance emphasizes the importance of appropriate model selection to improve prediction accuracy (Patel et al. 2023).

Prior research has consistently found that ensembles of models outperform individual GCMs (Raju and Kumar 2015, Ahmed et al. 2020, Patel et al. 2023). Studies have also suggested that ranking GCMs based on their performance indicators is effective for selecting the most suitable models for MMEs, which helps in reducing uncertainty. For instance, Yue et al. (2021) and Kim et al. (2020) have validated that MME models perform better than individual GCMs, while Yang et al. (2021) recommended ensemble methods based on optimally performing climate models. However, this study challenges that theory by showing that including both top-performing and less effective GCMs significantly enhances the performance of ensembles, as depicted in Fig. 8.5.

The study also acknowledges the advancements in machine learning, which have led to better results compared to traditional MME methods. Previous work has demonstrated the utility of ML-based ensemble approaches to improve GCM predictions for climate forecasting (Ahmed et al. 2020, Dey et al. 2022, Jose et al. 2022, Fu et al. 2023, Shetty et al. 2023, Wang et al. 2023). These studies showed that ML ensemble approaches consistently outperformed individual GCMs and simple model averages. However, many of these studies did not fully explore the potential of different ML techniques or the broader array of ensemble strategies that could offer more refined insights into model performance.

A critical gap in the literature is the integration of ranked GCMs with ML techniques, which could provide a deeper understanding of model performance. Moreover, many studies have used period-based data splitting for training and validation, which may impact the accurate performance assessment of GCMs. This study addresses these gaps by employing an MMLE approach that combines four different techniques to integrate both individual ML models and the top-performing ones. The results demonstrate that the MMLE approach outperforms most individual ML models, confirming its effectiveness in improving the accuracy of climate predictions.

Furthermore, this study utilizes a comprehensive set of CMIP6 GCMs and a wide array of ML algorithms to evaluate model performance across various climatic variables and regions. This extensive approach allows for a robust comparison of the predictive capabilities of both CMIP6 GCMs and diverse ML models, providing a comprehensive evaluation of their effectiveness in improving climate prediction accuracy.

Despite the success of the MMLE approach, the complexity introduced by utilizing 14 ML algorithms may pose challenges, particularly with overfitting, especially when applied to smaller datasets or highly variable climates. Future research could explore techniques such as regularization to prevent overfitting or investigate simpler ensemble models to maintain a balance between model accuracy and interpretability. Additionally, further improvements could be achieved by incorporating Deep Learning (DL) methods, such as Convolutional Neural Networks or Generative adversarial networks, either independently or in combination with ML approaches. These advanced methods have shown the potential to enhance model performance in various domains and may further boost the accuracy of climate predictions.

Another crucial aspect that requires attention is the data splitting strategy used in climate modeling. The way data is split for training and validation plays a significant role in model performance. Therefore, future studies should explore more robust and diverse data partitioning strategies to improve the predictive reliability of climate models. This research contributes valuable insights into the potential of combining traditional GCMs with modern

machine learning techniques to improve climate modeling and predictions. The results highlight the importance of ensemble-based approaches and the need to explore a broader spectrum of ML methodologies, ensemble strategies, and data partitioning techniques. This study improves the comprehension of climate dynamics while establishing a foundation for more precise and dependable climate projections, which are essential for formulating effective climate adaptation strategies.

8.6. Conclusions

This study evaluates the performance of 22 CMIP6 GCMs in simulating maximum temperature (T_{max}) over two locations, KKSD basins, and the Ujjain district. The models were assessed using feature importance rankings to prioritize the GCMs, followed by the construction of ensembles based on 14 ML algorithms and four MMLE techniques. Performance was evaluated using multiple metrics to estimate how well the models replicated temperature characteristics. The key conclusions derived from the study are outlined below:

- **Top-performing GCMs:** For KKSD basins, the best-performing GCMs for T_{max} simulation were MIROC-ES2L, GISS-E2, and ACCESS-ESM1-5. For Ujjain, the leading models were INM-CM-4-8, MRI-ESM2, and MIROC-ES2L.
- **Best-performing ML algorithms:** Among the 14 ML algorithms evaluated, KNN and ETR showed superior performance, achieving better agreement with observed T_{max} values across both locations.
- **MMLE performance:** The MMLE approach exhibited strong performance across various techniques, with the important exception of KNN.
- **Ensemble techniques:** Ensembles utilizing different ML techniques such as blending, bagging, voting, and stacking improved performance relative to individual models. The top three ensemble combinations KNN, ETR, and RF yielded the most significant enhancements in predictive accuracy.
- **Consistency across locations:** The performance consistency of the ensemble models across KKSD basins and Ujjain district suggests that the ensemble approach is reliable and effective in capturing climatic patterns, making it a robust tool for future projections. This consistency also demonstrates that ensemble methods can perform well in different geographical contexts.
- **Overall superiority of ensembles:** All ensemble-based models outperformed individual CMIP6 GCMs, highlighting the potential of ML ensembles in improving the overall accuracy of climate predictions.

These findings emphasize the value of CMIP6 GCMs in accurately simulating temperature time series, particularly in regions with significant climate variability. The use of an ensemble of GCMs coupled with ML techniques offers a strong foundation for enhancing the precision of climate projections.

In future climate studies, particularly when projecting under various Shared Socioeconomic Pathways, it is crucial to consider similar ensemble methodologies to maintain the consistency and comparability of projections. This approach helps ensure that future

climate scenarios are not only robust but also reliable, utilizing the strengths of both GCMs and machine learning algorithms.

The results of this study offer important insights for climate policymakers, suggesting that integrating MMLE with traditional GCMs can significantly enhance the reliability of T_{max} predictions. This is essential for developing targeted mitigation strategies and adaptation, especially in climate-sensitive regions like India, where accurate temperature projections are necessary for effective planning and resource management.

References

Ahmed, K., Sachindra, D.A., Shahid et al. (2020). Multi-model ensemble predictions of precipitation and temperature using machine learning algorithms. Atmos. Res., 236, 104806.

Breiman, L. (2001). Random Forests. Mach. Learn., 45(1), 5–32.

Chen, T. and Guestrin, C. (2016). XGBoost: A Scalable Tree Boosting System. In Proceedings of the 22nd ACM SIGKDD International Conference on Knowledge Discovery and Data Mining, 785–794.

Cover, T. and Hart, P. (1997). Nearest neighbor pattern classification. IEEE Trans. Inf. Theory 13(1), 21–27.

Cortes, C. and Vapnik, V. (1995). Support-vector networks. Mach. Learn., 20(3), 273–297.

Dey, A., Sahoo, D.P., Kumar, R. and Remesan, R. (2022). A multimodel ensemble machine learning approach for CMIP6 model projections in an Indian River basin. Int. J. Climatol. 42(16), 9215–9236.

Efron, B., Hastie, T., Johnstone, I. and Tibshirani, R. (2004). Least angle regression. Ann. Stat., 32(2), 407–499.

Eyring, V., Bony, S., Meehl et al. (2016). Overview of the Coupled Model Intercomparison Project Phase 6 (CMIP6) experimental design and organization. Geosci. Model Dev. 9(5), 1937–1958.

Friedman, J.H. (1991). Multivariate Adaptive Regression Splines. Ann. Statist., 19(1), 1–67.

Friedman, J.H. (2001). Greedy function approximation: A gradient boosting machine. Ann. Statist., 29(5), 1189–1232.

Freund, Y. and Schapire, R.E. (1997). A decision-theoretic generalization of on-line learning and an application to boosting. J. Comput. Syst. Sci., 55(1), 119–139.

Fu, Y., Zhuang, H., Shen, X. and Li, W. (2023). Assessment and prediction of regional climate based on multimodel ensemble machine learning method. Clim. Dyn., 61(9–10), 4139–4158.

Geurts, P., Ernst, D. and Wehenkel, L. (2006). Extremely randomized trees. Mach. Learn., 63(1), 3–42.

Guryanov, A. (2019). Histogram-Based Algorithm for Building Gradient Boosting Ensembles of Piecewise Linear Decision Trees. In: van der Aalst, W et al. Analysis of Images, Social Networks and Texts. AIST 2019. Lecture Notes in Computer Science, vol 11832. Springer, Cham.

Jose, D.M., Vincent, A.M. and Dwarakish, G.S. (2022). Improving multiple model ensemble predictions of daily precipitation and temperature through machine learning techniques. Sci. Rep., 12(1), 4678.

Ke, G., Meng, Q., Finley et al. (2017). LightGBM: a highly efficient gradient boosting decision tree. In Proceedings of the 31st International Conference on Neural Information Processing Systems (NIPS'17). Curran Associates Inc., Red Hook, NY, USA, 3149–3157.

Kim, Y.H., Min, S.K., Zhang et al. (2020). Evaluation of the CMIP6 multi-model ensemble for climate extreme indices. Weather Clim. Extrem., 29,100269.

Menze, B.H., Kelm, B.M., Masuch et al. (2009). A comparison of random forest and its Gini importance with standard chemometric methods for the feature selection and classification of spectral data. BMC Bioinformatics, 10, 213.

Patel, G., Das, S. and Das, R. (2023). Identification of Best CMIP6 Global Climate Model for Rainfall by Ensemble Implementation of MCDM Methods and Statistical Inference. Water Resour. Manage., 37(13), 5147–5170.

Prokhorenkova, L., Gusev, G., Vorobev et al. (2018). CatBoost: unbiased boosting with categorical features. In Proceedings of the 32nd International Conference on Neural Information Processing Systems (NIPS'18). Curran Associates Inc., Red Hook, NY, USA, 6639–6649.

Roy, A., Kim, L.S. and Mukhopadhyay, S. (1993). A polynomial time algorithm for the construction and training of a class of multilayer perceptrons. Neural Netw., 6(4), 535–545.

Shetty. S., Umesh, P. and Shetty, A. (2023). The effectiveness of machine learning-based multi-model ensemble predictions of CMIP6 in Western Ghats of India. Int. J. Climatol., 43(11), 5029–5054.

Srivastava, A.K., Rajeevan, M. and Kshirsagar, S.R. (2009). Development of a high resolution daily gridded temperature data set (1969–2005) for the Indian region. Atmosph. Sci. Lett., 10(4), 249–254.

Thrasher, B., Wang, W., Michaelis, A., Melton, F., Lee, T. and Nemani, R. (2022). NASA Global Daily Downscaled Projections, CMIP6. Sci. Data, 9(1), 262.

Wang, D., Liu, J., Luan et al. (2023). Projection of future precipitation change using CMIP6 multimodel ensemble based on fusion of multiple machine learning algorithms: A case in Hanjiang River Basin, China. Meteorol. Appl., 30(5), e2144.

Chapter 9

Projected Precipitation Changes Based on Selective GCMs

9.1. Introduction

Climate projections play a key role in planning and managing water resources, as climate change greatly impacts the global water sector by altering temperatures and rainfall patterns. Water resources are highly sensitive to climate variability and extreme events, leading to changes in water availability, more frequent and severe droughts, and a higher risk of floods.

Understanding future changes in precipitation and temperature is critical to addressing the impacts of climate change on mitigating hydrological extremes. Reliable climate projections enable policymakers, and stakeholders to anticipate potential changes and develop adaptive strategies to ensure water security. These projections also provide the scientific foundation for designing resilient water infrastructure, optimizing agricultural water use, and implementing effective flood control measures. Global Climate Models (GCMs) are widely recognized as the most reliable numerical tools for predicting future climate conditions. These models simulate historical climate patterns using observed greenhouse gas (GHG) concentrations and project future scenarios based on anticipated GHG emissions, making them indispensable for understanding climate change dynamics and guiding mitigation and adaptation efforts.

The Coupled Model Intercomparison Project Phase 6 (CMIP6) represents the latest advancement under the World Climate Research Program (WCRP). CMIP6 introduces several improvements, including refined greenhouse gas emission scenarios, enhanced land-use change projections, improved depiction of physical processes in the climate system, and advanced parameterizations of model components. These advancements aim to reduce uncertainties and improve the accuracy of climate projections.

Despite these improvements, GCM simulations within CMIP6 are not without challenges. Uncertainties persist, stemming from the parameterization of complex physical processes and the specification of initial and boundary conditions. As highlighted by Jose and Dwarakish (2020), these limitations emphasize the necessity of complementary strategies to enhance the utility of GCM outputs.

To address these uncertainties, researchers have developed various methodologies, including bias correction techniques to adjust systematic errors, statistical and dynamical downscaling methods to improve spatial and temporal resolution, and the formulation of multimodel ensembles (MMEs). MMEs, which combine outputs from multiple GCMs, have become the standard practice in recent years. This approach utilizes the strengths of individual models while mitigating their weaknesses, thereby increasing the reliability of climate projections.

While earlier studies often relied on single GCM outputs, the adoption of multi-GCM ensembles marks a significant shift in climate research. By integrating diverse model outputs, MMEs provide a more robust framework for capturing the complexities of climate systems, reducing uncertainties, and delivering more actionable insights for decision-makers addressing the impacts of climate change.

Patel et al. (2023) assessed the performance of 24 CMIP6 GCMs in the KKSD basins using multi-criteria decision-making (MCDM) techniques and statistical metrics. Building on their findings, this study focuses on utilizing the optimal GCMs identified for future climate projections. Specifically, five CMIP6 GCMs canESM5, MIROC-ES2L, IITM-ESM, BCC-CSM2-MR, and EC-Earth3-Veg-LR are selected for detailed analysis.

The primary objective is to apply machine learning (ML) techniques to ensembles of these top-performing GCMs, as recommended by Patel et al. (2023), to project climate conditions across three future periods: near-term (2015-2040), mid-term (2041-2060), and long-term (2061-2098). The simulations will be conducted under Shared Socioeconomic Pathway (SSP) scenarios to assess potential climate change impacts in the region.

This study evaluates and compares the performance of GCMs in simulating key climate variables over the defined time frames. By utilizing cutting-edge ML methods, the study aims to improve the precision and reliability of climate projections, providing a robust framework for analyzing future climate scenarios.

The results of this research have important significance for understanding and predicting the impacts of climate change, particularly from the perspective of water resources planning and management. By offering more accurate insights into future climate variability, this study supports the development of adaptive strategies to mitigate the adverse effects.

9.2. Empirical and Machine Learning-Based Projections

9.2.1. Selection of GCMs

The selection of GCMs was guided by a comprehensive approach incorporating both empirical and machine learning-based methods. Five GCMs were initially shortlisted following the recommendations of Patel et al. (2023), who employed MCDM techniques, alongside individual performance parameters and their integrated outputs.

To enable a comparison between the empirical approach and more advanced techniques, another method of GCM selection was implemented using machine learning models. These models included Extra Trees (ET), Random Forest (RF), K-Nearest Neighbors (KNN), Support Vector Machine (SVM), CatBoost (CB), XGBoost (XGB), Multi-Layer Perceptron (MLP), and AdaBoost (AB). The ML approach was based on feature selection criteria to recognize the most relevant GCMs and compare their outputs against those generated through the empirical method.

This dual methodology allows for a critical comparison of traditional and advanced techniques, providing a better understanding of the robustness and applicability of the selected GCMs for regional climatic analysis.

9.2.2. Splitting and tuning

To improve the performance and reliability of ML models used in GCM selection, the dataset was split into training and testing subsets. A manual split ratio of 68:32 was adopted, as it yielded better results compared to standard ratios. This splitting ensured that the models were trained on a significant percentage of the data while keeping a smaller portion for validation and performance evaluation.

Hyperparameter tuning was utilized to enhance the performance of each ML model. Advanced optimization techniques, including grid search, were employed to identify the ideal parameter configurations. The models tuned included ET, RF, KNN, SVM, CB, XGB, MLP, and AB.

The tuning process focused on improving key performance metrics, such as accuracy and error, to ensure robust predictions. Additionally, cross-validation was applied during the tuning process to mitigate overfitting and enhance the generalizability of the models. This rigorous approach to splitting and tuning was critical in ensuring the reliability of the machine learning models and their ability to identify the most suitable GCMs for regional climatic analysis.

9.3. Results and Discussion

The projections of canESM5, MIROC-ES2L, IITM-ESM, BCC-CSM2-MR, and EC-Earth3-Veg-LR are visualized in Figs. 9.1 to 9.5, with each model providing projections for four SSPs: SSP126, SSP245, SSP370, and SSP585. While these projections offer a range of outputs for future precipitation trends, they do not present a consistent pattern across the scenarios. The projections from canESM5, shown in Figs. 9.1 and 9.9, reveal varying precipitation trends across three time periods: the near-term (2015-2040), mid-term (2041-2060), and far-term (2061-2098).

In the near-term, for SSP126, the change in annual precipitation is not significant, while for SSP245 and SSP370, the relative percentage changes are -12.94% and -7.62%, respectively, and for SSP585, the change is a positive 2.56%. In the mid-term, SSP126 shows an 18.49% increase in precipitation, while SSP245 experiences a decrease of -9.50%, and SSP370 and SSP585 show increases of 5.6% and 7.9%, respectively. In the far-term, all SSP scenarios exhibit positive percentage changes in precipitation, with increasing trends across all pathways. These varying projections highlight the uncertainty and complexity inherent in climate model outputs, especially when considering different SSP scenarios and time periods.

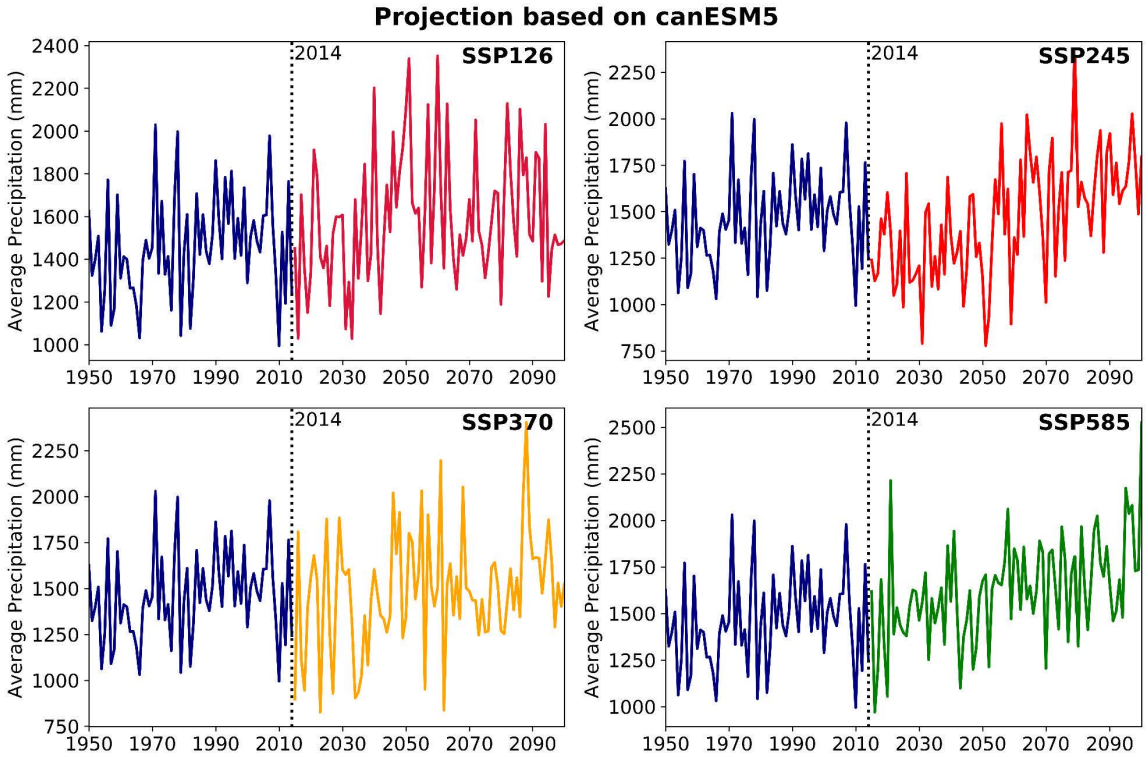

Fig. 9.1. Projections of average annual precipitation (mm) for the canESM5 model under different SSPs from 1950 to 2100. The dotted vertical line in 2014 represents the transition from historical to projected data.

The projections from MIROC-ES2L, shown in Figs. 9.2 and 9.9, reveal consistent precipitation trends across three time periods: the near-term, mid-term, and far-term. In the near-term, for all SSP scenarios, the change in annual precipitation is both significant and negative, with variations ranging from -10.45% for SSP126 to -20.37% for SSP585. A similar pattern is observed in the mid-term, where SSP126 shows a -10.45% decrease in precipitation, SSP245 experiences a decrease of -11.55%, and SSP370 and SSP585 show decreases of -17.58% and -11.29%, respectively. In the far-term, all SSP scenarios continue to exhibit negative percentage changes in precipitation. The magnitude of these decreases shows a consistent increase up to SSP370, ranging from -7.58% to -12.08%, but for SSP585, the decrease is less pronounced at -6.01%. Overall, it is evident that the near-term period experiences the most significant decrease in precipitation as projected by MIROC-ES2L, compared to the mid-term and far-term periods.

Similar to the MIROC-ES2L, the projections from IITM-ESM, illustrated in Figs. 9.3 and 9.9, indicate consistent declines in annual precipitation. During the near-term, significant negative changes are observed for all SSP scenarios, with reductions ranging from -5.68% under SSP126 to -11.94% under SSP585. This trend persists in the mid-term, where SSP126 shows a -6.66% decline, SSP245 records a -7.82% decrease, and SSP370 and SSP585 exhibit reductions of -9.93% and -14.91%, respectively. In the far-term, precipitation continues to decline, with percentage changes ranging from -3.12% to -6.03% across scenarios. Overall, IITM-ESM projections highlight the most pronounced decreases in precipitation during the far-term, with substantial declines evident throughout all periods.

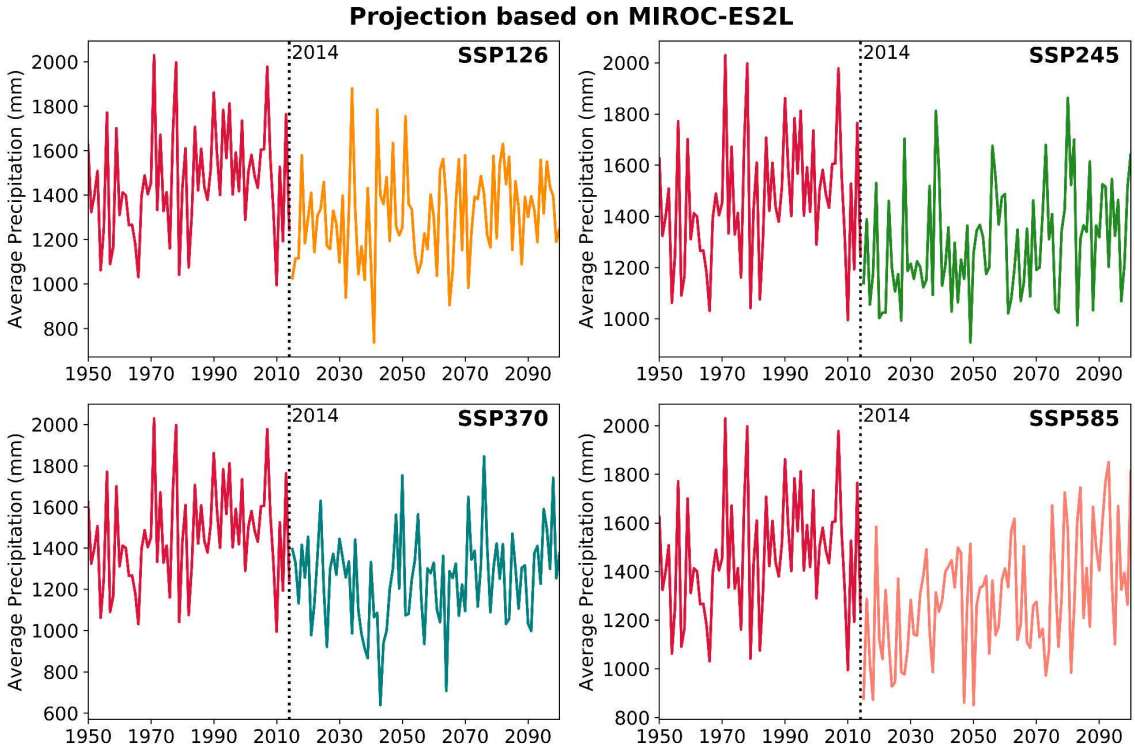

Fig. 9.2. Projections of average annual precipitation (mm) for the MIROC-ES2L model under different SSPs from 1950 to 2100. The dotted vertical line in 2014 represents the transition from historical to projected data.

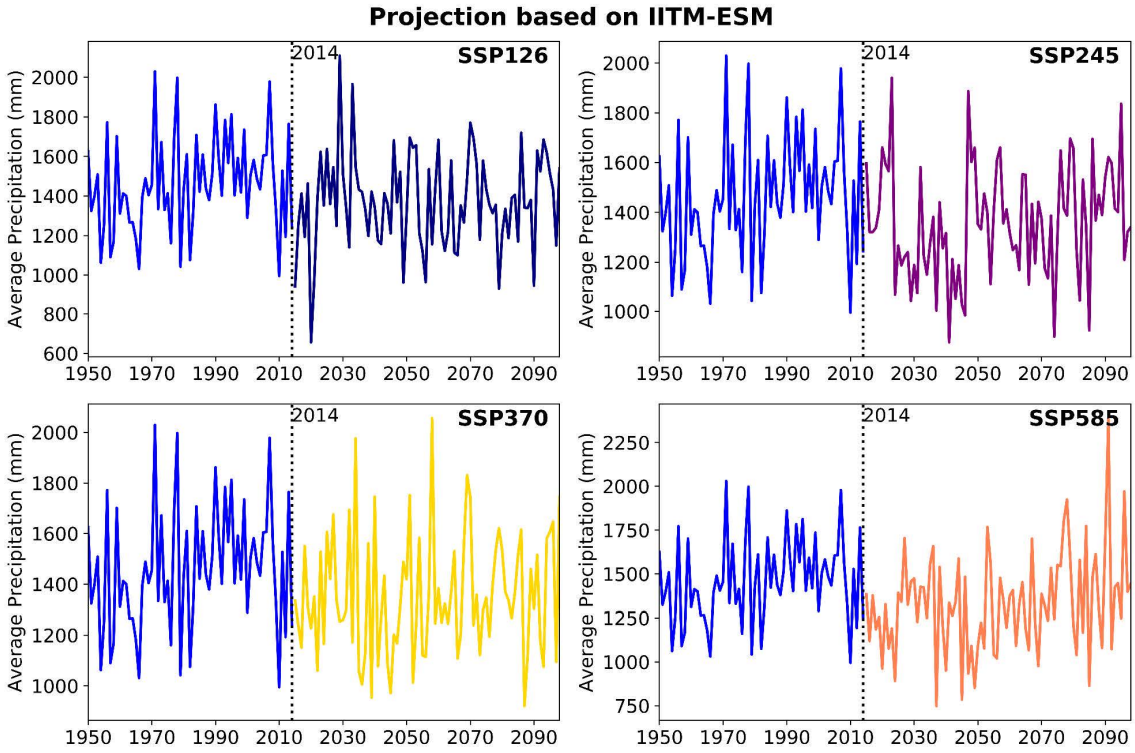

Fig. 9.3. Projections of average annual precipitation (mm) for the IITM-ESM model under different SSPs from 1950 to 2100. The dotted vertical line in 2014 represents the transition from historical to projected data.

Among the remaining two models, BCC-CSM2-MR exhibits a pattern similar to that of IITM-ESM, with a consistent negative trend in precipitation changes across all periods and SSP scenarios, as depicted in Figs. 9.4 and 9.9. In contrast, the EC-Earth3-Veg-LR model demonstrates variability in precipitation changes. For SSP126, it shows positive changes across all periods, whereas, for other scenarios, the changes are predominantly negative. Particularly, in the far-term, SSP245 and SSP370 show positive precipitation changes, diverging from the general negative trend observed in other scenarios and periods as shown in Figs. 9.5 and 9.9.

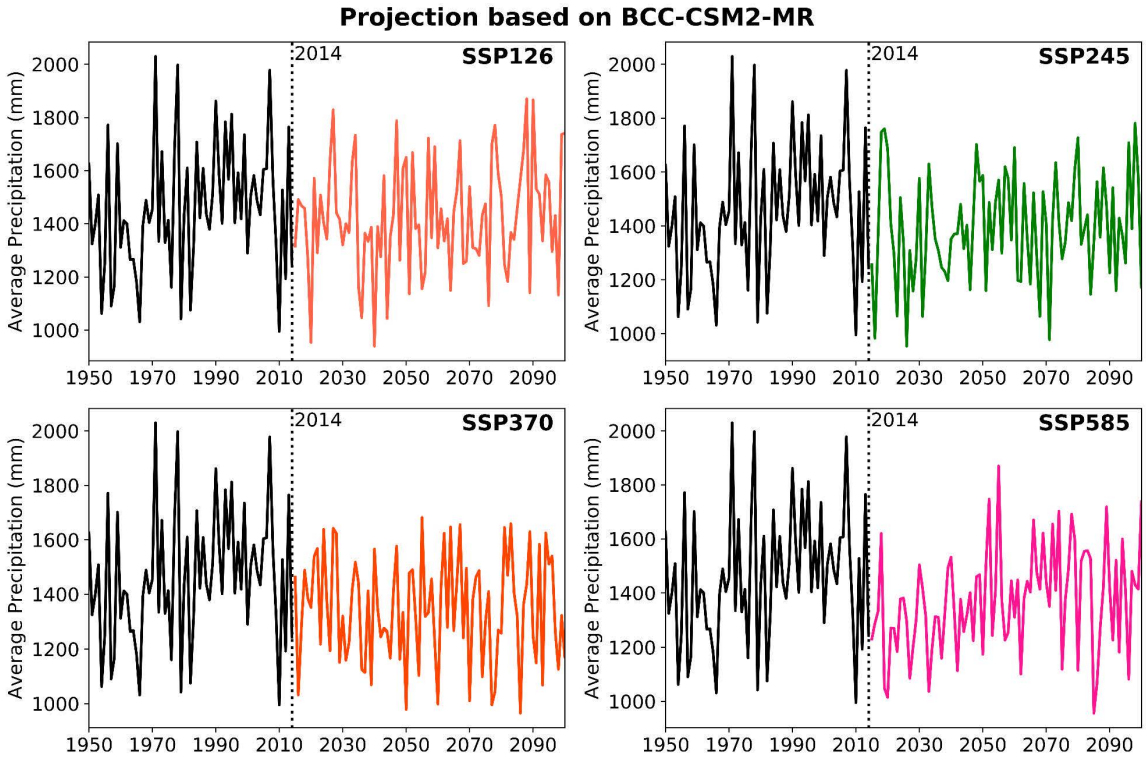

Fig. 9.4. Projections of average annual precipitation (mm) for the BCC-CSM2-MR model under different SSPs from 1950 to 2100. The dotted vertical line in 2014 represents the transition from historical to projected data.

The analysis of projected precipitation changes reveals that no individual GCM provides a definitive or consistent projection across scenarios and periods. To address this, we employed ML techniques to enhance the reliability of the projections by ensemble outputs based on feature selection criteria. Figure 9.6 compares the performance of ML models using all available GCMs versus the top five GCMs identified by Patel et al. (2023).

The outcomes demonstrate that no substantial difference in the outputs between these two cases. Among the ML models tested, the ET algorithm consistently outperformed others, leading to its selection for feature importance. Using ET, feature importance was analyzed to evaluate the contribution of individual GCMs in predicting outcomes. As shown in Fig 9.7, BCC-CSM2-MR emerged as the most influential model, followed closely by MIROC-ES2L. Interestingly, these findings differ from Patel et al. (2023), where canESM5 was identified as the leading GCM. Utilizing the ET model for projections, the results indicate that fluctuations

compared to individual GCMs are minimal, primarily due to the averaging effect inherent in ensemble methods.

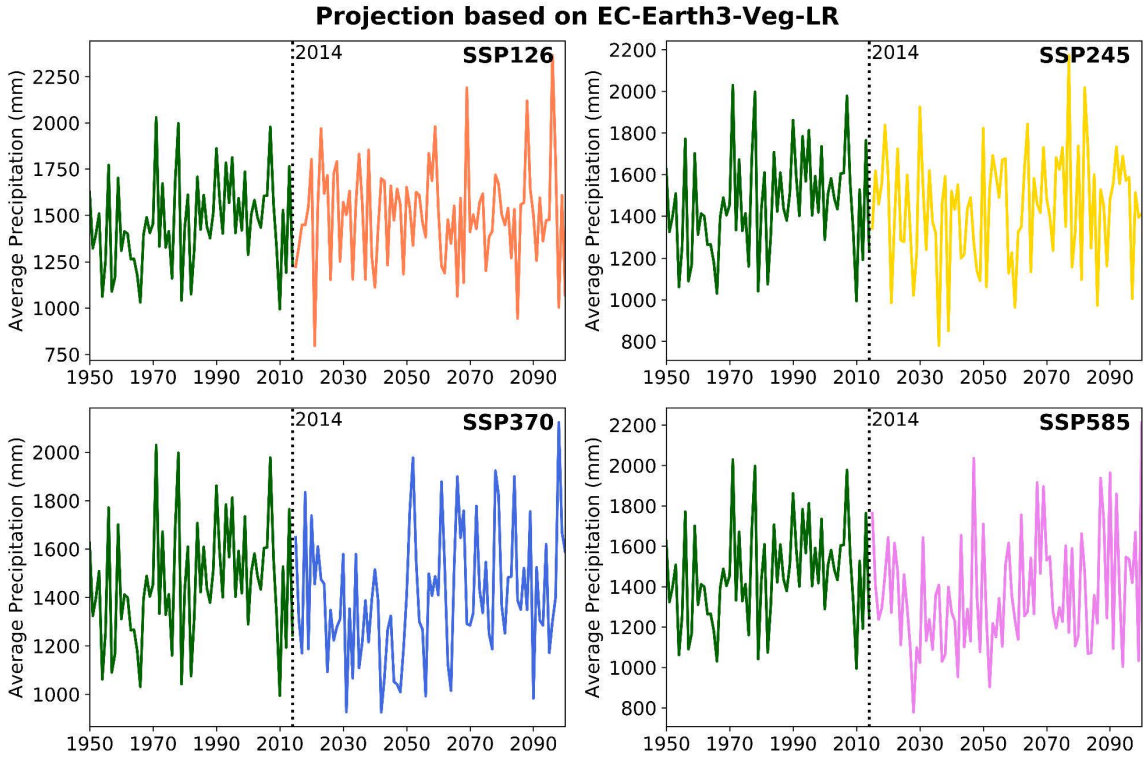

Fig. 9.5. Projections of average annual precipitation (mm) for the EC-Earth3-Veg-LR model under different SSPs from 1950 to 2100. The dotted vertical line in 2014 represents the transition from historical to projected data.

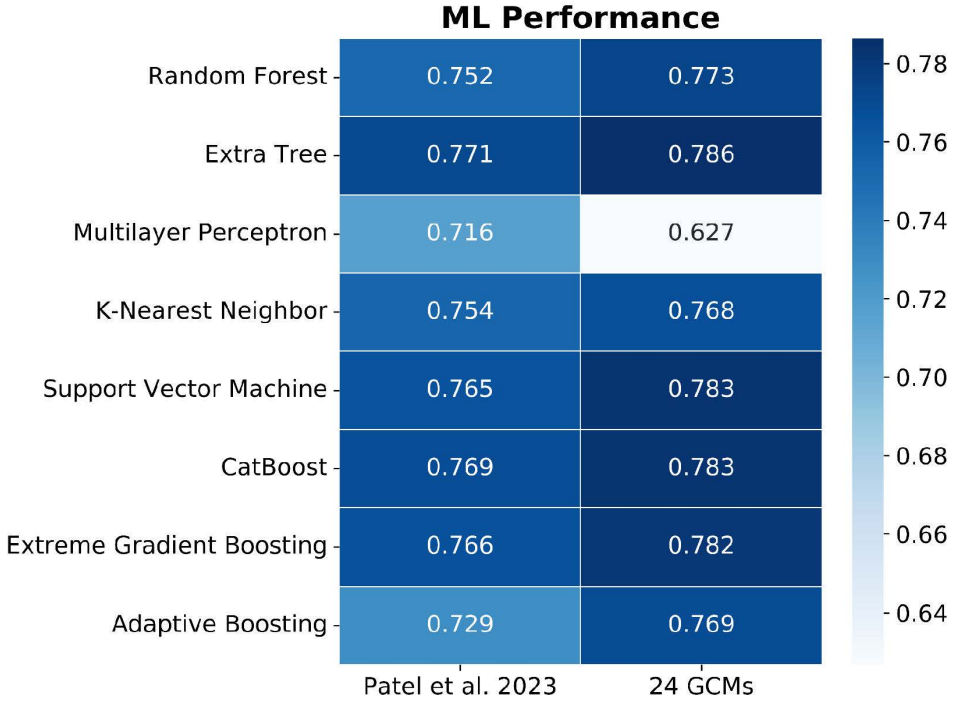

Fig. 9.6. Machine learning performance of top five models suggested by Patel et al. (2023) with overall model utilized.

For all SSP scenarios, as depicted in Fig 9.8, the projected trends exhibit a consistent upward trajectory. However, the average precipitation magnitude remains lower than the historical baseline across all scenarios.

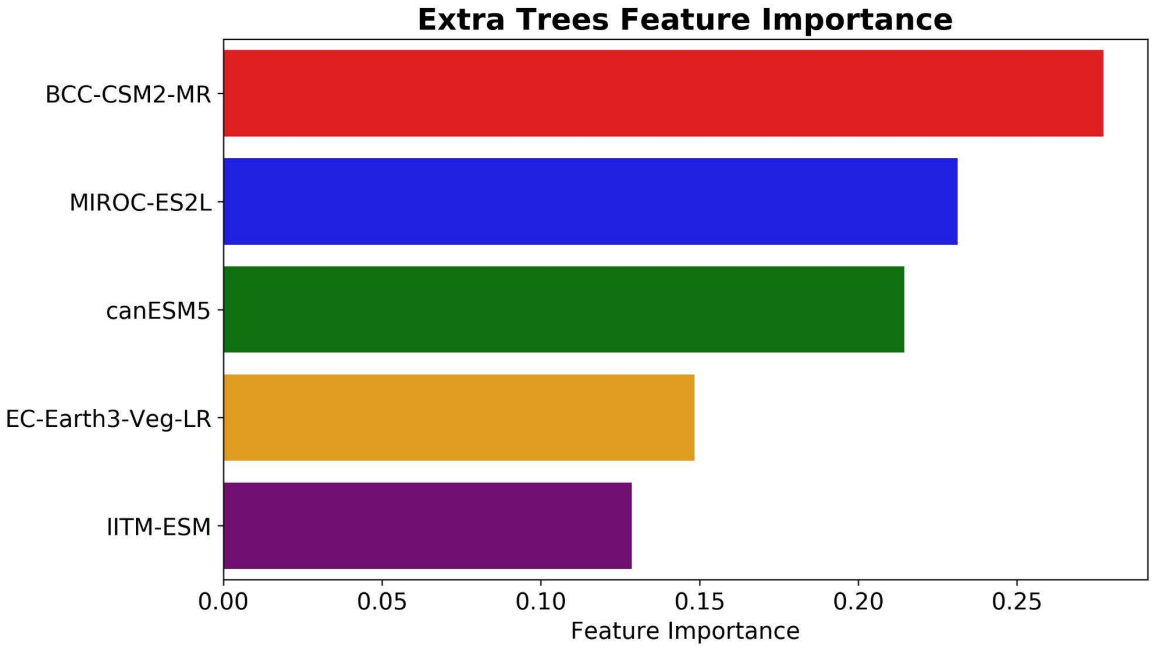

Fig. 9.7. Feature importance criteria based on an extra tree for top-performing models suggested by Patel et al. (2023).

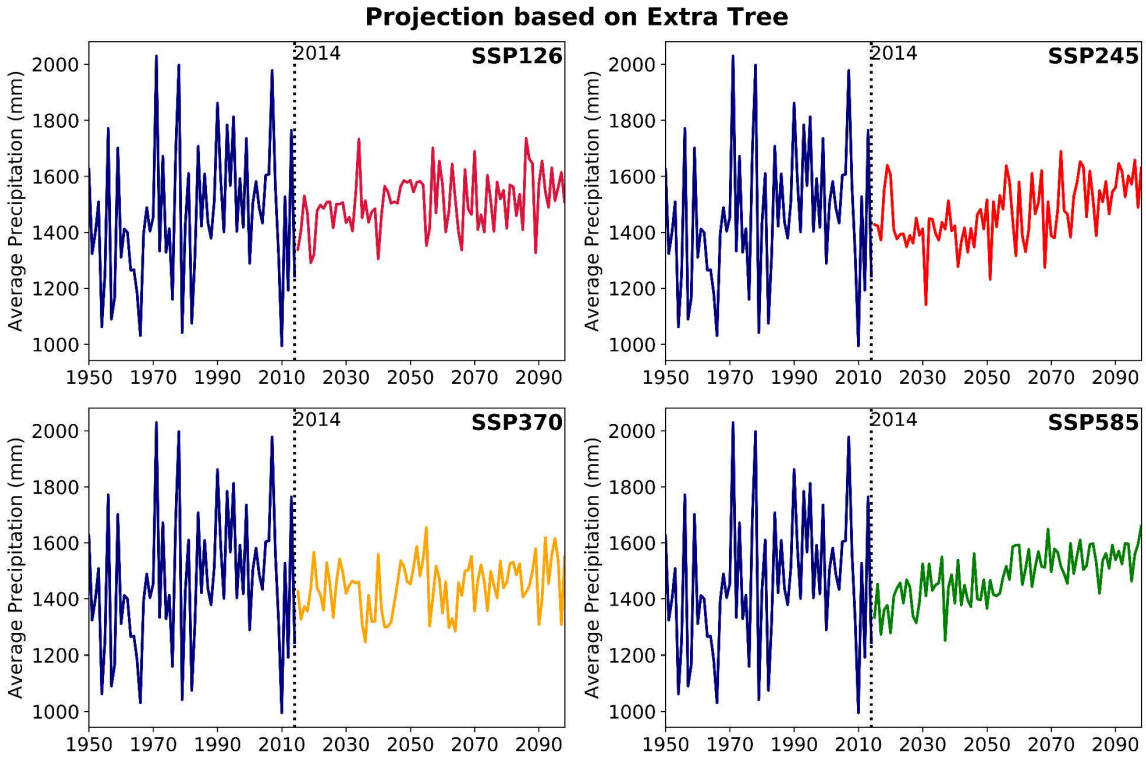

Fig. 9.8. Projections of average annual precipitation (mm) for the ML model under different SSPs from 1950 to 2100. The dotted vertical line in 2014 represents the transition from historical to projected data.

This demonstrates the stabilizing impact of ensemble modeling, providing a smoother and more coherent projection of future precipitation trends. The projected changes in precipitation, as derived from the ensemble approach, indicate distinct patterns across the time frames and scenarios. In the near-term, all scenarios exhibit negative changes except for SSP126, where the changes are negligible and non-significant.

Similarly, in the mid-term, SSP126 is the only scenario showing a positive change of 5.6%, while the remaining scenarios demonstrate negative but non-significant changes. In the far-term, however, all scenarios project positive changes in precipitation, with SSP126 showing a 4.34% increase, SSP245 indicating a 3.99% rise, and SSP585 demonstrating the highest increase at 5.54%. These results suggest that the long-term projections are more optimistic regarding precipitation trends compared to the near and mid-term projections.

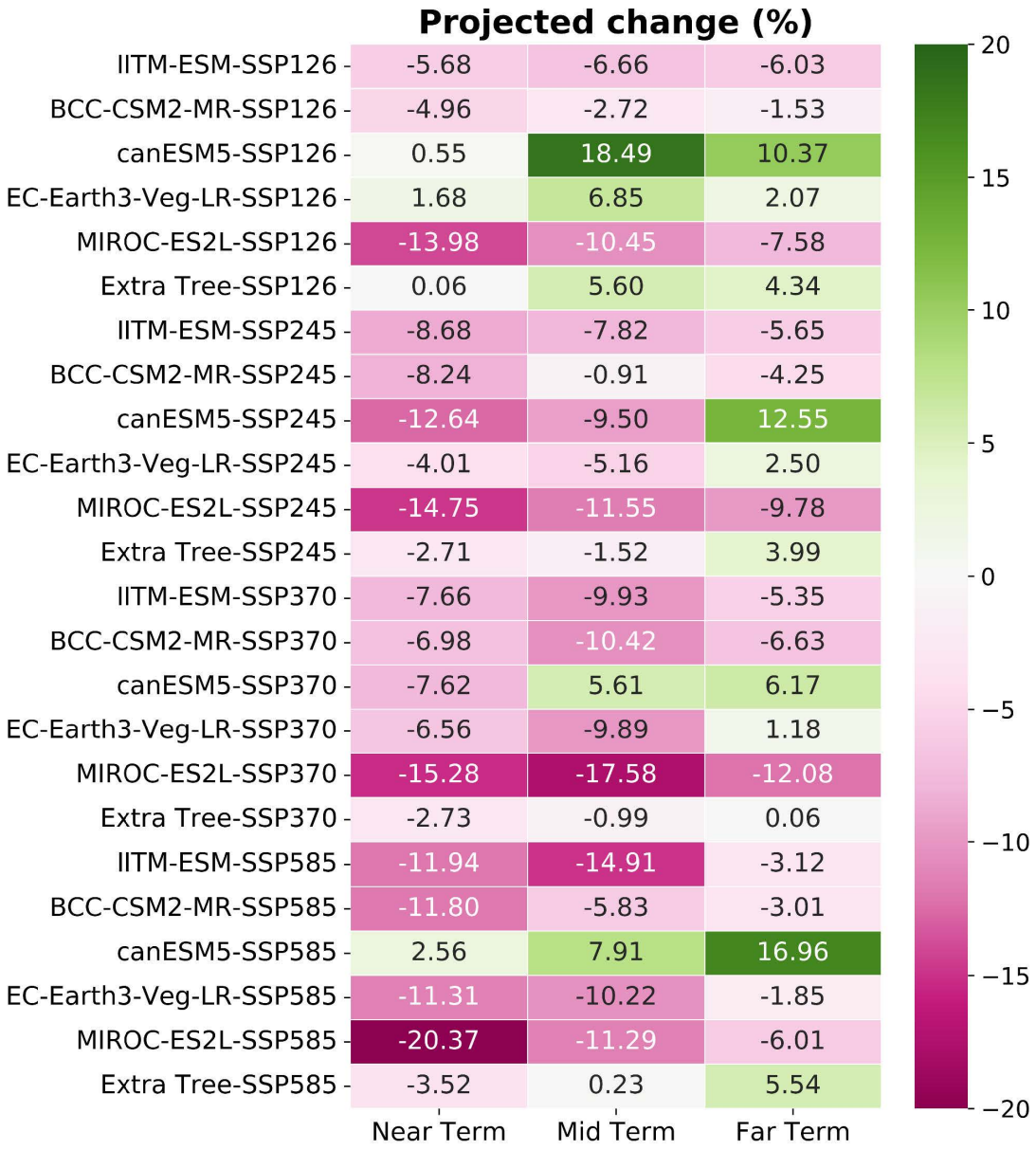

Fig. 9.9. The projected changes in precipitation based on different scenarios, time periods, and models, combined with machine learning model.

9.4. Conclusions

This chapter explored the projections of precipitation changes using five selected CMIP6 GCMs (canESM5, MIROC-ES2L, IITM-ESM, BCC-CSM2-MR, and EC-Earth3-Veg-LR) across three future periods under four SSP scenarios. The results revealed significant variability in the projections, with no single model providing a consistent or definitive pattern. While some models like canESM5 and MIROC-ES2L suggested more stable trends, others, such as EC-Earth3-Veg-LR, exhibited mixed behavior, including both positive and negative changes across scenarios and periods.

To address the inherent uncertainties in GCM outputs, ML techniques were employed to create an ensemble projection based on feature importance criteria. ET emerged as the most effective model, demonstrating that averaging effects reduce fluctuations compared to individual GCM outputs. The ensemble results showed less variability, with trends indicating a general upward trajectory in precipitation across scenarios, albeit with lower magnitudes than historical observations.

The ensemble-based projections highlighted refined trends: in the near-term, changes were largely negative but non-significant, except for SSP126. In the mid-term, SSP126 showed a modest positive change, while others remained negative. In the far-term, all scenarios indicated positive changes, with SSP585 showing the highest increase. These findings highlight the importance of ensemble approaches in improving the reliability of climate projections by mitigating the limitations of individual GCMs.

Overall, it concludes that integrating machine learning with multi-model ensembles provides a robust framework for analyzing climate projections, particularly for regions like the study area where high variability in precipitation trends poses challenges for water resource planning and climate adaptation strategies. The results not only enhance our understanding of future climate behavior but also support more informed decision-making for sustainable development in the face of climate change.

References

Jose, D.M. and Dwarakish, G.S. (2020). Uncertainties in predicting impacts of climate change on hydrology in basin scale: a review. Arab. J. Geosci., 13(19), 1037.

Patel, G., Das, S. and Das, R. (2023). Identification of Best CMIP6 Global Climate Model for Rainfall by Ensemble Implementation of MCDM Methods and Statistical Inference. Water Resour. Manage., 37(13), 5147–5170.

Chapter 10

Final Remarks

This thesis represents a comprehensive investigation into climate change impacts, focusing on temperature and precipitation variability and projections using advanced modeling techniques. By utilizing historical data, Global Climate Models (GCMs), and machine learning methods, the study offers valuable insights into future climate scenarios and their implications for water resource management and climate adaptation strategies. The findings contribute to the broader discourse on regional climate modeling, emphasizing the importance of accuracy and robustness in climate projections for informed decision-making.

- **Understanding Historical and Future Climate Variability**

The study began with an analysis of historical temperature and precipitation patterns to establish a baseline for understanding climatic trends. Utilizing observational datasets and statistical methods, we identified significant variability across spatial and temporal scales. This foundational analysis highlighted the critical need for accurate projections to predict future climatic behavior and assess its potential impacts on water resources and hydrological systems.

Future climate projections were explored using five CMIP6 GCMs: canESM5, MIROC-ES2L, IITM-ESM, BCC-CSM2-MR, and EC-Earth3-Veg-LR. These models were selected based on their performance in simulating historical climate conditions and recommendations from prior studies. Each model provided unique insights into precipitation changes under different Shared Socioeconomic Pathways (SSPs), covering near-term (2015-2040), mid-term (2041-2060), and far-term (2061-2098) timeframes. However, significant discrepancies were observed among the models, emphasizing the inherent uncertainties in GCM outputs.

- **Addressing Uncertainties Through Machine Learning**

Recognizing the variability and inconsistencies in GCM outputs, this study adopted machine learning techniques to enhance the reliability of climate projections. Ensemble methods were employed to integrate outputs from multiple GCMs. The machine learning framework was designed to address the challenges posed by individual model biases and uncertainties, offering a more holistic view of future climate scenarios.

Feature importance analysis played a crucial role in this approach, identifying the most influential GCMs in predicting precipitation changes. Interestingly, while previous studies recommended canESM5 and MIROC-ES2L as top-performing models, our analysis using Extra Trees suggested that BCC-CSM2-MR and MIROC-ES2L were more impactful in ensemble projections. This divergence underscores the importance of combining traditional model evaluations with advanced data-driven techniques to achieve a more refined understanding of climate dynamics.

- **Key Findings**

1. **Historical trends:**

   - The Innovative Trend Analysis (ITA) and Modified Mann-Kendall method consistently outperform other methods in detecting significant trends.
   - ITA exhibits greater performance in detecting sensitive trends.
   - The monsoon season contributes significantly to the total annual rainfall, there has been both significant increase and decrease trends for grids, contributing to the rise of extreme weather events like floods and droughts.
   - There has been a consistent decline in rainfall during the winter season.
   - T_{max} for 1951-2020: During the monsoon and autumn seasons, approximately 100% of the grids show positive trends, while winter, summer, and annual periods display decreasing trends across 80% of grids.
   - T_{max} for 2001-2020: Annual, monsoon, and autumn seasons reveal positive trends across about 64% of grids, while summer and winter show negative slopes at around 90% of grids with prominent magnitudes.
   - T_{min} for 1951-2020: All seasons exhibit increasing trends across more than 80% of grids.
   - T_{min} for 2001-2020: Apart from the monsoon season, which shows a positive trend with significant magnitude across 100% of grids, all other seasons demonstrate negative slopes across more than 82% of grids.

2. **GCM Selection:**

   - The analysis identified five top-performing models for the KKSD basins: canESM5, MIROC-ES2L, IITM-ESM, BCC-CSM2-MR, and EC-Earth3-Veg-LR. These models exhibited the best overall performance across multiple MCDM criteria integrated with performance indicators for rainfall.
   - The multi-temporal assessment of CMIP6 GCMs for maximum temperature identified three top-performing models for the KKSD basins: MIROC-ES2L, ACCESS-ESM1-5, and GISS-E2.

3. **GCM Projections:**

   - GCMs exhibited significant variability in precipitation projections across timeframes and scenarios.
   - canESM5 and MIROC-ES2L showed relatively stable trends, while EC-Earth3-Veg-LR displayed mixed behavior with both positive and negative changes.
   - Overall, the projections indicated an upward trend in precipitation for the far-term, particularly under SSP585, although the magnitude was generally lower than historical observations.

4. **Machine Learning Insights:**

   - Extra Trees and K-Nearest Neighbors emerged as the most effective ensemble models, demonstrating superior performance in integrating GCM outputs.

- Ensemble projections reduced fluctuations and provided more consistent trends compared to individual GCMs.
- Feature importance analysis revealed BCC-CSM2-MR and MIROC-ES2L as the most influential models, differing from previous recommendations.

5. **Scenario-Based Trends:**

- Near-term projections showed predominantly negative changes, except for SSP126, which exhibited non-significant positive changes.
- Mid-term projections were largely negative, with SSP126 showing modest positive changes.
- Far-term projections indicated positive changes across all scenarios, with SSP585 showing the highest increase.

Final Thoughts

Climate change poses unprecedented challenges to water resources, ecosystems, and human livelihoods. This thesis underscores the importance of accurate and reliable climate projections in understanding and addressing these challenges. By integrating advanced modeling techniques with traditional approaches, this research provides a robust framework for analyzing temperature and precipitation variability and future trends.

The findings not only contribute to the scientific understanding of regional climate dynamics but also offer practical insights for policymakers and stakeholders. As the impacts of climate change continue to expose, it is needed to adopt innovative approaches and collaborative efforts to build resilience and ensure sustainable development. This thesis serves as a step toward that goal, emphasizing the need for rigorous research, data-driven decision-making, and proactive planning to navigate the complexities of a changing climate.

Limitations

Despite the contributions of this thesis to understanding climatic behavior, the selection of GCMs, and projections, several limitations need to be acknowledged:

- The study is limited to a specific geographic region, which may restrict the generalizability of the findings to other regions with different climatic conditions.
- The analysis relies on specific data resolution grids, which may not capture finer-scale climatic variations.
- The study considers data from specific time ranges, which may not fully account for long-term climatic variability or emerging trends beyond this period.
- The findings are dependent on the selection of models, which may introduce bias due to inherent limitations in model structures and assumptions.
- While MCDM techniques are employed, their effectiveness is contingent on the chosen criteria and weights, which might vary based on normalization, criteria, and weight technique used.
- Uncertainty in climatic projections arises from the variability among GCM outputs and assumptions regarding future scenarios, realization, initiation method, physics, and forcing.
- The study does not extensively explore sensitivity or reverse rank analysis, which could provide deeper insights into the robustness of the selected methods.
- Utilization of bias correction and downscaling techniques in the study

Future Scopes

A few aspects of the research may have been further expanded after completing the comprehensive study on the analysis, and development of ensemble models.

1. **Integration of Additional Variables:** Future studies could incorporate other climatic variables, such as evapotranspiration, and soil moisture, to provide a more comprehensive understanding of climate change impacts.
2. **Exploration of Advanced Techniques:** Advanced machine learning techniques, such as deep learning or autoML, could be explored to further enhance projection accuracy and address uncertainties.
3. **Focus on Extreme Events:** Analyzing the frequency and intensity of extreme precipitation and temperature events could provide critical insights into the risks associated with climate change.
4. **Physics-informed strategies:** This will enhance the overall projection and ranking involved during the process.
5. **Bias Correction**: Applying robust bias correction techniques could minimize systematic errors in climate model outputs and improve reliability.
6. **Downscaling:** Employing advanced downscaling methods would enable finer resolution climate projections, better suited for regional and local analysis.
7. **CORDEX Models:** Utilizing CORDEX (Coordinated Regional Climate Downscaling Experiment) models could provide region-specific insights and strengthen the reliability of the projections.
8. **Satellite data:** Utilization of satellite-based datasets might be very useful as reference data

GAURAV PATEL

Address: Vill. and Post- Leduka Bazar,
Jaunpur, Uttar Pradesh, India, 222109
Contact no.: +91-8256059608,8638549774
E-mail: gauravp.wre.rs@jadavpuruniversity.in
gauravpatelofficial@gmail.com
LinkedIn: www.linkedin.com/in/gaurav-patel
ORCID ID: 0000-0002-4672-9273
SCOPUS ID: 58547371500
WoS Researcher ID: ACZ-6759-2022

CAREER OBJECTIVE

To build a career in a research field, where I can get the opportunities to prove my strength and abilities by accepting challenges and climbing the career ladder through continuous learning and commitments.

INTERESTED AREAS

Climate Change, Hydrology, Data Analysis, Climate Modeling, Multi-Criteria Decision Making, Meta-learning, Optimization, AI in Climate Analysis, Data visualization

EDUCATION

Course	Institute	Board/University	Percentage/CGPA	Year of Completion
Ph.D. (Engineering)	Jadavpur University, Kolkata, India	Jadavpur University	9.25 CGPA	2025 (Submitted)
M.Tech (WRE)	National Institute of Technology, Hamirpur, H.P., India	MHRD	7.92 CGPA	2020
B.Tech (CE)	Tezpur University, Assam, India	Tezpur University	8.02 CGPA	2018
10+2	Radhika Bal Vidya Mandir Senior Secondary School	CBSE	80.40 %	2013
10th	Radhika Bal Vidya Mandir Senior Secondary School	CBSE	9.0 CGPA	2011

*WRE: Water Resources Engineering; CE: Civil Engineering

INTERNSHIPS | EXPERIENCE

- **Indian Institute of Science, Bengaluru** (02 Jun-27 July 2017) (IAS-NASI-INSA Focus Area Science and Technology – Summer Research Fellowship 2017)
- **MSME TOOL ROOM INDIA** (5 Jun-19 Jun 2016): Learn new software of Civil Engineering that gives the structural solution

PROJECTS

- Mathematical Modelling of Type I Settling (*B.Tech 2nd Year Project*)
- Modelling of Two Way Two Lane Vertical Summit Curve (*B.Tech 2nd Year Project*)
- Design of G+5 Earthquake Resistant Building (*B.Tech 3rd Year Project*)
- Pushover Analysis and Fragility Analysis of G+5 Residential Building (*B.Tech Final Year Project*)

- Impact of Climate Change on the Hydrology of Beas River Basin in Himachal Pradesh (*M.Tech Thesis*)
- Climatic Behavior and Associated Variations (*Ph.D. Thesis*)

TECHNICAL SKILLS

- Microsoft Office, Microsoft Visual Basic
- Python, R Studio, MATLAB
- Origin Pro, Mathtype, Minitab
- ArcGIS, QGIS, HEC RAS, HEC HMS, SWAT
- **Structure Simulation Software**: Staad PRO V8i, SAP2000, AutoCAD
- **Climate Data Processing Software**:
  - Command Line Operators and Viewers: CDO, ncview (NetCDF), Panoply
  - Interpreted Languages: NCL, GrADS, R, Python

PUBLICATIONS

- **Patel, G.** and Das, S. (2024). Multi-Temporal Evaluation of CMIP6 Models for Maximum Temperature in East India: Improving Climate Dynamics Understanding. *Stochastic Environmental Research and Risk Assessment* (**2nd Revision**)
- **Patel, G.**, Das, R., Das, S. and Mukherjee, I. (2024). Innovative trend analysis of long-term rainfall variation over West Bengal, India. *Mausam* (**Accepted**) (**Q4, SCIE, SCOPUS**)
- **Patel, G.**, Das, S. and Das, R. (2024). Accuracy of historical precipitation from CMIP6 global climate models under diversified climatic features over India. *Environmental Development,* 50, 100998. https://doi.org/10.1016/j.envdev.2024.100998 (**IF: 5.4, Q2, SCIE, SCOPUS**)
- Nandi, B., **Patel, G.** and Das, S. (2024). Prediction of maximum scour depth at clear water conditions: Multivariate and robust comparative analysis between empirical equations and machine learning approaches using extensive reference metadata. *Journal of Environmental Management,* 354(3), 120349. https://doi.org/10.1016/j.jenvman.2024.120349 (**IF: 8.7, Q1, SCI, SCIE, SCOPUS**)
- **Patel, G.**, Das, S. and Das, R. (2024). Determine the best method for analyzing long-term (120 years) annual and seasonal rainfall trends in four east India river basins. *Journal of Earth System Science*, 133(2), 70. https://doi.org/10.1007/s12040-024-02282-7 (**IF: 1.9, Q3, SCIE, SCOPUS**)
- **Patel, G.**, Das, S. and Das, R. (2023). Identification of Best CMIP6 Global Climate Model for Rainfall by Ensemble Implementation of MCDM Methods and Statistical Inference. *Water Resources Management,* 37(13), 5147–5170. https://doi.org/10.1007/s11269-023-03599-6 (**IF:4.3, Q1, SCIE, SCOPUS**)
- **Patel, G.**, Das, R. and Das, S. (2023). Is the extreme temperature trend changed in last two decades compared to last seven decades? Case study from Eastern India. *Journal of Earth System Science*, 132(3), 140. https://doi.org/10.1007/s12040-023-02158-2 (**IF: 1.9, Q3, SCIE, SCOPUS**)
- **Patel, G.**, Das, S. and Das, R. (2024). Influence of normalization techniques in CMIP model selection using an MCDM method MOORA. In Swain, B.P. and Dixit, U.S. (eds.), Recent Advances in Civil Engineering. ICSTE 2022. *Lecture Notes in Civil Engineering*, vol 431. Springer, Singapore. https://doi.org/10.1007/978-981-99-4665-5_6 (**SCOPUS**)
- **Patel, G.**, Das, S. and Das, R. (2022). MCDM approach to select best CMIP6 Global Climate Models (GCMs) for Dwarkeswer and Kangsabati basins in India. vol. 2022, Art. no. GC51B-01,

2022. [*based on the article presented in the **American Geophysical Union (AGU)** Fall Meeting 2022, Chicago, Illinois, 12-16 December, 2022. https://agu2022fallmeeting-agu.ipostersessions.com/default.aspx?s=E6-5E-C6-6C-C9-A9-54-5B-24-58-59-5D-20-A9-D8-23*].

- **Patel, G**. and Tripura, J. (2022). Analysis of Climate Parameters Trend over Long Time Horizons and their Probable Impacts in the Beas Basin, HP, India. *Indian Journal of Ecology. 49*(3), 954-963. https://doi.org/10.55362/IJE/2022/3621
- **Patel, G.** and Tripura, J. (2019). "Impact of Climate Change on the hydrology of Beas River Basin", in the *Proceedings of 8th APHW International Conference on Emerging Technologies in Urban Water Management*. CoEDMM, IIT Roorkee, India, 22-23 Nov., pp.79. ESS Open Archive. https://doi.org/10.22541/essoar.167267360.08474700/v2
- **Patel** et al. (2018). "Seismic analysis of G+5 RCC residential Apartment (A comparative study between the Indian Standard Code based equivalent Static and Dynamic Approach)", in the *Proceedings of National Conference on Advances in Civil and Infrastructure Engineering (ACIE 2018)*. Tezpur University, Assam, India, 16-17, Feb.

AWARDS

- AICTE Doctoral Fellowship 2020 (**Jadavpur University**)
- MHRD Post Graduate Fellowship 2018 (**NIT Hamirpur**)
- IAS-INSA-NASI Summer Research Fellowship 2017 (**IISc Bangalore**)

PERSONAL DETAILS

Name: Gaurav Patel
Date of Birth: 20 July 1996
Languages Understand: Hindi, English, Bhojpuri, Bengali
Personal Website: https://sites.google.com/view/gauravpatel

Verified by:

Water Resources Management
https://doi.org/10.1007/s11269-023-03599-6

Identification of Best CMIP6 Global Climate Model for Rainfall by Ensemble Implementation of MCDM Methods and Statistical Inference

Gaurav Patel[1] · **Subhasish Das**[1] · **Rajib Das**[1]

Received: 12 July 2023 / Accepted: 30 August 2023

Abstract

Global climate models (GCMs) are becoming more and more important due to their ability to accurately identify climatic factors, which will be highly helpful in establishing planning and strategizing for water resources engineers. Therefore, studying the performance of GCMs is essential, as it can simulate and predict climatic scenarios. This study examines the best performance of 24 GCMs using NASA NEX-GDDP dataset reproduced rainfall in four catchments: Silabati, Keliaghai, Kangsabati and Dwarkeswer from West Bengal, India. This study used historical period (1950–2014) rainfall data to evaluate the performance of 24 CMIP6 GCMs. The GCMs output was compared with observed data using 17 performance indicators (PIs). Five distinct techniques for Multicriteria Decision Making (MCDM) were applied to assess rankings, aiming to achieve a consistent evaluation of GCMs, despite encountering conflicting outcomes from both the parameters and the MCDM methods. A combined evaluation of PIs and MCDM was used to rank GCMs. The research uncovered that out of all the GCMs examined, five were identified as the top-performing ones in terms of accurately estimating rainfall based on comparisons with observed data. The top-ranked GCMs observed were canESM5, MIROC-ES2L, IITM-ESM, BCC-CSM2-MR and EC-Earth3-Veg-LR. The assessed GCMs, despite their advancements, struggle with accurately capturing regional intricacies, potentially affecting the precision of forecasts. The findings from this research will provide valuable insights for both climate researchers and decision-makers in selecting the most suitable CMIP6 GCMs. It can be asserted that the proposed methodology is readily adaptable to any situation, offering practical applicability.

Keywords Global climate models · CMIP6: rainfall · MCDM

✉ Subhasish Das
subhasish.das@jadavpuruniversity.in

Gaurav Patel
gauravp.wre.rs@jadavpuruniversity.in

Rajib Das
rajib.das@jadavpuruniversity.in

[1] School of Water Resources Engineering, Jadavpur University, Kolkata 700032, India

Influence of Normalization Techniques in CMIP Model Selection Using an MCDM Method MOORA

Gaurav Patel, Subhasish Das, and Rajib Das

1 Introduction

Researchers have been motivated to develop new techniques in response to the requirement for a variety of decision-making procedures for addressing various model selection difficulties. The use of multi-criteria decision-making (MCDM) methodologies has the potential to produce superior results. Finding a good model is critical for predicting forthcoming environmental difficulties. Global climate models (GCMs) are commonly used to forecast future climate. Various groups have created a significant number of GCMs. Climate datasets from many organizations are being used by the IPCC for climate impact assessments [1]. The Coupled Model Intercomparison Project Phase 6 (CMIP6) is commonly utilized for present and future climate analysis and projections. Despite substantial advancements in CMIP6, large uncertainty remains under a variety of climate circumstances. Many assumptions were made throughout the creation of GCMs due to a lack of accurate information on atmospheric events, leading to exaggerations or underestimations of climate change. This allows us to see where the climate models and observations diverge. Climate projection uncertainty can be decreased by using a proper collection of GCMs. The preliminary goal of any climate change impact research or climate modeling is to pick the best group of GCMs [2]. Typically, the ability of climate models to simulate past climate is utilized as the basis for selecting GCMs. The uncertainty in climate projections has a significant impact on impact estimation. A small adjustment in climate projection can drastically alter the return duration of hydrological disasters such as floods and droughts. As a result, selecting credible GCMs is regarded as one of the most successful methods of lowering uncertainty in climate change estimates. GCMs are typically chosen based on their capacity to recreate historical climates. To evaluate the performance measure of GCMs, time series of monthly or

G. Patel (✉) · S. Das · R. Das
School of Water Resources Engineering, Jadavpur University, Kolkata, West Bengal, India
e-mail: gauravp.wre.rs@jadavpuruniversity.in

B. P. Swain and U. S. Dixit (eds.), *Recent Advances in Civil Engineering*, Lecture Notes in Civil Engineering 431, https://doi.org/10.1007/978-981-99-4665-5_6

Environmental Development 50 (2024) 100998

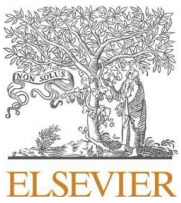

Contents lists available at ScienceDirect

Environmental Development

journal homepage: www.elsevier.com/locate/envdev

Accuracy of historical precipitation from CMIP6 global climate models under diversified climatic features over India

Gaurav Patel [a], Subhasish Das [b,*], Rajib Das [c]

[a] School of Water Resources Engineering, Jadavpur University, Kolkata, 700032, India
[b] School of Water Resources Engineering, Jadavpur University, Kolkata, 700032, India
[c] School of Water Resources Engineering, Jadavpur University, Kolkata, 700032, India

ARTICLE INFO

Keywords:
Global climate model
CMIP6
Overestimation
Underestimation
Precipitation

ABSTRACT

The importance of global climate models (GCMs) is increasingly recognized due to their excellent ability to accurately predict climatic factors. These capabilities prove invaluable to water resources engineers as they facilitate effective planning and strategic decision-making. Finally, evaluating the performance of GCMs is very important because it allows us to simulate and predict different climate scenarios, empowering us to make informed choices. Therefore, the purpose of this study is to determine the degree of discordance between historical simulated data produced by the CMIP6 models and historical observational data over different climate zones of India. The ability of 24 different GCMs to reproduce the geographical and seasonal distribution of Indian precipitation has been tested by analyzing the daily historical precipitation forecasts from these models. These models have been used to estimate the degree of uncertainty associated with the spatiotemporal variability of precipitation forecasts. More than 20% percent bias (PBIAS) is observed to occur predominantly in four climate classifications: polar tundra, temperate, cold, and tropical monsoon. In some regions of India, the CMIP6 models produce overestimated or underestimated results. The locations identified indicate that there have been changes of more than 20% PBIAS near Sivalik Range, Naga Hills, and Western Ghats. The precipitations of those regions that have been underestimated also imply that those locations have different climatic conditions. This study also highlights that CMIP6 GCMs are yet to produce better results near several Indian mountainous regions depending upon climates. The outcomes of this study will be very useful for reconstructing modeled data for that specific regions.

1. Introduction

Because of the detrimental consequences of climate change in a multitude of sectors, including water resources, healthcare, power, and agriculture, it is a problem that affects the entire world. To plan for climate change adaptation and mitigation methods effectively, it is essential to map any conceivable changes that may occur in the climatic parameters. It is of utmost importance in areas that are sensitive to the environment since even slight variations in climatic factors can have a big effect on the service industry. Greenhouse gas (GHG) emissions significantly impact climate systems, and global climate models (GCMs) can replicate these effects to expect

* Corresponding author.
E-mail addresses: gauravp.wre.rs@jadavpuruniversity.in (G. Patel), subhasish.das@jadavpuruniversity.in (S. Das), rajib.das@jadavpuruniversity.in (R. Das).

https://doi.org/10.1016/j.envdev.2024.100998
Received 26 October 2023; Received in revised form 1 May 2024; Accepted 2 May 2024
Available online 3 May 2024

Unraveling Extreme Temperature Dynamics Over West Bengal: A Decadal Investigation Utilizing Very High-Resolution Gridded Dataset

Gaurav Patel, Subhasish Das, and Rajib Das

Abstract Temperature fluctuations play a pivotal role in shaping regional climates and influencing various aspects of human life and the environment. West Bengal characterized by its geographical diversity, presents a complex tapestry of extreme temperature (T_{max}) dynamics that demands a nuanced approach for accurate analysis. The study employs 0.25 gridded resolutions for period of the last two decades (2000–2022) to unravel the intricate temperature variations spanning microscales. By utilizing geospatial, interpolation, and new Innovative Trend Analysis (ITA) techniques, the research unveils localized temperature trends, regional patterns, and the unique influence of geographical features. The findings not only shed light on West Bengal's climate complexities but also hold implications for climate adaptation strategies and urban planning. Through this study, we gain insights into the multidimensional nature of temperature dynamics and its implications for building climate resilience in a diverse and dynamic region.

Keywords Gridded · ITA · Interpolation · Geospatial · West Bengal

1 Introduction

Global warming, driven by the escalating emissions of greenhouse gases, continues to rise dramatically, resulting in discernible trends within hydro-meteorological records and a heightened occurrence of frequent and severe extreme events, often leading to inundation consequences in both urban and rural areas. Over the past two to three decades, the definition and analysis of these trends have gained substantial attention across various domains, including meteorology, hydrology, air quality, and water quality, as these time series data serve as critical indicators of the evolving impacts of climate change [1]. West Bengal, a diverse and populous state in eastern India, is known for its rich cultural heritage, agricultural prominence, and ecological

G. Patel (✉) · S. Das · R. Das
School of Water Resources Engineering, Jadavpur University, Kolkata, West Bengal, India
e-mail: gauravp.wre.rs@jadavpuruniversity.in

S. Vadhera et al. (eds.), *Advances in Green Energy Technologies*, Lecture Notes in Electrical Engineering 1314, https://doi.org/10.1007/978-981-96-0861-4_3

622979_1_En_3_Chapter ☑ TYPESET ☐ DISK ☐ LE ☑ CP Disp.:21/12/2024 Pages: 12 Layout: T1-Standard

J. Earth Syst. Sci. (2023)132 140
https://doi.org/10.1007/s12040-023-02158-2

Is the extreme temperature trend changed in last two decades compared to last seven decades? Case study from Eastern India

Gaurav Patel*, Rajib Das and Subhasish Das

School of Water Resources Engineering, Jadavpur University, Kolkata 700 032, India.
**Corresponding author. e-mail: gauravp.wre.rs@jadavpuruniversity.in*

MS received 19 January 2023; revised 22 May 2023; accepted 23 May 2023

Changes in global temperature have adverse influences on the environment, crop production, and public health. Temperature extreme investigation is necessary for those areas whose cropland and work cultures rely on effective climatic conditions. Therefore, identifying trends in climatic scenarios is important in determining the pattern of extreme temperatures. The previously mentioned trend analysis was based on a complete period that did not investigate the recent variability in temperature. We scrutinized a different decadal zone using the innovative trend analysis method (ITAM). We selected the annual and seasonal extreme temperature variations for 70 years (1951–2020) at 11 grid points in the Kangsabati–Silabati–Keliaghai–Dwarkeswar basins of West Bengal. The outcomes from two different time zones, 1951–2020 and 2001–2020, show some surprising results. For 1951–2020, T_{max} shows negative sloping patterns in winter and summer, whereas for 2001–2020, it shows the opposite pattern: year-round, winter and summer with excessive magnitudes. Similarly, for T_{min}, all the seasons from 1951 to 2020 show positive trends, but in recent decades (2001–2020), except the monsoon season, other seasons show negative trends. The normalized difference in vegetation and water indices also supports the results of trends. From the results obtained through the use of ITAM, we recognize that the results of the recent trends are more sensitive and of a higher magnitude of slope in nature than in the historical decade. This study may serve as scientific support for detecting and strategically minimizing the effects of climate change on water resources to reduce the risk of adverse weather soon.

Keywords. Gridded; extreme temperatures; innovative trend analysis method; NDVI; NDWI.

1. Introduction

One of the world's most important issues is global warming, which is considered an increase in global temperatures. They attributed it to the increase in the concentration of greenhouse gases (GHGs) in the atmosphere. Global warming has a negative impact on the hydrological cycle, which is vital to survival on Earth (Jose and Dwarakish 2022). There is a need to examine the spatiotemporal variability as an uneven atmospheric warming pattern over the world prompts climate change phenomena. It is now widely acknowledged that the Earth's climate is changing at a greater rate in recent history (IPCC 2021) than at any other time. From 1950 onwards, remarkable variations in

Published online: 23 August 2023

J. Earth Syst. Sci. (2024)133 70
https://doi.org/10.1007/s12040-024-02282-7

Determine the best method for analysing long-term (120 years) annual and seasonal rainfall trends in four east India river basins

Gaurav Patel, Subhasish Das* and Rajib Das

School of Water Resources Engineering, Jadavpur University, Kolkata 700 032, India.
**Corresponding author. e-mail: subhasish.das@jadavpuruniversity.in*

MS received 31 May 2023; revised 20 October 2023; accepted 11 December 2023

Studying rainfall patterns is very important because agricultural production and flood conditions depend on proper water management. Therefore, accurately identifying trends in climate scenarios is essential to achieve this goal. This study, therefore, analyses rainfall trends using the Mann–Kendall test (MKT), modified Mann–Kendall test (MMKT), Spearman rank correlation (SRC), Şen slope estimator (SSE), and innovative trend analysis method (ITAM). This investigation analyses annual, monsoon, autumn, summer, and winter rainfall trends using the most extensive hydrometeorological time series from 1901 to 2020. Five such methods of trend analysis use 120 years of gridded meteorological data from the India Meteorological Department for the neighbouring four river basins Kangsabati, Keliaghai, Silabati, and Dwarkeswer in east India. For the winter period, no significant trend is detected using the MKT, MMKT, SRC, and SSE. While the ITAM detects a significant trend at 88% of grid points of the study area. During other seasons, the MKT, MMKT, SRC and SSE notice trends for 76% of grid points with less significance than the ITAM method. Overall results obtained using the ITAM and MMKT methods are proved to be more effective in detecting sensitive trends. This study can serve as scientific support for the identification and strategic mitigation of climatic change impacts on water management to reduce the risk of climate change.

Keywords. Rainfall trends; modified Mann–Kendall test; innovative trend analysis; Şen slope estimator; Spearman rank correlation.

1. Introduction

Increased climate variability and changes due to anthropogenic activity have shifted rainfall patterns and trends around the world (Goswami *et al.* 2006; IPCC 2018). Regional rainfall trends tend to be distinctly unique. The most extensively utilised tests for hydrometeorological trend identification are the Mann–Kendall test (MKT) (Kendall 1938; Mann 1945), modified Mann–Kendall test (MMKT) (Hamed and Rao 1998; Yue and Wang 2004), Spearman rank correlation (SRC) (1904), Şen slope estimator (SSE), and innovative trend analysis method (ITAM) (Şen 2012).

The Mann–Kendall test (Kendall 1938; Mann 1945) is limited to a time series of independent, randomly ordered observations that are not normally distributed or auto-correlated (Hamed and

Published online: 04 April 2024

Gaurav Patel
27.01.25

Ph.D. Thesis

ORIGINALITY REPORT

8%
SIMILARITY INDEX

PRIMARY SOURCES

1	link.springer.com Internet	372 words — 1%
2	www.mdpi.com Internet	199 words — 1%
3	www.researchgate.net Internet	128 words — < 1%
4	www.frontiersin.org Internet	103 words — < 1%
5	dokumen.pub Internet	91 words — < 1%
6	www.nature.com Internet	77 words — < 1%
7	etd.aau.edu.et Internet	72 words — < 1%
8	ideas.repec.org Internet	72 words — < 1%
9	assets-eu.researchsquare.com Internet	70 words — < 1%
10	en.wikipedia.org Internet	

Subhasish Das 27/01/25

Dr. Subhasish Das
Associate Professor & Joint Director
School of Water Resources Engineering
Jadavpur University
Kolkata - 700032

Rajib Das 27/01/2025

Dr. RAJIB DAS
Assistant Professor
School of Water Resources Engineering
Jadavpur University
Kolkata-700 032

Gaurav Patel
27.01.2025